Global Carbon Budget 2023

Pierre Friedlingstein 1 2, Michael O'Sullivan 1, Matthew W. Jones 3, Robbie M. Andrew 4, Dorothee C. E. Bakker 5, Judith Hauck 6, Peter Landschützer 7, Corinne Le Quéré 3, Ingrid T. Luijkx 8, Glen P. Peters 4, Wouter Peters 8 9, Julia Pongratz 10 11, Clemens Schwingshackl 10, Stephen Sitch 1, Josep G. Canadell 12, Philippe Ciais 13, Robert B. Jackson 14, Simone R. Alin 15, Peter Anthoni 16, Leticia Barbero 17, Nicholas R. Bates 18 19, Meike Becker 20 21, Nicolas Bellouin 22, Bertrand Decharme 23, Laurent Bopp 2, Ida Bagus Mandhara Brasika 1 24, Patricia Cadule 25, Matthew A. Chamberlain 26, Naveen Chandra 27, Thi-Tuyet-Trang Chau 13, Frédéric Chevallier 13, Louise P. Chini 28, Margot Cronin 29, Xinyu Dou 30, Kazutaka Enyo 31, Wiley Evans 32, Stefanie Falk 10, Richard A. Feely 15, Liang Feng 33 34, Daniel. J. Ford 1, Thomas Gasser 35, Josefine Ghattas 13, Thanos Gkritzalis 7, Giacomo Grassi 36, Luke Gregor 37, Nicolas Gruber 38, Özgür Gürses 6, Ian Harris 39, Matthew Hefner 40, Jens Heinke 41, Richard A. Houghton 42, George C. Hurtt 43, Yosuke Iida 31, Tatiana Ilyina 11, Andrew R. Jacobson 44 45, Atul Jain 46, Tereza Jarníková 47, Annika Jersild 11, Fei Jiang 48, Zhe Jin 49 50, Fortunat Joos 51 52, Etsushi Kato 53, Ralph F. Keeling 54, Daniel Kennedy 55, Kees Klein Goldewijk 56, Jürgen Knauer 57 12, Jan Ivar Korsbakken 4, Arne Körtzinger 58, Xin Lan 44 45, Nathalie Lefèvre 59, Hongmei Li 11, Junjie Liu 60 61, Zhiqiang Liu 62, Lei Ma 28, Greg Marland 40 63, Nicolas Mayot 3, Patrick C. McGuire 64, G.A. McKinley 65, Gesa Meyer 66, Eric J. Morgan 54, David R. Munro 44 67, Shin-Ichiro Nakaoka 68, Yosuke Niwa 68 69, Kevin M. O'Brien 70 15, Are Olsen 20 21, Abdirahman M. Omar 71 21, Tsuneo Ono 72, Melf E. Paulsen 58, Denis Pierrot 73, Katie Pocock 74, Benjamin Poulter 75, Carter M. Powis 76, Gregor Rehder 77, Laure Resplandy 78, Eddy Robertson 79, Christian Rödenbeck 80, Thais M Rosan 1, Jörg Schwinger 21 81, Roland Séférian 82, T. Luke Smallman 33, Stephen M. Smith 76, Reinel Sospedra-Alfonso 83, Qing Sun 51 52, Adrienne J. Sutton 15, Colm Sweeney 45, Shintaro Takao 68, Pieter P. Tans 84, Hanqin Tian 85, Bronte Tilbrook 86 87, Hiroyuki Tsujino 88, Francesco Tubiello 89, Guido R. van der Werf 8, Erik van Ooijen 86, Rik Wanninkhof 73, Michio Watanabe 90, Cathy Wimart-Rousseau 58, Dongxu Yang 91, Xiaojuan Yang 92, Wenping Yuan 93, Xu Yue 94, Sönke Zaehle 80, Jiye Zeng 68, Bo Zheng 95

1 Faculty of Environment, Science and Economy, University of Exeter, Exeter EX4 4QF, UK
2 Laboratoire de Météorologie Dynamique / Institut Pierre-Simon Laplace, CNRS, Ecole Normale Supérieure / Université PSL, Sorbonne Université, Ecole Polytechnique, Paris, France
3 Tyndall Centre for Climate Change Research, School of Environmental Sciences, University of East Anglia, Norwich Research Park, Norwich NR4 7TJ, UK
4 CICERO Center for International Climate Research, Oslo 0349, Norway
5 School of Environmental Sciences, University of East Anglia, Norwich NR4 7TJ, UK
6 Alfred-Wegener-Institut, Helmholtz-Zentrum für Polar- und Meeresforschung, Am Handelshafen 12, 27570 Bremerhaven
7 VLIZ Flanders Marine Institute, Jacobsenstraat 1, 8400, Ostend, Belgium

8 Wageningen University, Environmental Sciences Group, P.O. Box 47, 6700AA, Wageningen, The Netherlands
9 University of Groningen, Centre for Isotope Research, Groningen, The Netherlands
10 Ludwig-Maximilians-Universität München, Luisenstr. 37, 80333 München, Germany
11 Max Planck Institute for Meteorology, Bundesstraße 53, 20146 Hamburg, Germany
12 CSIRO Environment, Canberra, ACT 2101, Australia
13 Laboratoire des Sciences du Climat et de l'Environnement, LSCE/IPSL, CEA-CNRS-UVSQ, Université Paris-Saclay, F-91198 Gif-sur-Yvette, France
14 Department of Earth System Science, Woods Institute for the Environment, and Precourt Institute for Energy, Stanford University, Stanford, CA 94305–2210, United States of America
15 National Oceanic and Atmospheric Administration, Pacific Marine Environmental Laboratory (NOAA/PMEL), 7600 Sand Point Way NE, Seattle, WA 98115, USA
16 Karlsruhe Institute of Technology, Institute of Meteorology and Climate Research/Atmospheric Environmental Research, 82467 Garmisch-Partenkirchen, Germany
17 Rosenstiel School of Marine Atmospheric and Earth Science, Cooperative Institute for Marine and Atmospheric Studies (CIMAS), University of Miami, 4600 Rickenbacker Causeway, Miami, FL, USA
18 School of Ocean Futures, Julie Ann Wrigley Global Futures Laboratory, Arizona State University, Tempe, Arizona, AZ 85287-5502, USA
19 Bermuda Institute of Ocean Sciences (BIOS), 17 Biological Lane, St. Georges, GE01, Bermuda
20 Geophysical Institute, University of Bergen, Allégaten 70, 5007 Bergen, Norway
21 Bjerknes Centre for Climate Research, Bergen, Norway
22 Department of Meteorology, University of Reading, Reading, RG6 6BB, UK
23 CNRM, Université de Toulouse, Météo-France, CNRS, Toulouse, France
24 Faculty of Marine Science & Fisheries, University of Udayana, Bali 80361, Indonesia
25 CNRS, Institut Pierre-Simon Laplace, Sorbonne Université, Paris, France
26 CSIRO Environment, Hobart, TAS, Australia
27 Research Institute for Global Change, JAMSTEC, 3173-25 Showa-machi, Kanazawa, Yokohama, 236-0001, Japan
28 Department of Geographical Sciences, University of Maryland, College Park, MD 20742, USA
29 Marine Institute, Rinville, Oranmore, Co Galway H91 R673, Ireland
30 Department of Earth System Science, Tsinghua University, Beijing, China
31 Japan Meteorological Agency, 3-6-9 Toranomon, Minato City, Tokyo 105-8431, Japan
32 Hakai Institute, 1713 Hyacinthe Bay Rd, Heriot Bay, BC, V0P 1H0, Canada
33 National Centre for Earth Observation, University of Edinburgh, Edinburgh, EH9 3FE, UK
34 School of Geosciences, University of Edinburgh, UK
35 International Institute for Applied Systems Analysis (IIASA), Schlossplatz 1, A-2361 Laxenburg, Austria
36 European Commission, Joint Research Centre, 21027 Ispra (VA), Italy
37 ETH Zuerich

38 Environmental Physics Group, ETH Zürich, Institute of Biogeochemistry and Pollutant Dynamics and Center for Climate Systems Modeling (C2SM)
39 NCAS-Climate, Climatic Research Unit, School of Environmental Sciences, University of East Anglia, Norwich Research Park, Norwich, NR4 7TJ, UK
40 Research Institute for Environment, Energy, and Economics, Appalachian State University, Boone, North Carolina, USA
41 Potsdam Institute for Climate Impact Research (PIK), member
of the Leibniz Association, P.O. Box 60 12 03, 14412 Potsdam, Germany
42 Woodwell Climate Research Center, Falmouth, MA 02540, USA
43 Department of Geographical Sciences, University of Maryland, College Park, Maryland 20742, USA
44 Cooperative Institute for Research in Environmental Sciences (CIRES), University of Colorado, Boulder, CO 80305, USA
45 National Oceanic and Atmospheric Administration, Global Monitoring Laboratory (NOAA/GML), 325 Broadway R/GML, Boulder, CO 80305, USA
46 Department of Atmospheric Sciences, University of Illinois, Urbana, IL 61821, USA
47 School of Environmental Sciences, University of East Anglia, Norwich Research Park, Norwich NR4 7TJ, UK
48 Jiangsu Provincial Key Laboratory of Geographic Information Science and Technology, International Institute for Earth System Science, Nanjing University, Nanjing, 210023, China
Nanjing University, Nanjing, China
49 State Key Laboratory of Tibetan Plateau Earth System and Resource Environment, Institute of Tibetan Plateau Research, Chinese Academy of Sciences, Beijing 100101, China
50 Institute of Carbon Neutrality, Peking University, Beijing 100871, China
51 Climate and Environmental Physics, Physics Institute, University of Bern, Bern, Switzerland
52 Oeschger Centre for Climate Change Research, University of Bern, Bern, Switzerland
53 Institute of Applied Energy (IAE), Minato-ku, Tokyo 105-0003, Japan
54 University of California, San Diego, Scripps Institution of Oceanography, La Jolla, CA 92093-0244, USA
55 National Center for Atmospheric Research, Climate and Global Dynamics, Terrestrial Sciences Section, Boulder, CO 80305, USA
56 Utrecht University, Faculty of Geosciences, Department IMEW, Copernicus Institute of Sustainable Development, Heidelberglaan 2, P.O. Box 80115, 3508 TC, Utrecht, the Netherlands
57 Hawkesbury Institute for the Environment, Western Sydney University, Penrith, New South Wales, Australia
58 GEOMAR Helmholtz Centre for Ocean Research, Wischhofstr. 1-3, 24148 Kiel, Germany
59 LOCEAN/IPSL laboratory, Sorbonne Université, CNRS/IRD/MNHN, Paris, France
60 NASA, Jet Propulsion Laboratory, California Institute of Technology, Pasadena, CA 91125, USA
61 Caltech, Pasadena, CA 91125
62 CMA Key Open Laboratory of Transforming Climate Resources to Economy, Chongqing Institute of Meteorological Sciences, Chongqing 401147, China

63 Department of Geological and Environmental Sciences, Appalachian State University, Boone, North Carolina, USA
64 Department of Meteorology & National Centre for Atmospheric Science (NCAS), University of Reading, Reading, United Kingdom
65 Columbia University
66 Climate Research Division, Environment and Climate Change Canada, Victoria, BC, Canada
67 National Oceanic and Atmospheric Administration/Global Monitoring Laboratory (NOAA/GML), 325 Broadway R/GML, Boulder, CO 80305, USA
68 Earth System Division, National Institute for Environmental Studies, 16-2 Onogawa, Tsukuba, Ibaraki, 305-8506 Japan
69 Department of Climate and Geochemistry Research, Meteorological Research Institute, 1-1 Nagamine, Tsukuba, Ibaraki 305-0052, Japan
70 Cooperative Institute for Climate, Ocean and Ecosystem Studies (CICOES), University of Washington, Seattle, WA 98105, USA
71 NORCE Norwegian Research Centre, Jahnebakken 5, 5007 Bergen, Norway
72 Marine Environment Division, Fisheries Resources Institute, Japan Fisheries Research and Education Agency, 2-12-4 Fukuura, Kanazawa-Ku, Yokohama 236-8648, Japan
73 National Oceanic & Atmospheric Administration, Atlantic Oceanographic & Meteorological Laboratory (NOAA/AOML), 4301 Rickenbacker Causeway, Miami, FL 33149, USA
74 Hakai Institute, 1713 Hyacinthe Bay Rd, Heriot Bay, BC, V0P 1H0, Canada
75 NASA Goddard Space Flight Center, Biospheric Sciences Laboratory, Greenbelt, Maryland 20771, USA
76 Smith School for Enterprise and the Environment, University of Oxford, Oxford, UK
77 Leibniz Institute for Baltic Sea Research Warnemünde (IOW), Seestrasse 15, 18119 Rostock, Germany
78 Princeton University, Department of Geosciences and Princeton Environmental Institute, Princeton, NJ, USA
79 Met Office Hadley Centre, FitzRoy Road, Exeter EX1 3PB, UK
80 Max Planck Institute for Biogeochemistry, P.O. Box 600164, Hans-Knöll-Str. 10, 07745 Jena, Germany
81 NORCE Climate & Environment, Jahnebakken 5, 5007 Bergen, Norway
82 CNRM (Météo-France/CNRS)-UMR 3589
83 Canadian Centre for Climate Modelling and Analysis, Victoria BC, Canada
84 Institute of Arctic and Alpine Research, University of Colorado, Boulder, CO 80309, USA
85 Schiller Institute of Integrated Science and Society, Department of Earth and Environmental Sciences, Boston College, Chestnut Hill, MA 02467, USA
86 CSIRO Environment, Castray Esplanade, Hobart, Tasmania 7004, Australia
87 Australian Antarctic Partnership Program, University of Tasmania, Hobart, Australia
88 JMA Meteorological Research Institute, Japan
89 Statistics Division, Food and Agriculture Organization of the United Nations, Via Terme di Caracalla, Rome 00153, Italy

90 Japan Agency for Marine-Earth Science and Technology (JAMSTEC), 3173-25, Showa-machi, Kanazawa-ku, Yokohama, 236-0001, Japan
91 Institute of Atmospheric Physics, Chinese Academy of Sciences
92 Environmental Sciences Division and Climate Change Science Institute, Oak Ridge National Laboratory, Oak Ridge, TN, 37831, USA
93 School of Atmospheric Sciences, Sun Yat-sen University, Zhuhai, Guangdong 510245, China
94 School of Environmental Science and Engineering, Nanjing University of Information Science and Technology (NUIST)
95 Shenzhen Key Laboratory of Ecological Remediation and Carbon Sequestration, Institute of Environment and Ecology, Tsinghua Shenzhen International Graduate School, Tsinghua University, Shenzhen 518055, China

Correspondence to: Pierre Friedlingstein (p.friedlingstein@exeter.ac.uk)

Abstract

Accurate assessment of anthropogenic carbon dioxide (CO_2) emissions and their redistribution among the atmosphere, ocean, and terrestrial biosphere in a changing climate is critical to better understand the global carbon cycle, support the development of climate policies, and project future climate change. Here we describe and synthesise data sets and methodology to quantify the five major components of the global carbon budget and their uncertainties. Fossil CO_2 emissions (E_{FOS}) are based on energy statistics and cement production data, while emissions from land-use change (E_{LUC}), mainly deforestation, are based on land-use and land-use change data and bookkeeping models. Atmospheric CO_2 concentration is measured directly, and its growth rate (G_{ATM}) is computed from the annual changes in concentration. The ocean CO_2 sink (S_{OCEAN}) is estimated with global ocean biogeochemistry models and observation-based fCO_2-products. The terrestrial CO_2 sink (S_{LAND}) is estimated with dynamic global vegetation models. Additional lines of evidence on land and ocean sinks are provided by atmospheric inversions, atmospheric oxygen measurements and Earth System Models. The resulting carbon budget imbalance (B_{IM}), the difference between the estimated total emissions and the estimated changes in the atmosphere, ocean, and terrestrial biosphere, is a measure of imperfect data and incomplete understanding of the contemporary carbon cycle. All uncertainties are reported as ±1σ.

For the year 2022, E_{FOS} increased by 0.9% relative to 2021, with fossil emissions at 9.9 ± 0.5 GtC yr^{-1} (10.2 ± 0.5 GtC yr^{-1} when the cement carbonation sink is not included), E_{LUC} was 1.2 ± 0.7 GtC yr^{-1}, for a total anthropogenic CO_2 emission (including the cement carbonation sink) of 11.1 ± 0.8 GtC yr^{-1} (40.7 ± 3.2 $GtCO_2$ yr^{-1}). Also, for 2022, G_{ATM} was 4.6 ± 0.2 GtC yr^{-1} (2.18 ± 0.1 ppm yr^{-1}), S_{OCEAN} was 2.8 ± 0.4 GtC yr^{-1} and S_{LAND} was 3.8 ± 0.8 GtC yr^{-1}, with a B_{IM} of -0.1 GtC yr^{-1} (i.e. total estimated sources marginally too low or sinks marginally too high). The global atmospheric CO_2 concentration averaged over 2022 reached 417.1 ± 0.1 ppm. Preliminary data for 2023, suggest an increase in E_{FOS} relative to 2022 of +1.1% (0.0% to 2.1%) globally, and atmospheric CO_2 concentration reaching 419.3 ppm, 51% above pre-industrial level (around 278 ppm in 1750). Overall, the mean and trend in the components of the global carbon budget are consistently estimated

over the period 1959-2022, with a near-zero overall budget imbalance, although discrepancies of up to around 1 GtC yr^{-1} persist for the representation of annual to semi-decadal variability in CO_2 fluxes. Comparison of estimates from multiple approaches and observations shows: (1) a persistent large uncertainty in the estimate of land-use changes emissions, (2) a low agreement between the different methods on the magnitude of the land CO_2 flux in the northern extra-tropics, and (3) a discrepancy between the different methods on the strength of the ocean sink over the last decade.

This living data update documents changes in methods and data sets applied to this most-recent global carbon budget as well as evolving community understanding of the global carbon cycle. The data presented in this work are available at https://doi.org/10.18160/GCP-2023 (Friedlingstein et al., 2023).

Executive Summary

Global fossil CO_2 emissions (including cement carbonation) are expected to further increase in 2023, to 1.4% above their pre-COVID-19 pandemic 2019 level. The 2022 emission increase was 0.09 GtC yr^{-1} (0.33 $GtCO_2$ yr^{-1}) relative to 2021, bringing 2022 fossil CO_2 emissions to 9.9 ± 0.5 GtC yr^{-1} (36.4 ± 1.8 $GtCO_2$ yr^{-1}), virtually equal to the emissions level of 2019. Preliminary estimates based on data available suggest fossil CO_2 emissions to increase further in 2023, by 1.1% relative to 2022 (0.0% to 2.1%), bringing emissions to 10.0 GtC yr^{-1} (36.8 $GtCO_2$ yr^{-1}), 1.4% above the 2019 level.

Emissions from coal, oil, and gas in 2023 are all expected to be slightly above their 2022 levels (by 1.1%, 1.5% and 0.5% respectively). Regionally, fossil emissions in 2022 are expected to decrease by 7.4% in the European Union (0.7 GtC, 2.6 $GtCO_2$), and by 3.0% in the United States (1.3 GtC, 4.9 $GtCO_2$), but to increase by 4.0% in China (3.2 GtC, 11.9 $GtCO_2$), 8.2% in India (0.8 GtC, 3.1 $GtCO_2$) and -0.4% for the rest of the world (3.8 GtC, 14.0 $GtCO_2$). International aviation and shipping (IAS) is expected to increase by 11.9% (0.3 GtC, 1.2 $GtCO_2$).

Fossil CO_2 emissions decreased in 18 countries during the decade 2013-2022. Altogether, these 18 countries contribute about 1.9 GtC yr^{-1} (7.1 $GtCO_2$) fossil fuel CO_2 emissions over the last decade, representing about 20% of world CO_2 fossil emissions.

Global CO_2 emissions from land-use, land-use change, and forestry (LULUCF) averaged 1.3 ± 0.7 GtC yr^{-1} (4.7 ± 2.6 $GtCO_2$ yr^{-1}) for the 2013-2022 period with a preliminary projection for 2023 of 1.1 ± 0.7 GtC yr^{-1} (4.0 ± 2.6 $GtCO_2$ yr^{-1}). A small decrease over the past two decades is not robust given the large model uncertainty. Emissions from deforestation, the main driver of global gross sources, remain high at around 1.9 GtC yr^{-1} over the 2013-2022 period, highlighting the strong potential of halting deforestation for emissions reductions. Sequestration of 1.3 GtC yr^{-1} through re-/afforestation and forestry offsets two third of the deforestation emissions. Emissions from other land-use transitions and from peat drainage and peat fire add further, smaller contributions. The highest emitters during 2013-2022 in descending order were Brazil, Indonesia, and the Democratic Republic of the Congo, with these 3 countries contributing more than half of global land-use CO_2 emissions.

Total anthropogenic emissions were 11.1 GtC yr^{-1} (40.7 $GtCO_2$ yr-1) in 2022, with a similar preliminary estimate of 11.1 GtC yr^{-1} (40.9 GtCO2 yr^{-1}) for 2023.

The remaining carbon budget for a 50% likelihood to limit global warming to 1.5°C, 1.7°C and 2°C has respectively reduced to 75 GtC (275 $GtCO_2$), 175 GtC (625 $GtCO_2$) and 315 GtC (1150 $GtCO_2$) from the beginning of 2024, equivalent to around 7, 15 and 28 years, assuming 2023 emissions levels.

The concentration of CO_2 in the atmosphere is set to reach 419.3 ppm in 2023, 51% above pre-industrial levels. The atmospheric CO_2 growth was 5.2 ± 0.02 GtC yr^{-1} during the decade 2013-2022 (47% of total CO_2 emissions) with a preliminary 2023 growth rate estimate of around 5.1 GtC (2.4 ppm).

The ocean CO_2 sink resumed a more rapid growth in the past two decades after low or no growth during the 1991-2002 period, overlaid with imprints of climate variability. The estimates based on *f*CO_2-products and models diverge with the growth of the ocean CO_2 sink in the past decade being a factor 2.5 larger than in the models. This discrepancy in the trend originates from all latitudes but is largest in the Southern Ocean. The ocean CO_2 sink was 2.9 ± 0.4 GtC yr^{-1} during the decade 2013-2022 (26% of total CO_2 emissions), and did not grow since 2019 due to a triple La Niña event. A similar value of 2.9 GtC yr^{-1} is preliminarily estimated for 2023, which marks an increase in the sink compared to the last two years due to the transition from La Niña to El Niño conditions in 2023.

The land CO_2 sink continued to increase during the 2013-2022 period primarily in response to increased atmospheric CO_2, albeit with large interannual variability. The land CO_2 sink was 3.3 ± 0.8 GtC yr^{-1} during the 2013-2022 decade (31% of total CO2 emissions), 0.4 GtC yr^{-1} larger than during the previous decade (2000-2009), with a preliminary 2023 estimate of around 2.9 GtC yr^{-1}, significantly lower than in 2022, and attributed to the response of the land biosphere to the emerging El Niño in 2023. Year to year variability in the land sink is about 1 GtC yr^{-1} and dominates the year-to-year changes in the global atmospheric CO_2 concentration, implying that small annual changes in anthropogenic emissions (such as the fossil fuel emission decrease in 2020) are hard to detect in the atmospheric CO_2 observations.

1 Introduction

The concentration of carbon dioxide (CO_2) in the atmosphere has increased from approximately 278 parts per million (ppm) in 1750 (Gulev et al., 2021), the beginning of the Industrial Era, to 417.1 ± 0.1 ppm in 2022 (Lan et al., 2023; Figure 1). The atmospheric CO_2 increase above pre-industrial levels was, initially, primarily caused by the release of carbon to the atmosphere from deforestation and other land-use change activities (Canadell et al., 2021). While emissions from fossil fuels started before the Industrial Era, they became the dominant source of anthropogenic emissions to the atmosphere from around 1950 and their relative share has continued to increase until present. Anthropogenic emissions occur on top of an active natural carbon cycle that circulates carbon between the reservoirs of the atmosphere, ocean, and terrestrial biosphere on time scales from sub-daily to millennia, while exchanges with geologic reservoirs occur at longer timescales (Archer et al., 2009).

The global carbon budget (GCB) presented here refers to the mean, variations, and trends in the perturbation of CO_2 in the environment, referenced to the beginning of the Industrial Era (defined here as 1750). This paper describes the components of the global carbon cycle over the historical period with a stronger focus on the recent period (since 1958, onset of robust atmospheric CO_2 measurements), the last decade (2013-2022), the last year (2022) and the current year (2023). Finally, it provides cumulative emissions from fossil fuels and land-use change since the year 1750 (the pre-industrial period), and since the year 1850 (the reference year for historical simulations in IPCC AR6) (Eyring et al., 2016).

We quantify the input of CO_2 to the atmosphere by emissions from human activities, the growth rate of atmospheric CO_2 concentration, and the resulting changes in the storage of carbon in the land and ocean reservoirs in response to increasing atmospheric CO_2 levels, climate change and variability, and other anthropogenic and natural changes (Figure 2). An understanding of this perturbation budget over time and the underlying variability and trends of the natural carbon cycle is necessary to understand the response of natural sinks to changes in climate, CO_2 and land-use change drivers, and to quantify emissions compatible with a given climate stabilisation target.

The components of the CO_2 budget that are reported annually in this paper include separate and independent estimates for the CO_2 emissions from (1) fossil fuel combustion and oxidation from all energy and industrial processes; also including cement production and carbonation (E_{FOS}; GtC yr^{-1}) and (2) the emissions resulting from deliberate human activities on land, including those leading to land-use change (E_{LUC}; GtC yr^{-1}); and their partitioning among (3) the growth rate of atmospheric CO_2 concentration (G_{ATM}; GtC yr^{-1}), and the uptake of CO_2 (the 'CO_2 sinks') in (4) the ocean (S_{OCEAN}; GtC yr^{-1}) and (5) on land (S_{LAND}; GtC yr^{-1}). The CO_2 sinks as defined here conceptually include the response of the land (including inland waters and estuaries) and ocean (including coastal and marginal seas) to elevated CO_2 and changes in climate and other environmental conditions, although in practice not all processes are fully accounted for (see Section 2.10). Global emissions and their partitioning among the atmosphere, ocean and land are in balance in the real world. Due to the combination of imperfect spatial and/or temporal data coverage, errors in each estimate, and smaller terms not

included in our budget estimate (discussed in Section 2.10), the independent estimates (1) to (5) above do not necessarily add up to zero. We therefore assess a set of additional lines of evidence derived from global atmospheric inversion system results (Section 2.7), observed changes in oxygen concentration (Section 2.8) and Earth System Models (ESMs) simulations (Section 2.9), all of which closing the global carbon balance. We also estimate a budget imbalance (B_{IM}), which is a measure of the mismatch between the estimated emissions and the estimated changes in the atmosphere, land and ocean, as follows:

$$B_{IM} = E_{FOS} + E_{LUC} - (G_{ATM} + S_{OCEAN} + S_{LAND}) \quad (1)$$

G_{ATM} is usually reported in ppm yr^{-1}, which we convert to units of carbon mass per year, GtC yr^{-1}, using 1 ppm = 2.124 GtC (Ballantyne et al., 2012; Table 1). All quantities are presented in units of gigatonnes of carbon (GtC, 10^{15} gC), which is the same as petagrams of carbon (PgC; Table 1). Units of gigatonnes of CO_2 (or billion tonnes of CO_2) used in policy are equal to 3.664 multiplied by the value in units of GtC.

We also quantify E_{FOS} and E_{LUC} by country, including both territorial and consumption-based accounting for E_{FOS} (see Section 2), and discuss missing terms from sources other than the combustion of fossil fuels (see Section 2.10, Supplement S1 and S2).

We now assess carbon dioxide removal (CDR) (see Sect. 2.2 and 2.3). Land-based CDR is significant, but already accounted for in E_{LUC} in equation (1) (Sect 3.2.2). Other CDR methods, not based on vegetation, are currently several orders of magnitude smaller than the other components of the budget (Sect. 3.3), hence these are not included in equation (1), or in the global carbon budget tables or figures (with the exception of Figure 2 where CDR is shown primarily for illustrative purpose).

The global CO_2 budget has been assessed by the Intergovernmental Panel on Climate Change (IPCC) in all assessment reports (Prentice et al., 2001; Schimel et al., 1995; Watson et al., 1990; Denman et al., 2007; Ciais et al., 2013; Canadell et al., 2021), and by others (e.g. Ballantyne et al., 2012). The Global Carbon Project (GCP, www.globalcarbonproject.org, last access: 9 November 2023) has coordinated this cooperative community effort for the annual publication of global carbon budgets for the year 2005 (Raupach et al., 2007; including fossil emissions only), year 2006 (Canadell et al., 2007), year 2007 (GCP, 2008), year 2008 (Le Quéré et al., 2009), year 2009 (Friedlingstein et al., 2010), year 2010 (Peters et al., 2012a), year 2012 (Le Quéré et al., 2013; Peters et al., 2013), year 2013 (Le Quéré et al., 2014), year 2014 (Le Quéré et al., 2015a; Friedlingstein et al., 2014), year 2015 (Jackson et al., 2016; Le Quéré et al., 2015b), year 2016 (Le Quéré et al., 2016), year 2017 (Le Quéré et al., 2018a; Peters et al., 2017), year 2018 (Le Quéré et al., 2018b; Jackson et al., 2018), year 2019 (Friedlingstein et al., 2019; Jackson et al., 2019; Peters et al., 2020), year 2020 (Friedlingstein et al., 2020; Le Quéré et al., 2021), year 2021 (Friedlingstein et al., 2022a; Jackson et al., 2022) and most recently the year 2022 (Friedlingstein et al., 2022b). Each of these papers updated previous estimates with the latest available information for the entire time series.

We adopt a range of ±1 standard deviation (σ) to report the uncertainties in our global estimates, representing a likelihood of 68% that the true value will be within the provided range if the errors have a gaussian distribution,

and no bias is assumed. This choice reflects the difficulty of characterising the uncertainty in the CO_2 fluxes between the atmosphere and the ocean and land reservoirs individually, particularly on an annual basis, as well as the difficulty of updating the CO_2 emissions from land-use change. A likelihood of 68% provides an indication of our current capability to quantify each term and its uncertainty given the available information. The uncertainties reported here combine statistical analysis of the underlying data, assessments of uncertainties in the generation of the data sets, and expert judgement of the likelihood of results lying outside this range. The limitations of current information are discussed in the paper and have been examined in detail elsewhere (Ballantyne et al., 2015; Zscheischler et al., 2017). We also use a qualitative assessment of confidence level to characterise the annual estimates from each term based on the type, amount, quality, and consistency of the different lines of evidence as defined by the IPCC (Stocker et al., 2013).

This paper provides a detailed description of the data sets and methodology used to compute the global carbon budget estimates for the industrial period, from 1750 to 2023, and in more detail for the period since 1959. This paper is updated every year using the format of 'living data' to keep a record of budget versions and the changes in new data, revision of data, and changes in methodology that lead to changes in estimates of the carbon budget. Additional materials associated with the release of each new version will be posted at the Global Carbon Project (GCP) website (http://www.globalcarbonproject.org/carbonbudget, last access: 9 November 2023), with fossil fuel emissions also available through the Global Carbon Atlas (http://www.globalcarbonatlas.org, last access: 9 November 2023). All underlying data used to produce the budget can also be found at https://globalcarbonbudget.org/ (last access: 9 November 2023). With this approach, we aim to provide the highest transparency and traceability in the reporting of CO_2, the key driver of climate change.

2 Methods

Multiple organisations and research groups around the world generated the original measurements and data used to complete the global carbon budget. The effort presented here is thus mainly one of synthesis, where results from individual groups are collated, analysed, and evaluated for consistency. We facilitate access to original data with the understanding that primary data sets will be referenced in future work (see Table 2 for how to cite the data sets, and Section on data availability). Descriptions of the measurements, models, and methodologies follow below, with more detailed descriptions of each component provided as Supplementary Information (S1 to S5).

This is the 18th version of the global carbon budget and the 12th revised version in the format of a living data update in Earth System Science Data. It builds on the latest published global carbon budget of Friedlingstein et al. (2022b). The main changes this year are: the inclusion of (1) data to year 2022 and a projection for the global carbon budget for year 2023; (2) CO_2 uptake from Carbon Dioxide Removal (CDR); (3) land and ocean net carbon fluxes estimates from changes in atmospheric oxygen concentration; (4) land and ocean net carbon fluxes estimates from ESMs; and (5) revised method to estimate the current year (2023) atmospheric CO_2. The main methodological differences between recent annual carbon budgets (2019 to 2023) are summarised in Table 3 and previous changes since 2006 are provided in Table S8.

2.1 Fossil CO_2 emissions (E_{FOS})

2.1.1 Historical period 1850-2022

The estimates of global and national fossil CO_2 emissions (E_{FOS}) include the oxidation of fossil fuels through both combustion (e.g., transport, heating) and chemical oxidation (e.g. carbon anode decomposition in aluminium refining) activities, and the decomposition of carbonates in industrial processes (e.g. the production of cement). We also include CO_2 uptake from the cement carbonation process. Several emissions sources are not estimated or not fully covered: coverage of emissions from lime production are not global, and decomposition of carbonates in glass and ceramic production are included only for the "Annex 1" countries of the United Nations Framework Convention on Climate Change (UNFCCC) for lack of activity data. These omissions are considered to be minor. Short-cycle carbon emissions - for example from combustion of biomass - are not included here but are accounted for in the CO_2 emissions from land use (see Section 2.2).

Our estimates of fossil CO_2 emissions rely on data collection by many other parties. Our goal is to produce the best estimate of this flux, and we therefore use a prioritisation framework to combine data from different sources that have used different methods, while being careful to avoid double counting and undercounting of emissions sources. The CDIAC-FF emissions dataset, derived largely from UN energy data, forms the foundation, and we extend emissions to year Y-1 using energy growth rates reported by the Energy Institute (a dataset formally produced by BP). We then proceed to replace estimates using data from what we consider to be superior sources, for example Annex 1 countries' official submissions to the UNFCCC. All data points are potentially subject to revision, not just the latest year. For full details see Andrew and Peters (2022).

Other estimates of global fossil CO_2 emissions exist, and these are compared by Andrew (2020a). The most common reason for differences in estimates of global fossil CO_2 emissions is a difference in which emissions sources are included in the datasets. Datasets such as those published by the energy company BP, the US Energy Information Administration, and the International Energy Agency's 'CO_2 emissions from fuel combustion' are all generally limited to emissions from combustion of fossil fuels. In contrast, datasets such as PRIMAP-hist, CEDS, EDGAR, and GCP's dataset aim to include all sources of fossil CO_2 emissions. See Andrew (2020a) for detailed comparisons and discussion.

Cement absorbs CO_2 from the atmosphere over its lifetime, a process known as 'cement carbonation'. We estimate this CO_2 sink, from 1931, onwards as the average of two studies in the literature (Cao et al., 2020; Guo et al., 2021). Both studies use the same model, developed by Xi et al. (2016), with different parameterisations and input data, with the estimate of Guo and colleagues being a revision of Xi et al. (2016). The trends of the two studies are very similar. Since carbonation is a function of both current and previous cement production, we extend these estimates to 2022 by using the growth rate derived from the smoothed cement emissions (10-year smoothing) fitted to the carbonation data. In the present budget, we always include the cement carbonation carbon sink in the fossil CO_2 emission component (E_{FOS}).

We use the Kaya Identity for a simple decomposition of CO_2 emissions into the key drivers (Raupach et al., 2007). While there are variations (Peters et al., 2017), we focus here on a decomposition of CO_2 emissions into population, GDP per person, energy use per GDP, and CO_2 emissions per energy. Multiplying these individual components together returns the CO_2 emissions. Using the decomposition, it is possible to attribute the change in CO_2 emissions to the change in each of the drivers. This method gives a first-order understanding of what causes CO_2 emissions to change each year.

2.1.2 2023 projection

We provide a projection of global fossil CO_2 emissions in 2022 by combining separate projections for China, USA, EU, India, and for all other countries combined. The methods are different for each of these. For China we combine monthly fossil fuel production data from the National Bureau of Statistics and trade data from the Customs Administration, giving us partial data for the growth rates to date of natural gas, petroleum, and cement, and of the apparent consumption itself for raw coal. We then use a regression model to project full-year emissions based on historical observations. For the USA our projection is taken directly from the Energy Information Administration's (EIA) Short-Term Energy Outlook (EIA, 2023), combined with the year-to-date growth rate of cement clinker production. For the EU we use monthly energy data from Eurostat to derive estimates of monthly CO_2 emissions through July, with coal emissions extended through September using a statistical relationship with reported electricity generation from coal and other factors. For natural gas we use Holt-Winters to project the last four months of the year. EU emissions from oil are derived using the EIA's projection of oil consumption for Europe. EU cement emissions are based on available year-to-date data from three of the largest producers, Germany, Poland, and Spain. India's projected emissions are derived from estimates through August (July for coal) using the methods of Andrew (2020b) and extrapolated assuming seasonal patterns from before 2019. Emissions for the rest of the world are derived using projected growth in economic production from the IMF (2023) combined with extrapolated changes in emissions intensity of economic production. More details on the E_{FOS} methodology and its 2023 projection can be found in Supplement S.1.

2.2 CO_2 emissions from land-use, land-use change and forestry (E_{LUC})

2.2.1 Historical period 1850-2022

The net CO_2 flux from land-use, land-use change and forestry (E_{LUC}, called land-use change emissions in the rest of the text) includes CO_2 fluxes from deforestation, afforestation, logging and forest degradation (including harvest activity), shifting cultivation (cycle of cutting forest for agriculture, then abandoning), and regrowth of forests (following wood harvest or agriculture abandonment). Emissions from peat burning and peat drainage are added from external datasets, peat drainage being averaged from three spatially explicit independent datasets (see Supplement S.2.1).

Three bookkeeping approaches (updated estimates each of BLUE (Hansis et al., 2015), OSCAR (Gasser et al., 2020), and H&C2023 (Houghton and Castanho, 2023)) were used to quantify gross emissions and gross

removals and the resulting net E_{LUC}. Uncertainty estimates were derived from the Dynamic Global Vegetation Models (DGVMs) ensemble for the time period prior to 1960, and using for the recent decades an uncertainty range of ±0.7 GtC yr^{-1}, which is a semi-quantitative measure for annual and decadal emissions and reflects our best value judgement that there is at least 68% chance (±1σ) that the true land-use change emission lies within the given range, for the range of processes considered here.

Our E_{LUC} estimates follow the definition of global carbon cycle models of CO_2 fluxes related to land use and land management and differ from IPCC definitions adopted in National GHG Inventories (NGHGI) for reporting under the UNFCCC, which additionally generally include, through adoption of the IPCC so-called managed land proxy approach, the terrestrial fluxes occurring on all land that countries define as managed. This partly includes fluxes due to environmental change (e.g. atmospheric CO_2 increase), which are part of S_{LAND} in our definition. This causes the global emission estimates to be smaller for NGHGI than for the global carbon budget definition (Grassi et al., 2018). The same is the case for the Food Agriculture Organization (FAO) estimates of carbon fluxes on forest land, which include both anthropogenic and natural sources on managed land (Tubiello et al., 2021). We translate the two definitions to each other, to provide a comparison of the anthropogenic carbon budget to the official country reporting to the climate convention.

E_{LUC} contains a range of fluxes that are related to Carbon Dioxide Removal (CDR). CDR can be defined as the set of anthropogenic activities that remove CO_2 from the atmosphere and store it in durable form, such as in forest biomass and soils, long-lived products, or in geological or ocean reservoirs. We quantify vegetation-based CDR that is implicitly or explicitly captured by land-use fluxes consistent with our updated model estimates (CDR not based on vegetation is discussed in Section 2.3; IPCC, 2023). We quantify re/afforestation from the three bookkeeping estimates by separating forest regrowth in shifting cultivation cycles from permanent increases in forest cover (see Supplement C.2.1). The latter count as CDR, but it should be noted that the permanence of the storage under climate risks such as fire is increasingly questioned. Other CDR activities contained in E_{LUC} include the transfer of carbon to harvested wood products (HWP), which is represented by the bookkeeping models with varying details concerning product usage and their lifetimes; bioenergy with carbon capture and storage (BECCS); and biochar production. Bookkeeping and TRENDY models currently only represent BECCS and biochar with regard to the CO_2 removal through photosynthesis, but not for the durable storage. HWP, BECCS, and biochar are typically counted as CDR when the transfer to the durable storage site occurs and not when the CO_2 is removed from the atmosphere, which complicates a direct comparison to the global carbon budgets approach to quantify annual fluxes to and from the atmosphere. Estimates for CDR through HWP, BECCS, and biochar are thus not indicated in this budget, but can be found elsewhere (see Section 3.2.2).

2.2.2 2023 Projection

We project the 2023 land-use emissions for BLUE, H&C2023, and OSCAR based on their E_{LUC} estimates for 2022 and adding the change in carbon emissions from peat fires and tropical deforestation and degradation fires (2023 emissions relative to 2022 emissions) estimated using active fire data (MCD14ML; Giglio et al., 2016).

Peat drainage is assumed to be unaltered as it has low interannual variability. More details on the E_{LUC} methodology can be found in Supplement S.2.

2.3 Carbon Dioxide Removal (CDR) not based on vegetation

CDR not based on terrestrial vegetation currently relies on enhanced rock weathering and Direct Air Carbon Capture and Storage (DACCS) projects. The majority of this (58%) derives from a single project: Climeworks' Orca DACCS plant based in Hellisheidi, Iceland. The remainder is generated by 13 small-scale projects including, for example, 500 tons of carbon dioxide sequestered through the spreading of crushed olivine on agricultural areas by Eion Carbon. We use data from the State of CDR Report (Smith et al., 2023), which quantifies all currently deployed CDR methods, including the land-use related activities already covered by Section 2.2. The State of CDR Report (Smith et al., 2023) combines estimates of carbon storage in managed land derived from NGHGI data with project-by-project storage rates obtained through 20 extant CDR databases and registries (status as of mid-year 2022) by Powis et al. (2023). They assessed the data quality on existing CDR projects to be poor, suffering from fragmentation, different reporting standards, limited geographical coverage, and inclusion of a number of pilot plants with uncertain lifespans. As a consequence, these numbers could change substantially from year-to-year in the near-term.

2.4 Growth rate in atmospheric CO_2 concentration (G_{ATM})

2.4.1 Historical period 1850-2022

The rate of growth of the atmospheric CO_2 concentration is provided for years 1959-2022 by the US National Oceanic and Atmospheric Administration Global Monitoring Laboratory (NOAA/GML; Lan et al., 2023), which includes recent revisions to the calibration scale of atmospheric CO_2 measurements (Hall et al., 2021). For the 1959-1979 period, the global growth rate is based on measurements of atmospheric CO_2 concentration averaged from the Mauna Loa and South Pole stations, as observed by the CO_2 Program at Scripps Institution of Oceanography (Keeling et al., 1976). For the 1980-2021 time period, the global growth rate is based on the average of multiple stations selected from the marine boundary layer sites with well-mixed background air (Ballantyne et al., 2012), after fitting a smooth curve through the data for each station as a function of time, and averaging by latitude band (Masarie and Tans, 1995). The annual growth rate is estimated by Lan et al. (2023) from atmospheric CO_2 concentration by taking the average of the most recent December-January months corrected for the average seasonal cycle and subtracting this same average one year earlier. The growth rate in units of ppm yr^{-1} is converted to units of GtC yr^{-1} by multiplying by a factor of 2.124 GtC per ppm, assuming instantaneous mixing of CO_2 throughout the atmosphere (Ballantyne et al., 2012; Table 1).

Since 2020, NOAA/GML provides estimates of atmospheric CO_2 concentrations with respect to a new calibration scale, referred to as WMO-CO2-X2019, in line with a recalibration agreed by the World Meteorological Organization (WMO) Global Atmosphere Watch (GAW) community (Hall et al., 2021). The re-calibrated data were first used to estimate G_{ATM} in the 2021 edition of the global carbon budget (Friedlingstein et al., 2022a). Friedlingstein et al. (2022a) verified that the change of scales from WMO-CO2-X2007 to WMO-

CO2-X2019 made a negligible difference to the value of G_{ATM} (-0.06 GtC yr^{-1} during 2010-2019 and -0.01 GtC yr^{-1} during 1959-2019, well within the uncertainty range reported below).

The uncertainty around the atmospheric growth rate is due to four main factors. First, the long-term reproducibility of reference gas standards (around 0.03 ppm for 1σ from the 1980s; Lan et al., 2023). Second, small unexplained systematic analytical errors that may have a duration of several months to two years come and go. They have been simulated by randomising both the duration and the magnitude (determined from the existing evidence) in a Monte Carlo procedure. Third, the network composition of the marine boundary layer with some sites coming or going, gaps in the time series at each site, etc (Lan et al., 2023). The latter uncertainty was estimated by NOAA/GML with a Monte Carlo method by constructing 100 "alternative" networks (Masarie and Tans, 1995; NOAA/GML, 2019). The second and third uncertainties, summed in quadrature, add up to 0.085 ppm on average (Lan et al., 2023). Fourth, the uncertainty associated with using the average CO_2 concentration from a surface network to approximate the true atmospheric average CO_2 concentration (mass-weighted, in 3 dimensions) as needed to assess the total atmospheric CO_2 burden. In reality, CO_2 variations measured at the stations will not exactly track changes in total atmospheric burden, with offsets in magnitude and phasing due to vertical and horizontal mixing. This effect must be very small on decadal and longer time scales, when the atmosphere can be considered well mixed. The CO2 increase in the stratosphere lags the increase (meaning lower concentrations) that we observe in the marine boundary layer, while the continental boundary layer (where most of the emissions take place) leads the marine boundary layer with higher concentrations. These effects nearly cancel each other. In addition the growth rate is nearly the same everywhere (Ballantyne et al, 2012). We therefore maintain an uncertainty around the annual growth rate based on the multiple stations data set ranges between 0.11 and 0.72 GtC yr^{-1}, with a mean of 0.61 GtC yr^{-1} for 1959-1979 and 0.17 GtC yr^{-1} for 1980-2022, when a larger set of stations were available as provided by Lan et al. (2023). We estimate the uncertainty of the decadal averaged growth rate after 1980 at 0.02 GtC yr^{-1} based on the calibration and the annual growth rate uncertainty but stretched over a 10-year interval. For years prior to 1980, we estimate the decadal averaged uncertainty to be 0.07 GtC yr^{-1} based on a factor proportional to the annual uncertainty prior and after 1980 (0.02 * [0.61/0.17] GtC yr^{-1}).

We assign a high confidence to the annual estimates of G_{ATM} because they are based on direct measurements from multiple and consistent instruments and stations distributed around the world (Ballantyne et al., 2012; Hall et al., 2021).

To estimate the total carbon accumulated in the atmosphere since 1750 or 1850, we use an atmospheric CO_2 concentration of 278.3 ± 3 ppm or 285.1 ± 3 ppm, respectively (Gulev et al., 2021). For the construction of the cumulative budget shown in Figure 3, we use the fitted estimates of CO_2 concentration from Joos and Spahni (2008) to estimate the annual atmospheric growth rate using the conversion factors shown in Table 1. The uncertainty of ±3 ppm (converted to ±1σ) is taken directly from the IPCC's AR5 assessment (Ciais et al., 2013). Typical uncertainties in the growth rate in atmospheric CO_2 concentration from ice core data are equivalent to ±0.1-0.15 GtC yr^{-1} as evaluated from the Law Dome data (Etheridge et al., 1996) for individual 20-year intervals over the period from 1850 to 1960 (Bruno and Joos, 1997).

2.4.2 2023 projection

We provide an assessment of G_{ATM} for 2023 as the average of two methods. The GCB regression method models monthly global-average atmospheric CO_2 concentrations and derives the increment and annual average from these. The model uses lagged observations of concentration (Lan et al., 2023): both a 12-month lag, and the lowest lag that will allow model prediction to produce an estimate for the following January, recalling that the G_{ATM} increment is derived from December/January pairs. The largest driver of interannual changes is the ENSO signal (Betts et al., 2016), so the monthly ENSO 3.4 index (Huang et al., 2023) is included in the model. Given the natural lag between sea-surface temperatures and effects on the biosphere, and in turn effects on globally mixed atmospheric CO_2 concentration, a lagged ENSO index is used, and we use both a 5-month and a 6-month lag. The combination of the two lagged ENSO values helps reduce possible effects of noise in a single month. To help characterise the seasonal variation, we add month as a categorical variable. Finally, we flag the period affected by the Pinatubo eruption (August 1991 - November 1993) as a categorical variable. Note that while emissions of CO_2 are the largest driver of the trend in atmospheric CO_2 concentration, our goal here is to predict divergence from that trend. Because changes in emissions from year to year are relatively minor, this has little effect on the variation of concentration from the trend line. Even the relatively large drop in emissions in 2020 due to the COVID-19 pandemic does not cause any problems for the model.

For the first time this year, we also use the multi-model mean and uncertainty of the 2023 G_{ATM} estimated by the ESMs prediction system (see Section 2.9). We then take the average of the GCB regression and ESMs G_{ATM} estimates, with their respective uncertainty combined quadratically.

Similarly, the projection of the 2023 global average CO_2 concentration (in ppm), is calculated as the average of the estimates from the two methods. For the GCB regression method, it is the annual average of global concentration over the 12 months of 2023; for the ESMs, it is the observed global average CO_2 concentration for 2022 plus the annual increase in 2023 of the global average CO_2 concentration predicted by the ESMs multi-model mean.

2.5 Ocean CO_2 sink

2.5.1 Historical period 1850-2022

The reported estimate of the global ocean anthropogenic CO_2 sink S_{OCEAN} is derived as the average of two estimates. The first estimate is derived as the mean over an ensemble of ten global ocean biogeochemistry models (GOBMs, Table 4 and Table S2). The second estimate is obtained as the mean over an ensemble of seven surface ocean fCO_2-observation-based data-products (Table 4 and Table S3). An eighth fCO_2-product (Watson et al., 2020) is shown, but is not included in the ensemble average as it differs from the other products by adjusting the flux to a cool, salty ocean surface skin (see Supplement S.3.1 for a discussion of the Watson product). The GOBMs simulate both the natural and anthropogenic CO_2 cycles in the ocean. They constrain the anthropogenic air-sea CO_2 flux (the dominant component of S_{OCEAN}) by the transport of carbon into the ocean interior, which is also the controlling factor of present-day ocean carbon uptake in the real world. They cover

the full globe and all seasons and were recently evaluated against surface ocean carbon observations, suggesting they are suitable to estimate the annual ocean carbon sink (Hauck et al., 2020). The fCO_2-products are tightly linked to observations of fCO_2 (fugacity of CO_2, which equals pCO_2 corrected for the non-ideal behaviour of the gas; Pfeil et al., 2013), which carry imprints of temporal and spatial variability, but are also sensitive to uncertainties in gas-exchange parameterizations and data-sparsity (Gloege et al., 2021, Hauck et al., 2023). Their asset is the assessment of the mean spatial pattern of variability and its seasonality (Hauck et al., 2020, Gloege et al. 2021, Hauck et al., 2023). We further use two diagnostic ocean models to estimate S_{OCEAN} over the industrial era (1781-1958).

The global fCO_2-based flux estimates were adjusted to remove the pre-industrial ocean source of CO_2 to the atmosphere of 0.65 ± 0.3 GtC yr^{-1} from river input to the ocean (Regnier et al., 2022), to satisfy our definition of S_{OCEAN} (Hauck et al., 2020). The river flux adjustment was distributed over the latitudinal bands using the regional distribution of Lacroix et al. (2020; North: 0.14 GtC yr^{-1}, Tropics: 0.42 GtC yr^{-1}, South: 0.09 GtC yr^{-1}). Acknowledging that this distribution is based on only one model, the advantage is that a gridded field is available and the river flux adjustment can be calculated for the three latitudinal bands and the RECCAP regions (REgional Carbon Cycle Assessment and Processes (RECCAP2; Ciais et al., 2020, Poulter et al., 2022, DeVries et al., 2023). This data set suggests that more of the riverine outgassing is located in the tropics than in the Southern Ocean, and is thus opposed to the previously used data set of Aumont et al. (2001). Accordingly, the regional distribution is associated with a major uncertainty in addition to the large uncertainty around the global estimate (Crisp et al., 2022; Gruber et al., 2023). Anthropogenic perturbations of river carbon and nutrient transport to the ocean are not considered (see Section 2.10 and Supplement S.6.3).

We derive S_{OCEAN} from GOBMs by using a simulation (sim A) with historical forcing of climate and atmospheric CO_2, accounting for model biases and drift from a control simulation (sim B) with constant atmospheric CO_2 and normal year climate forcing. A third simulation (sim C) with historical atmospheric CO_2 increase and normal year climate forcing is used to attribute the ocean sink to CO_2 (sim C minus sim B) and climate (sim A minus sim C) effects. A fourth simulation (sim D; historical climate forcing and constant atmospheric CO_2) is used to compare the change in anthropogenic carbon inventory in the interior ocean (sim A minus sim D) to the observational estimate of Gruber et al. (2019) with the same flux components (steady state and non-steady state anthropogenic carbon flux). The fCO_2-products are adjusted with respect to their original publications to represent the full ice-free ocean area, including coastal zones and marginal seas, when the area coverage is below 99%. This is done by either area filling following Fay et al. (2021) or a simple scaling approach. GOBMs and fCO_2-products fall within the observational constraints over the 1990s (2.2 ± 0.7 GtC yr^{-1}, Ciais et al., 2013) after applying adjustments.

S_{OCEAN} is calculated as the average of the GOBM ensemble mean and the fCO_2-product ensemble mean from 1990 onwards. Prior to 1990, it is calculated as the GOBM ensemble mean plus half of the offset between GOBMs and fCO_2-products ensemble means over 1990-2001.

We assign an uncertainty of ± 0.4 GtC yr^{-1} to the ocean sink based on a combination of random (ensemble standard deviation) and systematic uncertainties (GOBMs bias in anthropogenic carbon accumulation,

previously reported uncertainties in fCO_2-products; see Supplement S.3.4). We assess a medium confidence level to the annual ocean CO_2 sink and its uncertainty because it is based on multiple lines of evidence, it is consistent with ocean interior carbon estimates (Gruber et al., 2019, see Section 3.6.5) and the interannual variability in the GOBMs and data-based estimates is largely consistent and can be explained by climate variability. We refrain from assigning a high confidence because of the systematic deviation between the GOBM and fCO_2-product trends since around 2002. More details on the S_{OCEAN} methodology can be found in Supplement S.3.

2.5.2 2023 Projection

The ocean CO_2 sink forecast for the year 2023 is based on the annual historical (Lan et al., 2023) and our estimated 2023 atmospheric CO_2 concentration growth rate, the historical and our estimated 2023 annual global fossil fuel emissions from this year's carbon budget, and the spring (March, April, May) Oceanic Niño Index (ONI) (NCEP, 2023). Using a non-linear regression approach, i.e., a feed-forward neural network, atmospheric CO_2, ONI, and the fossil fuel emissions are used as training data to best match the annual ocean CO_2 sink (i.e. combined S_{OCEAN} estimate from GOBMs and data products) from 1959 through 2022 from this year's carbon budget. Using this relationship, the 2023 S_{OCEAN} can then be estimated from the projected 2022 input data using the non-linear relationship established during the network training. To avoid overfitting, the neural network was trained with a variable number of hidden neurons (varying between 2-5) and 20% of the randomly selected training data were withheld for independent internal testing. Based on the best output performance (tested using the 20% withheld input data), the best performing number of neurons was selected. In a second step, we trained the network 10 times using the best number of neurons identified in step 1 and different sets of randomly selected training data. The mean of the 10 trainings is considered our best forecast, whereas the standard deviation of the 10 ensembles provides a first order estimate of the forecast uncertainty. This uncertainty is then combined with the S_{OCEAN} uncertainty (0.4 GtC yr^{-1}) to estimate the overall uncertainty of the 2023 projection. As an additional line of evidence, we also assess the 2023 atmosphere-ocean carbon flux from the ESM prediction system (see Section 2.9).

2.6 Land CO_2 sink

2.6.1 Historical Period 1850-2022

The terrestrial land sink (S_{LAND}) is thought to be due to the combined effects of fertilisation by rising atmospheric CO_2 and N inputs on plant growth, as well as the effects of climate change such as the lengthening of the growing season in northern temperate and boreal areas. S_{LAND} does not include land sinks directly resulting from land-use and land-use change (e.g., regrowth of vegetation) as these are part of the land-use flux (E_{LUC}), although system boundaries make it difficult to attribute exactly CO_2 fluxes on land between S_{LAND} and E_{LUC} (Erb et al., 2013).

S_{LAND} is estimated from the multi-model mean of 20 DGVMs (Table S1) with an additional comparison of DGVMs with a data-driven, carbon data model framework (CARDAMOM) (Bloom and Williams, 2015; Bloom

et al., 2016), see Supplement S4. DGVMs simulations include all climate variability and CO_2 effects over land. In addition to the carbon cycle represented in all DGVMs, 14 models also account for the nitrogen cycle and hence can include the effect of N inputs on S_{LAND}. The DGVMs estimate of S_{LAND} does not include the export of carbon to aquatic systems or its historical perturbation, which is discussed in Supplement S.6.3. DGVMs need to meet several criteria to be included in this assessment. In addition, we use the International Land Model Benchmarking system (ILAMB; Collier et al., 2018) for the DGVMs evaluation (see Supplement S.4.2). The uncertainty on S_{LAND} is taken from the GGVMs standard deviation (see Supplement S.4.3). More details on the S_{LAND} methodology can be found in Supplement S.4.

2.6.2 2023 Projection

Like for the ocean forecast, the land CO_2 sink (S_{LAND}) forecast is based on the annual historical (Lan et al., 2023) and our estimated 2023 atmospheric CO_2 concentration, historical and our estimated 2023 annual global fossil fuel emissions from this year's carbon budget, and the summer (June, July, August) ONI (NCEP, 2022). All training data are again used to best match S_{LAND} from 1959 through 2022 from this year's carbon budget using a feed-forward neural network. To avoid overfitting, the neural network was trained with a variable number of hidden neurons (varying between 2-15), larger than for S_{OCEAN} prediction due to the stronger land carbon interannual variability. As done for S_{OCEAN}, a pre-training selects the optimal number of hidden neurons based on 20% withheld input data, and in a second step, an ensemble of 10 forecasts is produced to provide the mean forecast plus uncertainty. This uncertainty is then combined with the S_{LAND} uncertainty for 2022 (0.9 GtC yr^{-1}) to estimate the overall uncertainty of the 2023 projection.

2.7 Atmospheric inversion estimate

The world-wide network of in-situ atmospheric measurements and satellite derived atmospheric CO_2 column (xCO_2) observations put a strong constraint on changes in the atmospheric abundance of CO_2. This is true globally (hence our large confidence in G_{ATM}), but also regionally in regions with sufficient observational density found mostly in the extra-tropics. This allows atmospheric inversion methods to constrain the magnitude and location of the combined total surface CO_2 fluxes from all sources, including fossil and land-use change emissions and land and ocean CO_2 fluxes. The inversions assume E_{FOS} to be well known, and they solve for the spatial and temporal distribution of land and ocean fluxes from the residual gradients of CO_2 between stations that are not explained by fossil fuel emissions. By design, such systems thus close the carbon balance ($B_{IM} = 0$) and thus provide an additional perspective on the independent estimates of the ocean and land fluxes.

This year's release includes fourteen inversion systems that are described in Table S4, of which thirteen are included in the ensemble of inverse estimates presented in the text and figures. Each system is rooted in Bayesian inversion principles but uses different methodologies. These differences concern the selection of atmospheric CO_2 data or xCO_2, and the choice of a-priori fluxes to refine. They also differ in spatial and temporal resolution, assumed correlation structures, and mathematical approach of the models (see references in Table S4 for details). Importantly, the systems use a variety of transport models, which was demonstrated to be a driving factor behind differences in atmospheric inversion-based flux estimates, and specifically their

distribution across latitudinal bands (Gaubert et al., 2019; Schuh et al., 2019). Six inversion systems (CAMS-FT23r1, CMS-flux, GONGGA, THU, COLA, GCASv2) used satellite xCO_2 retrievals from GOSAT and/or OCO-2, scaled to the WMO 2019 calibration scale. Two inversions this year (CMS-Flux, COLA) used these xCO2 datasets in addition to the in-situ observational CO_2 mole fraction records.

The original products delivered by the inverse modellers were modified to facilitate the comparison to the other elements of the budget, specifically on two accounts: (1) global total fossil fuel emissions including cement carbonation CO_2 uptake, and (2) riverine CO_2 transport. Details are given below. We note that with these adjustments the inverse results no longer represent the net atmosphere-surface exchange over land/ocean areas as sensed by atmospheric observations. Instead, for land, they become the net uptake of CO_2 by vegetation and soils that is not exported by fluvial systems, similar to the DGVMs estimates. For oceans, they become the net uptake of anthropogenic CO_2, similar to the GOBMs estimates.

The inversion systems prescribe global fossil fuel emissions based on e.g. the GCP's Gridded Fossil Emissions Dataset versions 2023.1 (GCP-GridFED; Jones et al., 2023), which are updates to GCP-GridFEDv2021 presented by Jones et al. (2021b). GCP-GridFEDv2023 scales gridded estimates of CO_2 emissions from EDGARv4.3.2 (Janssens-Maenhout et al., 2019) within national territories to match national emissions estimates provided by the GCB for the years 1959-2022, which were compiled following the methodology described in Section 2.1. Small differences between the systems due to for instance regridding to the transport model resolution, or use of different fossil fuel emissions, are adjusted in the latitudinal partitioning we present, to ensure agreement with the estimate of E_{FOS} in this budget. We also note that the ocean fluxes used as prior by 8 out of 14 inversions are part of the suite of the ocean process model or fCO_2-products listed in Section 2.5. Although these fluxes are further adjusted by the atmospheric inversions, it makes the inversion estimates of the ocean fluxes not completely independent of S_{OCEAN} assessed here.

To facilitate comparisons to the independent S_{OCEAN} and S_{LAND}, we used the same corrections for transport and outgassing of carbon transported from land to ocean, as done for the observation-based estimates of S_{OCEAN} (see Supplement S.3).

The atmospheric inversions are evaluated using vertical profiles of atmospheric CO_2 concentrations (Figure S4). More than 30 aircraft programs over the globe, either regular programs or repeated surveys over at least 9 months (except for SH programs), have been used to assess system performance (with space-time observational coverage sparse in the SH and tropics, and denser in NH mid-latitudes; Table S7). The fourteen systems are compared to the independent aircraft CO_2 measurements between 2 and 7 km above sea level between 2001 and 2022. Results are shown in Figure S4 and discussed in Supplement S.5.2. One inversion was flagged for concerns after quality control with these observations, as well as assessment of their global growth rate. This makes the number of systems included in the ensemble to be N=13.

With a relatively small ensemble of systems that cover at least one full decade (N=9), and which moreover share some a-priori fluxes used with one another, or with the process-based models, it is difficult to justify using their mean and standard deviation as a metric for uncertainty across the ensemble. We therefore report their full range

(min-max) without their mean. More details on the atmospheric inversions methodology can be found in Supplement S.5.

2.8 Atmospheric oxygen based estimate

Long-term atmospheric O_2 and CO_2 observations allow estimation of the global ocean and land carbon sinks, due to the coupling of O_2 and CO_2 with distinct exchange ratios for fossil fuel emissions and land uptake, and uncoupled O_2 and CO_2 ocean exchange (Keeling and Manning, 2014). The global ocean and net land carbon sinks were calculated following methods and constants used in Keeling and Manning (2014) but modified to also include the effective O_2 source from metal refining (Battle et al., 2023), and using a value of 1.05 for the exchange ratio of the net land sink, following Resplandy et al. (2019). Atmospheric O_2 is observed as $\delta(O_2/N_2)$ and combined with CO_2 mole fraction observations into Atmospheric Potential Oxygen (APO, Stephens et al., 1998). The APO observations from 1990 to 2022 were taken from a weighted average of flask records from the three stations in the Scripps O_2 program network (Alert, Canada (ALT), La Jolla, California (LJO), and Cape Grim, Australia (CGO), weighted per Keeling and Manning (2014). Observed CO_2 was taken from the globally averaged marine surface annual mean growth rate from the NOAA/GML Global Greenhouse Gas Reference Network (Lan et al., 2023). The O_2 source from ocean warming is based on ocean heat content from updated data from NOAA/NCEI (Levitus et al., 2012). The effective O_2 source from metal refining is based on production data from Bray (2020), Flanagan (2021), and Tuck (2022). Uncertainty was determined through a Monte Carlo approach with 5,000 iterations, using uncertainties prescribed in Keeling and Manning (2014), including observational uncertainties from Keeling et al. (2007) and autoregressive errors in fossil fuel emissions (Ballantyne et al., 2015). The reported uncertainty is 1 standard deviation of the ensemble.

2.9 Earth System Models estimate

Reconstructions and predictions from decadal prediction systems based on Earth system models (ESMs) provide a novel line of evidence in assessing the atmosphere-land and atmosphere-ocean carbon fluxes in the past decades and predicting their changes for the current year. The decadal prediction systems based on ESMs used here consist of three sets of simulations: (i) uninitialized freely evolving historical simulations (1850-2014); (ii) assimilation reconstruction incorporating observational data into the model (1980-2022); (iii) initialized prediction simulations for the 1981-2023 period, starting every year from initial states obtained from the above assimilation simulations. The assimilations are designed to reconstruct the actual evolution of the Earth system by assimilating essential fields from data products. The assimilations' states, which are expected to be close to observations, are used to start the initialized prediction simulations used for the current year (2023) global carbon budget. Similar initialized prediction simulations starting every year (Nov. 1st or Jan. 1st) over the 1981-2022 period (i.e., hindcasts) are also performed for predictive skill quantification and for bias correction. More details on the illustration of a decadal prediction system based on an ESM can refer to Figure 1 of Li et al. (2023).

By assimilating physical atmospheric and oceanic data products into the ESMs, the models are able to reproduce the historical variations of the atmosphere-sea CO_2 fluxes, atmosphere-land CO_2 fluxes, and atmospheric CO_2

growth rate (Li et al., 2016, 2019; Lovenduski et al., 2019a,b; Ilyina et al., 2021; Li et al., 2023). Furthermore, the ESM-based predictions have proven their skill in predicting the air-sea CO_2 fluxes for up to 6 years, the air-land CO_2 fluxes and atmospheric CO_2 growth for 2 years (Lovenduski et al., 2019a,b; Ilyina et al., 2021; Li et al., 2023). The reconstructions from the fully coupled model simulations ensure a closed budget within the Earth system, i.e., no budget imbalance term.

Four ESMs, i.e., CanESM5 (Swart et al., 2019; Sospedra-Alfonso et al., 2021), IPSL-CM6A-CO2-LR (Boucher et al., 2020), MIROC-ES2L (Watanabe et al., 2020), and MPI-ESM1-2-LR (Mauritsen et al., 2019; Li et al., 2023), have performed the set of prediction simulations. Each ESM uses a different assimilation method and combination of data products incorporated in the system, more details on the models configuration can be found in Table 4. The ESMs use external forcings from the Coupled Model Intercomparison Project Phase 6 (CMIP6) historical (1980-2014) plus SSP2-4.5 baseline and CovidMIP two year blip scenario (2015-2023) (Eyring et al., 2016; Jones et al., 2021a). The CO_2 emissions forcing from 2015-2023 are substituted by GCB-GridFED (v2023.1, Jones et al., 2023) to provide a more realistic forcing. Reconstructions of atmosphere-ocean CO_2 fluxes (S_{OCEAN}) and atmosphere-land CO_2 fluxes (S_{LAND}-E_{LUC}) for the time period from 1980-2022 are assessed here. Predictions of the atmosphere-ocean CO_2 flux, atmosphere-land CO_2 flux, and atmospheric CO_2 growth for 2023 are calculated based on the predictions at a lead time of 1 year. The predictions are bias-corrected using the 1985-2014 climatology mean of GCB2022 (Friedlingstein et al., 2022), more details on methods can be found in Boer et al. (2016) and Li et al. (2023). The ensemble size of initialized prediction simulations is 10, and the ensemble mean for each individual model is used here. The ESMs are used here to support the assessment of S_{OCEAN} and net atmosphere-land CO_2 flux (S_{LAND} - E_{LUC}) over the 1980-2022 period, and to provide an estimate of the 2023 projection of G_{ATM}.

2.10 Processes not included in the global carbon budget

The contribution of anthropogenic CO and CH_4 to the global carbon budget is not fully accounted for in Eq. (1) and is described in Supplement S.6.1. The contributions to CO_2 emissions of decomposition of carbonates not accounted for is described in Supplement S.6.2. The contribution of anthropogenic changes in river fluxes is conceptually included in Eq. (1) in S_{OCEAN} and in S_{LAND}, but it is not represented in the process models used to quantify these fluxes. This effect is discussed in Supplement S.6.3. Similarly, the loss of additional sink capacity from reduced forest cover is missing in the combination of approaches used here to estimate both land fluxes (E_{LUC} and S_{LAND}) and its potential effect is discussed and quantified in Supplement S.6.4.

3 Results

For each component of the global carbon budget, we present results for three different time periods: the full historical period, from 1850 to 2022, the decades in which we have atmospheric concentration records from Mauna Loa (1960-2022), a specific focus on last year (2022), and the projection for the current year (2023). Subsequently, we assess the estimates of the budget components of the last decades against the top-down constraints from inverse modelling of atmospheric observations, the land/ocean partitioning derived from the atmospheric O_2 measurements, and the budget components estimates from the ESMs assimilation simulations.

Atmospheric inversions further allow for an assessment of the budget components with a regional breakdown of land and ocean sinks.

3.1 Fossil CO_2 Emissions

3.1.1 Historical period 1850-2022

Cumulative fossil CO_2 emissions for 1850-2022 were 477 ± 25 GtC, including the cement carbonation sink (Figure 3, Table 8, with all cumulative numbers rounded to the nearest 5GtC). In this period, 46% of global fossil CO_2 emissions came from coal, 35% from oil, 15% from natural gas, 3% from decomposition of carbonates, and 1% from flaring. In 1850, the UK stood for 62% of global fossil CO_2 emissions. In 1891 the combined cumulative emissions of the current members of the European Union reached and subsequently surpassed the level of the UK. Since 1917 US cumulative emissions have been the largest. Over the entire period 1850-2022, US cumulative emissions amounted to 115GtC (24% of world total), the EU's to 80 GtC (17%), China's to 70 GtC (15%), and India's to 15 GtC (3%).

In addition to the estimates of fossil CO_2 emissions that we provide here (see Methods), there are three global datasets with long time series that include all sources of fossil CO_2 emissions: CDIAC-FF (Gilfillan and Marland, 2021), CEDS version v_2021_04_21 (Hoesly et al., 2018; O'Rourke et al., 2021) and PRIMAP-hist version 2.4.2 (Gütschow et al., 2016; Gütschow and Pflüger, 2023), although these datasets are not entirely independent from each other (Andrew, 2020a). CDIAC-FF has the lowest cumulative emissions over 1750-2018 at 440 GtC, GCP has 444 GtC, CEDS 445 GtC, PRIMAP-hist TP 453 GtC, and PRIMAP-hist CR 452 GtC. CDIAC-FF excludes emissions from lime production. CEDS has higher emissions from international shipping in recent years, while PRIMAP-hist has higher fugitive emissions than the other datasets. However, in general these four datasets are in relative agreement as to total historical global emissions of fossil CO_2.

3.1.2 Recent period 1960-2022

Global fossil CO_2 emissions, E_{FOS} (including the cement carbonation sink), have increased every decade from an average of 3.0 ± 0.2 GtC yr^{-1} for the decade of the 1960s to an average of 9.6 ± 0.5 GtC yr^{-1} during 2013-2022 (Table 7, Figure 2 and Figure 5). The growth rate in these emissions decreased between the 1960s and the 1990s, from 4.3% yr^{-1} in the 1960s (1960-1969), 3.2% yr^{-1} in the 1970s (1970-1979), 1.6% yr^{-1} in the 1980s (1980-1989), to 1.0% yr^{-1} in the 1990s (1990-1999). After this period, the growth rate began increasing again in the 2000s at an average growth rate of 2.8% yr^{-1}, decreasing to 0.5% yr^{-1} for the last decade (2013-2022). China's emissions increased by +1.6% yr^{-1} on average over the last 10 years dominating the global trend, and India's emissions increased by +3.5% yr^{-1}, while emissions decreased in EU27 by –1.7% yr^{-1}, and in the USA by –1.0% yr^{-1}. Figure 6 illustrates the spatial distribution of fossil fuel emissions for the 2013-2022 period.

E_{FOS} reported here includes the uptake of CO_2 by cement via carbonation which has increased with increasing stocks of cement products, from an average of 18 MtC yr^{-1} (0.018 GtC yr^{-1}) in the 1960s to an average of 197 MtC yr^{-1} (0.197 GtC yr^{-1}) during 2013-2022 (Figure 5).

3.1.3 Final year 2022

Global fossil CO_2 emissions were slightly higher, 0.9%, in 2022 than in 2021, with an increase of less than 0.1 GtC to reach 9.9 ± 0.5 GtC (including the 0.2 GtC cement carbonation sink) in 2022 (Figure 5), distributed among coal (41%), oil (32%), natural gas (21%), cement (4%), flaring (1%), and others (<1%). Compared to the previous year, 2022 emissions from coal and oil increased by 1.6% and 3.2% respectively, while emissions from gas and cement respectively decreased by 2.2% and 5.1%. All growth rates presented are adjusted for the leap year, unless stated otherwise.

In 2022, the largest absolute contributions to global fossil CO_2 emissions were from China (31%), the USA (14%), India (8%), and the EU27 (7%). These four regions account for 59% of global fossil CO_2 emissions, while the rest of the world contributed 41%, including international aviation and marine bunker fuels (2.6% of the total). Growth rates for these countries from 2021 to 2022 were 0.5% (China), 0.5% (USA), -1.6% (EU27), and 5.8% (India), with +0.9% for the rest of the world. The per-capita fossil CO_2 emissions in 2022 were 1.3 tC person^{-1} yr^{-1} for the globe, and were 4.1 (USA), 2.2 (China), 1.7 (EU27) and 0.5 (India) tC person^{-1} yr^{-1} for the four highest emitters (Figure 5).

3.1.4 Year 2023 Projection

Globally, we estimate that global fossil CO_2 emissions (including cement carbonation, -0.21 GtC) will grow by 1.1% in 2023 (0.0% to 2.1%) to 10.0 GtC (36.8 $GtCO_2$), exceeding the pre-COVID19 2019 emission levels of 9.9 GtC (36.3 $GtCO_2$). Global increase in 2023 emissions per fuel types are projected to be +1.1% (range -0.1% to 2.4%) for coal, +1.5% (range 0.6% to 2.3%) for oil, +0.5% (range -0.9% to 1.8%) for natural gas, and 0.8% (range -0.7% to 2.4%) for cement.

For China, projected fossil emissions in 2023 are expected to increase by 4% (range 1.9% to 6.1%) compared with 2022 emissions, bringing 2023 emissions for China around 3.2 GtC yr^{-1} (11.9 $GtCO_2$ yr^{-1}). Changes in fuel specific projections for China are 3.3% for coal, 9.9% for oil, 6.5% natural gas, and -0.9% for cement.

For the USA, the Energy Information Administration (EIA) emissions projection for 2023 combined with cement clinker data from USGS gives an decrease of 3.0% (range -5.0% to -1.0%) compared to 2022, bringing USA 2023 emissions to around 1.3 GtC yr^{-1} (4.9 $GtCO_2$ yr^{-1}). This is based on separate projections for coal -18.3%, oil -0.3%, natural gas +1.4%, and cement -4.0%.

For the European Union, our projection for 2023 is for a decrease of 7.4% (range -9.9% to -4.9%) over 2022, with 2023 emissions around 0.7 GtC yr^{-1} (2.6 $GtCO_2$ yr^{-1}). This is based on separate projections for coal of -18.8%, oil -1.5%, natural gas -6.6%, and cement -8.7%.

For India, our projection for 2023 is an increase of 8.2% (range of 6.7% to 9.7%) over 2022, with 2023 emissions around 0.8 GtC yr^{-1} (3.1 $GtCO_2$ yr^{-1}). This is based on separate projections for coal of +9.5%, oil +5.3%, natural gas +5.6%, and cement +8.8%.

International aviation and shipping (2.8% of global emissions) are projected to increase by 11.9% in 2023, with international aviation projected to be up 28% over 2022, continuing to recover from pandemic lows, and international shipping projected to rise by 1%.

For the rest of the world, the expected change for 2023 is a decrease of 0.4% (range -2.4% to 1.6%) with 2023 emissions around 3.8 GtC yr^{-1} (14.0 $GtCO_2$ yr^{-1}). The fuel-specific projected 2023 growth rates for the rest of the world are: +0.8% for coal, -2.0% for oil, 0.0% for natural gas, +2.4% for cement.

3.2 Emissions from Land Use Changes

3.2.1 Historical period 1850-2022

Cumulative CO_2 emissions from land-use changes (E_{LUC}) for 1850-2022 were 220 ± 65 GtC (Table 8; Figure 3; Figure 15). The cumulative emissions from E_{LUC} show a large spread among individual estimates of 150 GtC (H&C2023), 290 GtC (BLUE), and 215 GtC (OSCAR) for the three bookkeeping models and a similar wide estimate of 210 ± 65 GtC for the DGVMs (all cumulative numbers are rounded to the nearest 5 GtC). These estimates are broadly consistent with indirect constraints from vegetation biomass observations, giving cumulative emissions of 155 ± 50 GtC over the 1901-2012 period (Li et al., 2017). However, given the large spread, a best estimate is difficult to ascertain.

3.2.2 Recent period 1960-2022

In contrast to growing fossil emissions, CO_2 emissions from land-use, land-use change, and forestry remained relatively constant over the 1960-1999 period. Since then, they have shown a slight decrease of about 0.1 GtC per decade, reaching 1.3 ± 0.7 GtC yr^{-1} for the 2013-2022 period (Table 7), but with large spread across estimates (Table 5, Figure 7). Different from the bookkeeping average, the DGVMs average grows slightly larger over the 1970-2022 period and shows no sign of decreasing emissions in the recent decades (Table 5, Figure 7). This is, however, expected as DGVM-based estimates include the loss of additional sink capacity, which grows with time, while the bookkeeping estimates do not (Supplement S.6.4).

We separate net E_{LUC} into five component fluxes to gain further insight into the drivers of net emissions: deforestation, forest (re-)growth, wood harvest and other forest management, peat drainage and peat fires, and all other transitions (Figure 7c; Sec. C.2.1). We further decompose the deforestation and the forest (re-)growth term into contributions from shifting cultivation vs permanent forest cover changes (Figure 7d). Averaged over the 2013-2022 period and over the three bookkeeping estimates, fluxes from deforestation amount to 1.9 [1.5 to 2.4] GtC yr^{-1} (Table 5), of which 1.1 [1.0, 1.2] GtC yr^{-1} are from permanent deforestation. Fluxes from forest (re-)growth amount to -1.3 [-1.5, -0.9] GtC yr^{-1} (Table 5), of which -0.5 [-0.8 to-0.2] GtC yr^{-1} are from re/afforestation and the remainder from forest regrowth in shifting cultivation cycles. Emissions from wood harvest and other forest management (0.2 [0.0, 0.6] GtC yr^{-1}), peat drainage and peat fires (0.3 [0.3, 0.3] GtC yr^{-1}) and the net flux from other transitions (0.1 [0.0, 0.3] GtC yr^{-1}) are substantially less important globally (Table 5). However, the small net flux from wood harvest and other forest management contains substantial gross

fluxes that largely compensate each other (see Figure S7): 1.3 [0.9, 2.0] GtC yr^{-1} emissions result from the decomposition of slash and the decay of wood products and -1.1 [-1.3, -0.8] GtC yr^{-1} removals result from regrowth after wood harvesting. This split into component fluxes clarifies the potentials for emission reduction and carbon dioxide removal: the emissions from permanent deforestation - the largest of our component fluxes - could be halted (largely) without compromising carbon uptake by forests, contributing substantially to emissions reduction. By contrast, reducing wood harvesting would have limited potential to reduce emissions as it would be associated with less forest regrowth; removals and emissions cannot be decoupled here on long timescales. A similar conclusion applies to removals and emissions from shifting cultivation, which we have therefore separated out. Carbon Dioxide Removal (CDR) in forests could instead be increased by permanently increasing the forest cover through re/afforestation. Our estimate of about -0.5 [-0.8, -0.2] GtC yr^{-1} (of which about two thirds are located in non-Annex-I countries, in particular in China) removed on average each year during 2013-2022 by re/afforestation is very similar to independent estimates that were derived from NGHGIs for 2022. Re/afforestation constitutes the vast majority of all current CDR (Powis et al., 2023). Though they cannot be compared directly to annual fluxes from the atmosphere, CDR through transfers between non-atmospheric reservoirs such as in durable HWPs, biochar or BECCS comprise much smaller amounts of carbon. 61 MtC yr^{-1} have been estimated to be transferred to HWPs in 2022, and BECCS projects have been estimated to store 0.5 MtC yr^{-1} in geological projects worldwide (Powis et al., 2023). “Blue carbon”, i.e. coastal wetland management such as restoration of mangrove forests, saltmarshes and seagrass meadows, though at the interface of land and ocean carbon fluxes, are counted towards the land-use sector as well. Currently, bookkeeping models do not include blue carbon; however, current CDR deployment in coastal wetlands is small globally, less than 0.003MtC yr^{-1} (Powis et al., 2023).

The small declining trend of E_{LUC} over the last three decades is a result of total deforestation emissions showing no clear trend, while forest regrowth has provided steadily increasing removals. Since the processes behind gross removals, foremost forest regrowth and soil recovery, are all slow, while gross emissions include a large instantaneous component, short-term changes in land-use dynamics, such as a temporary decrease in deforestation, influences gross emissions dynamics more than gross removals dynamics, which rather are a response to longer-term dynamics. Component fluxes often differ more across the three bookkeeping estimates than the net flux, which is expected due to different process representation; in particular, treatment of shifting cultivation, which increases both gross emissions and removals, differs across models, but also net and gross wood harvest fluxes show high uncertainty. By contrast, models agree relatively well for emissions from permanent deforestation emissions and removals by re/afforestation.

Overall, highest land-use emissions occur in the tropical regions of all three continents. The top three emitters (both cumulatively 1959-2022 and on average over 2013-2022) are Brazil (in particular the Amazon Arc of Deforestation), Indonesia and the Democratic Republic of the Congo, with these 3 countries contributing 0.7 GtC yr^{-1} or 55% of the global net land-use emissions (average over 2013-2022) (Figure 6b). This is related to massive expansion of cropland, particularly in the last few decades in Latin America, Southeast Asia, and sub-Saharan Africa (Hong et al., 2021), to a substantial part for export of agricultural products (Pendrill et al., 2019). Emission intensity is high in many tropical countries, particularly of Southeast Asia, due to high rates of land

conversion in regions of carbon-dense and often still pristine, undegraded natural forests (Hong et al., 2021). Emissions are further increased by peat fires in equatorial Asia (GFED4s, van der Werf et al., 2017). Uptake due to land-use change occurs, particularly in Europe, partly related to expanding forest area as a consequence of the forest transition in the 19th and 20th century and subsequent regrowth of forest (Figure 6b) (Mather 2001; McGrath et al., 2015).

While the mentioned patterns are robust and supported by independent literature, we acknowledge that model spread is substantially larger on regional than global levels, as has been shown for bookkeeping models (Bastos et al., 2021) as well as DGVMs (Obermeier et al., 2021). Assessments for individual regions will be performed as part of REgional Carbon Cycle Assessment and Processes (RECCAP2; Ciais et al., 2020, Poulter et al., 2022) or already exist for selected regions (e.g., for Europe by Petrescu et al., 2020, for Brazil by Rosan et al., 2021, for 8 selected countries/regions in comparison to inventory data by Schwingshackl et al., 2022).

As mentioned before, the NGHGI data under the LULUCF sector or data submitted by countries to FAOSTAT differ from the global models' definition of E_{LUC}. In the NGHGI reporting, the natural fluxes (S_{LAND}) are counted towards E_{LUC} when they occur on managed land (Grassi et al., 2018). To compare our results to the NGHGI approach, we perform a translation of our E_{LUC} estimates by subtracting S_{LAND} in managed forest from the DGVMs simulations (following the methodology described in Grassi et al., 2023) from the bookkeeping E_{LUC} estimate (see Supplement S.2.3). For the 2013-2022 period, we estimate that 2.0 GtC yr^{-1} of S_{LAND} occurred in managed forests. Subtracting this value from E_{LUC} changes E_{LUC} from being a source of 1.3 GtC yr^{-1} to a sink of 0.8 GtC yr^{-1}, very similar to the NGHGI estimate that yields a sink of 0.7 GtC yr^{-1} (Table 9). The translation approach has been shown to be generally applicable also on country-level (Grassi et al., 2023; Schwingshackl et al., 2022). Country-level analysis suggests, e.g., that the bookkeeping method estimates higher deforestation emissions than the national report in Indonesia, but less CO_2 removal by afforestation than the national report in China. The fraction of the natural CO_2 sinks that the NGHGI estimates include differs substantially across countries, related to varying proportions of managed vs total forest areas (Schwingshackl et al., 2022). By comparing E_{LUC} and NGHGI on the basis of the component fluxes used above, we find that our estimates reproduce very closely the NGHGI estimates for emissions from permanent deforestation (1.1 GtC yr^{-1} averaged over 2013-2022). Forest fluxes, that is, (re-)growth from re/afforestation plus the net flux from wood harvesting and other forest management, constitute a large sink in the NGHGI (-1.9 GtC yr^{-1} averaged over 2013-2022), since they also include S_{LAND} in managed forests. Summing up the bookkeeping estimates of (re-)growth from re/afforestation and the net flux from wood harvesting and other forest management and adding S_{LAND} in managed forests yields a flux of -2.3 GtC yr^{-1} (averaged over 2013-2022), which compares well with the NGHGI estimate. Emissions from organic soils in NGHGI are similar to the estimates based on the bookkeeping approach and the external peat drainage and burning datasets. The net flux from other transitions is small in both NGHGI and bookkeeping estimates, but a difference in sign (small source in bookkeeping estimates, small sink in NGHGI) creates a notable difference between NGHGI and bookkeeping estimates. Though estimates between NGHGI, FAOSTAT and the translated budget estimates still differ in value and need further analysis, the approach suggested by Grassi et al. (2023), which we adopt here, provides a feasible way to

relate the global models' and NGHGI approach to each other and thus link the anthropogenic carbon budget estimates of land CO_2 fluxes directly to the Global Stocktake, as part of UNFCCC Paris Agreement.

3.2.3 Final year 2022

The global CO_2 emissions from land-use change are estimated as 1.2 ± 0.7 GtC in 2022, similar to the 2020 and 2021 estimates. However, confidence in the annual change remains low. Effects of the COVID-19 pandemic on land-use change have turned out to be country-specific as global market mechanisms, national economics and changes in household income all could act to curb or enhance deforestation (Wunder et al., 2021). Concerns about enhanced deforestation due to weakened environmental protection and monitoring in tropical countries (Brancalion et al., 2020, Vale et al., 2021) have been confirmed only for some countries (Cespedes et al., 2023). For example, a recent study suggests slightly increased deforestation rates for the Democratic Republic of Congo linked in particular to post-pandemic economic recovery in the mining sector, while deforestation trends in Brazil seem to have been unaffected. Land use dynamics may be further altered by the Russian invasion of Ukraine, but scientific evidence related to international dependencies (like a shift to tropical palm oil to alleviate dependencies on sunflower oil) so far is very limited and recent changes will not be reflected by the land-use forcing applied in the global models. High food prices, which preceded but were exacerbated by the war (FAO, 2022), are generally linked to higher deforestation (Angelsen and Kaimowitz, 1999). A new wave of cropland abandonment in the conflict region may increase the substantial Eastern European carbon sink due to land-use changes, but sanctions being placed on trade may also incentivise domestic agricultural production, thus leading to recultivation of abandoned areas in Russia (Winkler et al., 2023).

3.2.4 Year 2023 Projection

In Indonesia, peat fire emissions are below average (12 Tg C through September 29 2023) despite El Niño conditions, which in general lead to more fires. Tropical deforestation and degradation fires in Indonesia are around average (13 Tg C through September 29 2023), but higher than in the previous year, which had a relatively wet dry season (GFED4.1s, van der Werf et al., 2017; see also https://www.geo.vu.nl/~gwerf/GFED/GFED4/tables/GFED4.1s_C.txt). In South America, emissions from tropical deforestation and degradation fires are among the lowest over the last decades (64 Tg C through September 29 2023). Effects of the El Niño in the Amazon, such as droughts, are not expected before 2024. Disentangling the degree to which interannual variability in rainfall patterns and stronger environmental protection measures in both Indonesia after their 2015 high fire season and in Brazil after the change in government in Brazil play a role in this is an important research topic. Cumulative fire emission estimates through September 29 2023 are 155 Tg C for global deforestation and degradation fires and 12 Tg C for peatland fires in Indonesia (https://www.geo.vu.nl/~gwerf/GFED/GFED4/tables/GFED4.1s_C.txt).

Based on these estimates, we expect E_{LUC} emissions of around 1.1 GtC (4.1 $GtCO_2$) in 2023. Our preliminary estimate of E_{LUC} for 2023 is substantially lower than the 2013-2022 average, which saw years of anomalously dry conditions in Indonesia and high deforestation fires in South America (Friedlingstein et al., 2022b). Note that although our extrapolation includes tropical deforestation and degradation fires, degradation attributable to

selective logging, edge-effects or fragmentation is not captured. Further, deforestation and fires in deforestation zones may become more disconnected, partly due to changes in legislation in some regions. For example, Van Wees et al. (2021) found that the contribution from fires to forest loss decreased in the Amazon and in Indonesia over the period of 2003-2018.

3.3 CDR not based on vegetation

Besides the CDR through land-use (Sec. 3.2), the atmosphere to geosphere flux of carbon resulting from carbon dioxide removal (CDR) activity is currently 0.003 MtC/yr, with 0.002 MtC/yr of DACCS and 0.001 MtC/yr of enhanced weathering projects. This is more than a million times smaller than current fossil CO_2 emissions.

3.4 Total anthropogenic emissions

Cumulative anthropogenic CO_2 emissions for 1850-2022 totalled 695 ± 70 GtC (2550 ± 260 $GtCO_2$), of which 70% (485 GtC) occurred since 1960 and 33% (235 GtC) since 2000 (Table 7 and 8). Total anthropogenic emissions more than doubled over the last 60 years, from 4.6 ± 0.7 GtC yr^{-1} for the decade of the 1960s to an average of 10.9 ± 0.8 GtC yr^{-1} during 2013-2022, and reaching 11.1 ± 0.9 GtC (40.7 ± 3.3 $GtCO_2$) in 2022. For 2023, we project global total anthropogenic CO_2 emissions from fossil and land use changes to be also around 11.2 GtC (40.9 $GtCO_2$). All values here include the cement carbonation sink (currently about 0.2 GtC yr^{-1}).

During the historical period 1850-2022, 31% of historical emissions were from land use change and 69% from fossil emissions. However, fossil emissions have grown significantly since 1960 while land use changes have not, and consequently the contributions of land use change to total anthropogenic emissions were smaller during recent periods (18% during the period 1960-2022 and down to 12% over the 2013-2022 period).

3.5 Atmospheric CO_2

3.5.1 Historical period 1850-2022

Atmospheric CO_2 concentration was approximately 278 parts per million (ppm) in 1750, reaching 300 ppm in the 1910s, 350 ppm in the late 1980s, and reaching 417.07 ± 0.1 ppm in 2022 (Lan et al., 2023; Figure 1). The mass of carbon in the atmosphere increased by 48% from 590 GtC in 1750 to 886 GtC in 2022. Current CO_2 concentrations in the atmosphere are unprecedented in the last 2 million years and the current rate of atmospheric CO_2 increase is at least 10 times faster than at any other time during the last 800,000 years (Canadell et al., 2021).

3.5.2 Recent period 1960-2022

The growth rate in atmospheric CO_2 level increased from 1.7 ± 0.07 GtC yr^{-1} in the 1960s to 5.2 ± 0.02 GtC yr^{-1} during 2013-2022 with important decadal variations (Table 7, Figure 3 and Figure 4). During the last decade (2013-2022), the growth rate in atmospheric CO_2 concentration continued to increase, albeit with large interannual variability (Figure 4).

The airborne fraction (AF), defined as the ratio of atmospheric CO_2 growth rate to total anthropogenic emissions:

$$AF = G_{ATM} / (E_{FOS} + E_{LUC}) \quad (2)$$

provides a diagnostic of the relative strength of the land and ocean carbon sinks in removing part of the anthropogenic CO_2 perturbation. The evolution of AF over the last 60 years shows no significant trend, remaining at around 44%, albeit showing a large interannual and decadal variability driven by the year-to-year variability in G_{ATM} (Figure 9). The observed stability of the airborne fraction over the 1960-2020 period indicates that the ocean and land CO_2 sinks have been removing on average about 56% of the anthropogenic emissions (see Sections 3.6.2 and 3.7.2).

3.5.3 Final year 2022

The growth rate in atmospheric CO_2 concentration was 4.6 ± 0.2 GtC (2.18 ± 0.08 ppm) in 2022 (Figure 4; Lan et al., 2023), below the 2021 growth rate (5.2 ± 0.2 GtC) or the 2013-2022 average (5.2 ± 0.02 GtC).

3.5.4 Year 2023 Projection

The 2023 growth in atmospheric CO_2 concentration (G_{ATM}) is projected to be about 5.1 GtC (2.4 ppm). This is the average of the GCB regression method (5.07 GtC, 2.39 ppm) and ESMs the multi-model mean (5.11 GtC, 2.41 ppm). The 2023 atmospheric CO_2 concentration, averaged over the year, is expected to reach the level of 419.3 ppm, 51% over the pre-industrial level.

3.6 Ocean Sink

3.6.1 Historical period 1850-2022

Cumulated since 1850, the ocean sink adds up to 180 ± 35 GtC, with more than two thirds of this amount (125 GtC) being taken up by the global ocean since 1960. Over the historical period, the ocean sink increased in pace with the anthropogenic emissions exponential increase (Figure 3). Since 1850, the ocean has removed 26% of total anthropogenic emissions.

3.6.2 Recent period 1960-2022

The ocean CO_2 sink increased from 1.1 ± 0.4 GtC yr^{-1} in the 1960s to 2.8 ± 0.4 GtC yr^{-1} during 2013-2022 (Table 7), with interannual variations of the order of a few tenths of GtC yr^{-1} (Figure 10). The ocean-borne fraction ($S_{OCEAN}/(E_{FOS}+E_{LUC})$) has been remarkably constant around 25% on average (Figure 9c), with variations around this mean illustrating the decadal variability of the ocean carbon sink. So far, there is no indication of a decrease in the ocean-borne fraction from 1960 to 2022. The increase of the ocean sink is primarily driven by the increased atmospheric CO_2 concentration, with the strongest CO_2 induced signal in the North Atlantic and the Southern Ocean (Figure 11a). The effect of climate change is much weaker, reducing the ocean sink globally

by 0.16 ± 0.04 GtC yr^{-1} (-6.7% of S_{OCEAN}) during 2013-2022 (all models simulate a weakening of the ocean sink by climate change, range -4.3 to -10.3%), and does not show clear spatial patterns across the GOBMs ensemble (Figure 11b). This is the combined effect of change and variability in all atmospheric forcing fields, previously attributed, in one model, to wind and temperature changes (LeQuéré et al., 2010).

The global net air-sea CO_2 flux is a residual of large natural and anthropogenic CO_2 fluxes into and out of the ocean with distinct regional and seasonal variations (Figure 6 and B1). Natural fluxes dominate on regional scales, but largely cancel out when integrated globally (Gruber et al., 2009). Mid-latitudes in all basins and the high-latitude North Atlantic dominate the ocean CO_2 uptake where low temperatures and high wind speeds facilitate CO_2 uptake at the surface (Takahashi et al., 2009). In these regions, formation of mode, intermediate and deep-water masses transport anthropogenic carbon into the ocean interior, thus allowing for continued CO_2 uptake at the surface. Outgassing of natural CO_2 occurs mostly in the tropics, especially in the equatorial upwelling region, and to a lesser extent in the North Pacific and polar Southern Ocean, mirroring a well-established understanding of regional patterns of air-sea CO_2 exchange (e.g., Takahashi et al., 2009, Gruber et al., 2009). These patterns are also noticeable in the Surface Ocean CO2 Atlas (SOCAT) dataset, where an ocean fCO_2 value above the atmospheric level indicates outgassing (Figure S1). This map further illustrates the data-sparsity in the Indian Ocean and the southern hemisphere in general.

Interannual variability of the ocean carbon sink is driven by climate variability with a first-order effect from a stronger ocean sink during large El Niño events (e.g., 1997-1998) (Figure 10; Rödenbeck et al., 2014, Hauck et al., 2020; McKinley et al. 2017). The GOBMs show the same patterns of decadal variability as the mean of the fCO_2-products, with a stagnation of the ocean sink in the 1990s and a strengthening since the early 2000s (Figure 10; Le Quéré et al., 2007; Landschützer et al., 2015, 2016; DeVries et al., 2017; Hauck et al., 2020; McKinley et al., 2020, Gruber et al., 2023). Different explanations have been proposed for this decadal variability, ranging from the ocean's response to changes in atmospheric wind and pressure systems (e.g., Le Quéré et al., 2007, Keppler and Landschützer, 2019), including variations in upper ocean overturning circulation (DeVries et al., 2017) to the eruption of Mount Pinatubo and its effects on sea surface temperature and slowed atmospheric CO_2 growth rate in the 1990s (McKinley et al., 2020). The main origin of the decadal variability is a matter of debate with a number of studies initially pointing to the Southern Ocean (see review in Canadell et al., 2021), but also contributions from the North Atlantic and North Pacific (Landschützer et al., 2016, DeVries et al., 2019), or a global signal (McKinley et al., 2020) were proposed.

Although all individual GOBMs and fCO_2-products fall within the observational constraint, the ensemble means of GOBMs, and fCO_2-products adjusted for the riverine flux diverge over time with a mean offset increasing from 0.30 GtC yr^{-1} in the 1990s to 0.57 GtC yr^{-1} in the decade 2013-2022 and reaching 0.61 GtC yr^{-1} in 2022. The S_{OCEAN} positive trend over time diverges by a factor two since 2002 (GOBMs: 0.24 ± 0.07 GtC yr^{-1} per decade, fCO_2-products: 0.48 ± 0.11 GtC yr^{-1} per decade, S_{OCEAN}: 0.36 GtC yr^{-1} per decade) and by a factor of 2.5 since 2010 (GOBMs: 0.16 ± 0.15 GtC yr^{-1} per decade, fCO_2-products: 0.42 ± 0.18 GtC yr^{-1} per decade, S_{OCEAN}: 0.29 GtC yr^{-1} per decade). The fCO_2-product estimate is slightly different compared to Friedlingstein et al.

(2022b) as a result of an updated submission of the NIES-ML3 product (previously NIES-NN), however the difference in the integrated mean flux is small.

The discrepancy between the two types of estimates stems from a larger S_{OCEAN} trend in the northern and southern extra-tropics since around 2002 (Figure 13). Note that the discrepancy in the mean flux, which was located in the Southern Ocean in previous versions of the GCB, has been reduced due to the choice of the regional river flux adjustment (Lacroix et al., 2020 instead of Aumont et al., 2001). This comes at the expense of a new discrepancy in the mean S_{OCEAN} of about 0.2 GtC yr^{-1} in the tropics. Likely explanations for the discrepancy in the trends in the high-latitudes are data sparsity and uneven data distribution (Bushinsky et al., 2019, Gloege et al., 2021, Hauck et al., 2023). In particular, two fCO_2-products that are part of the GCB ensemble were shown to overestimate the Southern Ocean CO_2 flux trend by 50 and 130% based on current sampling in a model subsampling experiment (Hauck et al., 2023). Another likely contributor to the discrepancy between GOBMs and fCO_2-products are model biases (as indicated by the large model spread in the South, Figure 13, and the larger model-data fCO_2 mismatch, Figure S2).

In previous GCB releases, the ocean sink 1959-1989 was only estimated by GOBMs due to the absence of fCO_2 observations. Now, the first data-based estimates extending back to 1957/58 are becoming available (Jena-MLS, Rödenbeck et al., 2022, LDEO-HPD, Bennington et al., 2022; Gloege et al., 2022). These are based on a multi-linear regression of pCO_2 with environmental predictors (Rödenbeck et al., 2022) or on model-data pCO_2 misfits and their relation to environmental predictors (Bennington et al., 2022). The Jena-MLS and LDEO-HPD estimates fall well within the range of GOBM estimates and have a correlation of 0.99 and 0.98 respectively with S_{OCEAN} for the period 1959-2022 (and 0.98 and 0.97 for the 1959-1989 period). They agree well on the mean S_{OCEAN} estimate since 1977 with a slightly higher amplitude of variability (Figure 10). Until 1976, Jena-MLS and LDEO-HPD are respectively about 0.25 $GtCyr^{-1}$ and about 0.1 $GtCyr^{-1}$ below the central S_{OCEAN} estimate. The agreement especially on phasing of variability is impressive in both products, and the discrepancies in the mean flux 1959-1976 could be explained by an overestimated trend of Jena-MLS (Rödenbeck et al., 2022). Bennington et al. (2022) report a larger flux into the pre-1990 ocean than in Jena-MLS, although lower than S_{OCEAN}.

The reported S_{OCEAN} estimate from GOBMs and fCO_2-products is 2.2 ± 0.4 GtC yr^{-1} over the period 1994 to 2007, which is in excellent agreement with the ocean interior estimate of 2.2 ± 0.4 GtC yr^{-1}, which accounts for the climate effect on the natural CO_2 flux of -0.4 ± 0.24 GtC yr^{-1} (Gruber et al., 2019) to match the definition of S_{OCEAN} used here (Hauck et al., 2020). This comparison depends critically on the estimate of the climate effect on the natural CO_2 flux, which is smaller from the GOBMs (-0.1 GtC yr^{-1}) than in Gruber et al. (2019). Uncertainties of these two estimates would also overlap when using the GOBM estimate of the climate effect on the natural CO_2 flux.

During 2010-2016, the ocean CO_2 sink appears to have intensified in line with the expected increase from atmospheric CO_2 (McKinley et al., 2020). This effect is slightly stronger in the fCO_2-products (Figure 10, ocean sink 2016 minus 2010, GOBMs: +0.42 ± 0.10 GtC yr^{-1}, fCO_2-products: +0.48 ± 0.10 GtC yr^{-1}). The reduction of

-0.14 GtC yr^{-1} (range: -0.39 to +0.01 GtC yr^{-1}) in the ocean CO_2 sink in 2017 is consistent with the return to normal conditions after the El Niño in 2015/16, which caused an enhanced sink in previous years. After an increasing S_{OCEAN} in 2018 and 2019, 2017, the GOBM and fCO_2-product ensemble means suggest a decrease of S_{OCEAN}, related to the triple La Niña event 2020-2023.

3.6.3 Final year 2022

The estimated ocean CO_2 sink is 2.8 ± 0.4 GtC for 2022. This is a small decrease of 0.05 GtC compared to 2021, in line with the expected sink weakening from persistent La Niña conditions. GOBM and fCO_2-product estimates consistently result in a near-stagnation of S_{OCEAN} (GOBMs: -0.01 ±0.05 GtC, fCO_2-products: -0.09 ±0.10 GtC). Four models and six fCO_2-products show a decrease in S_{OCEAN} (GOBMs down to -0.09 GtC, fCO_2-products down to -0.25 GtC), while one model shows no change and five models and two fCO_2-products show an increase in S_{OCEAN} (GOBMs up to 0.07 GtC, fCO_2-products up to 0.15 GtC; Figure 10). The fCO_2-products have a larger uncertainty at the end of the reconstructed time series (tail effect, e.g., Watson et al., 2020). Specifically, the fCO_2-products' estimate of the last year is regularly adjusted in the following release owing to the tail effect and an incrementally increasing data availability. While the monthly grid cells covered may have a lag of only about a year (Figure 10 inset), the values within grid cells may change with 1-5 years lag (see absolute number of observations plotted in previous GCB releases).

3.6.4 Year 2023 Projection

Using a feed-forward neural network method (see Section 2.5.2) we project an ocean sink of 2.9 GtC for 2023. This is slightly higher than for the year 2022 (2.8 GtC) and could mark a reversal of the slight decrease of S_{OCEAN} sink since 2019, due to the transition from persisting La Niña conditions to emerging El Niño conditions in 2023. The new set of ESMs predictions support this estimate with a 2023 ocean sink of around 3.1 [2.9, 3.2] GtC.

3.6.5 Ocean Models Evaluation

The process-based model evaluation draws a generally positive picture with GOBMs scattered around the observational values for Southern Ocean sea-surface salinity, Southern Ocean stratification index and surface ocean Revelle factor (Section C3.3 and Table S10). However, the Atlantic Meridional Overturning Circulation at 26°N is underestimated by 8 out of 10 GOBMs. It is planned to derive skill scores for the GOBMs in future releases based on these metrics.

The model simulations allow to separate the anthropogenic carbon component (steady state and non-steady state, sim D - sim A) and to compare the model flux and DIC inventory change directly to the interior ocean estimate of Gruber et al. (2019) without further assumptions (Table S10). The GOBMs ensemble average of anthropogenic carbon inventory changes 1994-2007 amounts to 2.4 GtC yr^{-1} and is thus lower than the 2.6 ± 0.3 GtC yr^{-1} estimated by Gruber et al. (2019) although within the uncertainty. Only four models with the highest sink estimate fall within the range reported by Gruber et al. (2019). This suggests that the majority of the

GOBMs underestimate anthropogenic carbon uptake by 10-20%. Analysis of Earth System Models indicate that an underestimation by about 10% may be due to biases in ocean carbon transport and mixing from the surface mixed layer to the ocean interior (Goris et al., 2018, Terhaar et al., 2021, Bourgeois et al., 2022, Terhaar et al., 2022), biases in the chemical buffer capacity (Revelle factor) of the ocean (Vaittinada Ayar et al., 2022; Terhaar et al., 2022) and partly due to a late starting date of the simulations (mirrored in atmospheric CO_2 chosen for the preindustrial control simulation, Table S2, Bronselaer et al., 2017, Terhaar et al., 2022). Interestingly, and in contrast to the uncertainties in the surface CO_2 flux, we find the largest mismatch in interior ocean carbon accumulation in the tropics (96% of the mismatch), with minor contributions from the north (3%) and the south (<1%). These numbers deviate slightly from GCB2021 because of submission of the ACCESS model with a high anthropogenic carbon accumulation, particularly in the Southern Ocean. The large discrepancy in accumulation in the tropics highlights the role of interior ocean carbon redistribution for those inventories (Khatiwala et al., 2009, DeVries et al., 2023).

The evaluation of the ocean estimates with the fCO_2 observations from the SOCAT v2023 dataset for the period 1990-2022 shows an RMSE from annually detrended data of 0.4 to 2.4 µatm for the seven fCO_2-products over the globe (Figure S2). The GOBMs RMSEs are larger and range from 2.9 to 5.4 µatm. The RMSEs are generally larger at high latitudes compared to the tropics, for both the fCO_2-products and the GOBMs. The fCO_2-products have RMSEs of 0.3 to 2.8 µatm in the tropics, 0.7 to 2.3 µatm in the north, and 0.7 to 2.8 µatm in the south. Note that the fCO_2-products are based on the SOCAT v2023 database, hence the SOCAT is not an independent dataset for the evaluation of the fCO_2-products. The GOBMs RMSEs are more spread across regions, ranging from 2.5 to 5.0 µatm in the tropics, 3.0 to 7.2 µatm in the North, and 3.7 to 8.5 µatm in the South. The higher RMSEs occur in regions with stronger climate variability, such as the northern and southern high latitudes (poleward of the subtropical gyres). The upper range of the model RMSEs have increased somewhat relative to Friedlingstein et al. (2022b).

3.7 Land Sink

3.7.1 Historical period 1850-2022

Cumulated since 1850, the terrestrial CO_2 sink amounts to 225 ± 55 GtC, 32% of total anthropogenic emissions. Over the historical period, the sink increased in pace with the anthropogenic emissions exponential increase (Figure 3).

3.7.2 Recent period 1960-2022

The terrestrial CO_2 sink S_{LAND} increased from 1.3 ± 0.5 GtC yr^{-1} in the 1960s to 3.3 ± 0.8 GtC yr^{-1} during 2013-2022, with important interannual variations of up to 2 GtC yr^{-1} generally showing a decreased land sink during El Niño events (Figure 8), responsible for the corresponding enhanced growth rate in atmospheric CO_2 concentration. The larger land CO_2 sink during 2013-2022 compared to the 1960s is reproduced by all the DGVMs in response to the increase in both atmospheric CO_2, nitrogen deposition, and the changes in climate, and is consistent with constraints from the other budget terms (Table 5).

Over the period 1960 to present the increase in the global terrestrial CO_2 sink is largely attributed to the CO_2 fertilisation effect (Prentice et al., 2001, Piao et al., 2009, Schimel et al., 2015) and increased nitrogen deposition (Huntzinger et al., 2017, O'Sullivan et al., 2019), directly stimulating plant photosynthesis and increased plant water use in water limited systems, with a small negative contribution of climate change (Figure 11). There is a range of evidence to support a positive terrestrial carbon sink in response to increasing atmospheric CO_2, albeit with uncertain magnitude (Walker et al., 2021). As expected from theory, the greatest CO_2 effect is simulated in the tropical forest regions, associated with warm temperatures and long growing seasons (Hickler et al., 2008) (Figure 11a). However, evidence from tropical intact forest plots indicate an overall decline in the land sink across Amazonia (1985-2011), attributed to enhanced mortality offsetting productivity gains (Brienen et al., 2015, Hubau et al., 2020). During 2013-2022 the land sink is positive in all regions (Figure 6) with the exception of eastern Brazil, Bolivia, Paraguay, northern Venezuela, Southwest USA, central Europe and Central Asia, North and South Africa, and eastern Australia, where the negative effects of climate variability and change (i.e. reduced rainfall and/or increased temperature) counterbalance CO_2 effects. This is clearly visible on Figure 11 where the effects of CO_2 (Figure 11a) and climate (Figure 11b) as simulated by the DGVMs are isolated. The negative effect of climate is the strongest in most of South America, Central America, Southwest US, Central Europe, western Sahel, southern Africa, Southeast Asia and southern China, and eastern Australia (Figure 11b). Globally, over the 2013-2022 period, climate change reduces the land sink by 0.68 ± 0.62 GtC yr^{-1} (20% of S_{LAND}).

Most DGVMs have similar S_{LAND} averaged over 2013-2022, and 14/20 models fall within the 1σ range of the residual land sink [2.0-3.8 GtC yr^{-1}] (see Table 5), and all but one model are within the 2σ range [1.1-4.7 GtC yr^{-1}]. The ED model is an outlier, with a land sink estimate of 5.7 GtC yr^{-1}, driven by a strong CO_2 fertilisation effect (6.6 GtC yr^{-1} in the CO_2 only (S1) simulation), that is offset by correspondingly high land-use emissions. There are no direct global observations of the land sink, or the CO_2 fertilisation effect, and so we are not yet in a position to rule out models based on component fluxes if the net land sink (S_{LAND}-E_{LUC}) is within the observational uncertainty provided by atmospheric O_2 measurements (Table 5). Overall, therefore the spread among models for the estimate of S_{LAND} over the last decade has increased this year (0.8 GtC yr^{-1}) compared to GCB2022 (0.6 GtC yr^{-1}).

Furthermore, DGVMs were compared against a data-constrained intermediate complexity model of the land carbon cycle (CARDAMOM) (Bloom and Williams, 2015; Bloom et al., 2016). Results suggest good correspondence between approaches at the interannual timescales, but divergence in the recent trend with CARDAMOM simulating a stronger trend than the DGVMs (Figure S8).

Since 2020 the globe has experienced La Niña conditions which would be expected to lead to an increased land carbon sink. A clear peak in the global land sink is not evident in S_{LAND}, and we find that a La Niña- driven increase in tropical land sink is offset by a reduced high latitude extra-tropical land sink, which may be linked to the land response to recent climate extremes. A notable difference from GCB2022 (2012-2021 S_{LAND} mean) is the reduced carbon losses across tropical drylands. Further, central Europe has switched from a sink of carbon to a source, with the summer heatwave of 2022 (and associated drought and wildfire) causing widespread losses

(Peters et al., 2023). In the past years several regions experienced record-setting fire events. While global burned area has declined over the past decades mostly due to declining fire activity in savannas (Andela et al., 2017), forest fire emissions are rising and have the potential to counter the negative fire trend in savannas (Zheng et al., 2021). Noteworthy events include the 2019-2020 Black Summer event in Australia (emissions of roughly 0.2 GtC; van der Velde et al., 2021) and Siberia in 2021 where emissions approached 0.4 GtC or three times the 1997-2020 average according to GFED4s. While other regions, including Western US and Mediterranean Europe, also experienced intense fire seasons in 2021 their emissions are substantially lower.

Despite these regional negative effects of climate change on S_{LAND}, the efficiency of land to remove anthropogenic CO_2 emissions has remained broadly constant over the last six decades, with a land-borne fraction ($S_{LAND}/(E_{FOS}+E_{LUC})$) of around 30% (Figure 9b).

3.7.3 Final year 2022

The terrestrial CO_2 sink from the DGVMs ensemble was 3.8 ± 0.8 GtC in 2022, above the decadal average of 3.3 ± 0.8 GtC yr^{-1} (Figure 4, Table 7), and slightly above the 2021 sink of 3.5 ± 1.0 GtC, likely driven by the persistent La Niña conditions. We note that the DGVMs estimate for 2022 is similar to the 3.7 ± 1.0 GtC yr^{-1} estimate from the residual sink from the global budget ($E_{FOS}+E_{LUC}-G_{ATM}-S_{OCEAN}$) (Table 5).

3.7.4 Year 2023 Projection

Using a feed-forward neural network method we project a land sink of 2.9 GtC for 2023, 0.9 GtC smaller than the 2022 estimate. As for the ocean sink, we attribute this to the emerging El Niño conditions in 2023, leading to a reduced land sink. The ESMs do not provide an additional estimate of S_{LAND} as they only simulate the net atmosphere-land carbon flux ($S_{LAND}-E_{LUC}$).

3.7.5 Land Models Evaluation

The evaluation of the DGVMs shows generally high skill scores across models for runoff, and to a lesser extent for vegetation biomass, GPP, and ecosystem respiration. These conclusions are supported by a more comprehensive analysis of DGVM performance in comparison with benchmark data (Seiler et al., 2022). A relative comparison of DGVM performance (Figure S3) suggests several DGVMs (CABLE-POP, CLASSIC, OCN, ORCHIDEE) may outperform others at multiple carbon and water cycle benchmarks. However, results from Seiler et al., 2022, also show how DGVM differences are often of similar magnitude compared with the range across observational datasets. All models score high enough over the metrics tests to support their use here. There are a few anomalously low scores for individual metrics from a single model, and these can direct the effort to improve models for use in future budgets.

3.8 Partitioning the carbon sinks

3.8.1 Global sinks and spread of estimates

In the period 2013-2022, the bottom-up view of global net ocean and land carbon sinks provided by the GCB, S_{OCEAN} for the ocean and $S_{LAND} - E_{LUC}$ for the land, agrees closely with the top-down global carbon sinks delivered by the atmospheric inversions. This is shown in Figure 12, which visualises the individual decadal mean atmosphere-land and atmosphere-ocean fluxes from each, along with the constraints on their sum offered by the global fossil CO_2 emissions flux minus the atmospheric growth rate ($E_{FOS} - G_{ATM}$, 4.5 ± 0.5 Gt C yr^{-1}, Table 7, shown as diagonal line on Figure 12). The GCB estimate for net atmosphere-to-surface flux ($S_{OCEAN} + S_{LAND} - E_{LUC}$) during 2013-2022 is 4.9 ± 1.2 Gt C yr^{-1} (Table 7), with the difference to the diagonal representing the budget imbalance (B_{IM}) of 0.4 GtC yr^{-1} discussed in Section 3.9. By virtue of the inversion methodology, the imbalance of the top-down estimates is < 0.1 GtC yr^{-1} and thus scatter across the diagonal, inverse models trading land for ocean fluxes in their solution. The independent constraint on the net atmosphere-to-surface flux based on atmospheric O_2 is 4.5 ± 1.0 GtC yr^{-1} over the 2013-2022 period (orange symbol on Figure 12), while the ESMs estimate for the net atmosphere-to-surface flux over that period is 5.0 [4.2, 5.5] Gt C yr^{-1}, consistent with the GCB estimate (Tables 5 and 6).

The distributions based on the individual models and data products reveal substantial spread but converge near the decadal means quoted in Tables 5 to 7. Sink estimates for S_{OCEAN} and from inverse systems are mostly non-Gaussian, while the ensemble of DGVMs appears more normally distributed justifying the use of a multi-model mean and standard deviation for their errors in the budget. Noteworthy is that the tails of the distributions provided by the land and ocean bottom-up estimates would not agree with the global constraint provided by the fossil fuel emissions and the observed atmospheric CO_2 growth rate. This illustrates the power of the atmospheric joint constraint from G_{ATM} and the global CO_2 observation network it derives from.

3.8.1.1 Net atmosphere-to-land fluxes

The GCB net atmosphere-to-land fluxes ($S_{LAND} - E_{LUC}$), calculated as the difference between S_{LAND} from the DGVMs and E_{LUC} from the bookkeeping models, amounts to a 2.1 ± 1.1 GtC yr^{-1} sink during 2013-2022 (Table 5). Estimates of net atmosphere-to-land fluxes ($S_{LAND} - E_{LUC}$) from the DGVMs alone (1.7 ± 0.6 GtC yr^{-1}, Table 5, green symbol on Figure 12) are slightly lower, within the uncertainty of the GCB estimate and also with the global carbon budget constraint from the ocean sink ($E_{FOS} - G_{ATM} - S_{OCEAN}$, 1.6 ± 0.6 GtC yr^{-1}; Table 7). For the last decade (2013-2022), the inversions estimate the net atmosphere-to-land uptake to be 1.6 [0.5, 2.3] GtC yr^{-1}, similar to the DGVMs estimates (purple symbol on Figure 12). The ESMs estimate for the net atmosphere-to-land uptake during 2013-2022 is 2.4 [1.8, 3.3] GtC yr^{-1}, consistent with the GCB and DGVMs estimates of $S_{LAND} - E_{LUC}$ (Figure 13 top row). The independent constraint based on atmospheric O_2 is significantly lower, 1.2 ± 0.8 GtC yr^{-1}, although its relatively high uncertainty range overlaps with the central estimates from other approaches.

3.8.1.2 Net atmosphere-to-ocean fluxes

For the 2013-2022 period, the GOBMs (2.6 ± 0.4 GtC yr^{-1}) produce a lower estimate for the ocean sink than the fCO_2-products (3.1 [2.6, 3.3] GtC yr^{-1}), which shows up in Figure 12 as separate peaks in the distribution from the GOBMs (dark blue symbols) and from the fCO_2-products (light blue symbols). Atmospheric inversions (3.0 [2.4, 4.1] GtC yr^{-1}) suggest an ocean uptake more in line with the fCO_2-products for the recent decade (Table 7) , although the inversions range includes both the GOBMs and fCO_2-products estimates (Figure 13 top row). The ESMs 2.6 [2.2, 3.4] GtC yr^{-1} suggest a moderate estimate for the ocean carbon sink, comparable to the GOBMs estimate with regard to mean and spread. Conversely, the independent constraint based on atmospheric O_2 suggests a larger ocean sink (3.5 ± 0.6 GtC yr^{-1}), more consistent with the fCO_2-products and atmospheric inversions. We caution that the riverine transport of carbon taken up on land and outgassing from the ocean is a substantial (0.65 ± 0.3 GtC yr^{-1}) and uncertain term (Crisp et al., 2022; Gruber et al., 2023; DeVries et al., 2023) that separates the GOBMs, ESMs and oxygen-based estimates on the one hand from the fCO_2-products and atmospheric inversions on the other hand. However, the high ocean sink estimate based on atmospheric oxygen that is not subject to river flux adjustment, provides another line of evidence that most GOBMs and ESMs underestimate the ocean sink.

3.8.2 Regional partitioning

Figure 13 shows the latitudinal partitioning of the global atmosphere-to-ocean (S_{OCEAN}), atmosphere-to-land ($S_{LAND} - E_{LUC}$), and their sum ($S_{OCEAN} + S_{LAND} - E_{LUC}$) according to the estimates from GOBMs and ocean fCO_2-products (S_{OCEAN}), DGVMs ($S_{LAND} - E_{LUC}$), and from atmospheric inversions (S_{OCEAN} and $S_{LAND} - E_{LUC}$).

3.8.2.1 North

Despite being one of the most densely observed and studied regions of our globe, annual mean carbon sink estimates in the northern extra-tropics (north of 30°N) continue to differ. The atmospheric inversions suggest an atmosphere-to-surface sink (S_{OCEAN}+ $S_{LAND} - E_{LUC}$) for 2013-2022 of 2.8[1.7 to 3.3] GtC yr^{-1}, which is higher than the process models' estimate of 2.2 ± 0.4 GtC yr^{-1} (Figure 13). The GOBMs (1.2 ± 0.2 GtC yr^{-1}), fCO_2-products (1.3[1.2-1.4] GtC yr^{-1}), and inversion systems (1.2[0.7 to 1.4] GtC yr^{-1}) produce consistent estimates of the ocean sink. Thus, the difference mainly arises from the net land flux ($S_{LAND} - E_{LUC}$) estimate, which is 1.0 ± 0.4 GtC yr^{-1} in the DGVMs compared to 1.6[0.4 to 2.6] GtC yr^{-1} in the atmospheric inversions (Figure 13, second row). We note that the range among inversions driven by OCO-2 satellite data is smaller though (1.6 - 2.2 GtC yr^{-1} N=6), supporting the notion that northern extra-tropics land uptake was larger than suggested by the DGVMs at least in the 2015-2022 period covered by this data product.

Discrepancies in the northern land fluxes conforms with persistent issues surrounding the quantification of the drivers of the global net land CO_2 flux (Arneth et al., 2017; Huntzinger et al., 2017; O'Sullivan et al., 2022) and the distribution of atmosphere-to-land fluxes between the tropics and high northern latitudes (Baccini et al., 2017; Schimel et al., 2015; Stephens et al., 2007; Ciais et al., 2019; Gaubert et al., 2019).

In the northern extra-tropics, the process models, inversions, and fCO_2-products consistently suggest that most of the variability stems from the land (Figure 13). Inversions generally estimate similar interannual variations (IAV) over land to DGVMs (0.28-0.35 vs 0.8-0.64 GtC yr^{-1}, averaged over 1990-2022), and they have higher IAV in ocean fluxes (0.05-0.10 GtC yr^{-1}) relative to GOBMs (0.02-0.06 GtC yr^{-1}, Figure S2), and fCO_2-products (0.03-0.10 GtC yr^{-1}).

3.8.2.2 Tropics

In the tropics (30°S-30°N), both the atmospheric inversions and process models estimate a net carbon balance ($S_{OCEAN} + S_{LAND} - E_{LUC}$) that is close to neutral over the past decade. The GOBMs (-0.03 ± 0.24 GtC yr^{-1}), fCO_2-products (0.2 [0.2, 0.3] GtC yr^{-1}), and inversion systems (-0.3 [-0.1, 0.8] GtC yr^{-1}) all indicate an approximately neutral tropical ocean flux (see Figure S1 for spatial patterns). DGVMs indicate a net land sink ($S_{LAND} - E_{LUC}$) of 0.6 ±0.4 GtC yr^{-1}, whereas the inversion systems indicate a net land flux of 0.03 [-0.8, 1.1] GtC yr^{-1}, though with high uncertainty (Figure 13, third row).

The tropical lands are the origin of most of the atmospheric CO_2 interannual variability (Ahlström et al., 2015), consistently among the process models and inversions (Figure 13). The interannual variability in the tropics is similar among the ocean fCO_2-products (0.07-0.16 GtC yr−1) and the GOBMs (0.07-0.16 GtC yr^{-1}, Figure S2), which is the highest ocean sink variability of all regions. The DGVMs and inversions indicate that atmosphere-to-land CO_2 fluxes are more variable than atmosphere-to-ocean CO_2 fluxes in the tropics, with interannual variability of 0.35 to 1.61 and 0.77-0.92 GtC yr^{-1} for DGVMs and inversions, respectively.

3.8.2.3 South

In the southern extra-tropics (south of 30°S), the atmospheric inversions suggest a net atmosphere-to-surface sink ($S_{OCEAN}+S_{LAND}-E_{LUC}$) for 2013-2022 of 1.5 [1.2, 1.9] GtC yr^{-1}, slightly higher than the process models' estimate of 1.5 ± 0.4 GtC yr^{-1} (Figure 13). An approximately neutral net land flux ($S_{LAND}-E_{LUC}$) for the southern extra-tropics is estimated by both the DGVMs (0.05 ± 0.07 GtC yr^{-1}) and the inversion systems (sink of 0.02 [-0.2, 0.2] GtC yr^{-1}). This means nearly all carbon uptake is due to oceanic sinks south of 30°S. The Southern Ocean flux in the fCO_2-products (1.6[1.3, 1.7 GtC] yr^{-1}) and inversion estimates (1.5 [1.3, 1.9] GtCyr-1) is slightly higher than in the GOBMs (1.4 ± 0.3 GtC yr^{-1}) (Figure 13, bottom row). This discrepancy in the mean flux is smaller this year than in previous releases due to the change in data set of the regional distribution of the river flux adjustment applied to fCO_2-products and inverse systems to isolate the anthropogenic S_{OCEAN} flux. The data set used (Lacroix et al., 2020) has less river-induced carbon outgassing in the Southern Ocean than the previously used data set (Aumont et al., 2001). Nevertheless, the time-series of atmospheric inversions and fCO_2-products diverge from the GOBMs. A substantial overestimation of the trends in the fCO_2-products could be explained by sparse and unevenly distributed observations, especially in wintertime (Figure S1; Hauck et al., 2023; Gloege et al., 2021). Model biases may contribute as well, with biases in mode water formation, stratification, and the chemical buffer capacity known to play a role in Earth System Models (Terhaar et al., 2021, Bourgeois et al., 2022, Terhaar et al., 2022).

The interannual variability in the southern extra-tropics is low because of the dominance of ocean areas with low variability compared to land areas. The split between land (S_{LAND}-E_{LUC}) and ocean (S_{OCEAN}) shows a substantial contribution to variability in the south coming from the land, with no consistency between the DGVMs and the inversions or among inversions. This is expected due to the difficulty of separating exactly the land and oceanic fluxes when viewed from atmospheric observations alone. The S_{OCEAN} interannual variability was found to be higher in the *f*CO_2-products (0.04-0.18 GtC yr^{-1}) compared to GOBMs (0.03 to 0.06 GtC yr^{-1}) in 1990-2022 (Figure S2). Model subsampling experiments recently illustrated that *f*CO_2-products may overestimate decadal variability in the Southern Ocean carbon sink by 30% and the trend since 2000 by 50-130% due to data sparsity, based on one and two *f*CO_2-products with strong variability (Gloege et al., 2021, Hauck et al., 2023).

3.8.2.4 RECCAP2 regions

Aligning with the RECCAP-2 initiative (Ciais et al., 2022; Poulter et al., 2022; DeVries et al., 2023), we provide a breakdown of this GCB paper estimate of the E_{LUC}, S_{LAND}, Net land (S_{LAND} - E_{LUC}), and S_{OCEAN} fluxes over the 10 land, and 5 ocean RECCAP-2 regions, averaged over the period 2013-2022. The DGVMs and inversions suggest a positive net land sink in all regions, except for South America and Africa, where the inversions indicate a small net source of respectively -0.1 [-0.5, 0.3] GtC yr^{-1} and -0.3 [-0.6, -0.1] GtC yr^{-1}, compared to a small sink of 0.1±0.3 GtC yr^{-1} and 0.3±0.2 GtC yr^{-1} for the DGVMs. However, for South America, there is substantial uncertainty in both products (ensembles span zero). For the DGVMs, this is driven by uncertainty in both S_{LAND} (0.6±0.5 GtC yr^{-1}) and E_{LUC} (0.4±0.2 GtC yr^{-1}). The bookkeeping models also suggest an E_{LUC} source of around 0.4 GtC yr^{-1} in South America and Africa, in line with the DGVMs estimates. Bookkeeping models and DGVMs similarly estimate a source of 0.4 GtC yr^{-1} in Southeast Asia, with DGVMs suggesting a near neutral net land sink (0.03±0.12 GtC yr^{-1}). This contrasts with the inversion estimate of a 0.2 [-0.3,0.6] GtC yr^{-1} sink, although the inversions spread is substantial. The inversions suggest the largest net land sinks are located in North America (0.5 [-0.1,0.8] GtC yr^{-1}), Russia (0.7 [0.5,1.1] GtC yr^{-1}), and East Asia (0.3 [0.0,0.9] GtC yr^{-1}). This agrees well with the DGVMs in North America (0.4±0.2 GtC yr^{-1}), which indicate a large natural land sink (S_{LAND}) of 0.6±0.2 GtC yr^{-1}, being slightly reduced by land-use related carbon losses (0.2±0.1 GtC yr^{-1}). The DGVMs suggest a smaller net land sink in Russia compared to inversions (0.4±0.2 GtC yr^{-1}), and a similar net sink in East Asia (0.2±0.1 GtC yr^{-1}).

There is generally a higher level of agreement in the estimates of regional S_{OCEAN} between the different data streams (GOBMs, *f*CO_2-products and atmospheric inversions) on decadal scale, compared to the agreement between the different land flux estimates. All data streams agree that the largest contribution to S_{OCEAN} stems from the Southern Ocean due to a combination of high flux density and large surface area, but with important contributions also from the Atlantic (high flux density) and Pacific (large area) basins. In the Southern Ocean, GOBMs suggest a sink of 1.0±0.3 GtC yr^{-1}, in line with the *f*CO_2-products (1.1 [0.9,1.2] GtC yr^{-1}) and atmospheric inversions (1.0 [0.8,1.4] GtC yr^{-1}). There is similar agreement in the Pacific ocean, with GOBMs,

fCO_2-products, and atmospheric inversions indicating a sink of 0.5±0.1 GtC yr^{-1}, 0.7 [0.5,0.9] GtC yr^{-1}, and 0.6 [0.2,1.0] GtC yr^{-1}, respectively. However, in the Atlantic ocean, GOBMs simulate a sink of 0.5±0.1 GtC yr^{-1}, noticeably lower than both the *f*CO_2-products (0.8 [0.7,0.9] GtC yr^{-1}) and atmospheric inversions (0.8 [0.5,1.2] GtC yr^{-1}). It is important to note the *f*CO_2-products and atmospheric inversions have a substantial and uncertain river flux adjustment in the Atlantic ocean (0.3 GtC yr^{-1}) that also leads to a mean offset between GOBMs and *f*CO_2-products/inversions in the latitude band of the tropics (Figure 13). The Indian Ocean due its smaller size and the Arctic Ocean due to its size and sea-ice cover that prevents air-sea gas-exchange are responsible for smaller but non negligible S_{OCEAN} fluxes (Indian Ocean: (0.3 [0.2,0.4] GtC yr^{-1}, 0.3 [0.3,0.4] GtC yr^{-1}, and 0.4 [0.3,0.6] GtC yr^{-1} for GOBMs, *f*CO_2-products, and atmospheric inversions, respectively, and Arctic Ocean: (0.1 [0.1,0.1] GtC yr^{-1}, 0.2 [0.2,0.2] GtC yr^{-1}, and 0.1 [0.1,0.1] GtC yr^{-1} for GOBMs, *f*CO_2-products, and atmospheric inversions, respectively). Note that the S_{OCEAN} numbers presented here deviate from numbers reported in RECCAP-2 where the net air-sea CO_2 flux is reported (i.e. without river flux adjustment for *f*CO_2-products and inversions, and with river flux adjustment subtracted from GOBMs in most chapters, or comparing unadjusted data sets with discussion of uncertain regional riverine fluxes as major uncertainty, e.g. Sarma et al., 2023, DeVries et al., 2023).

3.8.2.5 Tropical vs northern land uptake

A continuing conundrum is the partitioning of the global atmosphere-land flux between the northern hemisphere land and the tropical land (Stephens et al., 2017; Pan et al., 2011; Gaubert et al., 2019). It is of importance because each region has its own history of land-use change, climate drivers, and impact of increasing atmospheric CO_2 and nitrogen deposition. Quantifying the magnitude of each sink is a prerequisite to understanding how each individual driver impacts the tropical and mid/high-latitude carbon balance.

We define the North-South (N-S) difference as net atmosphere-land flux north of 30°N minus the net atmosphere-land flux south of 30°N. For the inversions, the N-S difference ranges from -0.5 GtC yr^{-1} to +3.0 GtC yr^{-1} across this year's inversion ensemble, but with a clear cluster of solutions driven by the OCO-2 satellite product with a NH land sink of 1.6-2.2 GtC yr^{-1} , along with a tropical land flux of -0.6 to +0.2 GtC yr^{-1}, and a dipole between +1.4 and +2.8 GtC yr^{-1} for the period 2015-2022. Whether this tighter clustering relative to the surface-observation based inversions is driven by (a) additional information on tropical fluxes delivered by tropical retrievals contained in OCO-2, (b) a tighter constraint on the NH land sink from that same product, or (c) a reduced sensitivity to vertical transport differences between models when using CO_2 column integrals, requires further investigation.

In the ensemble of DGVMs the N-S difference is 0.5 ± 0.6 GtC yr^{-1}, a much narrower range than the one from atmospheric inversions. Five DGVMs have a N-S difference larger than 1.0 GtC yr^{-1}, compared to only two from last year's ensemble. This is still only 25% of DGVMs, compared to most inversion systems simulating a difference at least this large. The smaller spread across DGVMs than across inversions is to be expected as there is no correlation between Northern and Tropical land sinks in the DGVMs as opposed to the inversions where

the sum of the two regions being well-constrained by atmospheric observations leads to an anti-correlation between these two regions. This atmospheric N-S gradient could be used as an additional way to evaluate tropical and NH uptake in DGVMs, if their fluxes were combined with multiple transport models. Vice versa, the much smaller spread in the N-S difference between the DGVMs could help to scrutinise the inverse systems further. For example, a large northern land sink and a tropical land source in an inversion would suggest a large sensitivity to CO_2 fertilisation (the dominant factor driving the land sinks) for Northern ecosystems, which would be not mirrored by tropical ecosystems. Such a combination could be hard to reconcile with the process understanding gained from the DGVM ensembles and independent measurements (e.g. Free Air CO_2 Enrichment experiments).

3.8.3 Fire Emissions in 2023

Fire emissions so far in 2023 have been above the average of recent decades, due to an extreme wildfire season in North America. Figure S9 shows global and regional emissions estimates for the period 1st Jan-30th September in each year 2003-2023. Estimates derive from two global fire emissions products: the global fire emissions database (GFED, version 4.1s; van der Werf et al., 2017), and; the global fire assimilation system (GFAS, operated by the Copernicus Atmosphere Service; Di Giuseppe et al., 2018). The two products estimate that global emissions from fires were 1.9-2.3 GtC yr^{-1} during January-October 2023. These estimates are 19-33% above the 2013-2022 average for the same months (1.6-1.7 GtC yr^{-1}) and 10-28% above the 2003-2022 average (1.8 GtC yr^{-1} in both products).

The above-average global fire emissions during January-October 2023 have occurred despite below-average fire emissions from major source regions. On average during 2013-2022, 75-80% of global fire emissions through October occur in the tropics (1.2-1.4 GtC yr^{-1}) and around 41-48% of global fire emissions through October occur in Africa (0.7-0.8 GtC yr^{-1}). This year, through October, fire emissions in the tropics were approximately equal to the 2013-2022 average and 7-9% below the 2003-2022 average, while in Africa the fire emissions were approximately equal to the 2013-2022 average and 4-13% below the 2003-2022 average.

In contrast, fire emissions from the Northern extra-tropics so far in 2023 have exceeded the values of all previous years. Northern extra-tropical fire emissions during January-October 2023 (0.7-0.9 GtC yr^{-1}) were 84-183% above the average for the same months in 2013-2022 (0.3-0.4 GtC yr^{-1}) and 76-190% above the average for the same months in 2003-2022 (0.3-0.4 GtC yr^{-1}). Fire emissions in North America alone (0.5-0.8 GtC yr^{-1}) were 239-438% above the average of 2013-2022 (0.2 GtC yr^{-1} for both products) and 215-410% above the average for 2003-2022 (0.2 GtC yr^{-1} for both products). Extreme fires in Canada were the largest contributor to the anomaly in 2023, with emissions reaching 0.5-0.8 GtC yr^{-1} or 527-874% above the 2013-2022 average (0.1 Gt C yr^{-1} in both products) and 450-709% above the 2003-2022 average (0.1 Gt C yr^{-1} in both products).

While the fire emission fluxes presented above point towards a highly unusual Northern Hemisphere fire season so far in 2023, we caution that the fluxes presented should not be compared directly with other fluxes of the budget (e.g. S_{LAND} or E_{LUC}) due to incompatibilities between the observable fire emission fluxes and what is quantified in the S_{LAND} and E_{LUC} components of the budget. The fire emission estimates from global fire

products relate to all fire types that can be observed in Earth Observations (Giglio et al., 2018; Randerson et al., 2012; Kaiser et al., 2012), including (i) fires occurring as part of natural disturbance-recovery cycles that would also have occurred in the pre-industrial period (Yue et al., 2016; Keeley and Pausas, 2019; Zou et al., 2019), (ii) fires occurring above and beyond natural disturbance-recovery cycle due to changes in climate, CO_2 and N fertilisation and to an increased frequency of extreme drought and heatwave events (Abatzoglou et al., 2019; Jones et al., 2022; Zheng et al., 2021; Burton et al., 2023), and (iii) fires occurring in relation to land use and land use change, such as deforestation fires and agricultural fires (van der Werf et al., 2010; Magi et al., 2012). In the context of the global carbon budget, only the portion of fire emissions associated with (ii) should be included in the S_{LAND} component, and fire emissions associated with (iii) should already be accounted for in the E_{LUC} component. Emissions associated with (i) should not be included in the global carbon budget. It is not currently possible to derive specific estimates for fluxes (i), (ii), and (iii) using global fire emission products such as GFED or GFAS. In addition, the fire emissions estimates from global fire emissions products represent a gross flux of carbon to the atmosphere, whereas the S_{LAND} component of the budget is a net flux that should also include post-fire recovery fluxes. Even if emissions from fires of type (ii) could be separated from those of type (i), these fluxes may be partially or wholly offset in subsequent years by post-fire fluxes as vegetation recovers, sequestering carbon from the atmosphere to the terrestrial biosphere (Yue et al., 2016).

3.9 Closing the Global Carbon Cycle

3.9.1 Partitioning of Cumulative Emissions and Sink Fluxes

The global carbon budget over the historical period (1850-2021) is shown in Figure 3.

Emissions during the period 1850-2022 amounted to 695 ± 70 GtC and were partitioned among the atmosphere (280 ± 5 GtC; 40%), ocean (180 ± 35 GtC; 26%), and land (225 ± 55 GtC; 32%). The cumulative land sink is almost equal to the cumulative land-use emissions (220 ± 70 GtC), making the global land nearly neutral over the whole 1850-2022 period.

The use of nearly independent estimates for the individual terms of the global carbon budget shows a cumulative budget imbalance of 15 GtC (2% of total emissions) during 1850-2022 (Figure 3, Table 8), which, if correct, suggests that emissions could be slightly too high by the same proportion (2%) or that the combined land and ocean sinks are slightly underestimated (by about 3%), although these are well within the uncertainty range of each component of the budget. Nevertheless, part of the imbalance could originate from the estimation of significant increase in E_{FOS} and E_{LUC} between the mid 1920s and the mid 1960s which is unmatched by a similar growth in atmospheric CO_2 concentration as recorded in ice cores (Figure 3). However, the known loss of additional sink capacity of 30-40 GtC (over the 1850-2020 period) due to reduced forest cover has not been accounted for in our method and would exacerbate the budget imbalance (see Section 2.10 and Supplement S.6.4).

For the more recent 1960-2022 period where direct atmospheric CO_2 measurements are available, total emissions (E_{FOS} + E_{LUC}) amounted to 485 ± 50 GtC, of which 395 ± 20 GtC (82%) were caused by fossil CO_2

emissions, and 90 ± 45 GtC (18%) by land-use change (Table 8). The total emissions were partitioned among the atmosphere (215 ± 5 GtC; 44%), ocean (125 ± 25 GtC; 25%), and the land (150 ± 35 GtC; 31%), with a near zero (-5 GtC) unattributed budget imbalance. All components except land-use change emissions have significantly grown since 1960, with important interannual variability in the growth rate in atmospheric CO_2 concentration and in the land CO_2 sink (Figure 4), and some decadal variability in all terms (Table 7). Differences with previous budget releases are documented in Figure S5.

The global carbon budget averaged over the last decade (2013-2022) is shown in Figure 2, Figure 14 (right panel) and Table 7. For this period, 88% of the total emissions ($E_{FOS} + E_{LUC}$) were from fossil CO_2 emissions (E_{FOS}), and 12% from land-use change (E_{LUC}). The total emissions were partitioned among the atmosphere (47%), ocean (26%) and land (31%), with a small unattributed budget imbalance (~4%). For single years, the budget imbalance can be larger (Figure 4). For 2022, the combination of our estimated sources (11.1 ± 0.9 GtC yr^{-1}) and sinks (11.2 ± 0.9 GtC yr^{-1}) leads to a B_{IM} of -0.09 GtC, suggesting a near closure of the global carbon budget, although there is relatively high uncertainty on B_{IM} (±1.3 GtC for 2022) as this is calculated as the residual of the five budget terms.

3.9.2 Trend and Variability in the Carbon Budget Imbalance

The carbon budget imbalance (B_{IM}; Eq. 1, Figure 4) quantifies the mismatch between the estimated total emissions and the estimated changes in the atmosphere, land, and ocean reservoirs. The budget imbalance from 1960 to 2022 is very small (-3.0 GtC over the period, i.e. average of 0.05 GtC yr^{-1}) and shows no trend over the full time series (Figure 4e). The process models (GOBMs and DGVMs) and data-products have been selected to match observational constraints in the 1990s, but no further constraints have been applied to their representation of trend and variability. Therefore, the near-zero mean and trend in the budget imbalance is seen as evidence of a coherent community understanding of the emissions and their partitioning on those time scales (Figure 4). However, the budget imbalance shows substantial variability of the order of ±1 GtC yr^{-1}, particularly over semi-decadal time scales, although most of the variability is within the uncertainty of the estimates. The positive carbon imbalance during the 1960s, and early 1990s, indicates that either the emissions were overestimated, or the sinks were underestimated during these periods. The reverse is true for the 1970s, and to a lesser extent for the 1980s and 2013-2022 period (Figure 4, Table 7).

We cannot attribute the cause of the variability in the budget imbalance with our analysis, we only note that the budget imbalance is unlikely to be explained by errors or biases in the emissions alone because of its large semi-decadal variability component, a variability that is atypical of emissions and has not changed in the past 60 years despite a near tripling in emissions (Figure 4). Errors in S_{LAND} and S_{OCEAN} are more likely to be the main cause for the budget imbalance, especially on interannual to semi-decadal timescales. For example, underestimation of the S_{LAND} by DGVMs has been reported following the eruption of Mount Pinatubo in 1991 possibly due to missing responses to changes in diffuse radiation (Mercado et al., 2009). Although since GCB2021 we accounted for aerosol effects on solar radiation quantity and quality (diffuse vs direct), most DGVMs only used the former as input (i.e., total solar radiation) (Table S1). Thus, the ensemble mean may not capture the full

effects of volcanic eruptions, i.e. associated with high light scattering sulphate aerosols, on the land carbon sink (O'Sullivan et al., 2021). DGVMs are suspected to overestimate the land sink in response to the wet decade of the 1970s (Sitch et al., 2008). Quasi-decadal variability in the ocean sink has also been reported, with all methods agreeing on a smaller than expected ocean CO_2 sink in the 1990s and a larger than expected sink in the 2000s (Figure 10; Landschützer et al., 2016, DeVries et al., 2019, Hauck et al., 2020, McKinley et al., 2020, Gruber et al., 2023) and the climate-driven variability could be substantial but is not well constrained (DeVries et al., 2023, Müller et al., 2023). Errors in sink estimates could also be driven by errors in the climatic forcing data, particularly precipitation for S_{LAND} and wind for S_{OCEAN}. Also, the B_{IM} shows substantial departure from zero on yearly time scales (Figure 4e), highlighting unresolved variability of the carbon cycle, likely in the land sink (S_{LAND}), given its large year to year variability (Figure 4d and 8).

Both the budget imbalance (B_{IM}, Table 7) and the residual land sink from the global budget (E_{FOS}+E_{LUC}-G_{ATM}-S_{OCEAN}, Table 5) include an error term due to the inconsistencies that arises from combining E_{LUC} from bookkeeping models with S_{LAND} from DGVMs, most notably the loss of additional sink capacity (see Section 2.10 and Supplement S.6.4). Other differences include a better accounting of land use changes practices and processes in bookkeeping models than in DGVMs, or the bookkeeping models error of having present-day observed carbon densities fixed in the past. That the budget imbalance shows no clear trend towards larger values over time is an indication that these inconsistencies probably play a minor role compared to other errors in S_{LAND} or S_{OCEAN}.

Although the budget imbalance is near zero for the recent decades, it could be due to a compensation of errors. We cannot exclude an overestimation of CO_2 emissions, particularly from land-use change, given their large uncertainty, as has been suggested elsewhere (Piao et al., 2018), and/or an underestimate of the sinks. A larger DGVM estimate of the atmosphere-land CO_2 flux (S_{LAND}-E_{LUC}) over the extra-tropics would reconcile model results with inversion estimates for fluxes in the total land during the past decade (Figure 13; Table 5). Likewise, a larger S_{OCEAN} is also possible given the higher estimates from the fCO_2-products (see Section 3.6.2, Figure 10 and Figure 13), the underestimation of interior ocean anthropogenic carbon accumulation in the GOBMs (Section 3.6.5), and the recently suggested upward adjustments of the ocean carbon sink in Earth System Models (Terhaar et al., 2022), and in fCO_2-products, here related to a potential temperature bias and skin effects (Watson et al., 2020; Dong et al., 2022; Figure 10). If S_{OCEAN} were to be based on fCO_2-products alone, with all fCO_2-products including this adjustment, this would result in a 2013-2022 S_{OCEAN} of 3.7 GtC yr^{-1} (Dong et al., 2022) or >3.9 GtC yr^{-1} (Watson et al., 2020), i.e., outside of the range supported by the atmospheric inversions and with an implied negative B_{IM} of more than -1 GtC yr^{-1} indicating that a closure of the budget could only be achieved with either anthropogenic emissions being significantly larger and/or the net land sink being substantially smaller than estimated here. A recent model study suggests that the skin effect is smaller (about 0.1 GtC yr^{-1} or 5%) due to feedbacks with surface carbon concentration (Bellenger et al., 2023), which would nevertheless lead to a larger S_{OCEAN} even in the GOBMs. More integrated use of observations in the Global Carbon Budget, either on their own or for further constraining model results, should help resolve some of the budget imbalance (Peters et al., 2017).

4 Tracking progress towards mitigation targets

The average growth in global fossil CO_2 emissions peaked at nearly +3% per year during the 2000s, driven by the rapid growth in emissions in China. In the last decade, however, the global growth rate has slowly declined, reaching a low +0.5% per year over 2013-2022. While this slowdown in global fossil CO_2 emissions growth is welcome, global fossil CO_2 emissions continue to grow, far from the rapid emission decreases needed to be consistent with the temperature goals of the Paris Agreement.

Since the 1990s, the average growth rate of fossil CO_2 emissions has continuously declined across the group of developed countries of the Organisation for Economic Co-operation and Development (OECD), with emissions peaking in around 2005 and now declining at around 1% yr^{-1} (Le Quéré et al., 2021). In the decade 2013-2022, territorial fossil CO_2 emissions decreased significantly (at the 95% confidence level) in 26 countries/economies whose economies grew significantly : Belgium, Brazil, Czechia, Denmark, Estonia, Finland, France, Germany, Greece, Hong Kong, Israel, Italy, Jamaica, Japan, Luxembourg, Netherlands, Norway, Portugal, Romania, Slovenia, South Africa, Sweden, Switzerland, United Kingdom, USA, Zimbabwe (updated from Le Quéré et al., 2019). Altogether, these 26 countries emitted 2.7 GtC yr^{-1} (10.0 $GtCO_2$ yr^{-1}) on average over the last decade, about 28% of world CO_2 fossil emissions. For comparison, 22 countries showed a significant decrease in territorial fossil CO_2 emissions over the previous decade (2003-2012). Figure 16 shows that the emission declines in the USA and the EU27 are primarily driven by slightly weaker economic growth in the last decade compared to the 1990s, sustained declines in energy per GDP (though, weakening in the USA), and sustained declines in CO_2 emissions per unit energy (decarbonisation) with a slight acceleration in the USA in the last decade.

In contrast, fossil CO_2 emissions continue to grow in non-OECD countries, although the growth rate has slowed from more than 6% yr^{-1} during the 2000s to less than 2% yr^{-1} in the last decade. Representing 47% of non-OECD emissions in 2022, a large part of this slowdown is due to China, which has seen emissions growth decline from 9% yr^{-1} in the 2000s to 1.6% yr^{-1} in the last decade. Excluding China, non-OECD emissions grew at 3.1% yr^{-1} in the 2000s compared to 1.5% yr^{-1} in the last decade. China has had weaker economic growth in the 2000s compared to the 2010s and a higher decarbonisation rate from 2005 to 2015 comparable to the highs in the 1990s, though the decarbonisation rate has slowed considerably since 2016 (Figure 16). India and the rest of the world have strong economic growth that is not offset by decarbonisation or declines in energy per GDP, driving up fossil CO_2 emissions. Despite the high deployment of renewables in some countries (e.g., India), fossil energy sources continue to grow to meet growing energy demand (Le Quéré et al., 2019).

Globally, fossil CO_2 emissions growth is slowing, and this is due in part to the emergence of climate policy (Eskander and Fankhauser 2020; Le Quere et al 2019) and technological change, which is leading to a shift from coal to gas and growth in renewable energies, and reduced expansion of coal capacity. At the aggregated global level, decarbonisation shows a strong and growing signal in the last decade, with smaller contributions from lower economic growth and declines in energy per GDP. Altogether, global emissions are still growing (average

of 0.5% per year over the 2013-2022 decade), far from the reductions needed to meet the ambitious climate goals of the UNFCCC Paris agreement.

This year we updated the remaining carbon budget (RCB) based on two studies, the IPCC AR6 (Canadell et al, 2021) as used in GCB2022, and a recent revision of the IPCC AR6 estimates (Forster et al 2023, Lamboll et al., 2023). We update the RCB assessed by the IPCC AR6 (Canadell et al., 2021), accounting for the 2020 to 2023 estimated emissions from fossil fuel combustion (E_{FOS}) and land use changes (E_{LUC}). From January 2024, the IPCC AR6 RCB (50% likelihood) for limiting global warming to 1.5°C, 1.7°C and 2°C is estimated to amount to 95, 190, and 325 GtC (340, 690, 1190 $GtCO_2$). The Forster et al. (2023) study proposed a significantly lower RCB than IPCC AR6, with the largest reduction being due to an update of the climate emulator (MAGICC) used to estimate the warming contribution of non-CO_2 agents, and to the warming (i.e. emissions) that occurred over the 2020-2022 period. We update the Forster et al., budget accounting for the 2023 estimated emissions from fossil fuel combustion (E_{FOS}) and land use changes (E_{LUC}). From January 2024, the Forster et al., (2023) RCB (50% likelihood) for limiting global warming to 1.5°C, 1.7°C and 2°C is estimated to amount to 55, 155, and 305 GtC (210, 560, 1110 $GtCO_2$), significantly smaller than the updated IPCC AR6 estimate. Both the original IPCC AR6 and Forster et al. (2023) estimates include an uncertainty due to the climate response to cumulative CO_2 emissions, which is reflected through the percent likelihood of exceeding the given temperature threshold, an additional uncertainty of 220$GtCO_2$ due to alternative non-CO_2 emission scenarios, and other sources of uncertainties (see Canadell et al., 2021). The two sets of estimates overlap when considering all uncertainties. The IPCC AR6 estimates have the advantage of a consensus building approach, while the Forster et al. (2023) estimates include significant update estimates but without the backing of the IPCC yet. Here, we take the average of our update of both IPCC AR6 and Forster et al. (2023) estimates, giving a remaining carbon (50% likelihood) for limiting global warming to 1.5°C, 1.7°C and 2°C of respectively 75, 175, and 315 GtC (275, 625, 1150 $GtCO_2$) starting from January 2024. We emphasise the large uncertainties, particularly when close to the global warming limit of 1.5°C. These 1.5°C, 1.7°C and 2°C average remaining carbon budgets correspond respectively to about 7, 15 and 28 years from the beginning of 2024, at the 2023 level of total anthropogenic CO_2 emissions. Reaching net-zero CO_2 emissions by 2050 entails cutting total anthropogenic CO_2 emissions by about 0.4 GtC (1.5 $GtCO_2$) each year on average, comparable to the decrease in E_{FOS} observed in 2020 during the COVID-19 pandemic. However, this would lead to cumulative emissions over 2024-2050 of 150 GtC (550 $GtCO_2$), well above the remaining carbon budget of 75 GtC to limit global warming to 1.5°C, but still below the remaining budget of 175 GtC to limit warming to 1.7°C (in phase with the "well below 2°C" ambition of the Paris Agreement). Even reaching net zero CO_2 globally by 2040, which would require annual emissions cuts of 0.7 GtC (2.4 $GtCO_2$) on average, would still exceed the remaining carbon budget, with 95 GtC (350 $GtCO_2$) cumulative emissions over 2024-2050, unless the global emissions trajectory becomes net negative (i.e. more anthropogenic CO_2 sinks than emissions) after 2040.

5 Discussion

Each year when the global carbon budget is published, each flux component is updated for all previous years to consider corrections that are the result of further scrutiny and verification of the underlying data in the primary

input data sets. Annual estimates may be updated with improvements in data quality and timeliness (e.g., to eliminate the need for extrapolation of forcing data such as land-use). Of all terms in the global budget, only the fossil CO_2 emissions and the growth rate in atmospheric CO_2 concentration are based primarily on empirical inputs supporting annual estimates in this carbon budget. The carbon budget imbalance, yet an imperfect measure, provides a strong indication of the limitations in observations, in understanding and representing processes in models, and/or in the integration of the carbon budget components.

The persistent unexplained variability in the carbon budget imbalance limits our ability to verify reported emissions (Peters et al., 2017) and suggests we do not yet have a complete understanding of the underlying carbon cycle dynamics on annual to decadal timescales. Resolving most of this unexplained variability should be possible through different and complementary approaches. First, as intended with our annual updates, the imbalance as an error term should be reduced by improvements of individual components of the global carbon budget that follow from improving the underlying data and statistics and by improving the models through the resolution of some of the key uncertainties detailed in Table 10. Second, additional clues to the origin and processes responsible for the variability in the budget imbalance could be obtained through a closer scrutiny of carbon variability in light of other Earth system data (e.g., heat balance, water balance), and the use of a wider range of biogeochemical observations to better understand the land-ocean partitioning of the carbon imbalance such as the constraint from atmospheric oxygen included this year. Finally, additional information could also be obtained through better inclusion of process knowledge at the regional level, and through the introduction of inferred fluxes such as those based on satellite xCO_2 retrievals. The limit of the resolution of the carbon budget imbalance is yet unclear, but most certainly not yet reached given the possibilities for improvements that lie ahead.

Estimates of global fossil CO_2 emissions from different datasets are in relatively good agreement when the different system boundaries of these datasets are considered (Andrew, 2020a). But while estimates of E_{FOS} are derived from reported activity data requiring much fewer complex transformations than some other components of the budget, uncertainties remain, and one reason for the apparently low variation between datasets is precisely the reliance on the same underlying reported energy data. The budget excludes some sources of fossil CO_2 emissions, which available evidence suggests are relatively small (<1%). We have added emissions from lime production in China and the US, but these are still absent in most other non-Annex I countries, and before 1990 in other Annex I countries.

Estimates of E_{LUC} suffer from a range of intertwined issues, including the poor quality of historical land-cover and land-use change maps, the rudimentary representation of management processes in most models, and the confusion in methodologies and boundary conditions used across methods (e.g., Arneth et al., 2017; Pongratz et al., 2014, see also Supplement S.6.4 on the loss of sink capacity; Bastos et al., 2021). Uncertainties in current and historical carbon stocks in soils and vegetation also add uncertainty in the E_{LUC} estimates. Unless a major effort to resolve these issues is made, little progress is expected in the resolution of E_{LUC}. This is particularly concerning given the growing importance of E_{LUC} for climate mitigation strategies, and the large issues in the quantification of the cumulative emissions over the historical period that arise from large uncertainties in E_{LUC}.

By adding the DGVMs estimates of CO_2 fluxes due to environmental change from countries' managed forest areas (part of S_{LAND} in this budget) to the budget E_{LUC} estimate, we successfully reconciled the large gap between our E_{LUC} estimate and the land use flux from NGHGIs using the approach described in Grassi et al. (2021) for future scenarios and in Grassi et al. (2023) using data from the Global Carbon Budget 2021. The updated data presented here can be used as potential adjustment in the policy context, e.g., to help assess the collective countries' progress towards the goal of the Paris Agreement and avoiding double-accounting for the sink in managed forests. In the absence of this adjustment, collective progress would hence appear better than it is (Grassi et al., 2021). The application of this adjustment is also recommended in the UNFCCC Synthesis report for the first Global Stocktake (UNFCCC, 2022) whenever a comparison between LULUCF fluxes reported by countries and the global emission estimates of the IPCC is conducted. However, this adjustment should be seen as a short-term and pragmatic fix based on existing data, rather than a definitive solution to bridge the differences between global models and national inventories. Additional steps are needed to understand and reconcile the remaining differences, some of which are relevant at the country level (Grassi, et al., 2023, Schwingshackl, et al., 2022).

The comparison of GOBMs, fCO_2-products, and inversions highlights substantial discrepancy in the temporal evolution of S_{OCEAN} in the Southern Ocean and northern high-latitudes (Figure 13, Hauck et al., 2023) and in the mean S_{OCEAN} in the tropics. A large part of the uncertainty in the mean fluxes stems from the regional distribution of the river flux adjustment term. The current distribution simulates the largest share of the outgassing to occur in the tropics (Lacroix et al., 2020) in contrast to the regional distribution previously used with the largest riverine outgassing flux south of 20°S (Aumont et al., 2001). The long-standing sparse data coverage of fCO_2 observations in the Southern compared to the Northern Hemisphere (e.g., Takahashi et al., 2009) continues to exist (Bakker et al., 2016, 2022, Figure S1) and to lead to substantially higher uncertainty in the S_{OCEAN} estimate for the Southern Hemisphere (Watson et al., 2020, Gloege et al., 2021, Hauck et al., 2023). This discrepancy, which also hampers model improvement, points to the need for increased high-quality fCO_2 observations especially in the Southern Ocean. At the same time, model uncertainty is illustrated by the large spread of individual GOBM estimates (indicated by shading in Figure 13) and highlights the need for model improvement. The diverging trends in S_{OCEAN} from different methods is a matter of concern. Recent and on-going work suggests that the fCO_2-products may overestimate the trend (Hauck et al., 2023), though many products remain to be tested, whereas evidence is accumulating that GOBMs likely underestimate the mean flux (Section 3.6.2, Terhaar et al., 2022, DeVries et al., 2023, Müller et al., 2023). The independent constraint from atmospheric oxygen measurements is consistent within errors with the relatively larger ocean sink in the fCO_2-products. The assessment of the net land-atmosphere exchange from DGVMs and atmospheric inversions also shows substantial discrepancy, particularly for the estimate of the net land flux over the northern extra-tropic. This discrepancy highlights the difficulty to quantify complex processes (CO_2 fertilisation, nitrogen deposition and fertilisers, climate change and variability, land management, etc.) that collectively determine the net land CO_2 flux. Resolving the differences in the Northern Hemisphere land sink will require the consideration and inclusion of larger volumes of observations.

We provide metrics for the evaluation of the ocean and land models and the atmospheric inversions (Figures B2 to B4, Table S10). These metrics expand the use of observations in the global carbon budget, helping 1) to support improvements in the ocean and land carbon models that produce the sink estimates, and 2) to constrain the representation of key underlying processes in the models and to allocate the regional partitioning of the CO_2 fluxes. The introduction of process-based metrics targeted to evaluate the simulation of S_{OCEAN} in the ocean biogeochemistry models is an important addition to the evaluation based on ocean carbon observations. This is an initial step towards the introduction of a broader range of observations and more stringent model evaluation that we hope will support continued improvements in the annual estimates of the global carbon budget.

We assessed before that a sustained decrease of –1% in global emissions could be detected at the 66% likelihood level after a decade only (Peters et al., 2017). Similarly, a change in behaviour of the land and/or ocean carbon sink would take as long to detect, and much longer if it emerges more slowly. To continue reducing the carbon imbalance on annual to decadal time scales, regionalising the carbon budget, and integrating multiple variables are powerful ways to shorten the detection limit and ensure the research community can rapidly identify issues of concern in the evolution of the global carbon cycle under the current rapid and unprecedented changing environmental conditions.

6 Conclusions

The estimation of global CO_2 emissions and sinks is a major effort by the carbon cycle research community that requires a careful compilation and synthesis of measurements, statistical estimates, and model results. The delivery of an annual carbon budget serves two purposes. First, there is a large demand for up-to-date information on the state of the anthropogenic perturbation of the climate system and its underpinning causes. A broad stakeholder community relies on the data sets associated with the annual carbon budget including scientists, policy makers, businesses, journalists, and non-governmental organisations engaged in adapting to and mitigating human-driven climate change. Second, over the last decades we have seen unprecedented changes in the human and biophysical environments (e.g., changes in the growth of fossil fuel emissions, impact of COVID-19 pandemic, Earth's warming, and strength of the carbon sinks), which call for frequent assessments of the state of the planet, a better quantification of the causes of changes in the contemporary global carbon cycle, and an improved capacity to anticipate its evolution in the future. Building this scientific understanding to meet the extraordinary climate mitigation challenge requires frequent, robust, transparent, and traceable data sets and methods that can be scrutinised and replicated. This paper via 'living data' helps to keep track of new budget updates.

7 Data availability

The data presented here are made available in the belief that their wide dissemination will lead to greater understanding and new scientific insights of how the carbon cycle works, how humans are altering it, and how we can mitigate the resulting human-driven climate change. Full contact details and information on how to cite the data shown here are given at the top of each page in the accompanying database and summarised in Table 2.

The accompanying database includes three Excel files organised in the following spreadsheets:

File Global_Carbon_Budget_2023v1.0.xlsx includes the following:

1. Summary
2. The global carbon budget (1959-2022);
3. The historical global carbon budget (1750-2022);
4. Global CO_2 emissions from fossil fuels and cement production by fuel type, and the per-capita emissions (1850-2022);
5. CO_2 emissions from land-use change from the individual bookkeeping models (1959-2022);
6. Ocean CO_2 sink from the individual global ocean biogeochemistry models and fCO_2-products (1959-2022);
7. Terrestrial CO_2 sink from the individual DGVMs (1959-2022);
8. Cement carbonation CO_2 sink (1959-2022).

File National_Fossil_Carbon_Emissions_2023v1.0.xlsx includes the following:

1. Summary
2. Territorial country CO_2 emissions from fossil fuels and cement production (1850-2022);
3. Consumption country CO_2 emissions from fossil fuels and cement production and emissions transfer from the international trade of goods and services (1990-2020) using CDIAC/UNFCCC data as reference;
4. Emissions transfers (Consumption minus territorial emissions; 1990-2020);
5. Country definitions.

File National_LandUseChange_Carbon_Emissions_2023v1.0.xlsx includes the following:

1. Summary
2. Territorial country CO_2 emissions from Land Use Change (1850-2022) from three bookkeeping models;

All three spreadsheets are published by the Integrated Carbon Observation System (ICOS) Carbon Portal and are available at https://doi.org/10.18160/GCP-2023 (Friedlingstein et al., 2023). National emissions data are also available on Zenodo (Andrew and Peters, 2022), from the Global Carbon Atlas (http://www.globalcarbonatlas.org/, last access: 9 November 2023) and from Our World in Data (https://ourworldindata.org/co2-emissions, last access: 9 November 2023).

Author contributions

PF, MO, MWJ, RMA, DCEB, JH, PL, CLQ, ITL, GPP, WP, JP, CSc, and SSi designed the study, conducted the analysis, and wrote the paper with input from JGC, PCi and RBJ. RMA, GPP and JIK produced the fossil CO_2 emissions and their uncertainties and analysed the emissions data. MH and GMa provided fossil fuel emission data. JP, TGa, CSc and RAH provided the bookkeeping land-use change emissions with synthesis by JP and CSc. FJo provided peat drainage emission estimates. SSm and CMP provided the estimates of non-vegetation CDR fluxes. LBo, MCh, ÖG, NG, TI, TJ, LR, JS, RS, and HiT provided an update of the global ocean biogeochemical models, TTTC, DF, LG, YI, AJ, GMc, ChR, and JZ provided an update of the ocean *f*CO2-data products, with synthesis on both streams by JH, PL and NMa. SRA, LBa, NRB, MB, MCr, KE, WE, RAF, TGk, AK, NL, DRM, SN, AO, AMO, TO, MEP, DP, KP, GR, AJS, CSw, ST, BT, EvO, RW, and CWR provided ocean fCO_2 measurements for the year 2022, with synthesis by DCEB and KMO. PA, DB, SF, JG, HJ, AKJ, EK, DK, JK, GMe, LM, PM, MO, BP, TLS, QS, HTi, WY, XYua, XYue, and SZ provided an update of the Dynamic Global Vegetation Models, with synthesis by SSi and MO. HL, RSA, MW, and PCa provided estimates of land and ocean sinks from Earth System Models, as well as a projection of the atmospheric growth rate for 2023. FC, ITL, NC, LF, ARJ, FJi, JL, ZJin, ZLiu, YN, CR, DY, and BZ provided an updated atmospheric inversion, WP, FC, and ITL developed the protocol and produced the synthesis and evaluation of the atmospheric inversions. RMA provided projections of the 2023 fossil emissions and atmospheric CO2 growth rate. PL provided the predictions of the 2023 ocean and land sinks. IBMB, LPC, GCH, KKG, TMR, and GRvdW provided forcing data for land-use change. FT and GG provided data for the land-use change NGHGI harmonisation. RK provided key atmospheric CO2 data. EJM and RFK provided the atmospheric oxygen constraint on surface net carbon sinks. XL, PPT and MWJ provided the historical atmospheric CO2 concentration and growth rate. MO and NB produced the aerosol diffuse radiative forcing for the DGVMs. IH provided the climate forcing data for the DGVMs. ER provided the evaluation of the DGVMs. MWJ provided the emissions prior for use in the inversion systems. XD provided seasonal emissions data for most recent years for the emission prior. PF, MO and MWJ coordinated the effort, revised all figures, tables, text and numbers to ensure the update was clear from the 2022 edition and in line with the globalcarbonatlas.org.

Competing interests.

At least one of the (co-)authors is a member of the editorial board of Earth System Science Data

Acknowledgements

We thank all people and institutions who provided the data used in this global carbon budget 2023 and the Global Carbon Project members for their input throughout the development of this publication. We thank Nigel Hawtin for producing Figure 2 and Figure 15. We thank Alex Vermeulen and Hanna Ritchie for respectively hosting the Global Carbon Budget datasets on the ICOS portal and the Our World in Data website. We thank Ian G. C. Ashton, Sebastian Brune, Fatemeh Cheginig, Sam Ditkovsky, Christian Ethé, Amanda R. Fay, Lonneke Goddijn-Murphy, T. Holding, Yawen Kong, Fabrice Lacroix, Yi Liu, Damian Loher, Naiqing Pan, Paridhi Rustogi, Shijie Shu, J. D. Shutler, Richard Sims, Phillip Townsend, Jing Wang, Andrew J. Watson, and David K. Woolf for their involvement in the development, use and analysis of the models and data-products used here. We thank Toste Tanhua, Marcos Fontela, Claire Lo Monaco and Nicolas Metzl who contributed to the provision of surface ocean CO_2 observations for the year 2022 (see Table S6). We also thank Stephen D. Jones of the Ocean Thematic Centre of the EU Integrated Carbon Observation System (ICOS) Research Infrastructure, Eugene Burger of NOAA's Pacific Marine Environmental Laboratory and Alex Kozyr of NOAA's National Centers for Environmental Information, for their contribution to surface ocean CO_2 data and metadata management. This is PMEL contribution 5550. We thank the scientists, institutions, and funding agencies responsible for the collection and quality control of the data in SOCAT as well as the International Ocean Carbon Coordination Project (IOCCP), the Surface Ocean Lower Atmosphere Study (SOLAS) and the Integrated Marine Biosphere Research (IMBeR) program for their support. We thank Nadine Goris and Lavinia Patara for support in calculating observational ocean evaluation metrics. We thank Fortunat Joos, Samar Khatiwala and Timothy DeVries for providing historical atmospheric and ocean data. We thank data providers ObsPack GLOBALVIEWplus v8.0 and NRT v8.1 for atmospheric CO_2 observations. Ingrid T Luijkx and Wouter Peters thank the CarbonTracker Europe team at Wageningen University, including Remco de Kok, Joram Hooghiem, Linda Kooijmans and Auke van der Woude. Daniel Kennedy thanks all the scientists, software engineers, and administrators who contributed to the development of CESM2. Josefine Ghattas thanks the whole ORCHIDEE group. Ian Harris thanks the Japan Meteorological Agency (JMA) for producing the Japanese 55-year Reanalysis (JRA-55). Reinel Sospedra-

Alfonso thanks Barbara Winter, Woosung Lee, and William J. Merryfield for their contribution to the preparation and production of CanESM5 runs. Patricia Cadule thanks Olivier Torres, Juliette Mignot, Didier Swingedouw, and Laurent Bopp for contributions to the IPSL-CM6-LR-ESMCO2 simulations. Yosuke Niwa thanks CSIRO, EC, EMPA, FMI, IPEN, JMA, LSCE, NCAR, NIES, NILU, NIWA, NOAA, SIO, and TU/NIPR for providing data for NISMON-CO2. Zhe Jin thanks Xiangjun Tian, Yilong Wang, Hongqin Zhang, Min Zhao, Tao Wang, Jinzhi Ding and Shilong Piao for their contributions to the GONGGA inversion system. Bo Zheng thanks Yawen Kong for running the THU inversion system. Frédéric Chevallier thanks Zoé Lloret who maintained the atmospheric transport model for the CAMS inversions. Frédéric Chevallier and Thi-Tuyet-Trang Chau thank Marion Gehlen for her contribution to the CMEMS-LSCE-FFNNv2 product. Lian Fang thanks Paul I. Palmer and acknowledges ongoing support from the National Centre for Earth Observation. Junjie Liu thanks the Jet Propulsion Laboratory, California Institute of Technology. Zhiqiang Liu thanks Ning Zeng, Yun Liu, Eugenia Kalnay, and Gassem Asrar for their contributions to the COLA system. Fei Jiang acknowledges ongoing support from Frontiers Science Center for Critical Earth Material Cycling, Nanjing University. Andy Jacobson thanks the team at NOAA GML, Boulder, Colorado, USA, who provided the CarbonTracker CT2022 and CT-NRT.v2023-3 results from the website at http://carbontracker.noaa.gov. Meike Becker and Are Olsen thank Sparebanken Vest / Agenda Vestlandet for their support for the observations on the Statsraad Lehmkuhl. Margot Cronin thanks Anthony English, Clynt Gregory and Gordon Furey (P&O Maritime Services), Tobias Steinhoff and Aodhan Fitzgerald (Marine Institute) for their support. Wiley Evans and Katie Pocock thank the Tula Foundation for funding support. Thanos Gkritzalis and the VLIZ ICOS team are thankful to the crew of the research vessel Simon Stevin for all the support and help they provide. Data providers Nicolas Metzl and Claire LoMonaco thank the French Institut National des Sciences de l'Univers (INSU), Institut Polaire français, Paul-Emile Victor(IPEV), Observatoire des sciences de l'univers Ecce-Terra (OSU at Sorbonne Université), Institut de recherche français sur les ressources marines (IFREMER), French Oceanographic Fleet (FOF) for the Marion Dufresne data set (http://dx.doi.org/10.17600/18001858). Bronte Tilbrook and Erik van Ooijen thank Australia's Integrated Marine Observing System (IMOS) for sourcing of CO_2 data. IMOS is enabled by the National Collaborative Research Infrastructure Strategy (NCRIS). FAOSTAT is funded by FAO member states through their contributions to the FAO Regular Programme, data contributions by national experts are greatly acknowledged. The views expressed in this paper are the authors' only and do not necessarily reflect those of FAO. Finally, we thank all funders who

have supported the individual and joint contributions to this work (see details below), as well as the two anonymous reviewers of this manuscript, and the many researchers who have provided feedback.

Financial and computing support

This research was supported by the following sources of funding: Integrated Marine Observing System (IMOS) [Australia]; ICOS Flanders [Belgium]; Research Foundation Flanders (grant no. I001821N) [Belgium]; Tula Foundation [Canada]; Chinese Academy of Science Project for Young Scientists in Basic Research (Grant No. YSBR-037) [China]; National Key R&D Program of China (Grant No: 2020YFA0607504); National Natural Science Foundation (grant no. 42141020, 42275128) [China]; National Natural Science Foundation (grant no. 42275128) [China]; National Natural Science Foundation (grant no. 41921005) [China]; Scientific Research Start-up Funds (grant no. QD2021024C) from Tsinghua Shenzhen International Graduate School [China]; Second Tibetan Plateau Scientific Expedition and Research Program (Grant: 2022QZKK0101) [China]; Young Elite Scientists Sponsorship Program by CAST (grant no. YESS20200135) [China]; Copernicus Atmosphere Monitoring Service, implemented by ECMWF (Grant: CAMS2 55) [EC]; Copernicus Marine Environment Monitoring Service, implemented by MOi (Grant: CAMS2 55) [EC]; H2020 (Horizon 2020) 4C (grant no. 821003) [European Commission, EC]; H2020 ESM2025 – Earth System Models for the Future (grant no. 101003536) [European Commission, EC]; H2020 EuroSea (grant no. 862626) [EC]; H2020 GEORGE (grant no. 101094716) [EC]; H2020 JERICO-S3 (grant no. 871153) [EC]; ICOS France [France]; Institut de Recherche pour le Développement (IRD) [France]; Federal Ministry of Education and Research (BMBF) (grant no. 03F0885AL1) [Germany]; Federal Ministry of Education and Research, collaborative project C-SCOPE (Towards Marine Carbon Observations 2.0: Socializing, COnnecting, Perfecting and Expanding, project no. 03F0877A) [Germany]; Helmholtz Association ATMO programme [Germany]; Helmholtz Association of German Research Centres (project MOSES; Modular Observation Solutions for Earth Systems) [Germany]; ICOS (Integrated Carbon Observation System) Germany [Germany]; Ludwig-Maximilians-University Munich, Department of Geography [Germany]; Marine Institute [Ireland]; Arctic Challenge for Sustainability phase II project (ArCS-II; grant no. JP-MXD1420318865) [Japan]; Environment Research and Technology Development Fund (grant no. JP-MEERF21S20800) [Japan]; Fundamental Research Funds for the Central Universities (Grant No: 090414380031); Global Environmental Research Coordination System, Ministry of the Environment (grant no. E2252) [Japan]; Japan Meteorological Agency [Japan]; Ministry of Education, Culture, Sports, Science and Technology, MEXT program for the advanced studies of climate change projection (SENTAN) (grant numbers

JPMXD0722680395, JPMXD0722681344) [Japan]; Ministry of Environment, Environmental Restoration and Conservation Agency, Environment Research and Technology Development Fund (grant no. JPMEERF21S20810) [Japan]; National Institute for Environmental Studies [Japan]; Research Council of Norway (N-ICOS-2, grant no. 296012) [Norway]; Swiss National Science Foundation (grant no. 200020-200511) [Switzerland]; National Centre for Atmospheric Science [UK]; NERC (Natural Environment Research Council) Independent Research Fellowship (NE/V01417X/1) [UK]; NERC (NE/R016518/1) [UK]; Royal Society (grant no. RP\R1\191063) [UK]; UK Research and Innovation (UKRI) for Horizon Europe (GreenFeedBack, grant no. 10040851) [UK]; NASA Carbon Monitoring System program (80NSSC21K1059) [USA]; NASA OCO Science team program (80NM0018F0583) [USA]; National Center for Atmospheric Research (NCAR) cooperative agreement (NSF No. 1852977) [USA]; National Oceanic and Atmospheric Administration (NOAA) cooperative agreement (NA22OAR4320151) [USA]; National Science Foundation (NSF- 831361857) [USA]; NOAA (NA20OAR4320278) [USA]; NOAA Cooperative Agreement, Cooperative Institute for Climate, Ocean, & Ecosystem Studies (CIOCES; NA20OAR4320271) [USA]; NOAA Cooperative Agreement, Cooperative Institute for Marine and Atmospheric Studies (CIMAS) / University of Miami (NA20OAR4320472) [USA]; NOAA Global Ocean Monitoring and Observing Program (grant no. 100018302, 100007298, NA-03-AR4320179) [USA]; NOAA Ocean Acidification Program [USA]; National Science Foundation (OPP-1922922) [USA]. We also acknowledge support from the following computing facilities: Adapter Allocation Scheme from the National Computational Infrastructure (NCI) [Australia]; High-Performance Computing Center (HPCC) of Nanjing University [China]; GENCI -TGCC (A0130102201, A0130106328, A0140107732 and A0130107403) [France], CCRT awarded by CEA/DRF (CCRT2023-p24cheva) [France]; HPC cluster Aether at the University of Bremen, financed by DFG within the scope of the Excellence Initiative [Germany], the State of Baden-Württemberg, through bwHPC [Germany]; Earth Simulator (ES4) at JAMSTEC [Japan], JAMSTEC's Super Computer system [Japan], NIES supercomputer system [Japan], NIES (SX-Aurora) and MRI (FUJITSU Server PRIMERGY CX2550M5) [Japan]; ADA HPC cluster at the University of East Anglia [UK], UK CEDA JASMIN supercomputer [UK]; Cheyenne NCAR HPC resources managed by CISL (doi:10.5065/D6RX99HX) [USA].

References

Ahlström, A., Raupach, M. R., Schurgers, G., Smith, B., Arneth, A., Jung, M., Reichstein, M., Canadell, J. G., Friedlingstein, P., Jain, A. K., Kato, E., Poulter, B., Sitch, S., Stocker, B. D., Viovy, N., Wang, Y. P., Wiltshire, A., Zaehle, S., and Zeng, N.: The dominant role of semi-arid ecosystems in the trend and variability of the land CO2 sink, 348, 895–899, https://doi.org/10.1126/science.aaa1668, 2015.

Amador-Jiménez, M., Millner, N., Palmer, C., Pennington, R. T., and Sileci, L.: The Unintended Impact of Colombia's Covid-19 Lockdown on Forest Fires, Environ Resource Econ, 76, 1081–1105, https://doi.org/10.1007/s10640-020-00501-5, 2020.

Andela, N., Morton, D. C., Giglio, L., Chen, Y., van der Werf, G. R., Kasibhatla, P. S., DeFries, R. S., Collatz, G. J., Hantson, S., Kloster, S., Bachelet, D., Forrest, M., Lasslop, G., Li, F., Mangeon, S., Melton, J. R., Yue, C., and Randerson, J. T.: A human-driven decline in global burned area, Science, 356, 1356–1362, https://doi.org/10.1126/science.aal4108, 2017.

Andrew, R. M.: A comparison of estimates of global carbon dioxide emissions from fossil carbon sources, Earth Syst. Sci. Data, 12, 1437–1465, https://doi.org/10.5194/essd-12-1437-2020, 2020a.

Andrew, R. M.: Timely estimates of India's annual and monthly fossil CO2 emissions, Earth Syst. Sci. Data, 12, 2411–2421, https://doi.org/10.5194/essd-12-2411-2020, 2020b.

Andrew, R. M. and Peters, G. P.: The Global Carbon Project's fossil CO2 emissions dataset (2022v27), https://doi.org/10.5281/zenodo.7215364, 2022.

Angelsen, A. and Kaimowitz, D.: Rethinking the Causes of Deforestation: Lessons from Economic Models, World Bank Res. Obs., 14, 73–98, https://doi.org/10.1093/wbro/14.1.73, 1999.

Aragão, L. E. O. C., Anderson, L. O., Fonseca, M. G., Rosan, T. M., Vedovato, L. B., Wagner, F. H., Silva, C. V. J., Silva Junior, C. H. L., Arai, E., Aguiar, A. P., Barlow, J., Berenguer, E., Deeter, M. N., Domingues, L. G., Gatti, L., Gloor, M., Malhi, Y., Marengo, J. A., Miller, J. B., Phillips, O. L., and Saatchi, S.: 21st Century drought-related fires counteract the decline of Amazon deforestation carbon emissions, Nat Commun, 9, 536, https://doi.org/10.1038/s41467-017-02771-y, 2018.

Archer, D., Eby, M., Brovkin, V., Ridgwell, A., Cao, L., Mikolajewicz, U., Caldeira, K., Matsumoto, K., Munhoven, G., Montenegro, A., and Tokos, K.: Atmospheric Lifetime of Fossil Fuel Carbon Dioxide, Annu. Rev. Earth Planet. Sci., 37, 117–134, https://doi.org/10.1146/annurev.earth.031208.100206, 2009.

Arneth, A., Sitch, S., Pongratz, J., Stocker, B. D., Ciais, P., Poulter, B., Bayer, A. D., Bondeau, A., Calle, L., Chini, L. P., Gasser, T., Fader, M., Friedlingstein, P., Kato, E., Li, W., Lindeskog, M., Nabel, J. E. M. S., Pugh, T. A. M., Robertson, E., Viovy, N., Yue, C., and Zaehle, S.: Historical carbon dioxide emissions caused by land-use changes are possibly larger than assumed, Nature Geosci, 10, 79–84, https://doi.org/10.1038/ngeo2882, 2017.

Asaadi, A., Arora, V. K., Melton, J. R., and Bartlett, P.: An improved parameterization of leaf area index (LAI) seasonality in the Canadian Land Surface Scheme (CLASS) and Canadian Terrestrial Ecosystem Model (CTEM) modelling framework, 15, 6885–6907, https://doi.org/10.5194/bg-15-6885-2018, 2018.

Aumont, O., Orr, J. C., Monfray, P., Ludwig, W., Amiotte-Suchet, P., and Probst, J.-L.: Riverine-driven interhemispheric transport of carbon, Global Biogeochem. Cycles, 15, 393–405, https://doi.org/10.1029/1999GB001238, 2001.

Aumont, O., Ethé, C., Tagliabue, A., Bopp, L., and Gehlen, M.: PISCES-v2: an ocean biogeochemical model for carbon and ecosystem studies, 8, 2465–2513, https://doi.org/10.5194/gmd-8-2465-2015, 2015.

Baccini, A., Walker, W., Carvalho, L., Farina, M., Sulla-Menashe, D., and Houghton, R. A.: Tropical forests are a net carbon source based on aboveground measurements of gain and loss, Science, 358, 230–234, https://doi.org/10.1126/science.aam5962, 2017.

Bakker, D. C. E., Pfeil, B., Landa, C. S., Metzl, N., O'Brien, K. M., Olsen, A., Smith, K., Cosca, C., Harasawa, S., Jones, S. D., Nakaoka, S., Nojiri, Y., Schuster, U., Steinhoff, T., Sweeney, C., Takahashi, T., Tilbrook, B., Wada, C., Wanninkhof, R., Alin, S. R., Balestrini, C. F., Barbero, L., Bates, N. R., Bianchi, A. A., Bonou, F., Boutin, J., Bozec, Y., Burger, E. F., Cai, W.-J., Castle, R. D., Chen, L., Chierici, M., Currie, K., Evans, W., Featherstone, C., Feely, R. A., Fransson, A., Goyet, C., Greenwood, N., Gregor, L., Hankin, S., Hardman-Mountford, N. J., Harlay, J., Hauck, J., Hoppema, M., Humphreys, M. P., Hunt, C. W., Huss, B., Ibánhez, J. S. P., Johannessen, T., Keeling, R., Kitidis, V., Körtzinger, A., Kozyr, A., Krasakopoulou, E., Kuwata, A., Landschützer, P., Lauvset, S. K., Lefèvre, N., Lo Monaco, C., Manke, A., Mathis, J. T., Merlivat, L., Millero, F. J., Monteiro, P. M. S., Munro, D. R., Murata, A., Newberger, T., Omar, A. M., Ono, T., Paterson, K., Pearce, D., Pierrot, D., Robbins, L. L., Saito, S., Salisbury, J., Schlitzer, R., Schneider, B., Schweitzer, R., Sieger, R., Skjelvan, I., Sullivan, K. F., Sutherland, S. C., Sutton, A. J., Tadokoro, K., Telszewski, M., Tuma, M., van Heuven, S. M. A. C., Vandemark, D., Ward, B., Watson, A. J., and Xu, S.: A multi-decade record of high-quality CO2 data in version 3 of the Surface Ocean CO2 Atlas (SOCAT), Earth Syst. Sci. Data, 8, 383–413, https://doi.org/10.5194/essd-8-383-2016, 2016.

Bakker, Dorothee C. E.; Alin, Simone R.; Bates, Nicholas; Becker, Meike; Feely, Richard A.; Gkritzalis, Thanos; Jones, Steve D.; Kozyr, Alex; Lauvset, Siv K.; Metzl, Nicolas; Munro, David R.; Nakaoka, Shin-ichiro; Nojiri, Yukihiro; O'Brien, Kevin M.; Olsen, Are; Pierrot, Denis; Rehder, Gregor; Steinhoff, Tobias; Sutton, Adrienne J.; Sweeney, Colm; Tilbrook, Bronte; Wada, Chisato; Wanninkhof, Rik; Akl, John; Barbero, Leticia; Beatty, Cory M.; Berghoff, Carla F.; Bittig, Henry C.; Bott, Randy; Burger, Eugene F.; Cai, Wei-Jun; Castaño-Primo, Rocío; Corredor, Jorge E.; Cronin, Margot; De Carlo, Eric H.; DeGrandpre, Michael D.; Dietrich, Colin; Drennan, William M.; Emerson, Steven R.; Enochs, Ian C.; Enyo, Kazutaka; Epherra, Lucía; Evans, Wiley; Fiedler, Björn; Fontela, Marcos; Frangoulis, Constantin; Gehrung, Martina; Giannoudi, Louisa; Glockzin, Michael; Hales, Burke; Howden, Stephan D.; Ibánhez, J. Severino P.; Kamb, Linus; Körtzinger, Arne; Lefèvre, Nathalie; Lo Monaco, Claire; Lutz, Vivian A.; Macovei, Vlad A.; Maenner Jones, Stacy; Manalang, Dana; Manzello, Derek P.; Metzl, Nicolas; Mickett, John; Millero, Frank J.; Monacci, Natalie M.; Morell, Julio M.; Musielewicz, Sylvia; Neill, Craig; Newberger, Tim; Newton, Jan; Noakes, Scott; Ólafsdóttir, Sólveig Rósa; Ono, Tsuneo; Osborne, John; Padín, Xose A.; Paulsen, Melf; Perivoliotis, Leonidas; Petersen, Wilhelm; Petihakis, George; Plueddemann, Albert J.; Rodriguez, Carmen; Rutgersson, Anna; Sabine, Christopher L.; Salisbury, Joseph E.; Schlitzer, Reiner; Skjelvan, Ingunn; Stamataki, Natalia; Sullivan, Kevin F.; Sutherland, Stewart C.; T'Jampens, Michiel; Tadokoro, Kazuaki; Tanhua, Toste; Telszewski, Maciej; Theetaert, Hannelore; Tomlinson, Michael; Vandemark, Douglas; Velo, Antón; Voynova, Yoana G.; Weller, Robert A.; Whitehead, Chris; Wimart-Rousseau, Cathy (2023). Surface Ocean CO2 Atlas Database Version 2023 (SOCATv2023) (NCEI Accession 0278913). [indicate subset used]. NOAA National Centers for Environmental Information. Dataset. https://doi.org/10.25921/r7xa-bt92, 2023.

Ballantyne, A. P., Alden, C. B., Miller, J. B., Tans, P. P., and White, J. W. C.: Increase in observed net carbon dioxide uptake by land and oceans during the past 50 years, Nature, 488, 70–72, https://doi.org/10.1038/nature11299, 2012.

Ballantyne, A. P., Andres, R., Houghton, R., Stocker, B. D., Wanninkhof, R., Anderegg, W., Cooper, L. A., DeGrandpre, M., Tans, P. P., Miller, J. B., Alden, C., and White, J. W. C.: Audit of the global carbon budget: estimate errors and their impact on uptake uncertainty, Biogeosciences, 12, 2565–2584, https://doi.org/10.5194/bg-12-2565-2015, 2015.

Bastos, A., Hartung, K., Nützel, T. B., Nabel, J. E. M. S., Houghton, R. A., and Pongratz, J.: Comparison of uncertainties in land-use change fluxes from bookkeeping model parameterisation, 12, 745–762, https://doi.org/10.5194/esd-12-745-2021, 2021.

Battle, M. O., Raynor, R., Kesler, S., and Keeling, R.: Technical Note: The impact of industrial activity on the amount of atmospheric O2, Atmospheric Chem. Phys. Discuss., 1–17, https://doi.org/10.5194/acp-2022-765, 2023.

Beckman, J. and Countryman, A. M.: The Importance of Agriculture in the Economy: Impacts from COVID-19, Am. J. Agr. Econ., 103, 1595–1611, https://doi.org/10.1111/ajae.12212, 2021.

Bellenger, H., Bopp, L., Ethé, C., Ho, D., Duvel, J. P., Flavoni, S., Guez, L., Kataoka, T., Perrot, X., Parc, L., and Watanabe, M.: Sensitivity of the Global Ocean Carbon Sink to the Ocean Skin in a Climate Model, J. Geophys. Res. Oceans, 128, e2022JC019479, https://doi.org/10.1029/2022JC019479, 2023.

Bennington, V., Gloege, L., and McKinley, G. A.: Variability in the Global Ocean Carbon Sink From 1959 to 2020 by Correcting Models with Observations, Geophys. Res. Lett., 49, e2022GL098632, https://doi.org/10.1029/2022GL098632, 2022.

Berthet, S., Séférian, R., Bricaud, C., Chevallier, M., Voldoire, A., and Ethé, C.: Evaluation of an Online Grid-Coarsening Algorithm in a Global Eddy-Admitting Ocean Biogeochemical Model, J. Adv. Model Earth Sy., 11, 1759–1783, https://doi.org/10.1029/2019MS001644, 2019.

Betts, R. A., Jones, C. D., Knight, J. R., Keeling, R. F., and Kennedy, J. J.: El Niño and a record CO2 rise, Nat. Clim. Change, 6, 806–810, https://doi.org/10.1038/nclimate3063, 2016.

Bloom, A. A. and Williams, M.: Constraining ecosystem carbon dynamics in a data-limited world: integrating ecological "common sense" in a model–data fusion framework, Biogeosciences, 12, 1299–1315, https://doi.org/10.5194/bg-12-1299-2015, 2015.

Bloom, A. A., Exbrayat, J.-F., van der Velde, I. R., Feng, L., and Williams, M.: The decadal state of the terrestrial carbon cycle: Global retrievals of terrestrial carbon allocation, pools, and residence times, Proc. Natl. Acad. Sci., 113, 1285–1290, https://doi.org/10.1073/pnas.1515160113, 2016.

Boer, G. J., Smith, D. M., Cassou, C., Doblas-Reyes, F., Danabasoglu, G., Kirtman, B., Kushnir, Y., Kimoto, M., Meehl, G. A., Msadek, R., Mueller, W. A., Taylor, K. E., Zwiers, F., Rixen, M., Ruprich-Robert, Y., and Eade, R.: The Decadal Climate Prediction Project (DCPP) contribution to CMIP6, Geosci. Model Dev., 9, 3751–3777, https://doi.org/10.5194/gmd-9-3751-2016, 2016.

Boucher, O., Servonnat, J., Albright, A. L., Aumont, O., Balkanski, Y., Bastrikov, V., Bekki, S., Bonnet, R., Bony, S., Bopp, L., Braconnot, P., Brockmann, P., Cadule, P., Caubel, A., Cheruy, F., Codron, F., Cozic, A., Cugnet, D., D'Andrea, F., Davini, P., de Lavergne, C., Denvil, S., Deshayes, J., Devilliers, M., Ducharne, A., Dufresne, J.-L., Dupont, E., Éthé, C., Fairhead, L., Falletti, L., Flavoni, S., Foujols, M.-A., Gardoll, S., Gastineau, G., Ghattas, J., Grandpeix, J.-Y., Guenet, B.,

Guez, E., Lionel, Guilyardi, E., Guimberteau, M., Hauglustaine, D., Hourdin, F., Idelkadi, A., Joussaume, S., Kageyama, M., Khodri, M., Krinner, G., Lebas, N., Levavasseur, G., Lévy, C., Li, L., Lott, F., Lurton, T., Luyssaert, S., Madec, G., Madeleine, J.-B., Maignan, F., Marchand, M., Marti, O., Mellul, L., Meurdesoif, Y., Mignot, J., Musat, I., Ottlé, C., Peylin, P., Planton, Y., Polcher, J., Rio, C., Rochetin, N., Rousset, C., Sepulchre, P., Sima, A., Swingedouw, D., Thiéblemont, R., Traore, A. K., Vancoppenolle, M., Vial, J., Vialard, J., Viovy, N., and Vuichard, N.: Presentation and Evaluation of the IPSL-CM6A-LR Climate Model, J. Adv. Model. Earth Syst., 12, e2019MS002010, https://doi.org/10.1029/2019MS002010, 2020.

Bourgeois, T., Goris, N., Schwinger, J., and Tjiputra, J. F.: Stratification constrains future heat and carbon uptake in the Southern Ocean between 30°S and 55°S, Nat. Commun., 13, 340, https://doi.org/10.1038/s41467-022-27979-5, 2022.

Bray, E.: 2017 Minerals Yearbook: Aluminum [Advance Release], Tech. rep., U.S. Geological Survey, https://d9-wret.s3-us-west-2.amazonaws.com/assets/palladium/production/atoms/files/myb1-2017-alumi.pdf, 2020.

Brancalion, P. H. S., Broadbent, E. N., de-Miguel, S., Cardil, A., Rosa, M. R., Almeida, C. T., Almeida, D. R. A., Chakravarty, S., Zhou, M., Gamarra, J. G. P., Liang, J., Crouzeilles, R., Hérault, B., Aragão, L. E. O. C., Silva, C. A., and Almeyda-Zambrano, A. M.: Emerging threats linking tropical deforestation and the COVID-19 pandemic, Perspectives in Ecology and Conservation, 18, 243–246, https://doi.org/10.1016/j.pecon.2020.09.006, 2020.

Brienen, R. J. W., Caldwell, L., Duchesne, L., Voelker, S., Barichivich, J., Baliva, M., Ceccantini, G., Di Filippo, A., Helama, S., Locosselli, G. M., Lopez, L., Piovesan, G., Schöngart, J., Villalba, R., and Gloor, E.: Forest carbon sink neutralized by pervasive growth-lifespan trade-offs, Nat. Commun., 11, 4241, https://doi.org/10.1038/s41467-020-17966-z, 2020.

Brienen, R. J. W., Phillips, O. L., Feldpausch, T. R., Gloor, E., Baker, T. R., Lloyd, J., Lopez-Gonzalez, G., Monteagudo-Mendoza, A., Malhi, Y., Lewis, S. L., Vásquez Martinez, R., Alexiades, M., Álvarez Dávila, E., Alvarez-Loayza, P., Andrade, A., Aragão, L. E. O. C., Araujo-Murakami, A., Arets, E. J. M. M., Arroyo, L., Aymard C., G. A., Bánki, O. S., Baraloto, C., Barroso, J., Bonal, D., Boot, R. G. A., Camargo, J. L. C., Castilho, C. V., Chama, V., Chao, K. J., Chave, J., Comiskey, J. A., Cornejo Valverde, F., da Costa, L., de Oliveira, E. A., Di Fiore, A., Erwin, T. L., Fauset, S., Forsthofer, M., Galbraith, D. R., Grahame, E. S., Groot, N., Hérault, B., Higuchi, N., Honorio Coronado, E. N., Keeling, H., Killeen, T. J., Laurance, W. F., Laurance, S., Licona, J., Magnussen, W. E., Marimon, B. S., Marimon-Junior, B. H., Mendoza, C., Neill, D. A., Nogueira, E. M., Núñez, P., Pallqui Camacho, N. C., Parada, A., Pardo-Molina, G., Peacock, J., Peña-Claros, M., Pickavance, G. C., Pitman, N. C. A., Poorter, L., Prieto, A., Quesada, C. A., Ramírez, F., Ramírez-Angulo, H., Restrepo, Z., Roopsind, A., Rudas, A., Salomão, R. P., Schwarz, M., Silva, N., Silva-Espejo, J. E., Silveira, M., Stropp, J., Talbot, J., ter Steege, H., Teran-Aguilar, J., Terborgh, J., Thomas-Caesar, R., Toledo, M., Torello-Raventos, M., Umetsu, R. K., van der Heijden, G. M. F., van der Hout, P., Guimarães Vieira, I. C., Vieira, S. A., Vilanova, E., Vos, V. A., and Zagt, R. J.: Long-term decline of the Amazon carbon sink, 519, 344–348, https://doi.org/10.1038/nature14283, 2015.

Bronselaer, B., Winton, M., Russell, J., Sabine, C. L., and Khatiwala, S.: Agreement of CMIP5 Simulated and Observed Ocean Anthropogenic CO2 Uptake, Geophys. Res. Lett., 44, 12,298-12,305, https://doi.org/10.1002/2017GL074435, 2017.

Bruno, M. and Joos, F.: Terrestrial carbon storage during the past 200 years: A Monte Carlo Analysis of CO 2 data from ice core and atmospheric measurements, Global Biogeochem. Cycles, 11, 111–124, https://doi.org/10.1029/96GB03611, 1997.

Burrows, S. M., Maltrud, M., Yang, X., Zhu, Q., Jeffery, N., Shi, X., Ricciuto, D., Wang, S., Bisht, G., Tang, J., Wolfe, J., Harrop, B. E., Singh, B., Brent, L., Baldwin, S., Zhou, T., Cameron-Smith, P., Keen, N., Collier, N., Xu, M., Hunke, E. C., Elliott, S. M., Turner, A. K., Li, H., Wang, H., Golaz, J.-C., Bond-Lamberty, B., Hoffman, F. M., Riley, W. J., Thornton, P. E., Calvin, K., and Leung, L. R.: The DOE E3SM v1.1 Biogeochemistry Configuration: Description and Simulated Ecosystem-Climate Responses to Historical Changes in Forcing, J. Adv. Model. Earth Syst., 12, e2019MS001766, https://doi.org/10.1029/2019MS001766, 2020.

Burton, C., Betts, R., Cardoso, M., Feldpausch, T. R., Harper, A., Jones, C. D., Kelley, D. I., Robertson, E., and Wiltshire, A.: Representation of fire, land-use change and vegetation dynamics in the Joint UK Land Environment Simulator vn4.9 (JULES), Geosci. Model Dev., 12, 179–193, https://doi.org/10.5194/gmd-12-179-2019, 2019.

Burton, C. et al.: Global burned area increasingly explained by climate change, *under review*, https://doi.org/10.21203/rs.3.rs-3168150/v1, 2023.

Bushinsky, S. M., Landschützer, P., Rödenbeck, C., Gray, A. R., Baker, D., Mazloff, M. R., Resplandy, L., Johnson, K. S., and Sarmiento, J. L.: Reassessing Southern Ocean Air-Sea CO 2 Flux Estimates With the Addition of Biogeochemical Float Observations, Global Biogeochem. Cycles, 33, 1370–1388, https://doi.org/10.1029/2019GB006176, 2019.

Canadell, J. G., Le Quere, C., Raupach, M. R., Field, C. B., Buitenhuis, E. T., Ciais, P., Conway, T. J., Gillett, N. P., Houghton, R. A., and Marland, G.: Contributions to accelerating atmospheric CO2 growth from economic activity, carbon intensity, and efficiency of natural sinks, Proceedings of the National Academy of Sciences, 104, 18866–18870, https://doi.org/10.1073/pnas.0702737104, 2007.

Canadell, J. G., Monteiro, P. M. S., Costa, M. H., Cotrim da Cunha, L., Cox, P. M., Eliseev, A. V., Henson, S., Ishii, M., Jaccard, S., Koven, C., Lohila, A., Patra, P. K., Piao, S., Rogelj, J., Syampungani, S., Zaehle, S., and Zickfeld, K.: Global Carbon and other Biogeochemical Cycles and Feedbacks. In: Climate Change 2021: The Physical Science Basis. Contribution of Working Group I to the Sixth Assessment Report of the Intergovernmental Panel on Climate Change [Masson-Delmotte, V., P. Zhai, A. Pirani, S. L. Connors, C. Péan, S. Berger, N. Caud, Y. Chen, L. Goldfarb, M. I. Gomis, M. Huang, K. Leitzell, E. Lonnoy, J.B.R. Matthews, T. K. Maycock, T. Waterfield, O. Yelekçi, R. Yu and B. Zhou (eds.)]. Cambridge University Press, Cambridge, United Kingdom and New York, NY, USA, pp. 673–816, doi: 10.1017/9781009157896.007., 2021.

Cao, Z., Myers, R. J., Lupton, R. C., Duan, H., Sacchi, R., Zhou, N., Reed Miller, T., Cullen, J. M., Ge, Q., and Liu, G.: The sponge effect and carbon emission mitigation potentials of the global cement cycle, Nat Commun, 11, 3777, https://doi.org/10.1038/s41467-020-17583-w, 2020.

Céspedes, J., Sylvester, J. M., Pérez-Marulanda, L., Paz-Garcia, P., Reymondin, L., Khodadadi, M., Tello, J. J., and Castro-Nunez, A.: Has global deforestation accelerated due to the COVID-19 pandemic?, J. For. Res., 34, 1153–1165, https://doi.org/10.1007/s11676-022-01561-7, 2023.

Chandra, N., Patra, P. K., Niwa, Y., Ito, A., Iida, Y., Goto, D., Morimoto, S., Kondo, M., Takigawa, M., Hajima, T., and Watanabe, M.: Estimated regional CO2 flux and uncertainty based on an ensemble of atmospheric CO2 inversions, Atmospheric Chem. Phys., 22, 9215–9243, https://doi.org/10.5194/acp-22-9215-2022, 2022.

Chatfield, C.: The Holt-Winters Forecasting Procedure, J. Roy. Stat. Soc. C., 27, 264–279, https://doi.org/10.2307/2347162, 1978.

Chau, T. T. T., Gehlen, M., and Chevallier, F.: A seamless ensemble-based reconstruction of surface ocean pCO_2 and air–sea CO_2 fluxes over the global coastal and open oceans, Biogeosciences, 19, 1087–1109, https://doi.org/10.5194/bg-19-1087-2022, 2022.

Chevallier, F., Fisher, M., Peylin, P., Serrar, S., Bousquet, P., Bréon, F.-M., Chédin, A., and Ciais, P.: Inferring CO 2 sources and sinks from satellite observations: Method and application to TOVS data, J. Geophys. Res., 110, D24309, https://doi.org/10.1029/2005JD006390, 2005.

Ciais, P., Sabine, C., Bala, G., Bopp, L., Brovkin, V., Canadell, J. G., Chhabra, A., DeFries, R., Galloway, J., Heimann, M., Jones, C., Le Quéré, C., Myneni, R., Piao, S., Thornton, P., Willem, J., Friedlingstein, P., and Munhoven, G.: Carbon and Other Biogeochemical Cycles, in Climate Change 2013: The Physical Science Basis, Contribution of Working Group I to the Fifth Assessment Report of the Intergovernmental Panel on Climate Change, edited by: Intergovernmental Panel on Climate Change, Cambridge University Press, Cambridge, United Kingdom and New York, NY, USA. doi:10.1017/CBO9781107415324.015, 2013.

Ciais, P., Tan, J., Wang, X., Roedenbeck, C., Chevallier, F., Piao, S.-L., Moriarty, R., Broquet, G., Le Quéré, C., Canadell, J. G., Peng, S., Poulter, B., Liu, Z., and Tans, P.: Five decades of northern land carbon uptake revealed by the interhemispheric CO2 gradient, Nature, 568, 221–225, https://doi.org/10.1038/s41586-019-1078-6, 2019.

Ciais, P., Bastos, A., Chevallier, F., Lauerwald, R., Poulter, B., Canadell, P., Hugelius, G., Jackson, R. B., Jain, A., Jones, M., Kondo, M., Luijkx, I. T., Patra, P. K., Peters, W., Pongratz, J., Petrescu, A. M. R., Piao, S., Qiu, C., Von Randow, C., Regnier, P., Saunois, M., Scholes, R., Shvidenko, A., Tian, H., Yang, H., Wang, X., and Zheng, B.: Definitions and methods to estimate regional land carbon fluxes for the second phase of the REgional Carbon Cycle Assessment and Processes Project (RECCAP-2), Geosci. Model Dev., 15, 1289–1316, https://doi.org/10.5194/gmd-15-1289-2022, 2022.

Collier, N., Hoffman, F. M., Lawrence, D. M., Keppel-Aleks, G., Koven, C. D., Riley, W. J., Mu, M., and Randerson, J. T.: The International Land Model Benchmarking (ILAMB) System: Design, Theory, and Implementation, J. Adv. Model. Earth Syst., 10, 2731–2754, https://doi.org/10.1029/2018MS001354, 2018.

Cox, P. M., Pearson, D., Booth, B. B., Friedlingstein, P., Huntingford, C., Jones, C. D., and Luke, C. M.: Sensitivity of tropical carbon to climate change constrained by carbon dioxide variability, Nature, 494, 341–344, https://doi.org/10.1038/nature11882, 2013.

De Kauwe, M. G., Medlyn, B. E., Zaehle, S., Walker, A. P., Dietze, M. C., Wang, Y.-P., Luo, Y., Jain, A. K., El-Masri, B., Hickler, T., Wårlind, D., Weng, E., Parton, W. J., Thornton, P. E., Wang, S., Prentice, I. C., Asao, S., Smith, B., McCarthy, H. R., Iversen, C. M., Hanson, P. J., Warren, J. M., Oren, R., and Norby, R. J.: Where does the carbon go? A model–data intercomparison of vegetation carbon allocation and turnover processes at two temperate forest free-air CO2 enrichment sites, New Phytol., 203, 883–899, https://doi.org/10.1111/nph.12847, 2014.

Delire, C., Séférian, R., Decharme, B., Alkama, R., Calvet, J.-C., Carrer, D., Gibelin, A.-L., Joetzjer, E., Morel, X., Rocher, M., and Tzanos, D.: The Global Land Carbon Cycle Simulated With ISBA-CTRIP: Improvements Over the Last Decade, J. Adv. Model. Earth Syst., 12, e2019MS001886, https://doi.org/10.1029/2019MS001886, 2020.

Denman, K. L., Brasseur, G., Chidthaisong, A., Ciais, P., Cox, P. M., Dickinson, R. E., Hauglustaine, D., Heinze, C., Holland, E., Jacob, D., Lohmann, U., Ramachandran, S., Leite da Silva Dias, P., Wofsy, S. C., and Zhang, X.: Couplings Between Changes in the Climate System and Biogeochemistry, in: Climate Change 2007: The Physical Science Basis.

Contribution of Working Group I to the Fourth Assessment Report of the Intergovernmental Panel on Climate Change, edited by: Solomon, S., Qin, D., Manning, M., Marquis, M., Averyt, K., Tignor, M. M. B., Miller, H. L., and Chen, Z. L., Cambridge University Press, Cambridge, UK and New York, USA, 499–587, ISBN: 9780521705967, 2007.

Denvil-Sommer, A., Gehlen, M., and Vrac, M.: Observation system simulation experiments in the Atlantic Ocean for enhanced surface ocean pCO2 reconstructions, Ocean Sci., 17, 1011–1030, https://doi.org/10.5194/os-17-1011-2021, 2021.

DeVries, T., Holzer, M., and Primeau, F.: Recent increase in oceanic carbon uptake driven by weaker upper-ocean overturning, Nature, 542, 215–218, https://doi.org/10.1038/nature21068, 2017.

DeVries, T., Quéré, C. L., Andrews, O., Berthet, S., Hauck, J., Ilyina, T., Landschützer, P., Lenton, A., Lima, I. D., Nowicki, M., Schwinger, J., and Séférian, R.: Decadal trends in the ocean carbon sink, PNAS, 116, 11646–11651, https://doi.org/10.1073/pnas.1900371116, 2019.

DeVries, T., Yamamoto, K., Wanninkhof, R., Gruber, N., Hauck, J., Müller, J. D., Bopp, L., Carroll, D., Carter, B., Chau, T.-T.-T., Doney, S. C., Gehlen, M., Gloege, L., Gregor, L., Henson, S., Kim, J. H., Iida, Y., Ilyina, T., Landschützer, P., Le Quéré, C., Munro, D., Nissen, C., Patara, L., Pérez, F. F., Resplandy, L., Rodgers, K. B., Schwinger, J., Séférian, R., Sicardi, V., Terhaar, J., Triñanes, J., Tsujino, H., Watson, A., Yasunaka, S., and Zeng, J.: Magnitude, trends, and variability of the global ocean carbon sink from 1985-2018, Glob. Biogeochem. Cycles, n/a, e2023GB007780, https://doi.org/10.1029/2023GB007780, 2023.

Forster, P. M., Smith, C. J., Walsh, T., Lamb, W. F., Lamboll, R., Hauser, M., Ribes, A., Rosen, D., Gillett, N., Palmer, M. D., Rogelj, J., von Schuckmann, K., Seneviratne, S. I., Trewin, B., Zhang, X., Allen, M., Andrew, R., Birt, A., Borger, A., Boyer, T., Broersma, J. A., Cheng, L., Dentener, F., Friedlingstein, P., Gutiérrez, J. M., Gütschow, J., Hall, B., Ishii, M., Jenkins, S., Lan, X., Lee, J.-Y., Morice, C., Kadow, C., Kennedy, J., Killick, R., Minx, J. C., Naik, V., Peters, G. P., Pirani, A., Pongratz, J., Schleussner, C.-F., Szopa, S., Thorne, P., Rohde, R., Rojas Corradi, M., Schumacher, D., Vose, R., Zickfeld, K., Masson-Delmotte, V., and Zhai, P.: Indicators of Global Climate Change 2022: annual update of large-scale indicators of the state of the climate system and human influence, Earth Syst. Sci. Data, 15, 2295–2327, https://doi.org/10.5194/essd-15-2295-2023, 2023.

Doney, S. C., Lima, I., Feely, R. A., Glover, D. M., Lindsay, K., Mahowald, N., Moore, J. K., and Wanninkhof, R.: Mechanisms governing interannual variability in upper-ocean inorganic carbon system and air–sea CO2 fluxes: Physical climate and atmospheric dust, Deep Sea Research Part II: Topical Studies in Oceanography, 56, 640–655, https://doi.org/10.1016/j.dsr2.2008.12.006, 2009.

Dong, Y., Bakker, D. C. E., Bell, T. G., Huang, B., Landschützer, P., Liss, P. S., and Yang, M.: Update on the Temperature Corrections of Global Air-Sea CO2 Flux Estimates, Glob. Biogeochem. Cycles, 36, e2022GB007360, https://doi.org/10.1029/2022GB007360, 2022.

Dou, X., Wang, Y., Ciais, P., Chevallier, F., Davis, S. J., Crippa, M., Janssens-Maenhout, G., Guizzardi, D., Solazzo, E., Yan, F., Huo, D., Zheng, B., Zhu, B., Cui, D., Ke, P., Sun, T., Wang, H., Zhang, Q., Gentine, P., Deng, Z., and Liu, Z.: Near-real-time global gridded daily CO2 emissions, The Innovation, 3, 100182, https://doi.org/10.1016/j.xinn.2021.100182, 2022.

Edson, J. B., Jampana, V., Weller, R. A., Bigorre, S. P., Plueddemann, A. J., Fairall, C. W., Miller, S. D., Mahrt, L., Vickers, D., and Hersbach, H.: On the Exchange of Momentum over the Open Ocean, J. Phys. Oceanogr., 43, 1589–1610, https://doi.org/10.1175/JPO-D-12-0173.1, 2013.

EIA. Short-Term Energy Outlook: September 2023. U.S. Energy Information Administration. Available at: http://www.eia.gov/forecasts/steo/outlook.cfm, last access: 9 November 2023, 2023.

Erb, K.-H., Kastner, T., Luyssaert, S., Houghton, R. A., Kuemmerle, T., Olofsson, P., and Haberl, H.: Bias in the attribution of forest carbon sinks, Nature Clim Change, 3, 854–856, https://doi.org/10.1038/nclimate2004, 2013.

Erb, K.-H., Kastner, T., Plutzar, C., Bais, A. L. S., Carvalhais, N., Fetzel, T., Gingrich, S., Haberl, H., Lauk, C., Niedertscheider, M., Pongratz, J., Thurner, M., and Luyssaert, S.: Unexpectedly large impact of forest management and grazing on global vegetation biomass, Nature, 553, 73–76, https://doi.org/10.1038/nature25138, 2018.

Eskander, S. M. S. U. and Fankhauser, S.: Reduction in greenhouse gas emissions from national climate legislation, Nat. Clim. Chang., 10, 750–756, https://doi.org/10.1038/s41558-020-0831-z, 2020.

Etheridge, D. M., Steele, L. P., Langenfelds, R. L., Francey, R. J., Barnola, J.-M., and Morgan, V. I.: Natural and anthropogenic changes in atmospheric CO 2 over the last 1000 years from air in Antarctic ice and firn, J. Geophys. Res., 101, 4115–4128, https://doi.org/10.1029/95JD03410, 1996.

Eyring, V., Bony, S., Meehl, G. A., Senior, C. A., Stevens, B., Stouffer, R. J., and Taylor, K. E.: Overview of the Coupled Model Intercomparison Project Phase 6 (CMIP6) experimental design and organization, Geosci. Model Dev., 9, 1937–1958, https://doi.org/10.5194/gmd-9-1937-2016, 2016.

FAO, Impact of the Ukraine-Russia conflict on global food security and related matters under the mandate of the Food and Agriculture Organization of the United Nations (FAO), Hundred and Seventieth Session of the Council, https://www.fao.org/3/nj164en/nj164en.pdf, last access: 9 November 2023, 2023.

Fay, A. R., Gregor, L., Landschützer, P., McKinley, G. A., Gruber, N., Gehlen, M., Iida, Y., Laruelle, G. G., Rödenbeck, C., Roobaert, A., and Zeng, J.: SeaFlux: harmonization of air–sea CO2 fluxes from surface pCO2 data products using a standardized approach, Earth System Science Data, 13, 4693–4710, https://doi.org/10.5194/essd-13-4693-2021, 2021.

Feng, L., Palmer, P. I., Bösch, H., and Dance, S.: Estimating surface CO2 fluxes from space-borne CO2 dry air mole fraction observations using an ensemble Kalman Filter, Atmospheric Chem. Phys., 9, 2619–2633, https://doi.org/10.5194/acp-9-2619-2009, 2009.

Feng, L., Palmer, P. I., Parker, R. J., Deutscher, N. M., Feist, D. G., Kivi, R., Morino, I., and Sussmann, R.: Estimates of European uptake of CO2 inferred from GOSAT XCO2 retrievals: sensitivity to measurement bias inside and outside Europe, Atmos. Chem. Phys., 16, 1289–1302, https://doi.org/10.5194/acp-16-1289-2016, 2016.

Flanagan, D.: 2017 Minerals Yearbook: Copper [Advance Release], Tech. rep., U.S. Geological Survey, https://pubs.usgs.gov/myb/vol1/2017/myb1-2017-copper.pdf, 2021.

Friedlingstein, P., Houghton, R. A., Marland, G., Hackler, J., Boden, T. A., Conway, T. J., Canadell, J. G., Raupach, M. R., Ciais, P., and Le Quéré, C.: Update on CO2 emissions, Nature Geosci, 3, 811–812, https://doi.org/10.1038/ngeo1022, 2010.

Friedlingstein, P., Andrew, R. M., Rogelj, J., Peters, G. P., Canadell, J. G., Knutti, R., Luderer, G., Raupach, M. R., Schaeffer, M., van Vuuren, D. P., and Le Quéré, C.: Persistent growth of CO2 emissions and implications for reaching climate targets, Nature Geosci, 7, 709–715, https://doi.org/10.1038/ngeo2248, 2014.

Friedlingstein, P., Jones, M. W., O'Sullivan, M., Andrew, R. M., Hauck, J., Peters, G. P., Peters, W., Pongratz, J., Sitch, S., Le Quéré, C., Bakker, D. C. E., Canadell, J. G., Ciais, P., Jackson, R. B., Anthoni, P., Barbero, L., Bastos, A., Bastrikov, V., Becker, M., Bopp, L., Buitenhuis, E., Chandra, N., Chevallier, F., Chini, L. P., Currie, K. I., Feely, R. A., Gehlen, M., Gilfillan, D., Gkritzalis, T., Goll, D. S., Gruber, N., Gutekunst, S., Harris, I., Haverd, V., Houghton, R. A., Hurtt, G., Ilyina, T., Jain, A. K., Joetzjer, E., Kaplan, J. O., Kato, E., Klein Goldewijk, K., Korsbakken, J. I., Landschützer, P., Lauvset, S. K., Lefèvre, N., Lenton, A., Lienert, S., Lombardozzi, D., Marland, G., McGuire, P. C., Melton, J. R., Metzl, N., Munro, D. R., Nabel, J. E. M. S., Nakaoka, S.-I., Neill, C., Omar, A. M., Ono, T., Peregon, A., Pierrot, D., Poulter, B., Rehder, G., Resplandy, L., Robertson, E., Rödenbeck, C., Séférian, R., Schwinger, J., Smith, N., Tans, P. P., Tian, H., Tilbrook, B., Tubiello, F. N., van der Werf, G. R., Wiltshire, A. J., and Zaehle, S.: Global Carbon Budget 2019, Earth Syst. Sci. Data, 11, 1783–1838, https://doi.org/10.5194/essd-11-1783-2019, 2019.

Friedlingstein, P., O'Sullivan, M., Jones, M. W., Andrew, R. M., Hauck, J., Olsen, A., Peters, G. P., Peters, W., Pongratz, J., Sitch, S., Le Quéré, C., Canadell, J. G., Ciais, P., Jackson, R. B., Alin, S., Aragão, L. E. O. C., Arneth, A., Arora, V., Bates, N. R., Becker, M., Benoit-Cattin, A., Bittig, H. C., Bopp, L., Bultan, S., Chandra, N., Chevallier, F., Chini, L. P., Evans, W., Florentie, L., Forster, P. M., Gasser, T., Gehlen, M., Gilfillan, D., Gkritzalis, T., Gregor, L., Gruber, N., Harris, I., Hartung, K., Haverd, V., Houghton, R. A., Ilyina, T., Jain, A. K., Joetzjer, E., Kadono, K., Kato, E., Kitidis, V., Korsbakken, J. I., Landschützer, P., Lefèvre, N., Lenton, A., Lienert, S., Liu, Z., Lombardozzi, D., Marland, G., Metzl, N., Munro, D. R., Nabel, J. E. M. S., Nakaoka, S.-I., Niwa, Y., O'Brien, K., Ono, T., Palmer, P. I., Pierrot, D., Poulter, B., Resplandy, L., Robertson, E., Rödenbeck, C., Schwinger, J., Séférian, R., Skjelvan, I., Smith, A. J. P., Sutton, A. J., Tanhua, T., Tans, P. P., Tian, H., Tilbrook, B., van der Werf, G., Vuichard, N., Walker, A. P., Wanninkhof, R., Watson, A. J., Willis, D., Wiltshire, A. J., Yuan, W., Yue, X., and Zaehle, S.: Global Carbon Budget 2020, Earth Syst. Sci. Data, 12, 3269–3340, https://doi.org/10.5194/essd-12-3269-2020, 2020.

Friedlingstein, P., Jones, M. W., O'Sullivan, M., Andrew, R. M., Bakker, D. C. E., Hauck, J., Le Quéré, C., Peters, G. P., Peters, W., Pongratz, J., Sitch, S., Canadell, J. G., Ciais, P., Jackson, R. B., Alin, S. R., Anthoni, P., Bates, N. R., Becker, M., Bellouin, N., Bopp, L., Chau, T. T. T., Chevallier, F., Chini, L. P., Cronin, M., Currie, K. I., Decharme, B., Djeutchouang, L. M., Dou, X., Evans, W., Feely, R. A., Feng, L., Gasser, T., Gilfillan, D., Gkritzalis, T., Grassi, G., Gregor, L., Gruber, N., Gürses, Ö., Harris, I., Houghton, R. A., Hurtt, G. C., Iida, Y., Ilyina, T., Luijkx, I. T., Jain, A., Jones, S. D., Kato, E., Kennedy, D., Klein Goldewijk, K., Knauer, J., Korsbakken, J. I., Körtzinger, A., Landschützer, P., Lauvset, S. K., Lefèvre, N., Lienert, S., Liu, J., Marland, G., McGuire, P. C., Melton, J. R., Munro, D. R., Nabel, J. E. M. S., Nakaoka, S.-I., Niwa, Y., Ono, T., Pierrot, D., Poulter, B., Rehder, G., Resplandy, L., Robertson, E., Rödenbeck, C., Rosan, T. M., Schwinger, J., Schwingshackl, C., Séférian, R., Sutton, A. J., Sweeney, C., Tanhua, T., Tans, P. P., Tian, H., Tilbrook, B., Tubiello, F., van der Werf, G. R., Vuichard, N., Wada, C., Wanninkhof, R., Watson, A. J., Willis, D., Wiltshire, A. J., Yuan, W., Yue, C., Yue, X., Zaehle, S., and Zeng, J.: Global Carbon Budget 2021, Earth Syst. Sci. Data, 14, 1917–2005, https://doi.org/10.5194/essd-14-1917-2022, 2022a.

Friedlingstein, P. and co-authors of the current study, Supplemental data of the Global Carbon Budget 2023, ICOS-ERIC Carbon Portal, https://doi.org/10.18160/GCP-2023, 2023.

Friedlingstein, P., O'Sullivan, M., Jones, M. W., Andrew, R. M., Gregor, L., Hauck, J., Le Quéré, C., Luijkx, I. T., Olsen, A., Peters, G. P., Peters, W., Pongratz, J., Schwingshackl, C., Sitch, S., Canadell, J. G., Ciais, P., Jackson, R. B., Alin, S. R.,

Alkama, R., Arneth, A., Arora, V. K., Bates, N. R., Becker, M., Bellouin, N., Bittig, H. C., Bopp, L., Chevallier, F., Chini, L. P., Cronin, M., Evans, W., Falk, S., Feely, R. A., Gasser, T., Gehlen, M., Gkritzalis, T., Gloege, L., Grassi, G., Gruber, N., Gürses, Ö., Harris, I., Hefner, M., Houghton, R. A., Hurtt, G. C., Iida, Y., Ilyina, T., Jain, A. K., Jersild, A., Kadono, K., Kato, E., Kennedy, D., Klein Goldewijk, K., Knauer, J., Korsbakken, J. I., Landschützer, P., Lefèvre, N., Lindsay, K., Liu, J., Liu, Z., Marland, G., Mayot, N., McGrath, M. J., Metzl, N., Monacci, N. M., Munro, D. R., Nakaoka, S.-I., Niwa, Y., O'Brien, K., Ono, T., Palmer, P. I., Pan, N., Pierrot, D., Pocock, K., Poulter, B., Resplandy, L., Robertson, E., Rödenbeck, C., Rodriguez, C., Rosan, T. M., Schwinger, J., Séférian, R., Shutler, J. D., Skjelvan, I., Steinhoff, T., Sun, Q., Sutton, A. J., Sweeney, C., Takao, S., Tanhua, T., Tans, P. P., Tian, X., Tian, H., Tilbrook, B., Tsujino, H., Tubiello, F., van der Werf, G. R., Walker, A. P., Wanninkhof, R., Whitehead, C., Willstrand Wranne, A., et al.: Global Carbon Budget 2022, Earth Syst. Sci. Data, 14, 4811–4900, https://doi.org/10.5194/essd-14-4811-2022, 2022b.

Ganzenmüller, R., Bultan, S., Winkler, K., Fuchs, R., Zabel, F., and Pongratz, J.: Land-use change emissions based on high-resolution activity data substantially lower than previously estimated, Environ. Res. Lett., 17, 064050, https://doi.org/10.1088/1748-9326/ac70d8, 2022.

Gasser, T., Crepin, L., Quilcaille, Y., Houghton, R. A., Ciais, P., and Obersteiner, M.: Historical CO2 emissions from land use and land cover change and their uncertainty, Biogeosciences, 17, 4075–4101, https://doi.org/10.5194/bg-17-4075-2020, 2020.

Gaubert, B., Stephens, B. B., Basu, S., Chevallier, F., Deng, F., Kort, E. A., Patra, P. K., Peters, W., Rödenbeck, C., Saeki, T., Schimel, D., Van der Laan-Luijkx, I., Wofsy, S., and Yin, Y.: Global atmospheric CO2 inverse models converging on neutral tropical land exchange, but disagreeing on fossil fuel and atmospheric growth rate, Biogeosciences, 16, 117–134, https://doi.org/10.5194/bg-16-117-2019, 2019.

GCP: The Global Carbon Budget 2007, available at: http://www. globalcarbonproject.org/carbonbudget/archive.htm, last access: 9 November 2023, 2007.

Giglio, L., Schroeder, W., and Justice, C. O.: The collection 6 MODIS active fire detection algorithm and fire products, Remote Sensing of Environment, 178, 31–41, https://doi.org/10.1016/j.rse.2016.02.054, 2016.

Gloege, L., McKinley, G. A., Landschützer, P., Fay, A. R., Frölicher, T. L., Fyfe, J. C., Ilyina, T., Jones, S., Lovenduski, N. S., Rodgers, K. B., Schlunegger, S., and Takano, Y.: Quantifying Errors in Observationally Based Estimates of Ocean Carbon Sink Variability, Global Biogeochem. Cy., 35, e2020GB006788, https://doi.org/10.1029/2020GB006788, 2021.

Gloege, L., Yan, M., Zheng, T., and McKinley, G. A.: Improved Quantification of Ocean Carbon Uptake by Using Machine Learning to Merge Global Models and pCO2 Data, J. Adv. Model. Earth Syst., 14, e2021MS002620, https://doi.org/10.1029/2021MS002620, 2022.

Golar, G., Malik, A., Muis, H., Herman, A., Nurudin, N., and Lukman, L.: The social-economic impact of COVID-19 pandemic: implications for potential forest degradation, Heliyon, 6, e05354, https://doi.org/10.1016/j.heliyon.2020.e05354, 2020.

Goris, N., Tjiputra, J. F., Olsen, A., Schwinger, J., Lauvset, S. K., and Jeansson, E.: Constraining Projection-Based Estimates of the Future North Atlantic Carbon Uptake, J. Clim., 31, 3959–3978, https://doi.org/10.1175/JCLI-D-17-0564.1, 2018.

Grassi, G., House, J., Kurz, W. A., Cescatti, A., Houghton, R. A., Peters, G. P., Sanz, M. J., Viñas, R. A., Alkama, R., Arneth, A., Bondeau, A., Dentener, F., Fader, M., Federici, S., Friedlingstein, P., Jain, A. K., Kato, E., Koven, C. D., Lee,

D., Nabel, J. E. M. S., Nassikas, A. A., Perugini, L., Rossi, S., Sitch, S., Viovy, N., Wiltshire, A., and Zaehle, S.: Reconciling global-model estimates and country reporting of anthropogenic forest CO2 sinks, Nature Clim Change, 8, 914–920, https://doi.org/10.1038/s41558-018-0283-x, 2018.

Grassi, G., Stehfest, E., Rogelj, J., van Vuuren, D., Cescatti, A., House, J., Nabuurs, G.-J., Rossi, S., Alkama, R., Viñas, R. A., Calvin, K., Ceccherini, G., Federici, S., Fujimori, S., Gusti, M., Hasegawa, T., Havlik, P., Humpenöder, F., Korosuo, A., Perugini, L., Tubiello, F. N., and Popp, A.: Critical adjustment of land mitigation pathways for assessing countries' climate progress, Nat. Clim. Chang., 11, 425–434, https://doi.org/10.1038/s41558-021-01033-6, 2021.

Grassi, G., Schwingshackl, C., Gasser, T., Houghton, R. A., Sitch, S., Canadell, J. G., Cescatti, A., Ciais, P., Federici, S., Friedlingstein, P., Kurz, W. A., Sanz Sanchez, M. J., Abad Viñas, R., Alkama, R., Bultan, S., Ceccherini, G., Falk, S., Kato, E., Kennedy, D., Knauer, J., Korosuo, A., Melo, J., McGrath, M. J., Nabel, J. E. M. S., Poulter, B., Romanovskaya, A. A., Rossi, S., Tian, H., Walker, A. P., Yuan, W., Yue, X., and Pongratz, J.: Harmonising the land-use flux estimates of global models and national inventories for 2000–2020, Earth Syst. Sci. Data, 15, 1093–1114, https://doi.org/10.5194/essd-15-1093-2023, 2023.

Gregor, L. and Gruber, N.: OceanSODA-ETHZ: a global gridded data set of the surface ocean carbonate system for seasonal to decadal studies of ocean acidification, 13, 777–808, https://doi.org/10.5194/essd-13-777-2021, 2021.

Gruber, N., Bakker, D. C. E., DeVries, T., Gregor, L., Hauck, J., Landschützer, P., McKinley, G. A., and Müller, J. D.: Trends and variability in the ocean carbon sink, Nat. Rev. Earth Environ., 4, 119–134, https://doi.org/10.1038/s43017-022-00381-x, 2023.

Gruber, N., Clement, D., Carter, B. R., Feely, R. A., van Heuven, S., Hoppema, M., Ishii, M., Key, R. M., Kozyr, A., Lauvset, S. K., Lo Monaco, C., Mathis, J. T., Murata, A., Olsen, A., Perez, F. F., Sabine, C. L., Tanhua, T., and Wanninkhof, R.: The oceanic sink for anthropogenic CO2 from 1994 to 2007, 363, 1193–1199, https://doi.org/10.1126/science.aau5153, 2019.

Guan, D., Liu, Z., Geng, Y., Lindner, S., and Hubacek, K.: The gigatonne gap in China's carbon dioxide inventories, Nature Clim Change, 2, 672–675, https://doi.org/10.1038/nclimate1560, 2012.

Gulev, S. K., Thorne, P. W., Ahn, J., Dentener, F. J., Domingues, C. M., Gerland, S., Gong, D. S., Kaufman, S., Nnamchi, H. C., Quaas, J., Rivera, J. A., Sathyendranath, S., Smith, S. L., Trewin, B., von Shuckmann, K., and Vose, R. S.: Changing State of the Climate System. In: Climate Change 2021: The Physical Science Basis. Contribution of Working Group I to the Sixth Assessment Report of the Intergovernmental Panel on Climate Change [Masson-Delmotte, V., Zhai, P., Pirani, A., Connors, S. L., Péan, C., Berger, S., Caud, N., Chen, Y., Goldfarb, L., Gomis, M. I., Huang, M., Leitzell, K., Lonnoy, E., Matthews, J.B.R., Maycock, T.K., Waterfield, T., Yelekçi, O., Yu, R. and Zhou, B. (eds.)]. Cambridge University Press, Cambridge, United Kingdom and New York, NY, USA, pp. 287–422, doi:10.1017/9781009157896.004, 2021.

Guo, R., Wang, J., Bing, L., Tong, D., Ciais, P., Davis, S. J., Andrew, R. M., Xi, F., and Liu, Z.: Global CO2 uptake by cement from 1930 to 2019, 13, 1791–1805, https://doi.org/10.5194/essd-13-1791-2021, 2021.

Gürses, Ö., Oziel, L., Karakuş, O., Sidorenko, D., Völker, C., Ye, Y., Zeising, M., Butzin, M., and Hauck, J.: Ocean biogeochemistry in the coupled ocean–sea ice–biogeochemistry model FESOM2.1–REcoM3, Geosci. Model Dev., 16, 4883–4936, https://doi.org/10.5194/gmd-16-4883-2023, 2023.

Gütschow, J., Jeffery, M. L., Gieseke, R., Gebel, R., Stevens, D., Krapp, M., and Rocha, M.: The PRIMAP-hist national historical emissions time series, 8, 571–603, https://doi.org/10.5194/essd-8-571-2016, 2016.

Gütschow, J., and Pflüger, M. (2023): The PRIMAP-hist national historical emissions time series v2.4.2 (1750-2021) [dataset]. https://doi.org/10.5281/zenodo.7727475, 2023.

Hall, B. D., Crotwell, A. M., Kitzis, D. R., Mefford, T., Miller, B. R., Schibig, M. F., and Tans, P. P.: Revision of the World Meteorological Organization Global Atmosphere Watch (WMO/GAW) CO2 calibration scale, 14, 3015–3032, https://doi.org/10.5194/amt-14-3015-2021, 2021.

Hansis, E., Davis, S. J., and Pongratz, J.: Relevance of methodological choices for accounting of land use change carbon fluxes, Global Biogeochem. Cycles, 29, 1230–1246, https://doi.org/10.1002/2014GB004997, 2015.

Hauck, J., Nissen, C., Landschützer, P., Rödenbeck, C., Bushinsky, S., and Olsen, A.: Sparse observations induce large biases in estimates of the global ocean CO2 sink: an ocean model subsampling experiment, Philos. Trans. R. Soc. Math. Phys. Eng. Sci., 381, 20220063, https://doi.org/10.1098/rsta.2022.0063, 2023.

Hauck, J., Zeising, M., Le Quéré, C., Gruber, N., Bakker, D. C. E., Bopp, L., Chau, T. T. T., Gürses, Ö., Ilyina, T., Landschützer, P., Lenton, A., Resplandy, L., Rödenbeck, C., Schwinger, J., and Séférian, R.: Consistency and Challenges in the Ocean Carbon Sink Estimate for the Global Carbon Budget, Front. Mar. Sci., 7, 571720, https://doi.org/10.3389/fmars.2020.571720, 2020.

Haverd, V., Smith, B., Nieradzik, L., Briggs, P. R., Woodgate, W., Trudinger, C. M., Canadell, J. G., and Cuntz, M.: A new version of the CABLE land surface model (Subversion revision r4601) incorporating land use and land cover change, woody vegetation demography, and a novel optimisation-based approach to plant coordination of photosynthesis, Geosci. Model Dev., 11, 2995–3026, https://doi.org/10.5194/gmd-11-2995-2018, 2018.

Heinke, J., Rolinski, S., and Müller, C.: Modelling the role of livestock grazing in C and N cycling in grasslands with LPJmL5.0-grazing, Geosci. Model Dev., 16, 2455–2475, https://doi.org/10.5194/gmd-16-2455-2023, 2023.

Hefner, M., Marland, G., Boden, T., Andres, R.: Global, Regional, and National Fossil-Fuel CO2 Emissions: 1751-2020 CDIAC-FF [dataset], available at: https://energy.appstate.edu/cdiac-appstate/data-products, last access: 9 November 2023, 2023.

Hickler, T., Smith, B., Prentice, I. C., Mjöfors, K., Miller, P., Arneth, A., and Sykes, M. T.: CO2 fertilization in temperate FACE experiments not representative of boreal and tropical forests, Glob. Change Biol., 14, 1531–1542, https://doi.org/10.1111/j.1365-2486.2008.01598.x, 2008.

Hoesly, R. M., Smith, S. J., Feng, L., Klimont, Z., Janssens-Maenhout, G., Pitkanen, T., Seibert, J. J., Vu, L., Andres, R. J., Bolt, R. M., Bond, T. C., Dawidowski, L., Kholod, N., Kurokawa, J., Li, M., Liu, L., Lu, Z., Moura, M. C. P., O'Rourke, P. R., and Zhang, Q.: Historical (1750–2014) anthropogenic emissions of reactive gases and aerosols from the Community Emissions Data System (CEDS), Geosci. Model Dev., 11, 369–408, https://doi.org/10.5194/gmd-11-369-2018, 2018.

Hong, C., Burney, J. A., Pongratz, J., Nabel, J. E. M. S., Mueller, N. D., Jackson, R. B., and Davis, S. J.: Global and regional drivers of land-use emissions in 1961–2017, Nature, 589, 554–561, https://doi.org/10.1038/s41586-020-03138-y, 2021.

Holding, T., Ashton, I. G., Shutler, J. D., Land, P. E., Nightingale, P. D., Rees, A. P., Brown, I., Piolle, J.-F., Kock, A., Bange, H. W., Woolf, D. K., Goddijn-Murphy, L., Pereira, R., Paul, F., Girard-Ardhuin, F., Chapron, B., Rehder, G., Ardhuin, F., and Donlon, C. J.: The FluxEngine air–sea gas flux toolbox: simplified interface and extensions for in situ analyses and multiple sparingly soluble gases, Ocean Sci., 15, 1707–1728, https://doi.org/10.5194/os-15-1707-2019, 2019.

Houghton, R. A. and Castanho, A.: Annual emissions of carbon from land use, land-use change, and forestry from 1850 to 2020, Earth Syst. Sci. Data, 15, 2025–2054, https://doi.org/10.5194/essd-15-2025-2023, 2023.

Houghton, R. A., House, J. I., Pongratz, J., van der Werf, G. R., DeFries, R. S., Hansen, M. C., Le Quéré, C., and Ramankutty, N.: Carbon emissions from land use and land-cover change, Biogeosciences, 9, 5125–5142, https://doi.org/10.5194/bg-9-5125-2012, 2012.

Huang, B., Thorne, P. W., Banzon, V. F., Boyer, T., Chepurin, G., Lawrimore, J. H., Menne, M. J., Smith, T. M., Vose, R. S., and Zhang, H.-M.: NOAA Extended Reconstructed Sea Surface Temperature (ERSST), Version 5, https://doi.org/10.7289/V5T72FNM, 2017.

Hubau, W., Lewis, S.L., Phillips, O.L., Affum-Baffoe, K., Beeckman, H., Cuní-Sanchez, A., Daniels, A.K., Ewango, C.E.N., Fauset, S., Mukinzi, J.M., Sheil, D., Sonké, B., Sullivan, M.J.P., Sunderland, T.C.H., Taedoumg, H., Thomas, S.C., White, L.J.T., Abernethy, K.A., Adu-Bredu, S., Amani, C.A., Baker, T.R., Banin, L.F., Baya, F., Begne, S.K., Bennett, A.C., Benedet, F., Bitariho, R., Bocko, Y.E., Boeckx, P., Boundja, P., Brienen, R.J.W., Brncic, T., Chezeaux, E., Chuyong, G.B., Clark, C.J., Collins, M., Comiskey, J.A., Coomes, D.A., Dargie, G.C., de Haulleville, T., Kamdem, M.N.D., Doucet, J.-L., Esquivel-Muelbert, A., Feldpausch, T.R., Fofanah, A., Foli, E.G., Gilpin, M., Gloor, E., Gonmadje, C., Gourlet-Fleury, S., Hall, J.S., Hamilton, A.C., Harris, D.J., Hart, T.B., Hockemba, M.B.N., Hladik, A., Ifo, S.A., Jeffery, K.J., Jucker, T., Yakusu, E.K., Kearsley, E., Kenfack, D., Koch, A., Leal, M.E., Levesley, A., Lindsell, J.A., Lisingo, J., Lopez-Gonzalez, G., Lovett, J.C., Makana, J.-R., Malhi, Y., Marshall, A.R., Martin, J., Martin, E.H., Mbayu, F.M., Medjibe, V.P., Mihindou, V., Mitchard, E.T.A., Moore, S., Munishi, P.K.T., Bengone, N.N., Ojo, L., Ondo, F.E., Peh, K.S.-H., Pickavance, G.C., Poulsen, A.D., Poulsen, J.R., Qie, L., Reitsma, J., Rovero, F., Swaine, M.D., Talbot, J., Taplin, J., Taylor, D.M., Thomas, D.W., Toirambe, B., Mukendi, J.T., Tuagben, D., Umunay, P.M., van der Heijden, G.M.F., Verbeeck, H., Vleminckx, J., Willcock, S., Wöll, H., Woods, J.T., Zemagho, L.: Asynchronous carbon sink saturation in African and Amazonian tropical forests, Nature, 579, 80–87, https://doi.org/10.1038/s41586-020-2035-0, 2020.

Humphrey, V., Zscheischler, J., Ciais, P., Gudmundsson, L., Sitch, S., and Seneviratne, S. I.: Sensitivity of atmospheric CO2 growth rate to observed changes in terrestrial water storage, Nature, 560, 628–631, https://doi.org/10.1038/s41586-018-0424-4, 2018.

Humphrey, V., Berg, A., Ciais, P., Gentine, P., Jung, M., Reichstein, M., Seneviratne, S. I., and Frankenberg, C.: Soil moisture–atmosphere feedback dominates land carbon uptake variability, Nature, 592, 65–69, https://doi.org/10.1038/s41586-021-03325-5, 2021.

Huntzinger, D. N., Michalak, A. M., Schwalm, C., Ciais, P., King, A. W., Fang, Y., Schaefer, K., Wei, Y., Cook, R. B., Fisher, J. B., Hayes, D., Huang, M., Ito, A., Jain, A. K., Lei, H., Lu, C., Maignan, F., Mao, J., Parazoo, N., Peng, S., Poulter, B., Ricciuto, D., Shi, X., Tian, H., Wang, W., Zeng, N., and Zhao, F.: Uncertainty in the response of terrestrial carbon sink to environmental drivers undermines carbon-climate feedback predictions, Sci Rep, 7, 4765, https://doi.org/10.1038/s41598-017-03818-2, 2017.

Iida, Y., Takatani, Y., Kojima, A., and Ishii, M.: Global trends of ocean CO2 sink and ocean acidification: an observation-based reconstruction of surface ocean inorganic carbon variables, J Oceanogr, 77, 323–358, https://doi.org/10.1007/s10872-020-00571-5, 2021.

Ilyina, T., Li, H., Spring, A., Müller, W. A., Bopp, L., Chikamoto, M. O., Danabasoglu, G., Dobrynin, M., Dunne, J., Fransner, F., Friedlingstein, P., Lee, W., Lovenduski, N. S., Merryfield, W. j., Mignot, J., Park, J. y., Séférian, R., Sospedra-Alfonso, R., Watanabe, M., and Yeager, S.: Predictable Variations of the Carbon Sinks and Atmospheric CO2 Growth in a Multi-Model Framework, Geophys. Res. Lett., 48, e2020GL090695, https://doi.org/10.1029/2020GL090695, 2021.

IMF: International Monetary Fund: World Economic Outlook, available at: http://www.imf.org, last access: 9 November 2023, 2023.

IPCC: Annex II: Glossary [Möller, V, J.B.R. Matthews, R. van Diemen, C. Méndez, S. Semenov, J.S. Fuglestvedt, A. Reisinger (eds.)]. In: Climate Change 2022: Impacts, Adaptation, and Vulnerability. Contribution of Working Group II to the Sixth Assessment Report of the Intergovernmental Panel on Climate Change [H.-O. Pörtner, D.C. Roberts, M. Tignor, E.S. Poloczanska, K. Mintenbeck, A. Alegría, M. Craig, S. Langsdorf, S. Löschke, V. Möller, A. Okem, B. Rama (eds.)], in: Climate Change 2022 – Impacts, Adaptation and Vulnerability: Working Group II Contribution to the Sixth Assessment Report of the Intergovernmental Panel on Climate Change [Möller, V, J.B.R. Matthews, R. van Diemen, C. Méndez, S. Semenov, J.S. Fuglestvedt, A. Reisinger (eds.)], Cambridge University Press, Cambridge, UK and New York, NY, 2897–2930, https://doi.org/10.1017/9781009325844.029, 2023.

Ito, A. and Inatomi, M.: Use of a process-based model for assessing the methane budgets of global terrestrial ecosystems and evaluation of uncertainty, 9, 759–773, https://doi.org/10.5194/bg-9-759-2012, 2012.

Jackson, R. B., Canadell, J. G., Le Quéré, C., Andrew, R. M., Korsbakken, J. I., Peters, G. P., and Nakicenovic, N.: Reaching peak emissions, Nature Clim Change, 6, 7–10, https://doi.org/10.1038/nclimate2892, 2016.

Jackson, R. B., Le Quéré, C., Andrew, R. M., Canadell, J. G., Korsbakken, J. I., Liu, Z., Peters, G. P., and Zheng, B.: Global energy growth is outpacing decarbonization, Environ. Res. Lett., 13, 120401, https://doi.org/10.1088/1748-9326/aaf303, 2018.

Jackson, R. B., Friedlingstein, P., Andrew, R. M., Canadell, J. G., Le Quéré, C., and Peters, G. P.: Persistent fossil fuel growth threatens the Paris Agreement and planetary health, Environ. Res. Lett., 14, 121001, https://doi.org/10.1088/1748-9326/ab57b3, 2019.

Jackson, R. B., Friedlingstein, P., Quéré, C. L., Abernethy, S., Andrew, R. M., Canadell, J. G., Ciais, P., Davis, S. J., Deng, Z., Liu, Z., Korsbakken, J. I., and Peters, G. P.: Global fossil carbon emissions rebound near pre-COVID-19 levels, Environ. Res. Lett., 17, 031001, https://doi.org/10.1088/1748-9326/ac55b6, 2022.

Jacobson, A. R., Schuldt, K. N., Tans, P., Arlyn Andrews, Miller, J. B., Oda, T., Mund, J., Weir, B., Ott, L., Aalto, T., Abshire, J. B., Aikin, K., Aoki, S., Apadula, F., Arnold, S., Baier, B., Bartyzel, J., Beyersdorf, A., Biermann, T., Biraud, S. C., Boenisch, H., Brailsford, G., Brand, W. A., Chen, G., Huilin Chen, Lukasz Chmura, Clark, S., Colomb, A., Commane, R., Conil, S., Couret, C., Cox, A., Cristofanelli, P., Cuevas, E., Curcoll, R., Daube, B., Davis, K. J., De Wekker, S., Coletta, J. D., Delmotte, M., DiGangi, E., DiGangi, J. P., Di Sarra, A. G., Dlugokencky, E., Elkins, J. W., Emmenegger, L., Shuangxi Fang, Fischer, M. L., Forster, G., Frumau, A., Galkowski, M., Gatti, L. V., Gehrlein, T., Gerbig, C., Francois Gheusi, Gloor,

E., Gomez-Trueba, V., Goto, D., Griffis, T., Hammer, S., Hanson, C., Haszpra, L., Hatakka, J., Heimann, M., Heliasz, M., Hensen, A., Hermansen, O., Hintsa, E., Holst, J., Ivakhov, V., Jaffe, D. A., Jordan, A., Joubert, W., Karion, A., Kawa, S. R., Kazan, V., Keeling, R. F., Keronen, P., Kneuer, T., Kolari, P., Kateřina Komínková, Kort, E., Kozlova, E., Krummel, P., Kubistin, D., Labuschagne, C., Lam, D. H. Y., Lan, X., Langenfelds, R. L., Laurent, O., Laurila, T., Lauvaux, T., Lavric, J., Law, B. E., Lee, J., Lee, O. S. M., Lehner, I., Lehtinen, K., Leppert, R., et al.: CarbonTracker CT2022, https://doi.org/10.25925/Z1GJ-3254, 2023a.

Jacobson, A. R., Schuldt, K. N., Tans, P., Arlyn Andrews, Miller, J. B., Oda, T., Mund, J., Weir, B., Ott, L., Aalto, T., Abshire, J. B., Aikin, K., Aoki, S., Apadula, F., Arnold, S., Baier, B., Bartyzel, J., Beyersdorf, A., Biermann, T., Biraud, S. C., Boenisch, H., Brailsford, G., Brand, W. A., Chen, G., Huilin Chen, Lukasz Chmura, Clark, S., Colomb, A., Commane, R., Conil, S., Couret, C., Cox, A., Cristofanelli, P., Cuevas, E., Curcoll, R., Daube, B., Davis, K. J., De Wekker, S., Coletta, J. D., Delmotte, M., DiGangi, E., DiGangi, J. P., Di Sarra, A. G., Dlugokencky, E., Elkins, J. W., Emmenegger, L., Shuangxi Fang, Fischer, M. L., Forster, G., Frumau, A., Galkowski, M., Gatti, L. V., Gehrlein, T., Gerbig, C., Francois Gheusi, Gloor, E., Gomez-Trueba, V., Goto, D., Griffis, T., Hammer, S., Hanson, C., Haszpra, L., Hatakka, J., Heimann, M., Heliasz, M., Hensen, A., Hermansen, O., Hintsa, E., Holst, J., Ivakhov, V., Jaffe, D. A., Jordan, A., Joubert, W., Karion, A., Kawa, S. R., Kazan, V., Keeling, R. F., Keronen, P., Kneuer, T., Kolari, P., Kateřina Komínková, Kort, E., Kozlova, E., Krummel, P., Kubistin, D., Labuschagne, C., Lam, D. H. Y., Lan, X., Langenfelds, R. L., Laurent, O., Laurila, T., Lauvaux, T., Lavric, J., Law, B. E., Lee, J., Lee, O. S. M., Lehner, I., Lehtinen, K., Leppert, R., et al.: CarbonTracker CT-NRT.v2023-3, https://doi.org/10.25925/7TAF-J322, 2023b.

Janssens-Maenhout, G., Crippa, M., Guizzardi, D., Muntean, M., Schaaf, E., Dentener, F., Bergamaschi, P., Pagliari, V., Olivier, J. G. J., Peters, J. A. H. W., van Aardenne, J. A., Monni, S., Doering, U., Petrescu, A. M. R., Solazzo, E., and Oreggioni, G. D.: EDGAR v4.3.2 Global Atlas of the three major greenhouse gas emissions for the period 1970–2012, Earth Syst. Sci. Data, 11, 959–1002, https://doi.org/10.5194/essd-11-959-2019, 2019.

Jean-Michel, L., Eric, G., Romain, B.-B., Gilles, G., Angélique, M., Marie, D., Clément, B., Mathieu, H., Olivier, L. G., Charly, R., Tony, C., Charles-Emmanuel, T., Florent, G., Giovanni, R., Mounir, B., Yann, D., and Pierre-Yves, L. T.: The Copernicus Global 1/12° Oceanic and Sea Ice GLORYS12 Reanalysis, Front. Earth Sci., 9, 2021.

Jiang, F., Ju, W., He, W., Wu, M., Wang, H., Wang, J., Jia, M., Feng, S., Zhang, L., and Chen, J. M.: A 10-year global monthly averaged terrestrial net ecosystem exchange dataset inferred from the ACOS GOSAT v9 XCO2 retrievals (GCAS2021), Earth Syst. Sci. Data, 14, 3013–3037, https://doi.org/10.5194/essd-14-3013-2022, 2022.

Jiang, F., Wang, H., Chen, J. M., Ju, W., Tian, X., Feng, S., Li, G., Chen, Z., Zhang, S., Lu, X., Liu, J., Wang, H., Wang, J., He, W., and Wu, M.: Regional CO2 fluxes from 2010 to 2015 inferred from GOSAT XCO2 retrievals using a new version of the Global Carbon Assimilation System, Atmospheric Chem. Phys., 21, 1963–1985, https://doi.org/10.5194/acp-21-1963-2021, 2021.

Jin, Z., Wang, T., Zhang, H., Wang, Y., Ding, J., and Tian, X.: Constraint of satellite CO2 retrieval on the global carbon cycle from a Chinese atmospheric inversion system, Sci. China Earth Sci., 66, 609–618, https://doi.org/10.1007/s11430-022-1036-7, 2023.

Joos, F. and Spahni, R.: Rates of change in natural and anthropogenic radiative forcing over the past 20,000 years, Proceedings of the National Academy of Sciences, 105, 1425–1430, https://doi.org/10.1073/pnas.0707386105, 2008.

Jones, C. D., Hickman, J. E., Rumbold, S. T., Walton, J., Lamboll, R. D., Skeie, R. B., Fiedler, S., Forster, P. M., Rogelj, J., Abe, M., Botzet, M., Calvin, K., Cassou, C., Cole, J. N. S., Davini, P., Deushi, M., Dix, M., Fyfe, J. C., Gillett, N. P., Ilyina, T., Kawamiya, M., Kelley, M., Kharin, S., Koshiro, T., Li, H., Mackallah, C., Müller, W. A., Nabat, P., van Noije, T., Nolan, P., Ohgaito, R., Olivié, D., Oshima, N., Parodi, J., Reerink, T. J., Ren, L., Romanou, A., Séférian, R., Tang, Y., Timmreck, C., Tjiputra, J., Tourigny, E., Tsigaridis, K., Wang, H., Wu, M., Wyser, K., Yang, S., Yang, Y., and Ziehn, T.: The Climate Response to Emissions Reductions Due to COVID-19: Initial Results From CovidMIP, Geophys. Res. Lett., 48, e2020GL091883, https://doi.org/10.1029/2020GL091883, 2021a.

Jones, M. W., Abatzoglou, J. T., Veraverbeke, S., Andela, N., Lasslop, G., Forkel, M., Smith, A. J. P., Burton, C., Betts, R. A., van der Werf, G. R., Sitch, S., Canadell, J. G., Santín, C., Kolden, C., Doerr, S. H., and Le Quéré, C.: Global and Regional Trends and Drivers of Fire Under Climate Change, Rev. Geophys., 60, e2020RG000726, https://doi.org/10.1029/2020RG000726, 2022.

Jones, M. W., Andrew, R. M., Peters, G. P., Janssens-Maenhout, G., De-Gol, A. J., Ciais, P., Patra, P. K., Chevallier, F., and Le Quéré, C.: Gridded fossil CO2 emissions and related O2 combustion consistent with national inventories 1959–2018, Sci Data, 8, 2, https://doi.org/10.1038/s41597-020-00779-6, 2021b.

Jones, M. W., Andrew, R. M., Peters, G. P., Janssens-Maenhout, G., De-Gol, A. J., Dou, X., Liu, Z., Pickers, P., Ciais, P., Patra, P. K., Chevallier, F., and Le Quéré, C.: Gridded fossil CO2 emissions and related O2 combustion consistent with national inventories 1959-2022, Zenodo [dataset], https://doi.org/10.5281/zenodo.8386803, 2023.

Jung, M., Reichstein, M., Schwalm, C. R., Huntingford, C., Sitch, S., Ahlström, A., Arneth, A., Camps-Valls, G., Ciais, P., Friedlingstein, P., Gans, F., Ichii, K., Jain, A. K., Kato, E., Papale, D., Poulter, B., Raduly, B., Rödenbeck, C., Tramontana, G., Viovy, N., Wang, Y.-P., Weber, U., Zaehle, S., and Zeng, N.: Compensatory water effects link yearly global land CO2 sink changes to temperature, Nature, 541, 516–520, https://doi.org/10.1038/nature20780, 2017.

Kaiser, J. W., Heil, A., Andreae, M. O., Benedetti, A., Chubarova, N., Jones, L., Morcrette, J.-J., Razinger, M., Schultz, M. G., Suttie, M., and van der Werf, G. R.: Biomass burning emissions estimated with a global fire assimilation system based on observed fire radiative power, Biogeosciences, 9, 527–554, https://doi.org/10.5194/bg-9-527-2012, 2012.

Kato, E., Kinoshita, T., Ito, A., Kawamiya, M., and Yamagata, Y.: Evaluation of spatially explicit emission scenario of land-use change and biomass burning using a process-based biogeochemical model, J. Land Use Sci., 8, 104–122, https://doi.org/10.1080/1747423X.2011.628705, 2013.

Kawasaki, T., Hasumi, H., and Tanaka, Y.: Role of tide-induced vertical mixing in the deep Pacific Ocean circulation, J. Oceanogr., 77, 173–184, https://doi.org/10.1007/s10872-020-00584-0, 2021.

Keeley, J. E. and Pausas, J. G.: Distinguishing disturbance from perturbations in fire-prone ecosystems, Int. J. Wildland Fire, 28, 282–287, https://doi.org/10.1071/WF18203, 2019.

Keeling, C. D., Bacastow, R. B., Bainbridge, A. E., Ekdahl, C. A., Guenther, P. R., Waterman, L. S., and Chin, J. F. S.: Atmospheric carbon dioxide variations at Mauna Loa Observatory, Hawaii, Tellus A., 28, 538–551, https://doi.org/10.1111/j.2153-3490.1976.tb00701.x, 1976.

Keeling, R. F., Manning, A. C., Paplawsky, W. J., and Cox, A. C.: On the long-term stability of reference gases for atmospheric O2/N2 and CO2 measurements, Tellus B Chem. Phys. Meteorol., 59, 3–14, https://doi.org/10.1111/j.1600-0889.2006.00196.x, 2007.

Keeling, R. F. and Manning, A. C.: 5.15 - Studies of Recent Changes in Atmospheric O2 Content, in: Treatise on Geochemistry (Second Edition), edited by: Holland, H. D. and Turekian, K. K., Elsevier, Oxford, 385–404, https://doi.org/10.1016/B978-0-08-095975-7.00420-4, 2014.

Keppler, L. and Landschützer, P.: Regional Wind Variability Modulates the Southern Ocean Carbon Sink, Sci Rep, 9, 7384, https://doi.org/10.1038/s41598-019-43826-y, 2019.

Khatiwala, S., Primeau, F., and Hall, T.: Reconstruction of the history of anthropogenic CO2 concentrations in the ocean, Nature, 462, 346–349, https://doi.org/10.1038/nature08526, 2009.

Khatiwala, S., Tanhua, T., Mikaloff Fletcher, S., Gerber, M., Doney, S. C., Graven, H. D., Gruber, N., McKinley, G. A., Murata, A., Ríos, A. F., and Sabine, C. L.: Global ocean storage of anthropogenic carbon, Biogeosciences, 10, 2169–2191, https://doi.org/10.5194/bg-10-2169-2013, 2013.

Kong, Y., Zheng, B., Zhang, Q., and He, K.: Global and regional carbon budget for 2015–2020 inferred from OCO-2 based on an ensemble Kalman filter coupled with GEOS-Chem, Atmospheric Chem. Phys., 22, 10769–10788, https://doi.org/10.5194/acp-22-10769-2022, 2022.

Korsbakken, J. I., Peters, G. P., and Andrew, R. M.: Uncertainties around reductions in China's coal use and CO2 emissions, Nature Clim Change, 6, 687–690, https://doi.org/10.1038/nclimate2963, 2016.

Krinner, G., Viovy, N., de Noblet-Ducoudré, N., Ogée, J., Polcher, J., Friedlingstein, P., Ciais, P., Sitch, S., and Prentice, I. C.: A dynamic global vegetation model for studies of the coupled atmosphere-biosphere system: DVGM for coupled climate studies, Global Biogeochem. Cycles, 19, GB1015, https://doi.org/10.1029/2003GB002199, 2005.

Lacroix, F., Ilyina, T., and Hartmann, J.: Oceanic CO2 outgassing and biological production hotspots induced by pre-industrial river loads of nutrients and carbon in a global modeling approach, Biogeosciences, 17, 55–88, https://doi.org/10.5194/bg-17-55-2020, 2020.

Lacroix, F., Ilyina, T., Mathis, M., Laruelle, G. G., and Regnier, P.: Historical increases in land-derived nutrient inputs may alleviate effects of a changing physical climate on the oceanic carbon cycle, Glob Change Biol, 27, 5491–5513, https://doi.org/10.1111/gcb.15822, 2021.

Lamboll, R. D., Nicholls, Z. R. J., Smith, C. J., Kikstra, J. S., Byers, E., and Rogelj, J.: Assessing the size and uncertainty of remaining carbon budgets, Nat. Clim. Change, https://doi.org/10.1038/s41558-023-01848-5, 2023.

Lan, X., Tans, P. and K.W. Thoning: Trends in globally-averaged CO2 determined from NOAA Global Monitoring Laboratory measurements, Version 2023-09. National Oceanic and Atmospheric Administration, Global Monitoring Laboratory (NOAA/GML), available at: https://gml.noaa.gov/ccgg/trends/global.html, last access: 9 November 2023, 2023.

Landschützer, P., Gruber, N., Haumann, F. A., Rödenbeck, C., Bakker, D. C. E., van Heuven, S., Hoppema, M., Metzl, N., Sweeney, C., Takahashi, T., Tilbrook, B., and Wanninkhof, R.: The reinvigoration of the Southern Ocean carbon sink, Science, 349, 1221–1224, https://doi.org/10.1126/science.aab2620, 2015.

Landschützer, P., Gruber, N., and Bakker, D. C. E.: Decadal variations and trends of the global ocean carbon sink: decadal air-sea CO2 flux variability, Global Biogeochem. Cycles, 30, 1396–1417, https://doi.org/10.1002/2015GB005359, 2016.

Law, R. M., Ziehn, T., Matear, R. J., Lenton, A., Chamberlain, M. A., Stevens, L. E., Wang, Y.-P., Srbinovsky, J., Bi, D., Yan, H., and Vohralik, P. F.: The carbon cycle in the Australian Community Climate and Earth System Simulator (ACCESS-ESM1) – Part 1: Model description and pre-industrial simulation, Geosci. Model Dev., 10, 2567–2590, https://doi.org/10.5194/gmd-10-2567-2017, 2017.

Lawrence, D. M., Fisher, R. A., Koven, C. D., Oleson, K. W., Swenson, S. C., Bonan, G., Collier, N., Ghimire, B., van Kampenhout, L., Kennedy, D., Kluzek, E., Lawrence, P. J., Li, F., Li, H., Lombardozzi, D., Riley, W. J., Sacks, W. J., Shi, M., Vertenstein, M., Wieder, W. R., Xu, C., Ali, A. A., Badger, A. M., Bisht, G., van den Broeke, M., Brunke, M. A., Burns, S. P., Buzan, J., Clark, M., Craig, A., Dahlin, K., Drewniak, B., Fisher, J. B., Flanner, M., Fox, A. M., Gentine, P., Hoffman, F., Keppel-Aleks, G., Knox, R., Kumar, S., Lenaerts, J., Leung, L. R., Lipscomb, W. H., Lu, Y., Pandey, A., Pelletier, J. D., Perket, J., Randerson, J. T., Ricciuto, D. M., Sanderson, B. M., Slater, A., Subin, Z. M., Tang, J., Thomas, R. Q., Val Martin, M., and Zeng, X.: The Community Land Model Version 5: Description of New Features, Benchmarking, and Impact of Forcing Uncertainty, J. Adv. Model Earth, Sy., 11, 4245–4287, https://doi.org/10.1029/2018MS001583, 2019.

Le Quéré, C., Rödenbeck, C., Buitenhuis, E. T., Conway, T. J., Langenfelds, R., Gomez, A., Labuschagne, C., Ramonet, M., Nakazawa, T., Metzl, N., Gillett, N., and Heimann, M.: Saturation of the Southern Ocean CO2 Sink Due to Recent Climate Change, Science, 316, 1735–1738, https://doi.org/10.1126/science.1136188, 2007.

Le Quéré, C., Raupach, M. R., Canadell, J. G., Marland, G., Bopp, L., Ciais, P., Conway, T. J., Doney, S. C., Feely, R. A., Foster, P., Friedlingstein, P., Gurney, K., Houghton, R. A., House, J. I., Huntingford, C., Levy, P. E., Lomas, M. R., Majkut, J., Metzl, N., Ometto, J. P., Peters, G. P., Prentice, I. C., Randerson, J. T., Running, S. W., Sarmiento, J. L., Schuster, U., Sitch, S., Takahashi, T., Viovy, N., van der Werf, G. R., and Woodward, F. I.: Trends in the sources and sinks of carbon dioxide, Nature Geosci, 2, 831–836, https://doi.org/10.1038/ngeo689, 2009.

Le Quéré, C., Andres, R. J., Boden, T., Conway, T., Houghton, R. A., House, J. I., Marland, G., Peters, G. P., van der Werf, G. R., Ahlström, A., Andrew, R. M., Bopp, L., Canadell, J. G., Ciais, P., Doney, S. C., Enright, C., Friedlingstein, P., Huntingford, C., Jain, A. K., Jourdain, C., Kato, E., Keeling, R. F., Klein Goldewijk, K., Levis, S., Levy, P., Lomas, M., Poulter, B., Raupach, M. R., Schwinger, J., Sitch, S., Stocker, B. D., Viovy, N., Zaehle, S., and Zeng, N.: The global carbon budget 1959–2011, Earth Syst. Sci. Data, 5, 165–185, https://doi.org/10.5194/essd-5-165-2013, 2013.

Le Quéré, C., Peters, G. P., Andres, R. J., Andrew, R. M., Boden, T. A., Ciais, P., Friedlingstein, P., Houghton, R. A., Marland, G., Moriarty, R., Sitch, S., Tans, P., Arneth, A., Arvanitis, A., Bakker, D. C. E., Bopp, L., Canadell, J. G., Chini, L. P., Doney, S. C., Harper, A., Harris, I., House, J. I., Jain, A. K., Jones, S. D., Kato, E., Keeling, R. F., Klein Goldewijk, K., Körtzinger, A., Koven, C., Lefèvre, N., Maignan, F., Omar, A., Ono, T., Park, G.-H., Pfeil, B., Poulter, B., Raupach, M. R., Regnier, P., Rödenbeck, C., Saito, S., Schwinger, J., Segschneider, J., Stocker, B. D., Takahashi, T., Tilbrook, B., van Heuven, S., Viovy, N., Wanninkhof, R., Wiltshire, A., and Zaehle, S.: Global carbon budget 2013, Earth Syst. Sci. Data, 6, 235–263, https://doi.org/10.5194/essd-6-235-2014, 2014.

Le Quéré, C., Moriarty, R., Andrew, R. M., Peters, G. P., Ciais, P., Friedlingstein, P., Jones, S. D., Sitch, S., Tans, P., Arneth, A., Boden, T. A., Bopp, L., Bozec, Y., Canadell, J. G., Chini, L. P., Chevallier, F., Cosca, C. E., Harris, I., Hoppema, M., Houghton, R. A., House, J. I., Jain, A. K., Johannessen, T., Kato, E., Keeling, R. F., Kitidis, V., Klein Goldewijk, K., Koven, C., Landa, C. S., Landschützer, P., Lenton, A., Lima, I. D., Marland, G., Mathis, J. T., Metzl, N., Nojiri, Y., Olsen, A., Ono, T., Peng, S., Peters, W., Pfeil, B., Poulter, B., Raupach, M. R., Regnier, P., Rödenbeck, C., Saito, S., Salisbury, J. E., Schuster, U., Schwinger, J., Séférian, R., Segschneider, J., Steinhoff, T., Stocker, B. D., Sutton, A. J., Takahashi, T., Tilbrook, B., van der Werf, G. R., Viovy, N., Wang, Y.-P., Wanninkhof, R., Wiltshire, A., and Zeng, N.: Global carbon budget 2014, Earth Syst. Sci. Data, 7, 47–85, https://doi.org/10.5194/essd-7-47-2015, 2015a.

Le Quéré, C., Moriarty, R., Andrew, R. M., Canadell, J. G., Sitch, S., Korsbakken, J. I., Friedlingstein, P., Peters, G. P., Andres, R. J., Boden, T. A., Houghton, R. A., House, J. I., Keeling, R. F., Tans, P., Arneth, A., Bakker, D. C. E., Barbero, L., Bopp, L., Chang, J., Chevallier, F., Chini, L. P., Ciais, P., Fader, M., Feely, R. A., Gkritzalis, T., Harris, I., Hauck, J., Ilyina, T., Jain, A. K., Kato, E., Kitidis, V., Klein Goldewijk, K., Koven, C., Landschützer, P., Lauvset, S. K., Lefèvre, N., Lenton, A., Lima, I. D., Metzl, N., Millero, F., Munro, D. R., Murata, A., Nabel, J. E. M. S., Nakaoka, S., Nojiri, Y., O'Brien, K., Olsen, A., Ono, T., Pérez, F. F., Pfeil, B., Pierrot, D., Poulter, B., Rehder, G., Rödenbeck, C., Saito, S., Schuster, U., Schwinger, J., Séférian, R., Steinhoff, T., Stocker, B. D., Sutton, A. J., Takahashi, T., Tilbrook, B., van der Laan-Luijkx, I. T., van der Werf, G. R., van Heuven, S., Vandemark, D., Viovy, N., Wiltshire, A., Zaehle, S., and Zeng, N.: Global Carbon Budget 2015, Earth Syst. Sci. Data, 7, 349–396, https://doi.org/10.5194/essd-7-349-2015, 2015b.

Le Quéré, C., Andrew, R. M., Canadell, J. G., Sitch, S., Korsbakken, J. I., Peters, G. P., Manning, A. C., Boden, T. A., Tans, P. P., Houghton, R. A., Keeling, R. F., Alin, S., Andrews, O. D., Anthoni, P., Barbero, L., Bopp, L., Chevallier, F., Chini, L. P., Ciais, P., Currie, K., Delire, C., Doney, S. C., Friedlingstein, P., Gkritzalis, T., Harris, I., Hauck, J., Haverd, V., Hoppema, M., Klein Goldewijk, K., Jain, A. K., Kato, E., Körtzinger, A., Landschützer, P., Lefèvre, N., Lenton, A., Lienert, S., Lombardozzi, D., Melton, J. R., Metzl, N., Millero, F., Monteiro, P. M. S., Munro, D. R., Nabel, J. E. M. S., Nakaoka, S., O'Brien, K., Olsen, A., Omar, A. M., Ono, T., Pierrot, D., Poulter, B., Rödenbeck, C., Salisbury, J., Schuster, U., Schwinger, J., Séférian, R., Skjelvan, I., Stocker, B. D., Sutton, A. J., Takahashi, T., Tian, H., Tilbrook, B., van der Laan-Luijkx, I. T., van der Werf, G. R., Viovy, N., Walker, A. P., Wiltshire, A. J., and Zaehle, S.: Global Carbon Budget 2016, Earth Syst. Sci. Data, 8, 605–649, https://doi.org/10.5194/essd-8-605-2016, 2016.

Le Quéré, C., Andrew, R. M., Friedlingstein, P., Sitch, S., Pongratz, J., Manning, A. C., Korsbakken, J. I., Peters, G. P., Canadell, J. G., Jackson, R. B., Boden, T. A., Tans, P. P., Andrews, O. D., Arora, V. K., Bakker, D. C. E., Barbero, L., Becker, M., Betts, R. A., Bopp, L., Chevallier, F., Chini, L. P., Ciais, P., Cosca, C. E., Cross, J., Currie, K., Gasser, T., Harris, I., Hauck, J., Haverd, V., Houghton, R. A., Hunt, C. W., Hurtt, G., Ilyina, T., Jain, A. K., Kato, E., Kautz, M., Keeling, R. F., Klein Goldewijk, K., Körtzinger, A., Landschützer, P., Lefèvre, N., Lenton, A., Lienert, S., Lima, I., Lombardozzi, D., Metzl, N., Millero, F., Monteiro, P. M. S., Munro, D. R., Nabel, J. E. M. S., Nakaoka, S., Nojiri, Y., Padin, X. A., Peregon, A., Pfeil, B., Pierrot, D., Poulter, B., Rehder, G., Reimer, J., Rödenbeck, C., Schwinger, J., Séférian, R., Skjelvan, I., Stocker, B. D., Tian, H., Tilbrook, B., Tubiello, F. N., van der Laan-Luijkx, I. T., van der Werf, G. R., van Heuven, S., Viovy, N., Vuichard, N., Walker, A. P., Watson, A. J., Wiltshire, A. J., Zaehle, S., and Zhu, D.: Global Carbon Budget 2017, Earth Syst. Sci. Data, 10, 405–448, https://doi.org/10.5194/essd-10-405-2018, 2018a.

Le Quéré, C., Andrew, R. M., Friedlingstein, P., Sitch, S., Hauck, J., Pongratz, J., Pickers, P. A., Korsbakken, J. I., Peters, G. P., Canadell, J. G., Arneth, A., Arora, V. K., Barbero, L., Bastos, A., Bopp, L., Chevallier, F., Chini, L. P., Ciais, P., Doney, S. C., Gkritzalis, T., Goll, D. S., Harris, I., Haverd, V., Hoffman, F. M., Hoppema, M., Houghton, R. A., Hurtt, G., Ilyina, T., Jain, A. K., Johannessen, T., Jones, C. D., Kato, E., Keeling, R. F., Klein Goldewijk, K., Landschützer, P., Lefèvre, N.,

Lienert, S., Liu, Z., Lombardozzi, D., Metzl, N., Munro, D. R., Nabel, J. E. M. S., Nakaoka, S., Neill, C., Olsen, A., Ono, T., Patra, P., Peregon, A., Peters, W., Peylin, P., Pfeil, B., Pierrot, D., Poulter, B., Rehder, G., Resplandy, L., Robertson, E., Rocher, M., Rödenbeck, C., Schuster, U., Schwinger, J., Séférian, R., Skjelvan, I., Steinhoff, T., Sutton, A., Tans, P. P., Tian, H., Tilbrook, B., Tubiello, F. N., van der Laan-Luijkx, I. T., van der Werf, G. R., Viovy, N., Walker, A. P., Wiltshire, A. J., Wright, R., Zaehle, S., and Zheng, B.: Global Carbon Budget 2018, Earth Syst. Sci. Data, 10, 2141–2194, https://doi.org/10.5194/essd-10-2141-2018, 2018b.

Le Quéré, C., Korsbakken, J. I., Wilson, C., Tosun, J., Andrew, R., Andres, R. J., Canadell, J. G., Jordan, A., Peters, G. P., and van Vuuren, D. P.: Drivers of declining CO2 emissions in 18 developed economies, Nat. Clim. Chang., 9, 213–217, https://doi.org/10.1038/s41558-019-0419-7, 2019.

Le Quéré, C., Peters, G. P., Friedlingstein, P., Andrew, R. M., Canadell, J. G., Davis, S. J., Jackson, R. B., and Jones, M. W.: Fossil CO2 emissions in the post-COVID-19 era, Nat. Clim. Chang., 11, 197–199, https://doi.org/10.1038/s41558-021-01001-0, 2021.

Levitus, S., Antonov, J. I., Boyer, T. P., Baranova, O. K., Garcia, H. E., Locarnini, R. A., Mishonov, A. V., Reagan, J. R., Seidov, D., Yarosh, E. S., and Zweng, M. M.: World ocean heat content and thermosteric sea level change (0–2000 m), 1955–2010, Geophys. Res. Lett., 39, https://doi.org/10.1029/2012GL051106, 2012.

Li, H., Ilyina, T., Müller, W. A., and Sienz, F.: Decadal predictions of the North Atlantic CO2 uptake, Nat. Commun., 7, 11076, https://doi.org/10.1038/ncomms11076, 2016.

Li, H., Ilyina, T., Müller, W. A., and Landschützer, P.: Predicting the variable ocean carbon sink, Sci. Adv., 5, eaav6471, https://doi.org/10.1126/sciadv.aav6471, 2019.

Li, H., Ilyina, T., Loughran, T., Spring, A., and Pongratz, J.: Reconstructions and predictions of the global carbon budget with an emission-driven Earth system model, Earth Syst. Dyn., 14, 101–119, https://doi.org/10.5194/esd-14-101-2023, 2023.

Li, W., Ciais, P., Peng, S., Yue, C., Wang, Y., Thurner, M., Saatchi, S. S., Arneth, A., Avitabile, V., Carvalhais, N., Harper, A. B., Kato, E., Koven, C., Liu, Y. Y., Nabel, J. E. M. S., Pan, Y., Pongratz, J., Poulter, B., Pugh, T. A. M., Santoro, M., Sitch, S., Stocker, B. D., Viovy, N., Wiltshire, A., Yousefpour, R., and Zaehle, S.: Land-use and land-cover change carbon emissions between 1901 and 2012 constrained by biomass observations, Biogeosciences, 14, 5053–5067, https://doi.org/10.5194/bg-14-5053-2017, 2017.

Liao, E., Resplandy, L., Liu, J., and Bowman, K. W.: Amplification of the Ocean Carbon Sink During El Niños: Role of Poleward Ekman Transport and Influence on Atmospheric CO2, Global Biogeochem. Cy., 34, e2020GB006574, https://doi.org/10.1029/2020GB006574, 2020.

Lienert, S. and Joos, F.: A Bayesian ensemble data assimilation to constrain model parameters and land-use carbon emissions, Biogeosciences, 15, 2909–2930, https://doi.org/10.5194/bg-15-2909-2018, 2018.

Liu, J., Baskaran, L., Bowman, K., Schimel, D., Bloom, A. A., Parazoo, N. C., Oda, T., Carroll, D., Menemenlis, D., Joiner, J., Commane, R., Daube, B., Gatti, L. V., McKain, K., Miller, J., Stephens, B. B., Sweeney, C., and Wofsy, S.: Carbon Monitoring System Flux Net Biosphere Exchange 2020 (CMS-Flux NBE 2020), 13, 299–330, https://doi.org/10.5194/essd-13-299-2021, 2021.

Liu, Z., Guan, D., Wei, W., Davis, S. J., Ciais, P., Bai, J., Peng, S., Zhang, Q., Hubacek, K., Marland, G., Andres, R. J., Crawford-Brown, D., Lin, J., Zhao, H., Hong, C., Boden, T. A., Feng, K., Peters, G. P., Xi, F., Liu, J., Li, Y., Zhao, Y., Zeng, N., and He, K.: Reduced carbon emission estimates from fossil fuel combustion and cement production in China, Nature, 524, 335–338, https://doi.org/10.1038/nature14677, 2015.

Liu, Z., Zeng, N., Liu, Y., Kalnay, E., Asrar, G., Wu, B., Cai, Q., Liu, D., and Han, P.: Improving the joint estimation of CO2 and surface carbon fluxes using a constrained ensemble Kalman filter in COLA (v1.0), Geosci. Model Dev., 15, 5511–5528, https://doi.org/10.5194/gmd-15-5511-2022, 2022.

Lovenduski, N. S., Bonan, G. B., Yeager, S. G., Lindsay, K., and Lombardozzi, D. L.: High predictability of terrestrial carbon fluxes from an initialized decadal prediction system, Environ. Res. Lett., 14, 124074, https://doi.org/10.1088/1748-9326/ab5c55, 2019a.

Lovenduski, N. S., Yeager, S. G., Lindsay, K., and Long, M. C.: Predicting near-term variability in ocean carbon uptake, Earth Syst. Dyn., 10, 45–57, https://doi.org/10.5194/esd-10-45-2019, 2019b.

Lutz, F., Herzfeld, T., Heinke, J., Rolinski, S., Schaphoff, S., von Bloh, W., Stoorvogel, J. J., and Müller, C.: Simulating the effect of tillage practices with the global ecosystem model LPJmL (version 5.0-tillage), Geosci. Model Dev., 12, 2419–2440, https://doi.org/10.5194/gmd-12-2419-2019, 2019.

Ma, L., Hurtt, G., Ott, L., Sahajpal, R., Fisk, J., Lamb, R., Tang, H., Flanagan, S., Chini, L., Chatterjee, A., and Sullivan, J.: Global evaluation of the Ecosystem Demography model (ED v3.0), Geosci. Model Dev., 15, 1971–1994, https://doi.org/10.5194/gmd-15-1971-2022, 2022.

Magi, B. I., Rabin, S., Shevliakova, E., and Pacala, S.: Separating agricultural and non-agricultural fire seasonality at regional scales, Biogeosciences, 9, 3003–3012, https://doi.org/10.5194/bg-9-3003-2012, 2012.

Masarie, K. A. and Tans, P. P.: Extension and integration of atmospheric carbon dioxide data into a globally consistent measurement record, J. Geophys. Res., 100, 11593, https://doi.org/10.1029/95JD00859, 1995.

Mather, A. S.: The transition from deforestation to reforestation in Europe, in: Agricultural technologies and tropical deforestation (eds. Angelsen, A.; Kaimowitz, D.), CABI in association with centre for international Forestry Research, 35–52, 2001.

Mauritsen, T., Bader, J., Becker, T., Behrens, J., Bittner, M., Brokopf, R., Brovkin, V., Claussen, M., Crueger, T., Esch, M., Fast, I., Fiedler, S., Fläschner, D., Gayler, V., Giorgetta, M., Goll, D. S., Haak, H., Hagemann, S., Hedemann, C., Hohenegger, C., Ilyina, T., Jahns, T., Jimenéz-de-la-Cuesta, D., Jungclaus, J., Kleinen, T., Kloster, S., Kracher, D., Kinne, S., Kleberg, D., Lasslop, G., Kornblueh, L., Marotzke, J., Matei, D., Meraner, K., Mikolajewicz, U., Modali, K., Möbis, B., Müller, W. A., Nabel, J. E. M. S., Nam, C. C. W., Notz, D., Nyawira, S.-S., Paulsen, H., Peters, K., Pincus, R., Pohlmann, H., Pongratz, J., Popp, M., Raddatz, T. J., Rast, S., Redler, R., Reick, C. H., Rohrschneider, T., Schemann, V., Schmidt, H., Schnur, R., Schulzweida, U., Six, K. D., Stein, L., Stemmler, I., Stevens, B., von Storch, J.-S., Tian, F., Voigt, A., Vrese, P., Wieners, K.-H., Wilkenskjeld, S., Winkler, A., and Roeckner, E.: Developments in the MPI-M Earth System Model version 1.2 (MPI-ESM1.2) and Its Response to Increasing CO2, J. Adv. Model Earth Sy., 11, 998–1038, https://doi.org/10.1029/2018MS001400, 2019.

McGrath, M. J., Luyssaert, S., Meyfroidt, P., Kaplan, J. O., Bürgi, M., Chen, Y., Erb, K., Gimmi, U., McInerney, D., Naudts, K., Otto, J., Pasztor, F., Ryder, J., Schelhaas, M.-J., and Valade, A.: Reconstructing European forest management from 1600 to 2010, 12, 4291–4316, https://doi.org/10.5194/bg-12-4291-2015, 2015.

McKinley, G. A., Fay, A. R., Eddebbar, Y. A., Gloege, L., and Lovenduski, N. S.: External Forcing Explains Recent Decadal Variability of the Ocean Carbon Sink, AGU Advances, 1, e2019AV000149, https://doi.org/10.1029/2019AV000149, 2020.

McKinley, G. A., Fay, A. R., Lovenduski, N. S., and Pilcher, D. J.: Natural Variability and Anthropogenic Trends in the Ocean Carbon Sink, Annu. Rev. Mar. Sci., 9, 125–150, https://doi.org/10.1146/annurev-marine-010816-060529, 2017.

Meiyappan, P., Jain, A. K., and House, J. I.: Increased influence of nitrogen limitation on CO 2 emissions from future land use and land use change, Global Biogeochem. Cycles, 29, 1524–1548, https://doi.org/10.1002/2015GB005086, 2015.

Melton, J. R., Arora, V. K., Wisernig-Cojoc, E., Seiler, C., Fortier, M., Chan, E., and Teckentrup, L.: CLASSIC v1.0: the open-source community successor to the Canadian Land Surface Scheme (CLASS) and the Canadian Terrestrial Ecosystem Model (CTEM) – Part 1: Model framework and site-level performance, Geosci. Model Dev., 13, 2825–2850, https://doi.org/10.5194/gmd-13-2825-2020, 2020.

Mercado, L. M., Bellouin, N., Sitch, S., Boucher, O., Huntingford, C., Wild, M., and Cox, P. M.: Impact of changes in diffuse radiation on the global land carbon sink, Nature, 458, 1014–1017, https://doi.org/10.1038/nature07949, 2009.

Merchant, C. J., Embury, O., Bulgin, C. E., Block, T., Corlett, G. K., Fiedler, E., Good, S. A., Mittaz, J., Rayner, N. A., Berry, D., Eastwood, S., Taylor, M., Tsushima, Y., Waterfall, A., Wilson, R., and Donlon, C.: Satellite-based time-series of sea-surface temperature since 1981 for climate applications, Sci. Data, 6, 223, https://doi.org/10.1038/s41597-019-0236-x, 2019.

Moorcroft, P. R., Hurtt, G. C., and Pacala, S. W.: A Method for Scaling Vegetation Dynamics: The Ecosystem Demography Model (ed), Ecol. Monogr., 71, 557–586, https://doi.org/10.1890/0012-9615(2001)071[0557:AMFSVD]2.0.CO;2, 2001.

Müller, J. D., Gruber, N., Carter, B., Feely, R., Ishii, M., Lange, N., Lauvset, S. K., Murata, A., Olsen, A., Pérez, F. F., Sabine, C., Tanhua, T., Wanninkhof, R., and Zhu, D.: Decadal Trends in the Oceanic Storage of Anthropogenic Carbon From 1994 to 2014, AGU Adv., 4, e2023AV000875, https://doi.org/10.1029/2023AV000875, 2023.

Nakano, H., Tsujino, H., Hirabara, M., Yasuda, T., Motoi, T., Ishii, M., and Yamanaka, G.: Uptake mechanism of anthropogenic CO2 in the Kuroshio Extension region in an ocean general circulation model, J. Oceanogr., 67, 765–783, https://doi.org/10.1007/s10872-011-0075-7, 2011.

NCEP: National Centers for Environmental Prediction. ONI Index. Cold & Warm Episodes by Season, available at: https://origin.cpc.ncep.noaa.gov/products/analysis_monitoring/ensostuff/ONI_v5.php, last access: 9 November 2023, 2023.

Niu, G.-Y., Yang, Z.-L., Mitchell, K. E., Chen, F., Ek, M. B., Barlage, M., Kumar, A., Manning, K., Niyogi, D., Rosero, E., Tewari, M., and Xia, Y.: The community Noah land surface model with multiparameterization options (Noah-MP): 1. Model description and evaluation with local-scale measurements, J. Geophys. Res. Atmospheres, 116, https://doi.org/10.1029/2010JD015139, 2011.

Niwa, Y., Ishijima, K., Ito, A., and Iida, Y.: Toward a long-term atmospheric CO2 inversion for elucidating natural carbon fluxes: technical notes of NISMON-CO2 v2021.1, Prog. Earth Planet Sci., 9, 42, https://doi.org/10.1186/s40645-022-00502-6, 2022.

Niwa, Y., Langenfelds, R., Krummel, P., Loh, Zoe, Worthy, Doug, Hatakka, Juha, Aalto, Tuula, Ramonet, Michel, Delmotte, Marc, Schmidt, Martina, Gheusi, Francois, Mihalopoulos, N., Morgui, J.A., Andrews, Arlyn, Dlugokencky, Ed, Lee, John, Sweeney, Colm, Thoning, Kirk, Tans, Pieter, De Wekker, Stephan, Fischer, Marc L., Jaffe, Dan, McKain, Kathryn, Viner, Brian, Miller, John B., Karion, Anna, Miller, Charles, Sloop, Christopher D., Saito, Kazuyuki, Aoki, Shuji, Morimoto, Shinji, Goto, Daisuke, Steinbacher, Martin, Myhre, Cathrine Lund, Hermanssen, Ove, Stephens, Britton, Keeling, Ralph, Afshar, Sara, Paplawsky, Bill, Cox, Adam, Walker, Stephen, Schuldt, Kenneth, Mukai, Hitoshi, Machida, Toshinobu, Sasakawa, Motoki, Nomura, Shohei, Ito, Akihiko, Iida, Yosuke, and Jones, Matthew W.: Long-term global CO2 fluxes estimated by NICAM-based Inverse Simulation for Monitoring CO2 (NISMON-CO2) (ver.2022.1), National Institute for Environmental Studies Japan [dataset], https://doi.org/10.17595/20201127.001, 2020.

Obermeier, W. A., Nabel, J. E. M. S., Loughran, T., Hartung, K., Bastos, A., Havermann, F., Anthoni, P., Arneth, A., Goll, D. S., Lienert, S., Lombardozzi, D., Luyssaert, S., McGuire, P. C., Melton, J. R., Poulter, B., Sitch, S., Sullivan, M. O., Tian, H., Walker, A. P., Wiltshire, A. J., Zaehle, S., and Pongratz, J.: Modelled land use and land cover change emissions – a spatio-temporal comparison of different approaches, 12, 635–670, https://doi.org/10.5194/esd-12-635-2021, 2021.

O'Rourke, P. R., Smith, S. J., Mott, A., Ahsan, H., McDuffie, E. E., Crippa, M., Klimont, Z., McDonald, B., Wang, S., Nicholson, M. B., Feng, L., and Hoesly, R. M.: CEDS v_2021_04_21 Release Emission Data, https://doi.org/10.5281/zenodo.4741285, 2021.

O'Sullivan, M., Zhang, Y., Bellouin, N., Harris, I., Mercado, L. M., Sitch, S., Ciais, P., and Friedlingstein, P.: Aerosol–light interactions reduce the carbon budget imbalance, Environ. Res. Lett., 16, 124072, https://doi.org/10.1088/1748-9326/ac3b77, 2021.

O'Sullivan, M., Friedlingstein, P., Sitch, S., Anthoni, P., Arneth, A., Arora, V. K., Bastrikov, V., Delire, C., Goll, D. S., Jain, A., Kato, E., Kennedy, D., Knauer, J., Lienert, S., Lombardozzi, D., McGuire, P. C., Melton, J. R., Nabel, J. E. M. S., Pongratz, J., Poulter, B., Séférian, R., Tian, H., Vuichard, N., Walker, A. P., Yuan, W., Yue, X., and Zaehle, S.: Process-oriented analysis of dominant sources of uncertainty in the land carbon sink, Nat. Commun., 13, 4781, https://doi.org/10.1038/s41467-022-32416-8, 2022.

O'Sullivan, M., Spracklen, D. V., Batterman, S. A., Arnold, S. R., Gloor, M., and Buermann, W.: Have Synergies Between Nitrogen Deposition and Atmospheric CO2 Driven the Recent Enhancement of the Terrestrial Carbon Sink?, Glob. Biogeochem. Cycles, 33, 163–180, https://doi.org/10.1029/2018GB005922, 2019.

Palmer, P. I., Feng, L., Baker, D., Chevallier, F., Bösch, H., and Somkuti, P.: Net carbon emissions from African biosphere dominate pan-tropical atmospheric CO2 signal, Nat Commun, 10, 3344, https://doi.org/10.1038/s41467-019-11097-w, 2019.

Pan, Y., Birdsey, R. A., Fang, J., Houghton, R., Kauppi, P. E., Kurz, W. A., Phillips, O. L., Shvidenko, A., Lewis, S. L., Canadell, J. G., Ciais, P., Jackson, R. B., Pacala, S. W., McGuire, A. D., Piao, S., Rautiainen, A., Sitch, S., and Hayes, D.: A Large and Persistent Carbon Sink in the World's Forests, Science, 333, 988–993, https://doi.org/10.1126/science.1201609, 2011.

Pendrill, F., Persson, U. M., Godar, J., Kastner, T., Moran, D., Schmidt, S., and Wood, R.: Agricultural and forestry trade drives large share of tropical deforestation emissions, Global Environmental Change, 56, 1–10, https://doi.org/10.1016/j.gloenvcha.2019.03.002, 2019.

Peters, G. P., Minx, J. C., Weber, C. L., and Edenhofer, O.: Growth in emission transfers via international trade from 1990 to 2008, Proceedings of the National Academy of Sciences, 108, 8903–8908, https://doi.org/10.1073/pnas.1006388108, 2011a.

Peters, G. P., Marland, G., Le Quéré, C., Boden, T., Canadell, J. G., and Raupach, M. R.: Rapid growth in CO2 emissions after the 2008–2009 global financial crisis, Nature Clim Change, 2, 2–4, https://doi.org/10.1038/nclimate1332, 2012a.

Peters, G. P., Andrew, R. M., Boden, T., Canadell, J. G., Ciais, P., Le Quéré, C., Marland, G., Raupach, M. R., and Wilson, C.: The challenge to keep global warming below 2 °C, Nature Clim Change, 3, 4–6, https://doi.org/10.1038/nclimate1783, 2013.

Peters, G. P., Le Quéré, C., Andrew, R. M., Canadell, J. G., Friedlingstein, P., Ilyina, T., Jackson, R. B., Joos, F., Korsbakken, J. I., McKinley, G. A., Sitch, S., and Tans, P.: Towards real-time verification of CO2 emissions, Nature Clim Change, 7, 848–850, https://doi.org/10.1038/s41558-017-0013-9, 2017.

Peters, G. P., Andrew, R. M., Canadell, J. G., Friedlingstein, P., Jackson, R. B., Korsbakken, J. I., Le Quéré, C., and Peregon, A.: Carbon dioxide emissions continue to grow amidst slowly emerging climate policies, Nat. Clim. Chang., 10, 3–6, https://doi.org/10.1038/s41558-019-0659-6, 2020.

Peters, W., Miller, J. B., Whitaker, J., Denning, A. S., Hirsch, A., Krol, M. C., Zupanski, D., Bruhwiler, L., and Tans, P. P.: An ensemble data assimilation system to estimate CO2 surface fluxes from atmospheric trace gas observations, J. Geophys. Res. Atmospheres, 110, https://doi.org/10.1029/2005JD006157, 2005.

Peters W, Woude Avd, Luijkx I, Joetzjer E, Lafont S, Loubet B, Herig-Coimbra P, Loustau D, Koren G, Ciais P, Ramonet M, Xu Y, Bastos A, Sitch S, Kneuer T, Kubistin D, De Kok R, Botía S. Temperature extremes of 2022 reduced carbon uptake by forests in Europe. doi:10.21203/rs.3.rs-2841861/v1. PPR:PPR653515, 2023.

Petrescu, A. M. R., Peters, G. P., Janssens-Maenhout, G., Ciais, P., Tubiello, F. N., Grassi, G., Nabuurs, G.-J., Leip, A., Carmona-Garcia, G., Winiwarter, W., Höglund-Isaksson, L., Günther, D., Solazzo, E., Kiesow, A., Bastos, A., Pongratz, J., Nabel, J. E. M. S., Conchedda, G., Pilli, R., Andrew, R. M., Schelhaas, M.-J., and Dolman, A. J.: European anthropogenic AFOLU greenhouse gas emissions: a review and benchmark data, Earth Syst. Sci. Data, 12, 961–1001, https://doi.org/10.5194/essd-12-961-2020, 2020.

Pfeil, B., Olsen, A., Bakker, D. C. E., Hankin, S., Koyuk, H., Kozyr, A., Malczyk, J., Manke, A., Metzl, N., Sabine, C. L., Akl, J., Alin, S. R., Bates, N., Bellerby, R. G. J., Borges, A., Boutin, J., Brown, P. J., Cai, W.-J., Chavez, F. P., Chen, A., Cosca, C., Fassbender, A. J., Feely, R. A., González-Dávila, M., Goyet, C., Hales, B., Hardman-Mountford, N., Heinze, C., Hood, M., Hoppema, M., Hunt, C. W., Hydes, D., Ishii, M., Johannessen, T., Jones, S. D., Key, R. M., Körtzinger, A., Landschützer, P., Lauvset, S. K., Lefèvre, N., Lenton, A., Lourantou, A., Merlivat, L., Midorikawa, T., Mintrop, L., Miyazaki, C., Murata, A., Nakadate, A., Nakano, Y., Nakaoka, S., Nojiri, Y., Omar, A. M., Padin, X. A., Park, G.-H., Paterson, K., Perez, F. F., Pierrot, D., Poisson, A., Ríos, A. F., Santana-Casiano, J. M., Salisbury, J., Sarma, V. V. S. S., Schlitzer, R., Schneider, B., Schuster, U., Sieger, R., Skjelvan, I., Steinhoff, T., Suzuki, T., Takahashi, T., Tedesco, K., Telszewski, M., Thomas, H., Tilbrook, B., Tjiputra, J., Vandemark, D., Veness, T., Wanninkhof, R., Watson, A. J., Weiss,

R., Wong, C. S., and Yoshikawa-Inoue, H.: A uniform, quality controlled Surface Ocean CO2 Atlas (SOCAT), Earth Syst. Sci. Data, 5, 125–143, https://doi.org/10.5194/essd-5-125-2013, 2013.

Piao, S., Ciais, P., Friedlingstein, P., de Noblet-Ducoudré, N., Cadule, P., Viovy, N., and Wang, T.: Spatiotemporal patterns of terrestrial carbon cycle during the 20th century, Global Biogeochem. Cy., 23, GB4026, https://doi.org/10.1029/2008GB003339, 2009.

Piao, S., Huang, M., Liu, Z., Wang, X., Ciais, P., Canadell, J. G., Wang, K., Bastos, A., Friedlingstein, P., Houghton, R. A., Le Quéré, C., Liu, Y., Myneni, R. B., Peng, S., Pongratz, J., Sitch, S., Yan, T., Wang, Y., Zhu, Z., Wu, D., and Wang, T.: Lower land-use emissions responsible for increased net land carbon sink during the slow warming period, Nature Geosci, 11, 739–743, https://doi.org/10.1038/s41561-018-0204-7, 2018.

Pongratz, J., Reick, C. H., Houghton, R. A., and House, J. I.: Terminology as a key uncertainty in net land use and land cover change carbon flux estimates, Earth Syst. Dynam., 5, 177–195, https://doi.org/10.5194/esd-5-177-2014, 2014.

Poulter, B., Bastos, A., Canadell, J., Ciais, P., Gruber, N., Hauck, J., Jackson, R., Ishii, M., Müller, J., Patra, P., and Tian, H.: Inventorying Earth's Land and Ocean Greenhouse Gases, Eos, 103, https://doi.org/10.1029/2022EO179084, 2022.

Poulter, B., Frank, D. C., Hodson, E. L., and Zimmermann, N. E.: Impacts of land cover and climate data selection on understanding terrestrial carbon dynamics and the CO2 airborne fraction, Biogeosciences, 8, 2027–2036, https://doi.org/10.5194/bg-8-2027-2011, 2011.

Poulter, B., Freeborn, P. H., Jolly, W. M., and Varner, J. M.: COVID-19 lockdowns drive decline in active fires in southeastern United States, PNAS, 118, e2105666118, https://doi.org/10.1073/pnas.2105666118, 2021.

Powis, C. M., Smith, S. M., Minx, J. C., and Gasser, T.: Quantifying global carbon dioxide removal deployment, Environ. Res. Lett., 18, 024022, https://doi.org/10.1088/1748-9326/acb450, 2023.

Prentice, I. C., Farquhar, G. D., Fasham, M. J. R., Goulden, M. L., Heimann, M., Jaramillo, V. J., Kheshgi, H. S., Le Quéré, C., Scholes, R. J., and Wallace, D. W. R.: The Carbon Cycle and Atmospheric Carbon Dioxide, in Climate Change 2001: The Scientific Basis. Contribution of Working Group I to the Third Assessment Report of the Intergovernmental Panel on Climate Change, edited by: Houghton, J. T., Ding, Y., Griggs, D. J., Noguer, M., van der Linden, P. J., Dai, X., Maskell, K., and Johnson, C. A., Cambridge University Press, Cambridge, United Kingdom and New York, NY, USA, 183–237, ISBN: 978-0521014953, 2001.

Price, J. T. and Warren, R.: Literature Review of the Potential of "Blue Carbon" Activities to Reduce Emissions, available at: https://avoid-net-uk.cc.ic.ac.uk/wp-content/uploads/delightful-downloads/2016/03/Literature-review-of-the-potential-of-blue-carbon-activities-to-reduce-emissions-AVOID2-WPE2.pdf, last access: 9 November 2023, 2016.

Qin, Y., Xiao, X., Wigneron, J.-P., Ciais, P., Brandt, M., Fan, L., Li, X., Crowell, S., Wu, X., Doughty, R., Zhang, Y., Liu, F., Sitch, S., and Moore, B.: Carbon loss from forest degradation exceeds that from deforestation in the Brazilian Amazon, Nat. Clim. Chang., 11, 442–448, https://doi.org/10.1038/s41558-021-01026-5, 2021.

Randerson, J. T., Chen, Y., van der Werf, G. R., Rogers, B. M., and Morton, D. C.: Global burned area and biomass burning emissions from small fires: BURNED AREA FROM SMALL FIRES, J. Geophys. Res. Biogeosciences, 117, n/a-n/a, https://doi.org/10.1029/2012JG002128, 2012.

Raupach, M. R., Marland, G., Ciais, P., Le Quere, C., Canadell, J. G., Klepper, G., and Field, C. B.: Global and regional drivers of accelerating CO2 emissions, Proceedings of the National Academy of Sciences, 104, 10288–10293, https://doi.org/10.1073/pnas.0700609104, 2007.

Regnier, P., Resplandy, L., Najjar, R. G., and Ciais, P.: The land-to-ocean loops of the global carbon cycle, Nature, 603, 401–410, https://doi.org/10.1038/s41586-021-04339-9, 2022.

Reick, C. H., Gayler, V., Goll, D., Hagemann, S., Heidkamp, M., Nabel, J. E. M. S., Raddatz, T., Roeckner, E., Schnur, R., 110 and Wilkenskjeld, S.: JSBACH 3 – The land component of the MPI Earth System Model: documentation of version 3.2, available at: https://doi.org/10.17617/2.3279802, 2021.

Remaud, M., Chevallier, F., Cozic, A., Lin, X., and Bousquet, P.: On the impact of recent developments of the LMDz atmospheric general circulation model on the simulation of CO2 transport, 11, 4489, https://doi.org/10.5194/gmd-11-4489-2018, 2018.

Resplandy, L., Keeling, R. F., Rödenbeck, C., Stephens, B. B., Khatiwala, S., Rodgers, K. B., Long, M. C., Bopp, L., and Tans, P. P.: Revision of global carbon fluxes based on a reassessment of oceanic and riverine carbon transport, Nature Geosci, 11, 504–509, https://doi.org/10.1038/s41561-018-0151-3, 2018.

Rodenbeck, C., Houweling, S., Gloor, M., and Heimann, M.: CO2 flux history 1982–2001 inferred from atmospheric data using a global inversion of atmospheric transport, Atmos Chem Phys, 3, 1919–1964, 2003.

Rödenbeck, C., Bakker, D. C. E., Metzl, N., Olsen, A., Sabine, C., Cassar, N., Reum, F., Keeling, R. F., and Heimann, M.: Interannual sea–air CO2 flux variability from an observation-driven ocean mixed-layer scheme, 11, 4599–4613, https://doi.org/10.5194/bg-11-4599-2014, 2014.

Rödenbeck, C., Zaehle, S., Keeling, R., and Heimann, M.: History of El Niño impacts on the global carbon cycle 1957–2017: a quantification from atmospheric CO2 data, 373, 20170303, https://doi.org/10.1098/rstb.2017.0303, 2018.

Rödenbeck, C., DeVries, T., Hauck, J., Le Quéré, C., and Keeling, R. F.: Data-based estimates of interannual sea–air CO2 flux variations 1957–2020 and their relation to environmental drivers, Biogeosciences, 19, 2627–2652, https://doi.org/10.5194/bg-19-2627-2022, 2022.

Rosan, T. M., Klein Goldewijk, K., Ganzenmüller, R., O'Sullivan, M., Pongratz, J., Mercado, L. M., Aragao, L. E. O. C., Heinrich, V., Randow, C. V., Wiltshire, A., Tubiello, F. N., Bastos, A., Friedlingstein, P., and Sitch, S.: A multi-data assessment of land use and land cover emissions from Brazil during 2000–2019, Environ. Res. Lett., 16, 074004, https://doi.org/10.1088/1748-9326/ac08c3, 2021.

Sakamoto, K., H. Nakano, S. Urakawa, T. Toyoda, Y. Kawakami, H. Tsujino, G. Yamanaka, 2023: Reference manual for the Meteorological Research Institute Community Ocean Model version 5 (MRI.COMv5), Technical Reports of the Meteorological Research Institute, No.87, https://doi.org/10.11483/mritechrepo.87.

Sarma, V. V. S. S., Sridevi, B., Metzl, N., Patra, P. K., Lachkar, Z., Chakraborty, K., Goyet, C., Levy, M., Mehari, M., and Chandra, N.: Air-Sea Fluxes of CO2 in the Indian Ocean Between 1985 and 2018: A Synthesis Based on Observation-Based Surface CO2, Hindcast and Atmospheric Inversion Models, Glob. Biogeochem. Cycles, 37, e2023GB007694, https://doi.org/10.1029/2023GB007694, 2023.

Schaphoff, S., von Bloh, W., Rammig, A., Thonicke, K., Biemans, H., Forkel, M., Gerten, D., Heinke, J., Jägermeyr, J., Knauer, J., Langerwisch, F., Lucht, W., Müller, C., Rolinski, S., and Waha, K.: LPJmL4 – a dynamic global vegetation model with managed land – Part 1: Model description, Geosci. Model Dev., 11, 1343–1375, https://doi.org/10.5194/gmd-11-1343-2018, 2018.

Schimel, D., Alves, D., Enting, I. G., Heimann, M., Joos, F., Raynaud, D., Wigley, T., Prater, M., Derwent, R., Ehhalt, D., Fraser, P., Sanhueza, E., Zhou, X., Jonas, P., Charlson, R., Rodhe, H., Sadasivan, S., Shine, K. P., Fouquart, Y., Ramaswamy, V., Solomon, S., Srinivasan, J., Albritton, D., Derwent, R., Isaksen, I., Lal, M., and Wuebbles, D.: Radiative Forcing of Climate Change, in: Climate Change 1995: The Science of Climate Change, Contribution of Working Group I to the Second Assessment Report of the Intergovernmental Panel on Climate Change [Houghton, J. T., Meira Rilho, L. G., Callander, B. A., Harris, N., Kattenberg, A., and Maskell, K. (eds.)], Cambridge University Press, Cambridge, United Kingdom and New York, NY, USA, ISBN: 978-0521559621, 1995.

Schimel, D., Stephens, B. B., and Fisher, J. B.: Effect of increasing CO 2 on the terrestrial carbon cycle, Proc Natl Acad Sci USA, 112, 436–441, https://doi.org/10.1073/pnas.1407302112, 2015.

Schuh, A. E., Jacobson, A. R., Basu, S., Weir, B., Baker, D., Bowman, K., Chevallier, F., Crowell, S., Davis, K. J., Deng, F., Denning, S., Feng, L., Jones, D., Liu, J., and Palmer, P. I.: Quantifying the Impact of Atmospheric Transport Uncertainty on CO 2 Surface Flux Estimates, Global Biogeochem. Cycles, 33, 484–500, https://doi.org/10.1029/2018GB006086, 2019.

Schwinger, J., Goris, N., Tjiputra, J. F., Kriest, I., Bentsen, M., Bethke, I., Ilicak, M., Assmann, K. M., and Heinze, C.: Evaluation of NorESM-OC (versions 1 and 1.2), the ocean carbon-cycle stand-alone configuration of the Norwegian Earth System Model (NorESM1), Geosci. Model Dev., 9, 2589–2622, https://doi.org/10.5194/gmd-9-2589-2016, 2016.

Schwingshackl, C., Obermeier, W. A., Bultan, S., Grassi, G., Canadell, J. G., Friedlingstein, P., Gasser, T., Houghton, R. A., Kurz, W. A., Sitch, S., and Pongratz, J.: Differences in land-based mitigation estimates reconciled by separating natural and land-use CO2 fluxes at the country level, One Earth, 5, 1367–1376, https://doi.org/10.1016/j.oneear.2022.11.009, 2022.

Séférian, R., Nabat, P., Michou, M., Saint-Martin, D., Voldoire, A., Colin, J., Decharme, B., Delire, C., Berthet, S., Chevallier, M., Sénési, S., Franchisteguy, L., Vial, J., Mallet, M., Joetzjer, E., Geoffroy, O., Guérémy, J.-F., Moine, M.-P., Msadek, R., Ribes, A., Rocher, M., Roehrig, R., Salas-y-Mélia, D., Sanchez, E., Terray, L., Valcke, S., Waldman, R., Aumont, O., Bopp, L., Deshayes, J., Éthé, C., and Madec, G.: Evaluation of CNRM Earth System Model, CNRM-ESM2-1: Role of Earth System Processes in Present-Day and Future Climate, Journal of Advances in Modeling Earth Systems, 11, 4182–4227, https://doi.org/10.1029/2019MS001791, 2019.

Seiler, C., Melton, J. R., Arora, V. K., Sitch, S., Friedlingstein, P., Anthoni, P., Goll, D., Jain, A. K., Joetzjer, E., Lienert, S., Lombardozzi, D., Luyssaert, S., Nabel, J. E. M. S., Tian, H., Vuichard, N., Walker, A. P., Yuan, W., and Zaehle, S.: Are Terrestrial Biosphere Models Fit for Simulating the Global Land Carbon Sink?, J. Adv. Model. Earth Syst., 14, e2021MS002946, https://doi.org/10.1029/2021MS002946, 2022.

Sellar, A. A., Jones, C. G., Mulcahy, J. P., Tang, Y., Yool, A., Wiltshire, A., O'Connor, F. M., Stringer, M., Hill, R., Palmieri, J., Woodward, S., Mora, L., Kuhlbrodt, T., Rumbold, S. T., Kelley, D. I., Ellis, R., Johnson, C. E., Walton, J., Abraham, N. L., Andrews, M. B., Andrews, T., Archibald, A. T., Berthou, S., Burke, E., Blockley, E., Carslaw, K., Dalvi, M., Edwards, J., Folberth, G. A., Gedney, N., Griffiths, P. T., Harper, A. B., Hendry, M. A., Hewitt, A. J., Johnson, B., Jones, A., Jones, C. D., Keeble, J., Liddicoat, S., Morgenstern, O., Parker, R. J., Predoi, V., Robertson, E., Siahaan, A.,

Smith, R. S., Swaminathan, R., Woodhouse, M. T., Zeng, G., and Zerroukat, M.: UKESM1: Description and Evaluation of the U.K. Earth System Model, J. Adv. Model. Earth Syst., 11, 4513–4558, https://doi.org/10.1029/2019MS001739, 2019.

Shu, S., Jain, A. K., Koven, C. D., and Mishra, U.: Estimation of Permafrost SOC Stock and Turnover Time Using a Land Surface Model With Vertical Heterogeneity of Permafrost Soils, Global Biogeochem. Cy., 34, e2020GB006585, https://doi.org/10.1029/2020GB006585, 2020.

Shutler, J. D., Land, P. E., Piolle, J.-F., Woolf, D. K., Goddijn-Murphy, L., Paul, F., Girard-Ardhuin, F., Chapron, B., and Donlon, C. J.: FluxEngine: A Flexible Processing System for Calculating Atmosphere–Ocean Carbon Dioxide Gas Fluxes and Climatologies, J. Atmospheric Ocean. Technol., 33, 741–756, https://doi.org/10.1175/JTECH-D-14-00204.1, 2016.

Sitch, S., Huntingford, C., Gedney, N., Levy, P. E., Lomas, M., Piao, S. L., Betts, R., Ciais, P., Cox, P., Friedlingstein, P., Jones, C. D., Prentice, I. C., and Woodward, F. I.: Evaluation of the terrestrial carbon cycle, future plant geography and climate-carbon cycle feedbacks using five Dynamic Global Vegetation Models (DGVMs): Uncertainty In Land Carbon Cycle Feedbacks, Glob. Change Biol., 14, 2015–2039, https://doi.org/10.1111/j.1365-2486.2008.01626.x, 2008.

Smallman, T. L., Milodowski, D. T., Neto, E. S., Koren, G., Ometto, J., and Williams, M.: Parameter uncertainty dominates C-cycle forecast errors over most of Brazil for the 21st century, Earth Syst. Dyn., 12, 1191–1237, https://doi.org/10.5194/esd-12-1191-2021, 2021.

Smith, B., Wårlind, D., Arneth, A., Hickler, T., Leadley, P., Siltberg, J., and Zaehle, S.: Implications of incorporating N cycling and N limitations on primary production in an individual-based dynamic vegetation model, Biogeosciences, 11, 2027–2054, https://doi.org/10.5194/bg-11-2027-2014, 2014.

Smith, S., Geden, O., Nemet, G., Gidden, M., Lamb, W., Powis, C., Bellamy, R., Callaghan, M., Cowie, A., Cox, E. and Fuss, S., 2023. The State of Carbon Dioxide Removal–1st Edition, http://dx.doi.org/10.17605/OSF.IO/W3B4Z, 2023.

Sospedra-Alfonso, R., Merryfield, W. J., Boer, G. J., Kharin, V. V., Lee, W.-S., Seiler, C., and Christian, J. R.: Decadal climate predictions with the Canadian Earth System Model version 5 (CanESM5), Geosci. Model Dev., 14, 6863–6891, https://doi.org/10.5194/gmd-14-6863-2021, 2021.

Stephens, B. B., Gurney, K. R., Tans, P. P., Sweeney, C., Peters, W., Bruhwiler, L., Ciais, P., Ramonet, M., Bousquet, P., Nakazawa, T., Aoki, S., Machida, T., Inoue, G., Vinnichenko, N., Lloyd, J., Jordan, A., Heimann, M., Shibistova, O., Langenfelds, R. L., Steele, L. P., Francey, R. J., and Denning, A. S.: Weak Northern and Strong Tropical Land Carbon Uptake from Vertical Profiles of Atmospheric CO2, Science, 316, 1732–1735, https://doi.org/10.1126/science.1137004, 2007.

Stephens, B. B., Keeling, R. F., Heimann, M., Six, K. D., Murnane, R., and Caldeira, K.: Testing global ocean carbon cycle models using measurements of atmospheric O2 and CO2 concentration, Glob. Biogeochem. Cycles, 12, 213–230, https://doi.org/10.1029/97GB03500, 1998.

Stocker, T., Qin, D., and Platner, G.-K.: Climate Change 2013: The Physical Science Basis. Contribution of Working Group I to the Fifth Assessment Report of the Intergovernmental Panel on Climate Change [Intergovernmental Panel on Climate Change (eds.)], Cambridge University Press, Cambridge, ISBN: 9789291691388, 2013.\

Swart, N. C., Cole, J. N. S., Kharin, V. V., Lazare, M., Scinocca, J. F., Gillett, N. P., Anstey, J., Arora, V., Christian, J. R., Hanna, S., Jiao, Y., Lee, W. G., Majaess, F., Saenko, O. A., Seiler, C., Seinen, C., Shao, A., Sigmond, M., Solheim, L., von Salzen, K., Yang, D., and Winter, B.: The Canadian Earth System Model version 5 (CanESM5.0.3), Geosci. Model Dev., 12, 4823–4873, https://doi.org/10.5194/gmd-12-4823-2019, 2019.

SX Coal: Monthly coal consumption estimates, http://www.sxcoal.com/, last access: 9 November 2023, 2022.

Takahashi, T., Sutherland, S. C., Wanninkhof, R., Sweeney, C., Feely, R. A., Chipman, D. W., Hales, B., Friederich, G., Chavez, F., Sabine, C., Watson, A., Bakker, D. C. E., Schuster, U., Metzl, N., Yoshikawa-Inoue, H., Ishii, M., Midorikawa, T., Nojiri, Y., Körtzinger, A., Steinhoff, T., Hoppema, M., Olafsson, J., Arnarson, T. S., Tilbrook, B., Johannessen, T., Olsen, A., Bellerby, R., Wong, C. S., Delille, B., Bates, N. R., and de Baar, H. J. W.: Climatological mean and decadal change in surface ocean pCO2, and net sea–air CO2 flux over the global oceans, Deep Sea Research Part II: Topical Studies in Oceanography, 56, 554–577, https://doi.org/10.1016/j.dsr2.2008.12.009, 2009.

Terhaar, J., Frölicher, T. L., and Joos, F.: Southern Ocean anthropogenic carbon sink constrained by sea surface salinity, Sci. Adv., 7, eabd5964, https://doi.org/10.1126/sciadv.abd5964, 2021.

Terhaar, J., Frölicher, T. L., and Joos, F.: Observation-constrained estimates of the global ocean carbon sink from Earth system models, Biogeosciences, 19, 4431–4457, https://doi.org/10.5194/bg-19-4431-2022, 2022.

Tian, H., Xu, X., Lu, C., Liu, M., Ren, W., Chen, G., Melillo, J., and Liu, J.: Net exchanges of CO2, CH4, and N2O between China's terrestrial ecosystems and the atmosphere and their contributions to global climate warming, J. Geophys. Res. Biogeosciences, 116, G02011, https://doi.org/10.1029/2010JG001393, 2011.

Tian, H., Chen, G., Lu, C., Xu, X., Hayes, D. J., Ren, W., Pan, S., Huntzinger, D. N., and Wofsy, S. C.: North American terrestrial CO2 uptake largely offset by CH4 and N2O emissions: toward a full accounting of the greenhouse gas budget, Climatic Change, 129, 413–426, https://doi.org/10.1007/s10584-014-1072-9, 2015.

Tubiello, F. N., Conchedda, G., Wanner, N., Federici, S., Rossi, S., and Grassi, G.: Carbon emissions and removals from forests: new estimates, 1990–2020, Earth Syst. Sci. Data, 13, 1681–1691, https://doi.org/10.5194/essd-13-1681-2021, 2021.

Tuck, C.: 2022 Mineral Commodity Summary: Iron Ore, Tech. rep., U.S. Geological Survey, https://pubs.usgs.gov/periodicals/mcs2022/mcs2022-iron-ore.pdf, 2022.

UNFCCC: Synthesis report for the technical assessment component of the first global stocktake, available at: https://unfccc.int/documents/461466, last access: 9 November 2023, 2022

Urakawa, L. S., Tsujino, H., Nakano, H., Sakamoto, K., Yamanaka, G., and Toyoda, T.: The sensitivity of a depth-coordinate model to diapycnal mixing induced by practical implementations of the isopycnal tracer diffusion scheme, Ocean Model., 154, 101693, https://doi.org/10.1016/j.ocemod.2020.101693, 2020.

Vale, M. M., Berenguer, E., Argollo de Menezes, M., Viveiros de Castro, E. B., Pugliese de Siqueira, L., and Portela, R. de C. Q.: The COVID-19 pandemic as an opportunity to weaken environmental protection in Brazil, Biological Conservation, 255, 108994, https://doi.org/10.1016/j.biocon.2021.108994, 2021.

van der Laan-Luijkx, I. T., van der Velde, I. R., van der Veen, E., Tsuruta, A., Stanislawska, K., Babenhauserheide, A., Zhang, H. F., Liu, Y., He, W., Chen, H., Masarie, K. A., Krol, M. C., and Peters, W.: The CarbonTracker Data Assimilation Shell (CTDAS) v1.0: implementation and global carbon balance 2001–2015, Geosci. Model Dev., 10, 2785–2800, https://doi.org/10.5194/gmd-10-2785-2017, 2017.

van der Velde, I. R., van der Werf, G. R., Houweling, S., Maasakkers, J. D., Borsdorff, T., Landgraf, J., Tol, P., van Kempen, T. A., van Hees, R., Hoogeveen, R., Veefkind, J. P., and Aben, I.: Vast CO2 release from Australian fires in 2019–2020 constrained by satellite, Nature, 597, 366–369, https://doi.org/10.1038/s41586-021-03712-y, 2021.

van der Werf, G. R., Randerson, J. T., Giglio, L., Collatz, G. J., Mu, M., Kasibhatla, P. S., Morton, D. C., DeFries, R. S., Jin, Y., and van Leeuwen, T. T.: Global fire emissions and the contribution of deforestation, savanna, forest, agricultural, and peat fires (1997–2009), Atmospheric Chem. Phys., 10, 11707–11735, https://doi.org/10.5194/acp-10-11707-2010, 2010.

van der Werf, G. R., Randerson, J. T., Giglio, L., van Leeuwen, T. T., Chen, Y., Rogers, B. M., Mu, M., van Marle, M. J. E., Morton, D. C., Collatz, G. J., Yokelson, R. J., and Kasibhatla, P. S.: Global fire emissions estimates during 1997–2016, Earth Syst. Sci. Data, 9, 697–720, https://doi.org/10.5194/essd-9-697-2017, 2017.

van Wees, D., van der Werf, G. R., Randerson, J. T., Andela, N., Chen, Y., and Morton, D. C.: The role of fire in global forest loss dynamics, Glob. Change Biol., 27, 2377–2391, https://doi.org/10.1111/gcb.15591, 2021.

von Bloh, W., Schaphoff, S., Müller, C., Rolinski, S., Waha, K., and Zaehle, S.: Implementing the nitrogen cycle into the dynamic global vegetation, hydrology, and crop growth model LPJmL (version 5.0), Geosci. Model Dev., 11, 2789–2812, https://doi.org/10.5194/gmd-11-2789-2018, 2018.

Vaittinada Ayar, P., Bopp, L., Christian, J. R., Ilyina, T., Krasting, J. P., Séférian, R., Tsujino, H., Watanabe, M., Yool, A., and Tjiputra, J.: Contrasting projections of the ENSO-driven CO2 flux variability in the equatorial Pacific under high-warming scenario, Earth Syst. Dynam., 13, 1097–1118, https://doi.org/10.5194/esd-13-1097-2022, 2022.

Vuichard, N., Messina, P., Luyssaert, S., Guenet, B., Zaehle, S., Ghattas, J., Bastrikov, V., and Peylin, P.: Accounting for carbon and nitrogen interactions in the global terrestrial ecosystem model ORCHIDEE (trunk version, rev 4999): multi-scale evaluation of gross primary production, Geosci. Model Dev., 12, 4751–4779, https://doi.org/10.5194/gmd-12-4751-2019, 2019.

Walker, A. P., Quaife, T., Bodegom, P. M., De Kauwe, M. G., Keenan, T. F., Joiner, J., Lomas, M. R., MacBean, N., Xu, C., Yang, X., and Woodward, F. I.: The impact of alternative trait-scaling hypotheses for the maximum photosynthetic carboxylation rate (V cmax) on global gross primary production, New Phytol., 215, 1370–1386, https://doi.org/10.1111/nph.14623, 2017.

Walker, A. P., De Kauwe, M. G., Bastos, A., Belmecheri, S., Georgiou, K., Keeling, R. F., McMahon, S. M., Medlyn, B. E., Moore, D. J. P., Norby, R. J., Zaehle, S., Anderson-Teixeira, K. J., Battipaglia, G., Brienen, R. J. W., Cabugao, K. G., Cailleret, M., Campbell, E., Canadell, J. G., Ciais, P., Craig, M. E., Ellsworth, D. S., Farquhar, G. D., Fatichi, S., Fisher, J. B., Frank, D. C., Graven, H., Gu, L., Haverd, V., Heilman, K., Heimann, M., Hungate, B. A., Iversen, C. M., Joos, F., Jiang, M., Keenan, T. F., Knauer, J., Körner, C., Leshyk, V. O., Leuzinger, S., Liu, Y., MacBean, N., Malhi, Y., McVicar, T. R., Penuelas, J., Pongratz, J., Powell, A. S., Riutta, T., Sabot, M. E. B., Schleucher, J., Sitch, S., Smith, W. K., Sulman, B., Taylor, B., Terrer, C., Torn, M. S., Treseder, K. K., Trugman, A. T., Trumbore, S. E., van Mantgem, P. J., Voelker, S. L.,

Whelan, M. E., and Zuidema, P. A.: Integrating the evidence for a terrestrial carbon sink caused by increasing atmospheric CO2, New Phytol., 229, 2413–2445, https://doi.org/10.1111/nph.16866, 2021.

Watanabe, M., Tatebe, H., Koyama, H., Hajima, T., Watanabe, M., and Kawamiya, M.: Importance of El Niño reproducibility for reconstructing historical CO2 flux variations in the equatorial Pacific, Ocean Sci., 16, 1431–1442, https://doi.org/10.5194/os-16-1431-2020, 2020.

Watson, A. J., Schuster, U., Shutler, J. D., Holding, T., Ashton, I. G. C., Landschützer, P., Woolf, D. K., and Goddijn-Murphy, L.: Revised estimates of ocean-atmosphere CO2 flux are consistent with ocean carbon inventory, Nat Commun, 11, 4422, https://doi.org/10.1038/s41467-020-18203-3, 2020.

Watson, R. T., Rohde, H., Oeschger, H., and Siegenthaler, U.: Greenhouse Gases and Aerosols, in: Climate Change: The IPCC Scientific Assessment. Intergovernmental Panel on Climate Change (IPCC), edited by: Houghton, J. T., Jenkins, G. J., and Ephraums, J. J., Cambridge University Press, Cambridge, ISBN: 978-0521403603, 1990.

Wenzel, S., Cox, P. M., Eyring, V., and Friedlingstein, P.: Projected land photosynthesis constrained by changes in the seasonal cycle of atmospheric CO2, Nature, 538, 499–501, https://doi.org/10.1038/nature19772, 2016.

Wilkenskjeld, S., Kloster, S., Pongratz, J., Raddatz, T., and Reick, C. H.: Comparing the influence of net and gross anthropogenic land-use and land-cover changes on the carbon cycle in the MPI-ESM, Biogeosciences, 11, 4817–4828, https://doi.org/10.5194/bg-11-4817-2014, 2014.

Wiltshire, A. J., Burke, E. J., Chadburn, S. E., Jones, C. D., Cox, P. M., Davies-Barnard, T., Friedlingstein, P., Harper, A. B., Liddicoat, S., Sitch, S., and Zaehle, S.: JULES-CN: a coupled terrestrial carbon–nitrogen scheme (JULES vn5.1), 14, 2161–2186, https://doi.org/10.5194/gmd-14-2161-2021, 2021.

Winkler, K., Yang, H., Ganzenmüller, R., Fuchs, R., Ceccherini, G., Duveiller, G., Grassi, G., Pongratz, J., Bastos, A., Shvidenko, A., Araza, A., Herold, M., Wigneron, J.-P., and Ciais, P.: Changes in land use and management led to a decline in Eastern Europe's terrestrial carbon sink, Commun. Earth Environ., 4, 1–14, https://doi.org/10.1038/s43247-023-00893-4, 2023.

Woodward, F. I. and Lomas, M. R.: Vegetation dynamics – simulating responses to climatic change, Biol. Rev., 79, 643–670, https://doi.org/10.1017/S1464793103006419, 2004.

Wright, R. M., Le Quéré, C., Buitenhuis, E., Pitois, S., and Gibbons, M. J.: Role of jellyfish in the plankton ecosystem revealed using a global ocean biogeochemical model, 18, 1291–1320, https://doi.org/10.5194/bg-18-1291-2021, 2021.

Wunder, S., Kaimowitz, D., Jensen, S., and Feder, S.: Coronavirus, macroeconomy, and forests: What likely impacts?, For. Policy Econ., 131, 102536, https://doi.org/10.1016/j.forpol.2021.102536, 2021.

Xi, F., Davis, S. J., Ciais, P., Crawford-Brown, D., Guan, D., Pade, C., Shi, T., Syddall, M., Lv, J., Ji, L., Bing, L., Wang, J., Wei, W., Yang, K.-H., Lagerblad, B., Galan, I., Andrade, C., Zhang, Y., and Liu, Z.: Substantial global carbon uptake by cement carbonation, Nature Geosci, 9, 880–883, https://doi.org/10.1038/ngeo2840, 2016.

Xia, J., Chen, Y., Liang, S., Liu, D., and Yuan, W.: Global simulations of carbon allocation coefficients for deciduous vegetation types, Tellus B, 67, 28016, https://doi.org/10.3402/tellusb.v67.28016, 2015.

Yang, D., Liu, Y., Feng, L., Wang, J., Yao, L., Cai, Z., Zhu, S., Lu, N., and Lyu, D.: The First Global Carbon Dioxide Flux Map Derived from TanSat Measurements, Adv. Atmospheric Sci., 38, 1433–1443, https://doi.org/10.1007/s00376-021-1179-7, 2021.

Yang, X., Thornton, P., Ricciuto, D., Wang, Y., and Hoffman, F.: Global evaluation of terrestrial biogeochemistry in the Energy Exascale Earth System Model (E3SM) and the role of the phosphorus cycle in the historical terrestrial carbon balance, Biogeosciences, 20, 2813–2836, https://doi.org/10.5194/bg-20-2813-2023, 2023.

Yu, Z., Ciais, P., Piao, S., Houghton, R. A., Lu, C., Tian, H., Agathokleous, E., Kattel, G. R., Sitch, S., Goll, D., Yue, X., Walker, A., Friedlingstein, P., Jain, A. K., Liu, S., and Zhou, G.: Forest expansion dominates China's land carbon sink since 1980, Nat. Commun., 13, 5374, https://doi.org/10.1038/s41467-022-32961-2, 2022.

Yue, X. and Unger, N.: The Yale Interactive terrestrial Biosphere model version 1.0: description, evaluation and implementation into NASA GISS ModelE2, Geosci. Model Dev., 8, 2399–2417, https://doi.org/10.5194/gmd-8-2399-2015, 2015.

Yuan, W., Liu, D., Dong, W., Liu, S., Zhou, G., Yu, G., Zhao, T., Feng, J., Ma, Z., Chen, J., Chen, Y., Chen, S., Han, S., Huang, J., Li, L., Liu, H., Liu, S., Ma, M., Wang, Y., Xia, J., Xu, W., Zhang, Q., Zhao, X., and Zhao, L.: Multiyear precipitation reduction strongly decreases carbon uptake over northern China, J. Geophys. Res.-Biogeo., 119, 881–896, https://doi.org/10.1002/2014JG002608, 2014.

Yue, C., Ciais, P., Zhu, D., Wang, T., Peng, S. S., and Piao, S. L.: How have past fire disturbances contributed to the current carbon balance of boreal ecosystems?, Biogeosciences, 13, 675–690, https://doi.org/10.5194/bg-13-675-2016, 2016.

Zaehle, S. and Friend, A. D.: Carbon and nitrogen cycle dynamics in the O-CN land surface model: 1. Model description, site-scale evaluation, and sensitivity to parameter estimates: Site-scale evaluation of a C-N model, Global Biogeochem. Cycles, 24, GB1005, https://doi.org/10.1029/2009GB003521, 2010.

Zaehle, S., Ciais, P., Friend, A. D., and Prieur, V.: Carbon benefits of anthropogenic reactive nitrogen offset by nitrous oxide emissions, Nature Geosci, 4, 601–605, https://doi.org/10.1038/ngeo1207, 2011.

Zaehle, S., Medlyn, B. E., De Kauwe, M. G., Walker, A. P., Dietze, M. C., Hickler, T., Luo, Y., Wang, Y.-P., El-Masri, B., Thornton, P., Jain, A., Wang, S., Warlind, D., Weng, E., Parton, W., Iversen, C. M., Gallet-Budynek, A., McCarthy, H., Finzi, A., Hanson, P. J., Prentice, I. C., Oren, R., and Norby, R. J.: Evaluation of 11 terrestrial carbon–nitrogen cycle models against observations from two temperate Free-Air CO2 Enrichment studies, New Phytol., 202, 803–822, https://doi.org/10.1111/nph.12697, 2014.

Zeng, J., Iida, Y., Matsunaga, T., and Shirai, T.: Surface ocean CO2 concentration and air-sea flux estimate by machine learning with modelled variable trends, Front. Mar. Sci., 9, https://doi.org/10.3389/fmars.2022.989233, 2022.

Zheng, B., Ciais, P., Chevallier, F., Chuvieco, E., Chen, Y., and Yang, H.: Increasing forest fire emissions despite the decline in global burned area, Sci. Adv., 7, eabh2646, https://doi.org/10.1126/sciadv.abh2646, 2021.

Zou, Y., Wang, Y., Ke, Z., Tian, H., Yang, J., and Liu, Y.: Development of a REgion-Specific Ecosystem Feedback Fire (RESFire) Model in the Community Earth System Model, J. Adv. Model. Earth Syst., 11, 417–445, https://doi.org/10.1029/2018MS001368, 2019.

Zscheischler, J., Mahecha, M. D., Avitabile, V., Calle, L., Carvalhais, N., Ciais, P., Gans, F., Gruber, N., Hartmann, J., Herold, M., Ichii, K., Jung, M., Landschützer, P., Laruelle, G. G., Lauerwald, R., Papale, D., Peylin, P., Poulter, B., Ray, D., Regnier, P., Rödenbeck, C., Roman-Cuesta, R. M., Schwalm, C., Tramontana, G., Tyukavina, A., Valentini, R., van der Werf, G., West, T. O., Wolf, J. E., and Reichstein, M.: Reviews and syntheses: An empirical spatiotemporal description of the global surface–atmosphere carbon fluxes: opportunities and data limitations, Biogeosciences, 14, 3685–3703, https://doi.org/10.5194/bg-14-3685-2017, 2017.

Tables

Unit 1	Unit 2	Conversion	Source
GtC (gigatonnes of carbon)	ppm (parts per million) (a)	2.124 (b)	Ballantyne et al. (2012)
GtC (gigatonnes of carbon)	PgC (petagrams of carbon)	1	SI unit conversion
GtCO2 (gigatonnes of carbon dioxide)	GtC (gigatonnes of carbon)	3.664	44.01/12.011 in mass equivalent
GtC (gigatonnes of carbon)	MtC (megatonnes of carbon)	1000	SI unit conversion
(a) Measurements of atmospheric CO2 concentration have units of dry-air mole fraction. 'ppm' is an abbreviation for micromole/mol, dry air.			
(b) The use of a factor of 2.124 assumes that all the atmosphere is well mixed within one year. In reality, only the troposphere is well mixed and the growth rate of CO2 concentration in the less well-mixed stratosphere is not measured by sites from the NOAA network. Using a factor of 2.124 makes the approximation that the growth rate of CO2 concentration in the stratosphere equals that of the troposphere on a yearly basis.			

Table 1. Factors used to convert carbon in various units (by convention, Unit 1 = Unit 2 × conversion).

Component	Primary reference
Global fossil CO2 emissions (EFOS), total and by fuel type	Updated from Andrew and Peters (2022)
National territorial fossil CO2 emissions (EFOS)	Gilfillan and Marland (2021), UNFCCC (2022)
National consumption-based fossil CO2 emissions (EFOS) by country (consumption)	Peters et al. (2011a) updated as described in this paper
Net land-use change flux (ELUC)	This paper (see Table 4 for individual model references).
Growth rate in atmospheric CO2 concentration (GATM)	Lan et al. (2023)
Ocean and land CO2 sinks (SOCEAN and SLAND)	This paper (see Table 4 for individual model and data products references).

Table 2. How to cite the individual components of the global carbon budget presented here.

Publication year	Fossil fuel emissions		LUC emissions	Reservoirs			Other changes
	Global	Country (territorial)		Atmosphere	Ocean	Land	
2019 Friedlingstein et al. (2019) GCB2019	Global emissions calculated as sum of all countries plus bunkers, rather than taken directly from CDIAC.		Average of two bookkeeping models; use of 15 DGVMs	Use of three atmospheric inversions	Based on nine models	Based on 16 models	
2020 Friedlingstein et al. (2020) GCB2020	Cement carbonation now included in the EFOS estimate, reducing EFOS by about 0.2GtC yr-1 for the last decade	India's emissions from Andrew (2020: India); Corrections to Netherland Antilles and Aruba and Soviet emissions before 1950 as per Andrew (2020: CO2); China's coal emissions in 2019 derived from official statistics, emissions now shown for EU27 instead of EU28. Projection for 2020 based on assessment of four approaches.	Average of three bookkeeping models; use of 17 DGVMs. Estimate of gross land use sources and sinks provided	Use of six atmospheric inversions	Based on nine models. River flux revised and partitioned NH, Tropics, SH	Based on 17 models	
2021 Friedlingstein et al. (2022a) GCB2021	Projections are no longer an assessment of four approaches.	Official data included for a number of additional countries, new estimates for South Korea, added emissions from lime	ELUC estimate compared to the estimates adopted in national GHG inventories (NGHGI)		Average of means of eight models and means of seven data-products. Current year prediction of SOCEAN using a feed-forward	Current year prediction of SLAND using a feed-forward neural network method	

		production in China.			neural network method		
2022 Friedlingstein et al. (2022) GCB2022			ELUC provided at country level. Revised components decomposition of ELUC fluxes. Revision of LUC maps for Brazil. New datasets for peat drainage.	Use of nine atmospheric inversions	Average of means of ten models and means of seven data-products	Based on 16 models. Revision of LUC maps for Brazil.	
2023 This study			Refined components decomposition of ELUC. Revision of LUC maps for Indonesia. Use of updated peat drainage estimates.	Use of 14 atmospheric inversions. Additional use of 4 Earth System Models to estimate current year CO2	Additional use of 4 Earth System Models and atmospheric oxygen method to assess SOCEAN. Regional distribution of river flux adjustment revised.	Based on 20 models. Additional use of 4 Earth System Models and atmospheric oxygen method to assess the net atmosphere-land flux.	Inclusion of an estimate of Carbon Dioxide Removal (CDR)

Table 3. Main methodological changes in the global carbon budget since 2019. Methodological changes introduced in one year are kept for the following years unless noted. Empty cells mean there were no methodological changes introduced that year. Table S8 lists methodological changes from the first global carbon budget publication up to 2018.

Model/data name	Reference	Change from Global Carbon Budget 2022 (Friedlingstein et al., 2022b)
Bookkeeping models for land-use change emissions		
BLUE	Hansis et al. (2015)	No change to model, but simulations performed with LUH2-GCB2023 forcing. Update in added peat drainage emissions.
H&C2023	Houghton and Castanho (2023)	H&C2023 replaces the formerly used H&N2017 model. Minor bug fix in fuel harvest estimates. Update in added peat drainage emissions.
OSCAR	Gasser et al. (2020)	No change to model, but land-use forcing changed to LUH2-GCB2023 and FRA2020 (extrapolated to 2022). Constraining based on GCB2022 data for SLAND over 1960-2021. Update in added peat drainage emissions.
Dynamic global vegetation models		
CABLE-POP	Haverd et al. (2018)	Improved representation of nitrogen retranslocation and plant uptake, minor bug fixes, parameter changes
CLASSIC	Melton et al. (2020), Asaadi et al. (2018)	Bug fixes, correct allocation of leaves after summer solstice for latitudes higher than 45°N, improved phenology for several PFTs
CLM5.0	Lawrence et al. (2019)	No change.
DLEM	Tian et al. (2011, 2015)	No change.
EDv3	Moorcroft et al. (2001), Ma et al. (2022)	New this year.
ELM	Yang et al.(2023), Burrows et al.(2020)	New this year.
IBIS	Yuan et al. (2014)	Changes in parameterisation and new module of soil nitrogen dynamics (Ma et al., 2022)
ISAM	Jain et al. (2013), Meiyappan et al. (2015), Shu et al. (2020)	Vertically resolved soil biogeochemistry (carbon and nitrogen) module, following Shu et al. (2020),
ISBA-CTRIP	Delire et al. (2020)	No change.
JSBACH	Mauritsen et al. (2019), Reick et al. (2021)	No change.
JULES-ES	Wiltshire et al. (2021), Sellar et al. (2019), Burton et al. (2019)	Minor bug fixes. (Using JULES v6.3, suite u-co002)
LPJ-GUESS	Smith et al. (2014)	Minor bug fixes.

LPJml	Schaphoff et al., 2018, von Bloh et al., 2018, Lutz et al., 2019 (tillage), Heinke et al., 2023 (livestock grazing)	New this year.
LPJwsl	Poulter et al. (2011) (d)	No change.
LPX-Bern	Lienert and Joos (2018)	No change.
OCN	Zaehle and Friend (2010), Zaehle et al. (2011)	Minor bug fixes
ORCHIDEEv3	Krinner et al. (2005), Zaehle and Friend (2010), Vuichard et al. (2019)	Small update for leaf senescence (ORCHIDEE - V3; revision 8119)
SDGVM	Woodward and Lomas (2004), Walker et al. (2017)	implement gross land-use transitions, tracking of carbon from wood & crop harvest, and tracking of primary & secondary vegetation
VISIT	Ito and Inatomi (2012), Kato et al. (2013)	No change.
YIBs	Yue and Unger (2015)	Inclusion of process-based water cycle from Noah-MP (Niu et al., 2011)
Intermediate complexity land carbon cycle model		
CARDAMOM	Bloom et al. (2016), Smallman et al. (2021)	New this year
Global ocean biogeochemistry models		
NEMO3.6-PISCESv2-gas (CNRM)	Berthet et al. (2019), Séférian et al. (2019)	No change.
FESOM-2.1-REcoM2	Gürses et al. (2023)	No change
NEMO-PISCES (IPSL)	Aumont et al. (2015)	No change.
MOM6-COBALT (Princeton)	Liao et al. (2020)	No change
MRI-ESM2-2	Nakano et al. (2011)	The ocean model has been updated to MRI.COMv5 (Sakamoto et al. 2023). The distribution of background vertical diffusivity is changed to the one proposed by Kawasaki et al. (2021). Model was spup-up with a preindustrial xCO2 of 278 ppm.
MICOM-HAMOCC (NorESM-OCv1.2)	Schwinger et al. (2016)	No change.
NEMO-PlankTOM12	Wright et al. (2021)	Minor bug fixes, switch to ERA5 forcing, salinity restoring

CESM-ETHZ	Doney et al. (2009)	Model was spup-up with a preindustrial xCO2 of 278 ppm.
MPIOM-HAMOCC6	Lacroix et al. (2021)	No change.
ACCESS (CSIRO)	Law et al. (2017)	Minor bug fixes, extended spinup since last participation 2020.
fCO2-products		
CMEMS-LSCE-FFNNv2	Chau et al. (2022)	Update to SOCATv2023 measurements and time period 1985-2022. The mapping approach by Chau et al (2022) has been upgraded by increasing spatial resolution from 1° to 0.25°.
JMA-MLR	Iida et al. (2021)	Updated to SOCATv2023
LDEO-HPD	Gloege et al. (2022), Bennington et al. (2022)	Updated with SOCATv2023. Updated with current GCB2023 models and extending back in time using Bennington et al. (2022) method.
MPI-SOMFFN	Landschützer et al. (2016)	update to SOCATv2023. Since GCB2022, fluxes cover open ocean and coastal domains as well as the Arctic Ocean extension.
NIES-ML3	Zeng et al. (2022)	New this year
OS-ETHZ-GRaCER	Gregor et al. (2021)	Updated to SOCATv2023
Jena-MLS	Rödenbeck et al. (2014, 2022)	update to SOCATv2023 measurements, time period extended to 1957-2022
UOEx-Watson	Watson et al. (2020)	Updated to SOCAT v2023. fCO2(sw) corrected to CCI SST v2.1 (Merchant et al. 2019) instead of OI SST v2.1. Updated interpolation datasets to CCI SST v2.1, CMEMS SSS and MLD (Jean-Michel et al. 2021). Monthly cool skin difference calculated using NOAA COARE 3.5 (Edson et al. 2013). CO2 flux computed using FluxEngine (Holding et al., 2019; Shutler et al., 2016).
Atmospheric inversions		
Jena CarboScope	Rödenbeck et al. (2003, 2018)	Extension to 2022, re-addition of a 2.5-year relaxation term.
CAMS	Chevallier et al. (2005), Remaud et al. (2018)	Increase of the 3D resolution (4.5 times more 3D cells than the previous submission); extension to year 2022; update of the prior fluxes.
CarbonTracker Europe (CTE)	van der Laan-Luijkx et al. (2017)	Extension to 2022, update of prior fluxes.
NISMON-CO2	Niwa et al. (2020, 2022)	Prior terrestrial fluxes include minor fluxes (BVOC and CH4) in addition to GPP, RE and LUC.
CT-NOAA	Peters et al. (2005), Jacobson et al. (2023a, 2023b)	New this year.
CMS-Flux	Liu et al. (2021)	Update of OCO-2 observations and prior fluxes.

CAMS-Satellite	Chevallier et al. (2005), Remaud et al. (2018)	Increase of the 3D resolution, extension to year 2022 and the first months of 2023; removal of the pre-OCO-2 period (2010-2014 with GOSAT); update of the prior fluxes.
GONGGA	Jin et al. (2023)	Update of OCO-2 observations and prior fluxes.
THU	Kong et al. (2022)	Updates to the OCO-2 product and the fossil fuel data.
COLA	Liu et al. (2022)	New this year.
GCASv2	Jiang et al. (2021, 2022)	New this year.
UoE in-situ	Feng et al. (2009), Feng et al. (2016), Palmer et al. (2019)	Update of the inversion system by using new version of GEOS-Chem
IAPCAS	Feng et al. (2016), Yang et al. (2021)	New this year.
MIROC4-ACTM	Chandra et al. (2022)	New this year
Earth System Models		
CanESM5	Swart et al. (2019), Sospedra-Alfonso et al. (2021)	New this year.
IPSL-CM6a-CO2-LR	Boucher et al. (2020)	New this year.
MIROC-ES2L	Watanabe et al. (2020)	New this year.
MPI-ESM1-2-LR	Mauritsen et al. (2019), Li et al. (2023)	New this year.

Table 4. References for the process models, bookkeeping models, ocean data products, and atmospheric inversions. All models and products are updated with new data to the end of year 2022, and the atmospheric forcing for the DGVMs has been updated as described in Section C.2.2 and C.4.1.

		1960s	1970s	1980s	1990s	2000s	2013-2022	2022
Land-use change emissions (ELUC)	Bookkeeping (BK) Net flux (1a)	1.5±0.7	1.3±0.7	1.4±0.7	1.6±0.7	1.4±0.7	1.3±0.7	1.2±0.7
	BK - deforestation (total)	1.7 [1.3,2.1]	1.6 [1.2,1.9]	1.7 [1.3,2.1]	1.9 [1.6,2.2]	2 [1.6,2.4]	1.9 [1.5,2.4]	1.9 [1.4,2.5]
	BK - forest regrowth (total)	-0.8 [-1.1,-0.6]	-0.9 [-1.1,-0.7]	-0.9 [-1.1,-0.7]	-1 [-1.2,-0.7]	-1.1 [-1.3,-0.8]	-1.3 [-1.5,-0.9]	-1.3 [-1.6,-1]
	BK - other transitions	0.4 [0.3,0.4]	0.2 [0.1,0.3]	0.2 [0.2,0.3]	0.1 [0,0.2]	0.1 [0,0.2]	0.1 [0,0.3]	0.1 [0,0.2]
	BK - peat drainage & peat fires	0.2 [0.1,0.2]	0.2 [0.1,0.2]	0.2 [0.2,0.3]	0.3 [0.3,0.3]	0.3 [0.2,0.3]	0.3 [0.3,0.3]	0.2 [0.2,0.3]
	BK - wood harvest & forest management	0.2 [-0.2,0.6]	0.2 [-0.2,0.6]	0.2 [-0.2,0.6]	0.2 [-0.1,0.6]	0.2 [-0.1,0.6]	0.2 [0,0.6]	0.2 [0,0.7]
	DGVMs-net flux (1b)	1.5±0.5	1.3±0.5	1.6±0.6	1.8±0.6	1.8±0.7	1.7±0.6	1.7±0.6
Terrestrial sink (SLAND)	Residual sink from global budget ($E_{FOS}+E_{LUC}$(1a)-G_{ATM}-S_{OCEAN}) (2a)	1.7±0.8	1.8±0.8	1.7±0.9	2.7±0.9	2.9±0.9	2.9±0.9	3.7±1
	DGVMs (2b)	1.3±0.5	2±0.7	1.9±0.8	2.5±0.6	2.9±0.7	3.3±0.8	3.8±0.8
Net land fluxes (SLAND-ELUC)	GCB2023 Budget (2b-1a)	-0.2±0.8	0.8±1	0.5±1	0.9±0.9	1.4±1	2.1±1.1	2.6±1.1
	Atmospheric O_2	---	---	---	1.2±1	1.1±1.1	1.1±1.3	-
	DGVMs-net (2b-1b)	-0.2±0.4	0.7±0.7	0.3±0.6	0.7±0.5	1.1±0.4	1.7±0.6	2.1±0.6
	Inversions*	- [-,-]	- [-,-]	0.5 [0.4,0.6] (2)	0.9 [0.6,1.3] (3)	1.3 [0.7,2] (4)	1.6 [0.5,2.3] (8)	2.7 [1.4-3.8] (13)
	ESMs	---	---	0.6 [0.1,1]	1.7 [1.3,2]	2 [1.4,2.7]	2.4 [1.8,3.3]	3.9 [2.8-5.5]

*Estimates are adjusted for the pre-industrial influence of river fluxes, for the cement carbonation sink, and adjusted to common E_{FOS} (Sect. 2.7). The ranges given include varying numbers (in parentheses) of inversions in each decade (Table S4).

Table 5. Comparison of results from the bookkeeping method and budget residuals with results from the DGVMs, as well as additional estimates from atmospheric oxygen, atmospheric inversions and Earth System Models (ESMs) for different periods, the last decade, and the last year available. All values are in GtCyr−1. See Figure 7 for explanation of the bookkeeping component fluxes. The DGVM uncertainties represent ±1σ of the decadal or annual (for 2022) estimates from the individual DGVMs: for the inverse systems the mean and range of available results is given. All values are rounded to the nearest 0.1 GtC and therefore columns do not necessarily add to zero.

Product	1960s	1970s	1980s	1990s	2000s	2013-2022	2022
fCO_2 -products	---	---	---	2.3 [2,2.9]	2.4 [2.2,2.7]	3.1 [2.6,3.3]	3.1 [2.5,3.3]
GOBMs	1±0.3	1.2±0.3	1.7±0.3	2±0.3	2.1±0.4	2.6±0.4	2.5±0.4
GCB2023 Budget	1.1±0.4	1.4±0.4	1.9±0.4	2.1±0.4	2.3±0.4	2.8±0.4	2.8±0.4
Atmospheric O_2	---	---	---	2±0.7	2.6±0.6	3.3±0.6	-
Inversions	- [-,-]	- [-,-]	1.7 [1.6,1.8] (2)	2.2 [1.9,2.5] (3)	2.4 [1.8,3.1] (4)	3 [2.4,4.1] (8)	3 [2.2-4.2] (13)
ESMs	---	---	1.6 [0.7,2.4]	1.8 [1.1,2.5]	2.1 [1.5,2.8]	2.6 [2.2,3.4]	2.7 [2.3-3.5]

Table 6: Comparison of results for the ocean sink from the *f*CO2-products, from global ocean biogeochemistry models (GOBMs), the best estimate for GCB2023 as calculated from fCO2-products and GOBMs that is used in the budget Table 7, as well as additional estimates from atmospheric oxygen, atmospheric inversions and Earth System Models (ESMs) for different periods, the last decade, and the last year available. All values are in GtCyr−1. Uncertainties represent ±1σ of the estimates from the GOBMs (N>10) and range of ensemble members is given for ensembles with N<10 (*f*CO2-products, inversions, ESMs). The uncertainty of the GCB2023 budget estimate is based on expert judgement (Section 2 and Supplementary S1 to S4) and for oxygen it is the standard deviation of a Monte Carlo ensemble (Section 2.8).

		1960s	1970s	1980s	1990s	2000s	2013-2022	2022	2023 (Projection)
Total emissions (EFOS + ELUC)	Fossil CO2 emissions (EFOS)*	3±0.2	4.7±0.2	5.5±0.3	6.4±0.3	7.8±0.4	9.6±0.5	9.9±0.5	10±0.5
	Land-use change emissions (ELUC)	1.5±0.7	1.3±0.7	1.4±0.7	1.6±0.7	1.4±0.7	1.3±0.7	1.2±0.7	1.1±0.7
	Total emissions	4.6±0.7	6±0.7	6.9±0.8	7.9±0.8	9.2±0.8	10.9±0.8	11.1±0.9	11.1±0.9
Partitioning	Growth rate in atmos CO2 (GATM)	1.7±0.07	2.8±0.07	3.4±0.02	3.1±0.02	4±0.02	5.2±0.02	4.6±0.2	5.1±0.4
	Ocean sink (SOCEAN)	1.1±0.4	1.4±0.4	1.9±0.4	2.1±0.4	2.3±0.4	2.8±0.4	2.8±0.4	2.9±0.6
	Terrestrial sink (SLAND)	1.3±0.5	2±0.7	1.9±0.8	2.5±0.6	2.9±0.7	3.3±0.8	3.8±0.8	2.9±1.2
Budget Imbalance	BIM=EFOS+ELUC-(GATM+SOCEAN+SLAND)	0.4	-0.2	-0.2	0.2	0	-0.4	-0.1	0.3

*Fossil emissions excluding the cement carbonation sink amount to 3±0.2 GtC/yr, 4.7±0.2 GtC/yr, 5.5±0.3 GtC/yr, 6.4±0.3 GtC/yr, 7.9±0.4 GtC/yr, and 9.8±0.5 GtC/yr for the decades 1960s to 2010s respectively and to 10.1±0.5 GtC/yr for 2022, and 10.2±0.5 GtC/yr for 2023.

Table 7: Decadal mean in the five components of the anthropogenic CO2 budget for different periods, and last year available. All values are in GtC yr-1, and uncertainties are reported as ±1σ. Fossil CO_2 emissions include cement carbonation. The table also shows the budget imbalance (B_{IM}), which provides a measure of the discrepancies among the nearly independent estimates. A positive imbalance means the emissions are overestimated and/or the sinks are too small. All values are rounded to the nearest 0.1 GtC and therefore columns do not necessarily add to zero.

		1750-2022	1850-2014	1850-2022	1960-2022	1850-2023
Emissions	Fossil CO2 emissions (EFOS)	480±25	400±20	475±25	395±20	485±25
	Land-use change emissions (ELUC)	250±75	210±65	220±65	90±45	220±65
	Total emissions	730±80	610±65	695±70	485±50	705±70
Partitioning	Growth rate in atmos CO2 (GATM)	300±5	235±5	280±5	215±5	285±5
	Ocean sink (SOCEAN)	190±40	155±30	180±35	125±25	180±35
	Terrestrial sink (SLAND)	245±60	200±50	225±55	150±35	225±55
Budget imbalance	BIM=EFOS+ELUC-(GATM+SOCEAN+SLAND)	-5	20	15	-5	15

Table 8. Cumulative CO_2 for different time periods in gigatonnes of carbon (GtC). Fossil CO_2 emissions include cement carbonation. The budget imbalance (B_{IM}) provides a measure of the discrepancies among the nearly independent estimates. All values are rounded to the nearest 5 GtC and therefore columns do not necessarily add to zero. Uncertainties are reported as follows: E_{FOS} is 5% of cumulative emissions; E_{LUC} prior to 1959 is 1$\boldsymbol{\sigma}$ spread from the DGVMs, E_{LUC} post-1959 is 0.7*number of years (where 0.7 GtC/yr is the uncertainty on the annual E_{LUC} flux estimate); G_{ATM} uncertainty is held constant at 5 GtC for all time periods; S_{OCEAN} uncertainty is 20% of the cumulative sink (20% relates to the annual uncertainty of 0.4 GtC/yr, which is ~20% of the current ocean sink); and S_{LAND} is the 1$\boldsymbol{\sigma}$ spread from the DGVMs estimates.

	2003-2012	2013-2022
ELUC from bookkeeping estimates (from Table 5)	1.4	1.3
SLAND on non-intact forest from DGVMs	1.9	2.0
ELUC subtract SLAND on non-intact forests	-0.5	-0.8
National Greenhouse Gas Inventories	-0.4	-0.7

Table 9: Translation of global carbon cycle models' land flux definitions to the definition of the LULUCF net flux used in national Greenhouse Gas Inventories reported to UNFCCC. See Sec. C.2.3 and Table S9 for detail on methodology and comparison to other datasets. Units are GtC yr-1.

Source of uncertainty	Time scale (years)	Location	Evidence
Fossil CO2 emissions (EFOS; Section 2.1)			
energy statistics	annual to decadal	global, but mainly China & major developing countries	(Korsbakken et al., 2016, Guan et al., 2012)
carbon content of coal	annual to decadal	global, but mainly China & major developing countries	(Liu et al., 2015)
system boundary	annual to decadal	all countries	(Andrew, 2020a)
Net land-use change flux (ELUC; section 2.2)			
land-cover and land-use change statistics	continuous	global; in particular tropics	(Houghton et al., 2012, Gasser et al., 2020, Ganzenmüller et al., 2022, Yu et al. 2022)
sub-grid-scale transitions	annual to decadal	global	(Wilkenskjeld et al., 2014)
vegetation biomass	annual to decadal	global; in particular tropics	(Houghton et al., 2012, Bastos et al., 2021)
forest degradation (fire, selective logging)	annual to decadal	tropics	(Aragão et al., 2018, Qin et al., 2021)
wood and crop harvest	annual to decadal	global; SE Asia	(Arneth et al., 2017, Erb et al., 2018)
peat burning	multi-decadal trend	global	(van der Werf et al., 2010, 2017)
loss of additional sink capacity	multi-decadal trend	global	(Pongratz et al, 2014, Gasser et al, 2020; Obermeier et al., 2021)
Atmospheric growth rate (GATM; section 2.4) no demonstrated uncertainties larger than ±0.3 GtC yr-1 . The uncertainties in GATM have been estimated as ±0.2 GtC yr-1, although the conversion of the growth rate into a global annual flux assuming instantaneous mixing throughout the atmosphere introduces additional errors that have not yet been quantified.			
Ocean sink (SOCEAN; section 2.5)			
sparsity in surface fCO2 observations	mean, decadal variability and trend	global, in particular southern hemisphere	(Gloege et al., 2021, Denvil-Sommer et al., 2021, Hauck et al., 2023)

riverine carbon outgassing and its anthropogenic perturbation	annual to decadal	global, in particular partitioning between Tropics and South	(Aumont et al., 2001, Lacroix et al., 2020, Cris et al., 2022)
Models underestimate interior ocean anthropogenic carbon storage	annual to decadal	global	(Friedlingstein et al., 2021, this study, DeVries et al., 2023, see also Terhaar et al., 2022)
near-surface temperature and salinity gradients	mean on all time-scales	global	(Watson et al., 2020, Dong et al., 2022, Bellenger et al., 2023)
Land sink (SLAND; section 2.6)			
strength of CO2 fertilisation	multi-decadal trend	global	(Wenzel et al., 2016; Walker et al., 2021)
response to variability in temperature and rainfall	annual to decadal	global; in particular tropics	(Cox et al., 2013; Jung et al., 2017; Humphrey et al., 2018; 2021)
nutrient limitation and supply	annual to decadal	global	(Zaehle et al., 2014)
carbon allocation and tissue turnover rates	annual to decadal	global	(De Kauwe et al., 2014; O'Sullivan et al., 2022)
tree mortality	annual	global in particular tropics	(Hubau et al., 2021; Brienen et al., 2020)
response to diffuse radiation	annual	global	(Mercado et al., 2009; O'Sullivan et al., 2021)

Table 10. Major known sources of uncertainties in each component of the Global Carbon Budget, defined as input data or processes that have a demonstrated effect of at least ±0.3 GtC yr-1.

Figures and Captions

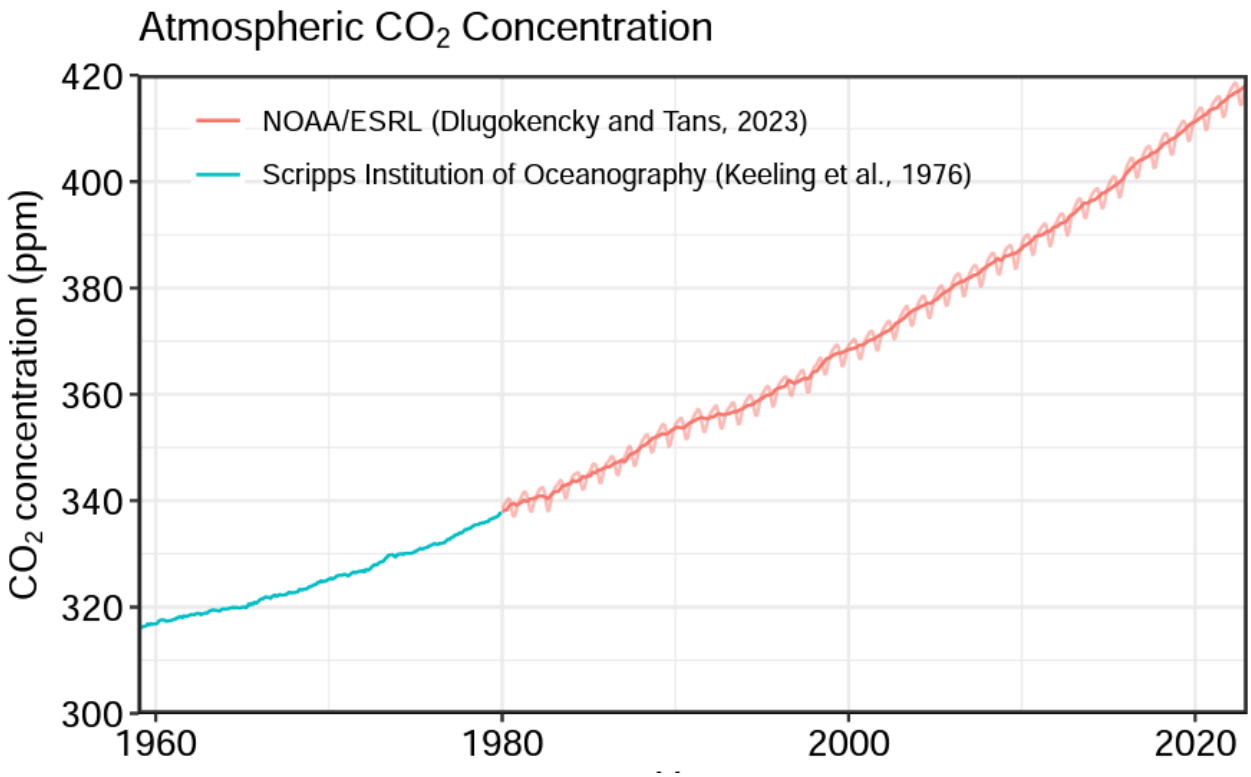

Figure 1. Surface average atmospheric CO_2 concentration (ppm). Since 1980, monthly data are from NOAA/GML (Lan et al., 2023) and are based on an average of direct atmospheric CO_2 measurements from multiple stations in the marine boundary layer (Masarie and Tans, 1995). The 1958-1979 monthly data are from the Scripps Institution of Oceanography, based on an average of direct atmospheric CO_2 measurements from the Mauna Loa and South Pole stations (Keeling et al., 1976). To account for the difference of mean CO_2 and seasonality between the NOAA/GML and the Scripps station networks used here, the Scripps surface average (from two stations) was de-seasonalised and adjusted to match the NOAA/GML surface average (from multiple stations) by adding the mean difference of 0.667 ppm, calculated here from overlapping data during 1980-2012.

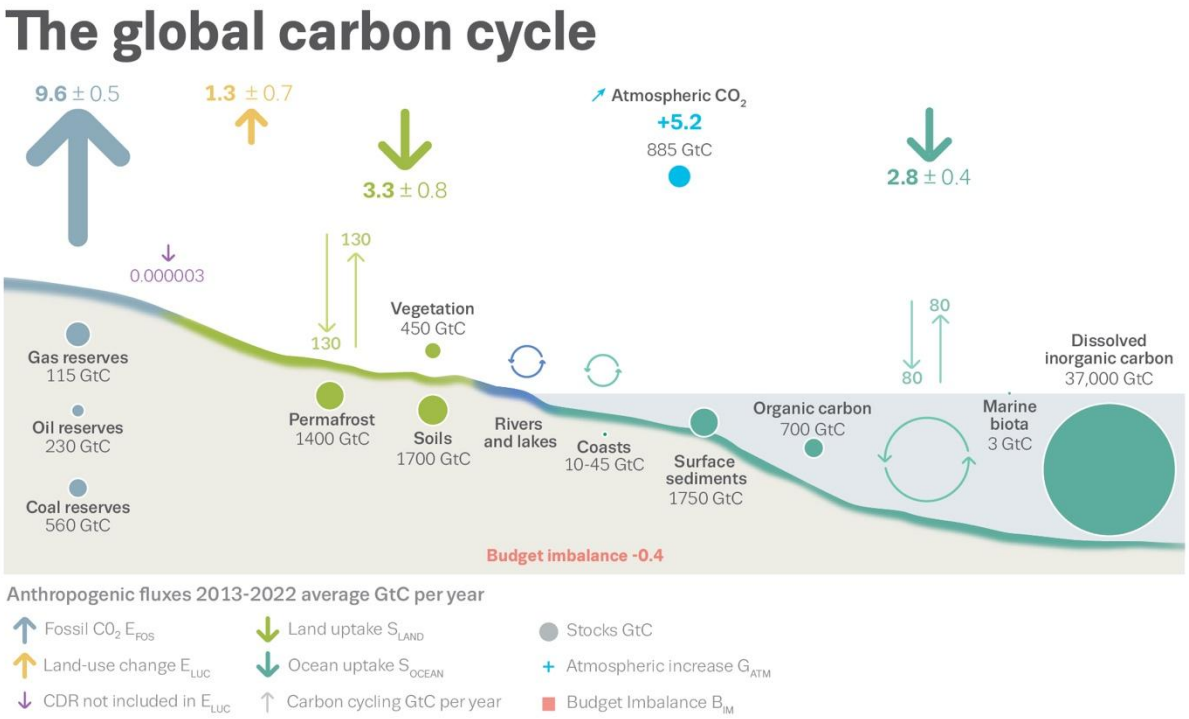

Figure 2. Schematic representation of the overall perturbation of the global carbon cycle caused by anthropogenic activities, averaged globally for the decade 2013-2022. See legends for the corresponding arrows. Fluxes estimates and their 1 standard deviation uncertainty are as reported in Table 7. The uncertainty in the atmospheric CO_2 growth rate is very small (±0.02 GtC yr^{-1}) and is neglected for the figure. The anthropogenic perturbation occurs on top of an active carbon cycle, with fluxes and stocks represented in the background and taken from Canadell et al. (2021) for all numbers, except for the carbon stocks in coasts which is from a literature review of coastal marine sediments (Price and Warren, 2016). Fluxes are in GtC yr^{-1} and reservoirs in GtC.

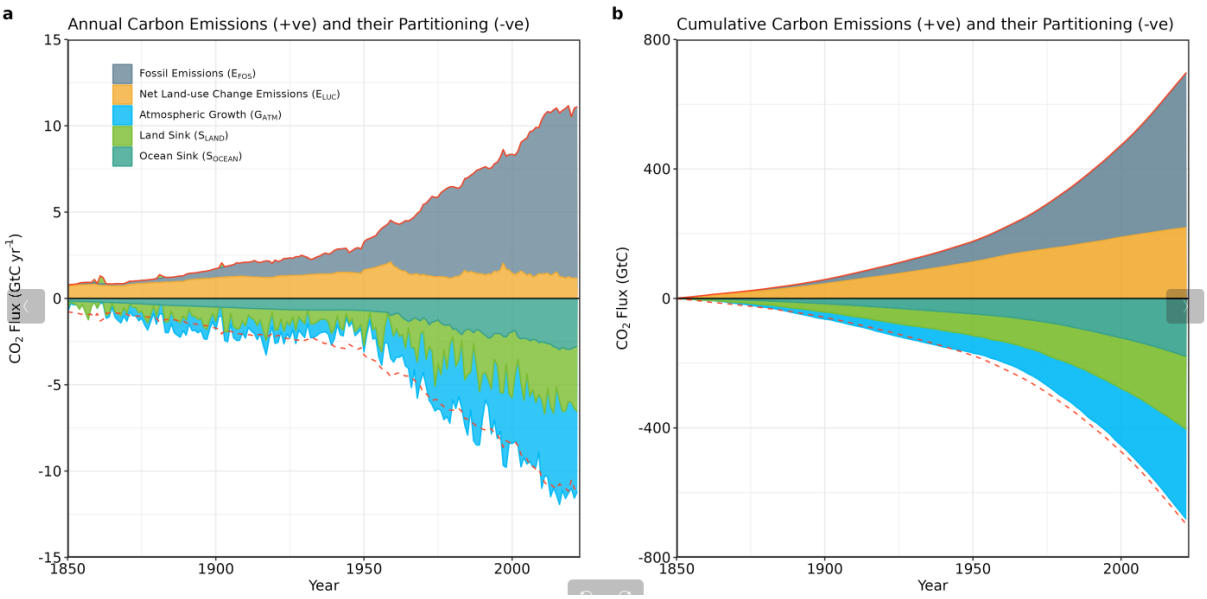

Figure 3. Combined components of the global carbon budget as a function of time, for fossil CO_2 emissions (E_{FOS}, including a small sink from cement carbonation; grey) and emissions from land-use change (E_{LUC}; brown), as well as their partitioning among the atmosphere (G_{ATM}; cyan), ocean (S_{OCEAN}; blue), and land (S_{LAND}; green). Panel (a) shows annual estimates of each flux (in GtC yr^{-1}) and panel (b) the cumulative flux (the sum of all prior annual fluxes, in GtC) since the year 1850. The partitioning is based on nearly independent estimates from observations (for G_{ATM}) and from process model ensembles constrained by data (for S_{OCEAN} and S_{LAND}) and does not exactly add up to the sum of the emissions, resulting in a budget imbalance (B_{IM}) which is represented by the difference between the bottom red line (mirroring total emissions) and the sum of carbon fluxes in the ocean, land, and atmosphere reservoirs. All data are in GtC yr^{-1} (panel a) and GtC (panel b). The E_{FOS} estimate is based on a mosaic of different datasets, and has an uncertainty of ±5% (±1σ). The E_{LUC} estimate is from three bookkeeping models (Table 4) with uncertainty of ±0.7 GtC yr^{-1}. The G_{ATM} estimates prior to 1959 are from Joos and Spahni (2008) with uncertainties equivalent to about ±0.1-0.15 GtC yr-1 and from Lan et al. (2023) since 1959 with uncertainties of about +-0.07 GtC yr^{-1} during 1959-1979 and ±0.02 GtC yr^{-1} since 1980. The S_{OCEAN} estimate is the average from Khatiwala et al. (2013) and DeVries (2014) with uncertainty of about ±30% prior to 1959, and the average of an ensemble of models and an ensemble of fCO_2-products (Table 4) with uncertainties of about ±0.4 GtC yr^{-1} since 1959. The S_{LAND} estimate is the average of an ensemble of models

(Table 4) with uncertainties of about ±1 GtC yr^{-1}. See the text for more details of each component and their uncertainties.

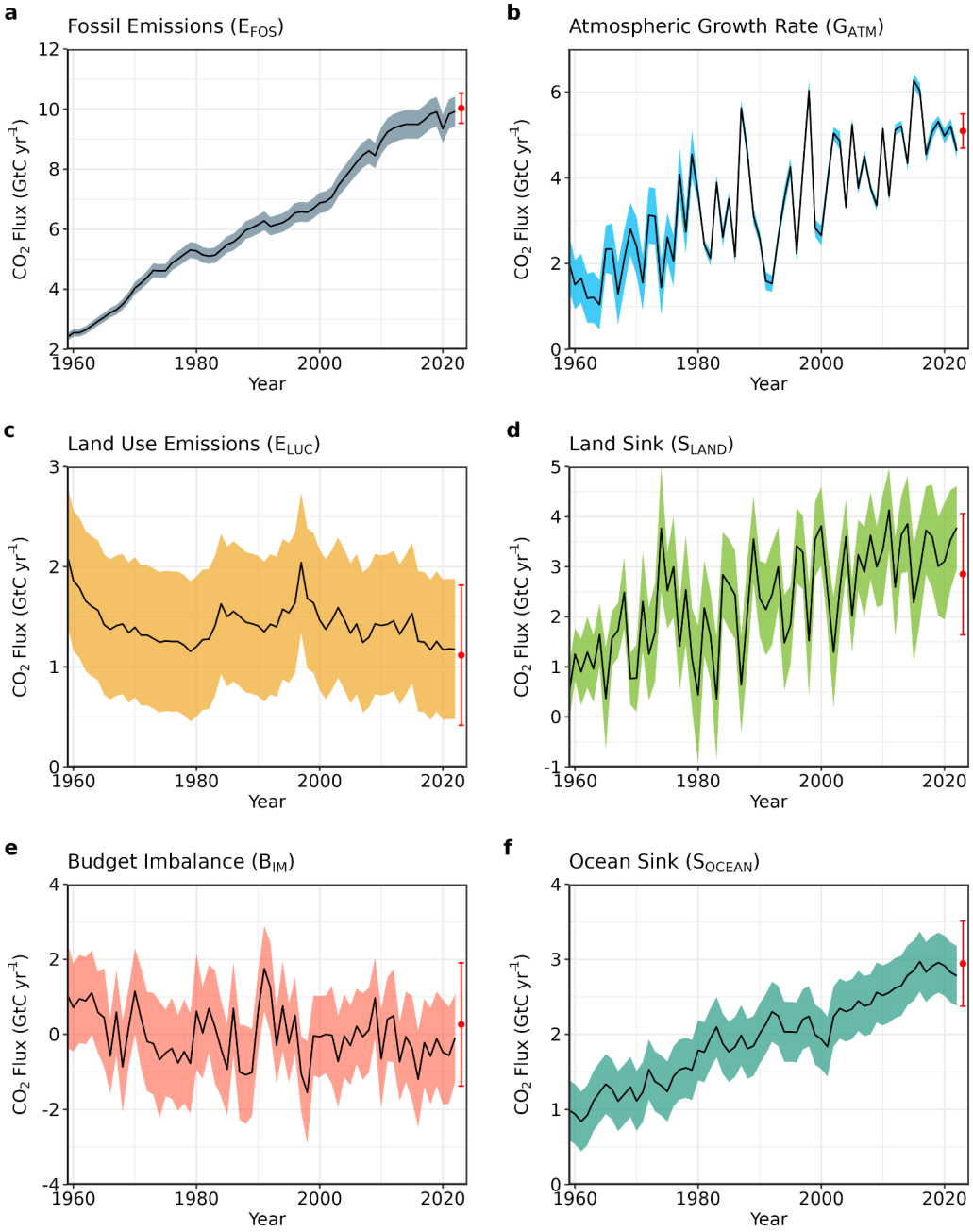

Figure 4. Components of the global carbon budget and their uncertainties as a function of time, presented individually for (a) fossil CO_2 and cement carbonation emissions (E_{FOS}), (b) growth rate in atmospheric CO_2 concentration (G_{ATM}), (c) emissions from land-use change (E_{LUC}), (d) the land CO_2 sink (S_{LAND}), (e) the ocean CO_2 sink (S_{OCEAN}), (f) the budget imbalance that is not accounted for by the other terms. Positive values of S_{LAND} and S_{OCEAN} represent a flux from the atmosphere to land or the ocean. All data are in GtC yr^{-1} with the uncertainty bounds representing ±1 standard deviation in shaded colour. Data sources are as in Figure 3. The red dots indicate our projections for the year 2023 and the red error bars the uncertainty in the projections (see methods).

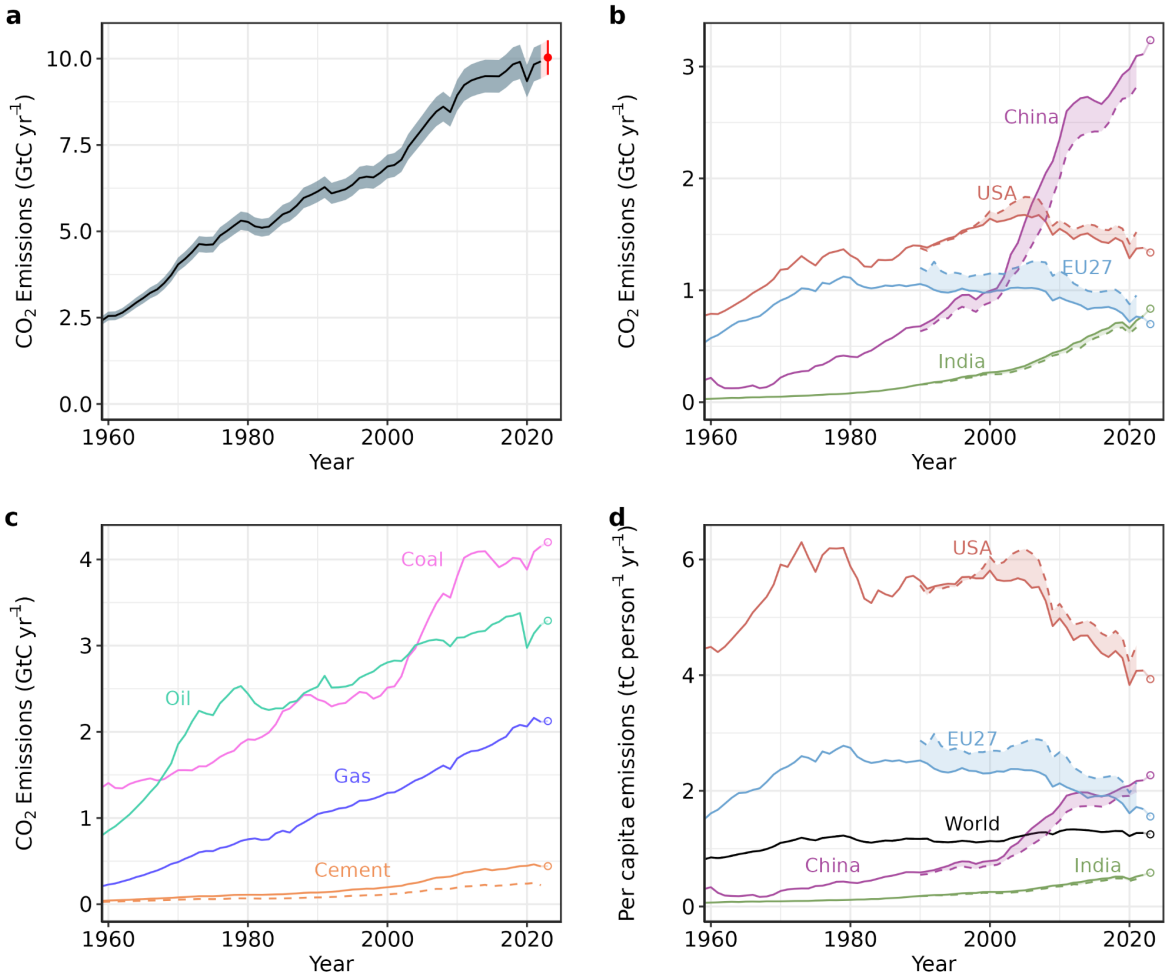

Figure 5. Fossil CO_2 emissions for (a) the globe, including an uncertainty of ± 5% (grey shading) and a projection through the year 2023 (red dot and uncertainty range), (b) territorial (solid lines) and consumption (dashed lines) emissions for the top three country emitters (USA, China, India) and for the European Union (EU27), (c) global emissions by fuel type, including coal, oil, gas, and cement, and cement minus cement carbonation (dashed), and (d) per-capita emissions the world and for the large emitters as in panel (b). Territorial emissions are primarily from a draft update of Gilfillan and Marland (2021) except for national data for Annex I countries for 1990-2021, which are reported to the UNFCCC as detailed in the text, as well as some improvements in individual countries, and extrapolated forward to 2022 using data from Energy Institute. Consumption-based emissions are updated from Peters et al. (2011a). See Section 2.1 and Supplement S.1 for details of the calculations and data sources.

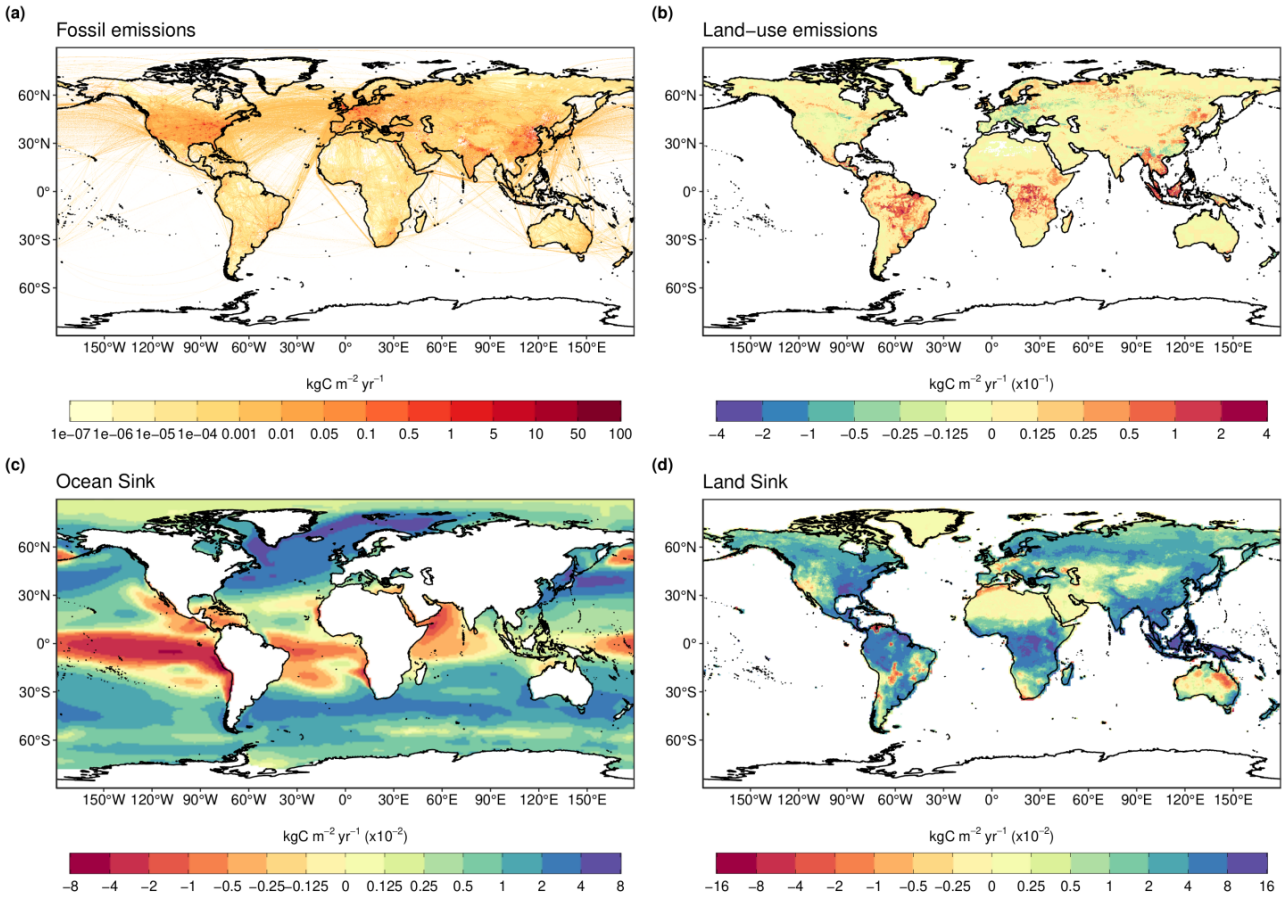

Figure 6. The 2013-2022 decadal mean components of the global carbon budget, presented for (a) fossil CO_2 emissions (E_{FOS}), (b) land-use change emissions (E_{LUC}), (c) the ocean CO_2 sink (S_{OCEAN}), and (d) the land CO_2 sink (S_{LAND}). Positive values for E_{FOS} and E_{LUC} represent a flux to the atmosphere, whereas positive values of S_{OCEAN} and S_{LAND} represent a flux from the atmosphere to the ocean or the land (carbon sink). In all panels, yellow/red colours represent a source (flux from the land/ocean to the atmosphere), green/blue colours represent a sink (flux from the atmosphere into the land/ocean). All units are in kgC m^{-2} yr^{-1}. Note the different scales in each panel. E_{FOS} data shown is from GCP-GridFEDv2023.1 and does not include cement carbonation. The E_{LUC} map shows the average E_{LUC} from the three bookkeeping models plus emissions from peat drainage and peat fires. Gridded E_{LUC} estimates for H&C2023 and OSCAR are derived by spatially distributing their national data based on the spatial patterns of BLUE gross fluxes in each country (see Schwingshackl et al., 2022, for more details about the methodology). S_{OCEAN} data shown is the average of GOBMs and data-products means, using GOBMs simulation A, no adjustment for bias and drift applied to the gridded fields (see Section 2.5). S_{LAND} data shown is the average of the DGVMs for simulation S2 (see Section 2.6).

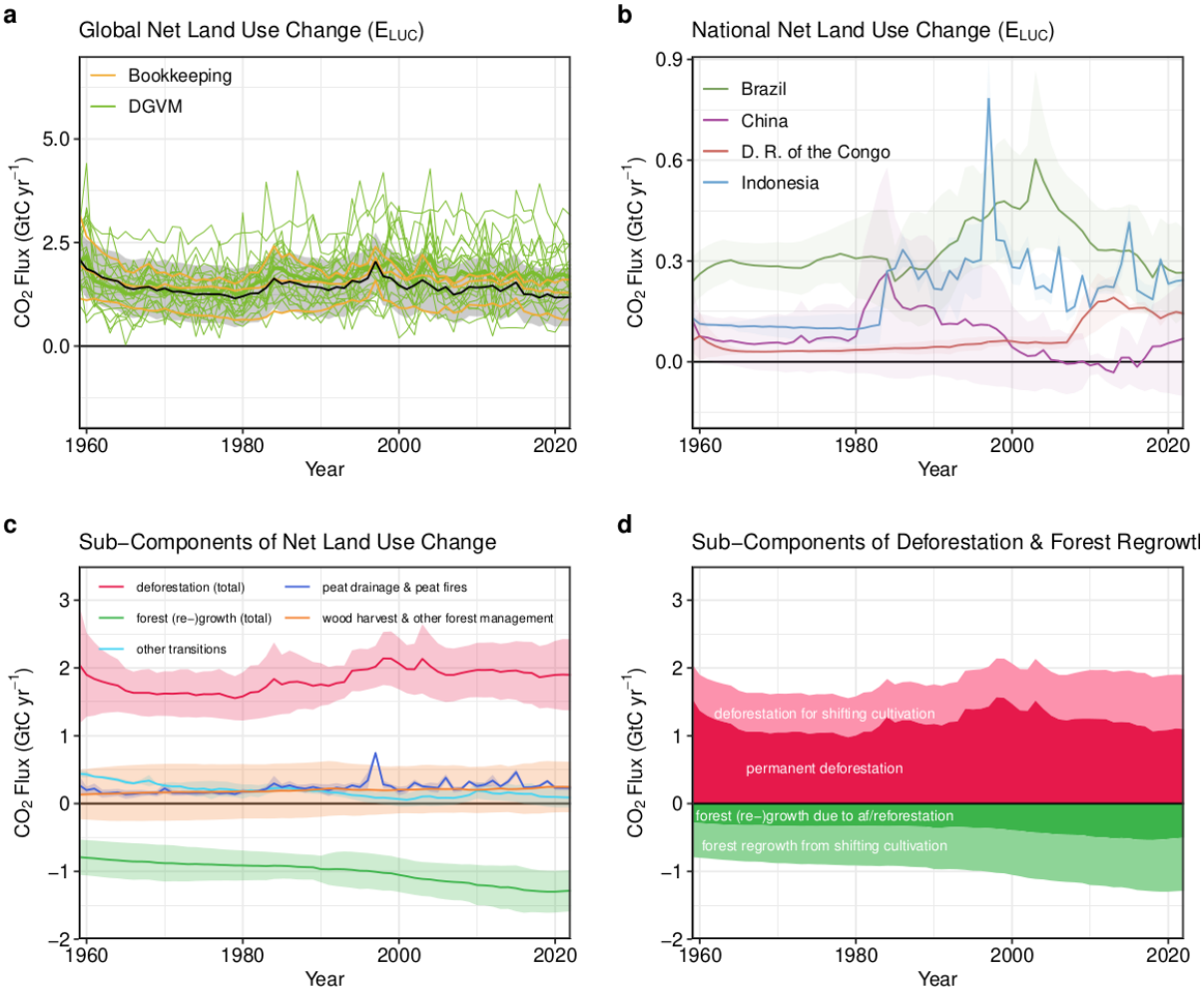

Figure 7. Net CO_2 exchanges between the atmosphere and the terrestrial biosphere related to land use change. (a) Net CO_2 emissions from land-use change (E_{LUC}) with estimates from the three bookkeeping models (yellow lines) and the budget estimate (black with ±1σ uncertainty), which is the average of the three bookkeeping models. Estimates from individual DGVMs (narrow green lines) and the DGVM ensemble mean (thick green line) are also shown. (b) Net CO_2 emissions from land-use change from the four countries with largest cumulative emissions since 1959. Values shown are the average of the three bookkeeping models, with shaded regions as ±1σ uncertainty. (c) Sub-components of E_{LUC}: (i) emissions from deforestation (including permanent deforestation and deforestation in shifting cultivation cycles), (ii) emissions from peat drainage & peat fires, (iii) removals from forest (re-)growth (including forest (re-)growth due to afforestation and reforestation and forest regrowth in shifting cultivation cycles), (iv) fluxes from wood harvest and other forest management (comprising slash and product decay following wood harvest, regrowth after wood harvest, and fire suppression), and (v) emissions and removals related to other land-use transitions. The sum of the five components is E_{LUC} shown in panel (a). (d) Sub-components of 'deforestation (total)' and of 'forest (re-)growth (total)': (i) deforestation in shifting cultivation cycles, (ii) permanent deforestation, (iii) forest (re-)growth due to afforestation and/or reforestation, and (iv) forest regrowth in shifting cultivation cycles.

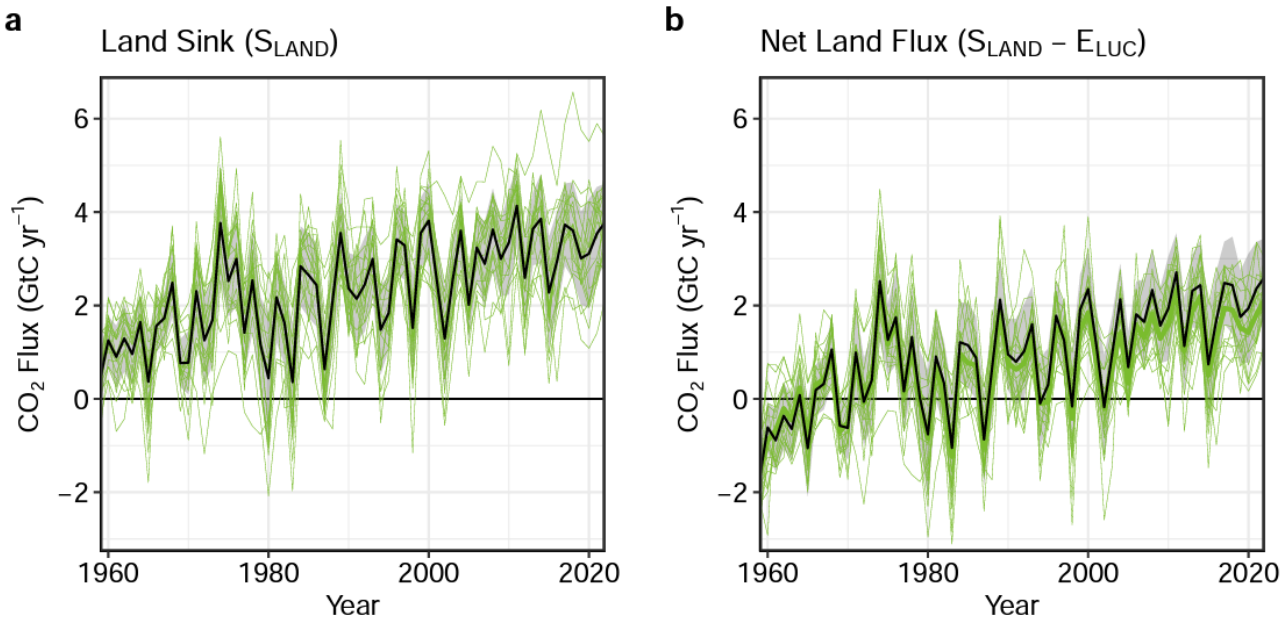

Figure 8. (a) The land CO_2 sink (S_{LAND}) estimated by individual DGVMs (green), as well as the budget estimate (black with ±1σ uncertainty), which is the average of all DGVMs. (b) Net atmosphere-land CO_2 fluxes (S_{LAND} – E_{LUC}). The budget estimate of the net land flux (black with ±1σ uncertainty) combines the DGVM estimate of S_{LAND} from panel (a) with the bookkeeping estimate of E_{LUC} from Figure 7a. Uncertainties are similarly propagated in quadrature. DGVMs also provide estimates of E_{LUC} (see Figure 7a), which can be combined with their own estimates of the land sink. Hence panel (b) also includes an estimate for the net land flux for individual DGVMs (thin green lines) and their multi-model mean (thick green line).

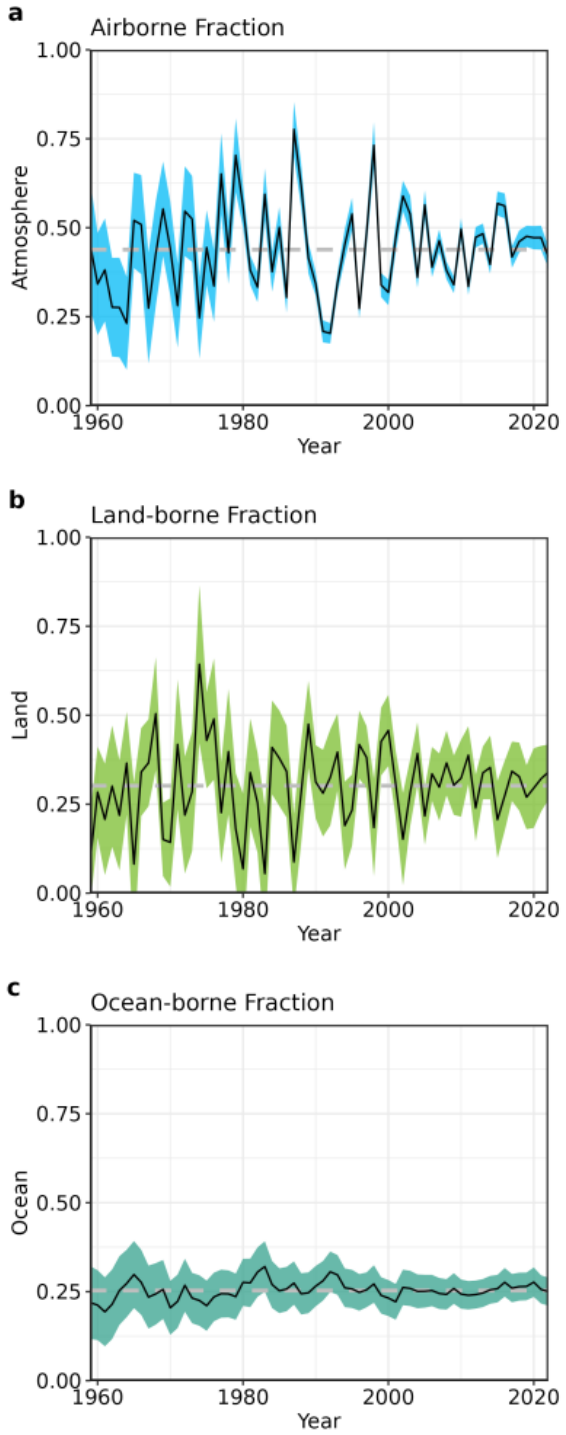

Figure 9. The partitioning of total anthropogenic CO_2 emissions (E_{FOS} + E_{LUC}) across (a) the atmosphere (airborne fraction), (b) land (land-borne fraction), and (c) ocean (ocean-borne fraction). Black lines represent the central estimate, and the coloured shading represents the uncertainty. The grey dashed lines represent the long-term average of the airborne (44%), land-borne (30%) and ocean-borne (25%) fractions during 1960-2022 (with a B_{IM} of 1%).

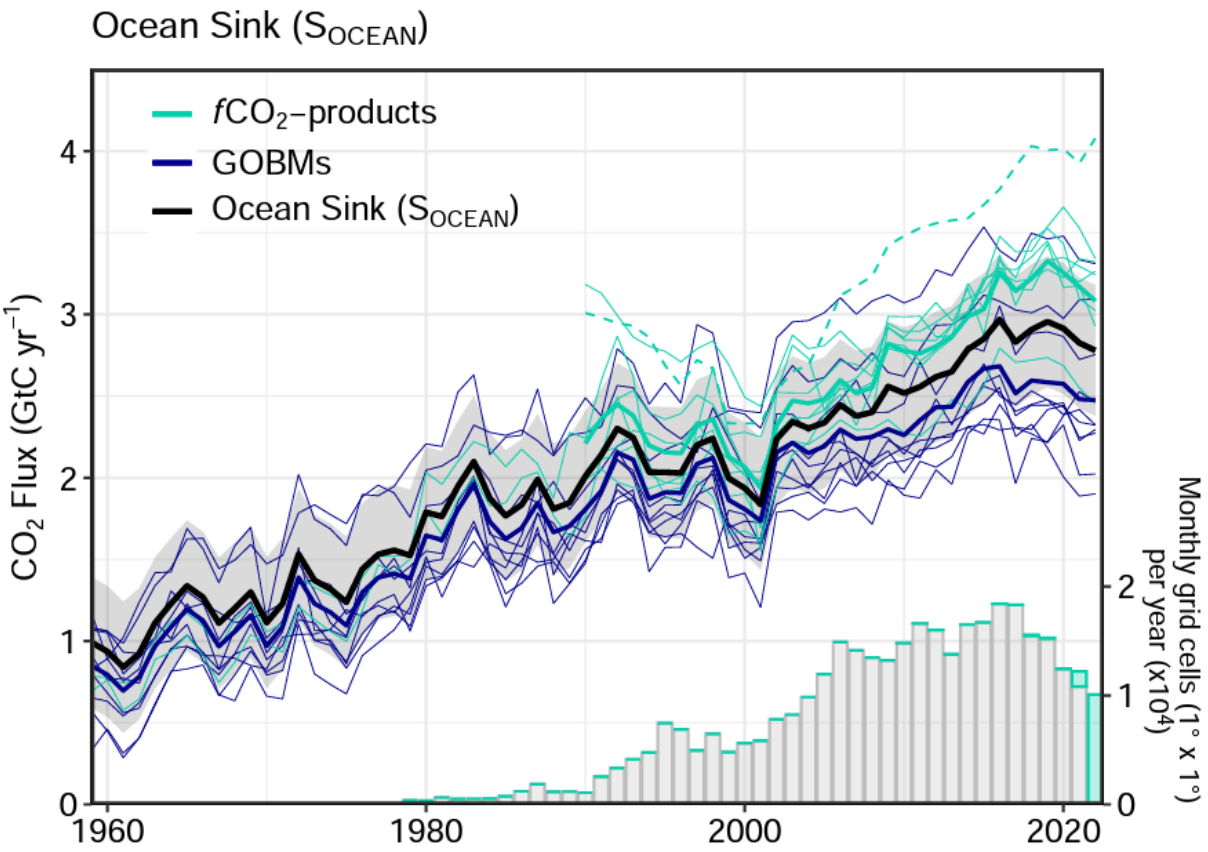

Figure 10. Comparison of the anthropogenic atmosphere-ocean CO_2 flux showing the budget values of S_{OCEAN} (black; with the uncertainty in grey shading), individual ocean models (royal blue), and the ocean fCO_2-products (cyan; with Watson et al. (2020) in dashed line as not used for ensemble mean). Only one fCO_2-product (Jena-MLS) extends back to 1959 (Rödenbeck et al., 2022). The fCO_2-products were adjusted for the pre-industrial ocean source of CO_2 from river input to the ocean, by subtracting a source of 0.65 GtC yr^{-1} to make them comparable to S_{OCEAN} (see Section 2.5). Bar-plot in the lower right illustrates the number of fCO_2 observations in the SOCAT v2023 database (Bakker et al., 2023). Grey bars indicate the number of data points in SOCAT v2022, and coloured bars the newly added observations in v2023.

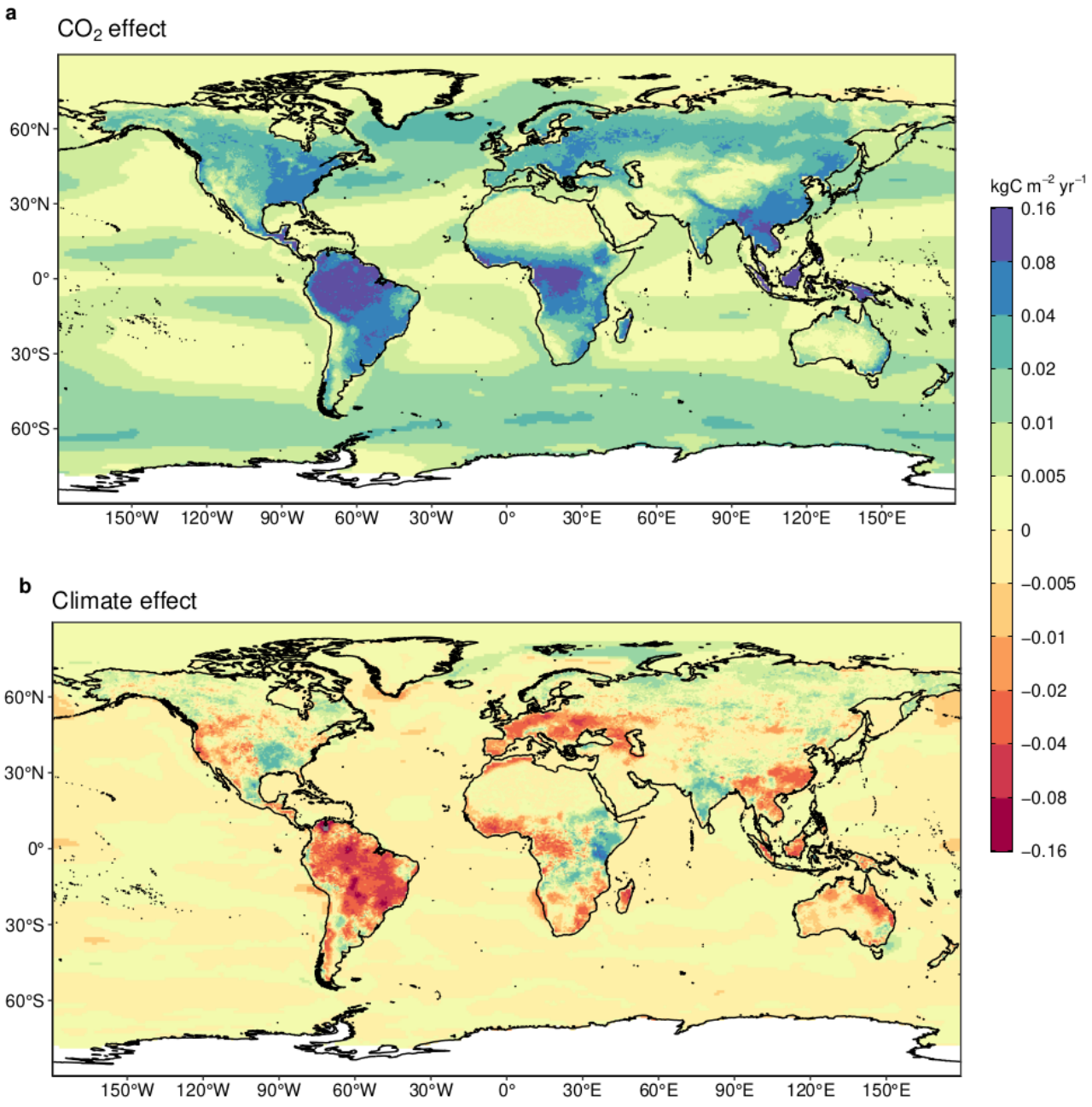

Figure 11. Attribution of the atmosphere-ocean (S_{OCEAN}) and atmosphere-land (S_{LAND}) CO_2 fluxes to (a) increasing atmospheric CO_2 concentrations and (b) changes in climate, averaged over the previous decade 2013-2022. All data shown is from the processed-based GOBMs and DGVMs. Note that the sum of ocean CO_2 and climate effects shown here will not equal the ocean sink shown in Figure 6 which includes the fCO_2-products. See Supplement S.3.2 and S.4.1 for attribution methodology. Units are in kgC m^{-2} yr^{-1} (note the non-linear colour scale).

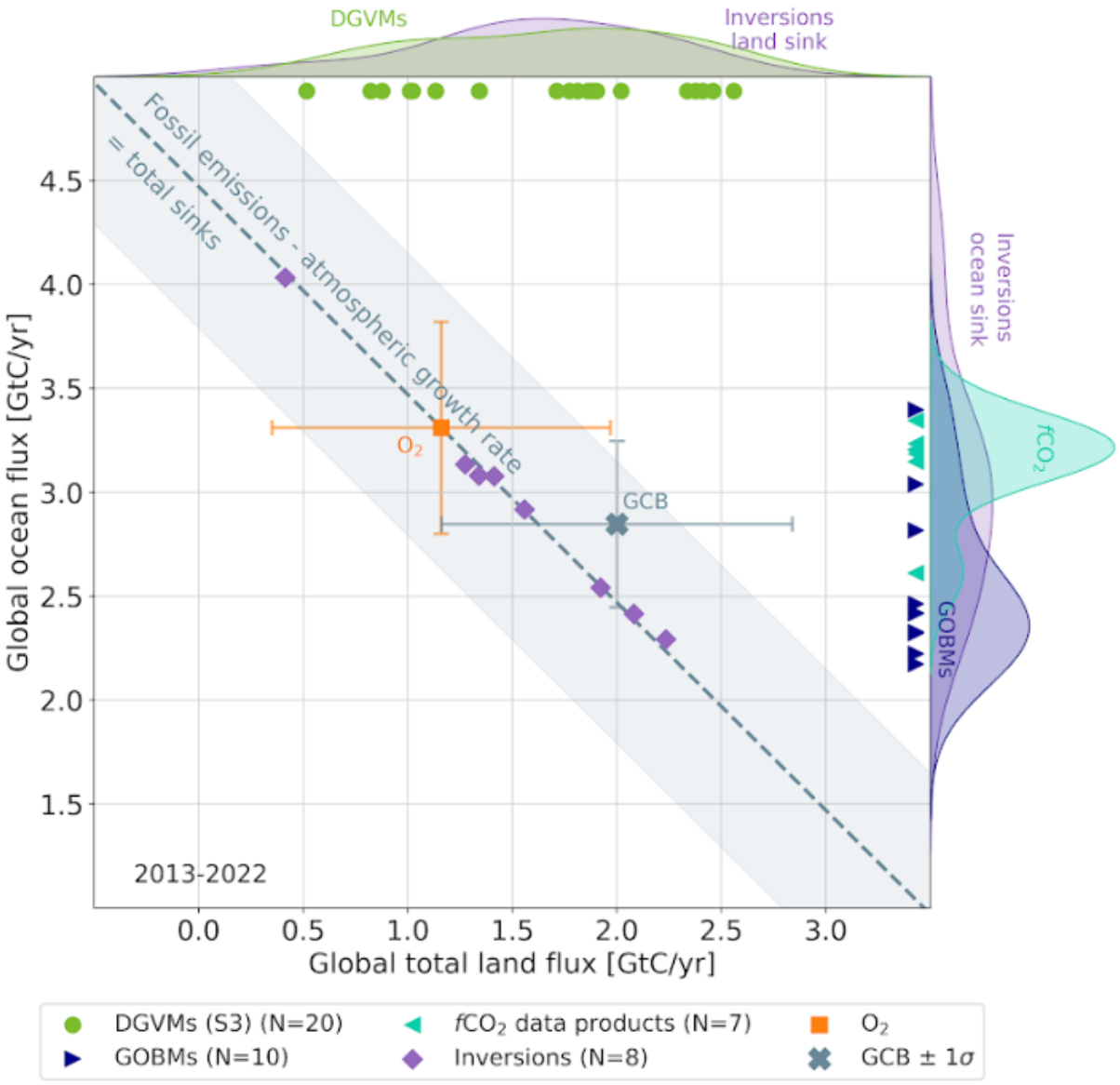

Figure 12. The 2013-2022 decadal mean global net atmosphere-ocean and atmosphere-land fluxes derived from the ocean models and fCO_2 products (y-axis, right and left pointing blue triangles respectively), and from the DGVMs (x-axis, green symbols), and the same fluxes estimated from the atmospheric inversions (purple symbols). The shaded distributions show the densities of the ensembles of individual estimates. The grey central cross is the mean (±1σ) of S_{OCEAN} and (S_{LAND} – E_{LUC}) as assessed in this budget. The grey diagonal line represents the constraint on the global land + ocean net flux, i.e. global fossil fuel emissions minus the atmospheric growth rate from this budget ($E_{FOS} - G_{ATM}$). The orange cross represents the same global net atmosphere-ocean and atmosphere-land fluxes as estimated from the atmospheric O_2 constraint (±1σ for each of the fluxes although caution is needed to interpret these error bars, since solutions outside the grey band are unlikely, as outside of the 1σ uncertainty). Positive values are CO_2 sinks. Note that the inverse estimates have been scaled for a minor difference between E_{FOS} and GridFEDv2023.1 (Jones et al., 2023).

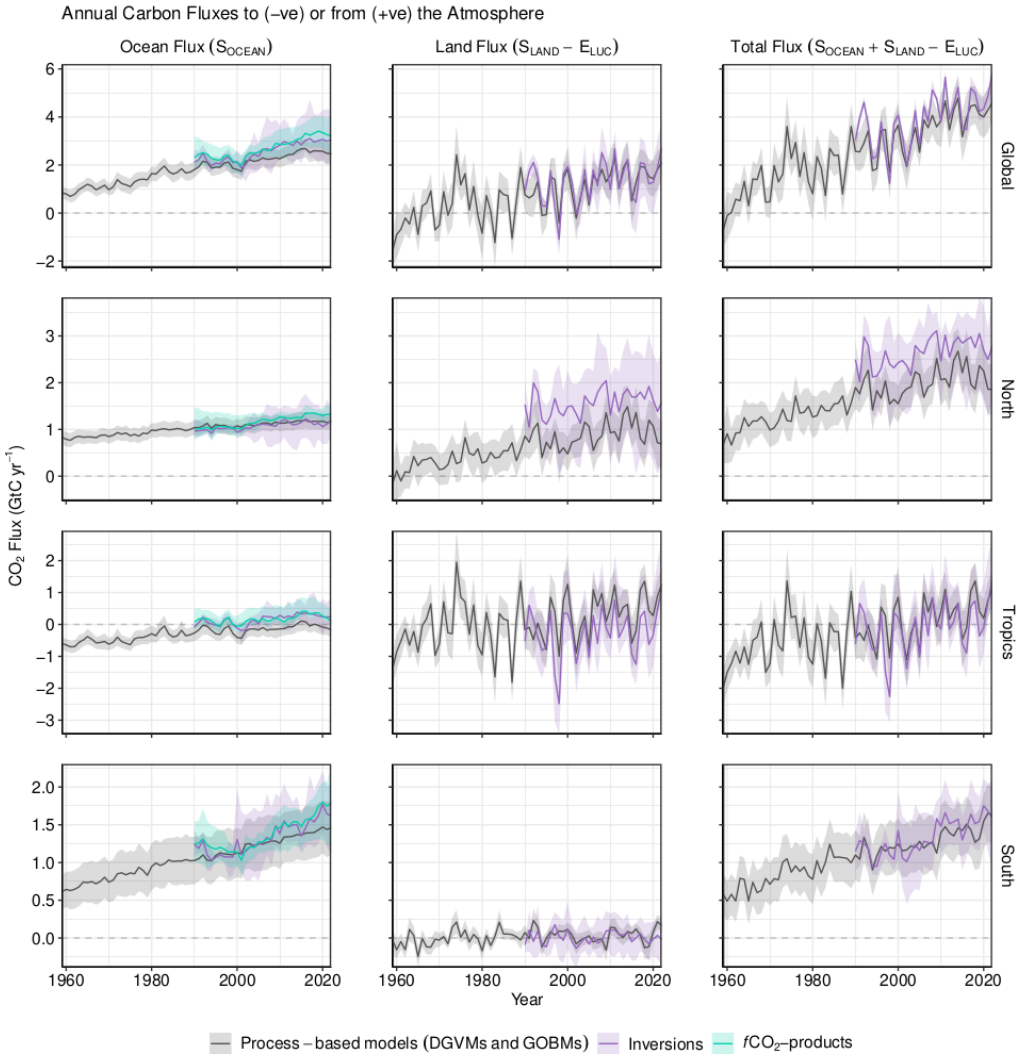
Annual Carbon Fluxes to (–ve) or from (+ve) the Atmosphere
Ocean Flux (S_{OCEAN})
Land Flux ($S_{LAND} - E_{LUC}$)
Total Flux ($S_{OCEAN} + S_{LAND} - E_{LUC}$)
Global
North
Tropics
South
CO_2 Flux (GtC yr^{-1})
Year
1960
1980
2000
2020
Process – based models (DGVMs and GOBMs)
Inversions
fCO_2–products

Figure 13. CO_2 fluxes between the atmosphere and the Earth's surface separated between land and oceans, globally and in three latitude bands. The ocean flux is S_{OCEAN} and the land flux is the net atmosphere-land fluxes from the DGVMs. The latitude bands are (top row) global, (2nd row) north (>30°N), (3rd row) tropics (30°S-30°N), and (bottom row) south (<30°S), and over ocean (left column), land (middle column), and total (right column). Estimates are shown for: process-based models (DGVMs for land, GOBMs for oceans); inversion systems (land and ocean); and *f*CO_2-products (ocean only). Positive values are CO_2 sinks. Mean estimates from the combination of the process models for the land and oceans are shown (black line) with ±1 σ of the model ensemble (grey shading). For the total uncertainty in the process-based estimate of the total sink, uncertainties are summed in quadrature. Mean estimates from the atmospheric inversions are shown (purple lines) with their full spread (purple shading). Mean estimates from the *f*CO_2-products are shown for the ocean domain (light blue lines) with full model spread (light blue shading). The global S_{OCEAN} (upper left) and the sum of S_{OCEAN} in all three regions represents the anthropogenic atmosphere-to-ocean flux based on the assumption that the preindustrial ocean sink was 0 GtC yr^{-1} when riverine fluxes are not considered. This assumption does not hold at the regional level, where preindustrial fluxes can be significantly different from zero. Hence, the regional panels for S_{OCEAN} represent a combination of natural and anthropogenic fluxes. Bias-correction and area-weighting were only applied to global S_{OCEAN}; hence the sum of the regions is slightly different from the global estimate (<0.05 GtC yr^{-1}).

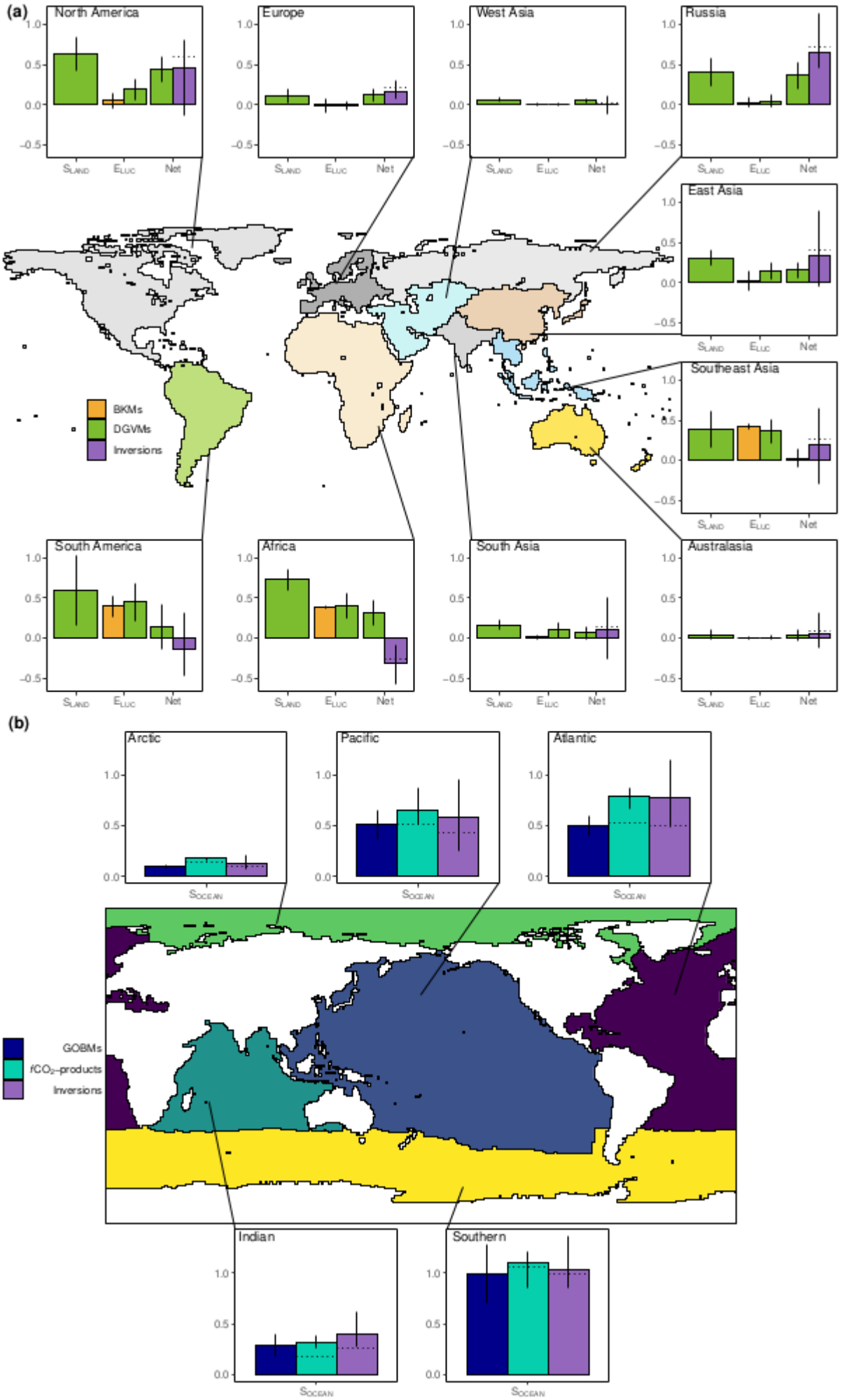
(a)
North America
Europe
West Asia
Russia
East Asia
Southeast Asia
South America
Africa
South Asia
Australasia
BIMs
DGVMs
Inversions
(b)
Arctic
Pacific
Atlantic
Indian
Southern
GOBMs
fCO2−products
Inversions

Figure 14. Decadal mean (a) land and (b) ocean fluxes for RECCAP-2 regions over 2013-2022. For land fluxes, S_{LAND} is estimated by the DGVMs (green bars), with the error bar as ±1σ spread among models. A positive S_{LAND} is a net transfer of carbon from the atmosphere to the land. E_{LUC} fluxes are shown for both DGVMs (green) and bookkeeping models (orange), again with the uncertainty calculated as the ±1σ spread. Note, a positive E_{LUC} flux indicates a loss of carbon from the land. The net land flux is shown for both DGVMs (green) and atmospheric inversions (purple), including the full model spread for inversions. The net ocean sink (S_{OCEAN}) is estimated by GOBMs (royal blue), *f*CO_2-products (cyan), and atmospheric inversions (purple). Uncertainty is estimated as the ±1σ spread for GOBMs, and the full model spread for the other two products. The dotted lines show the *f*CO_2-products and inversion results without river flux adjustment. Positive values are CO_2 sinks.

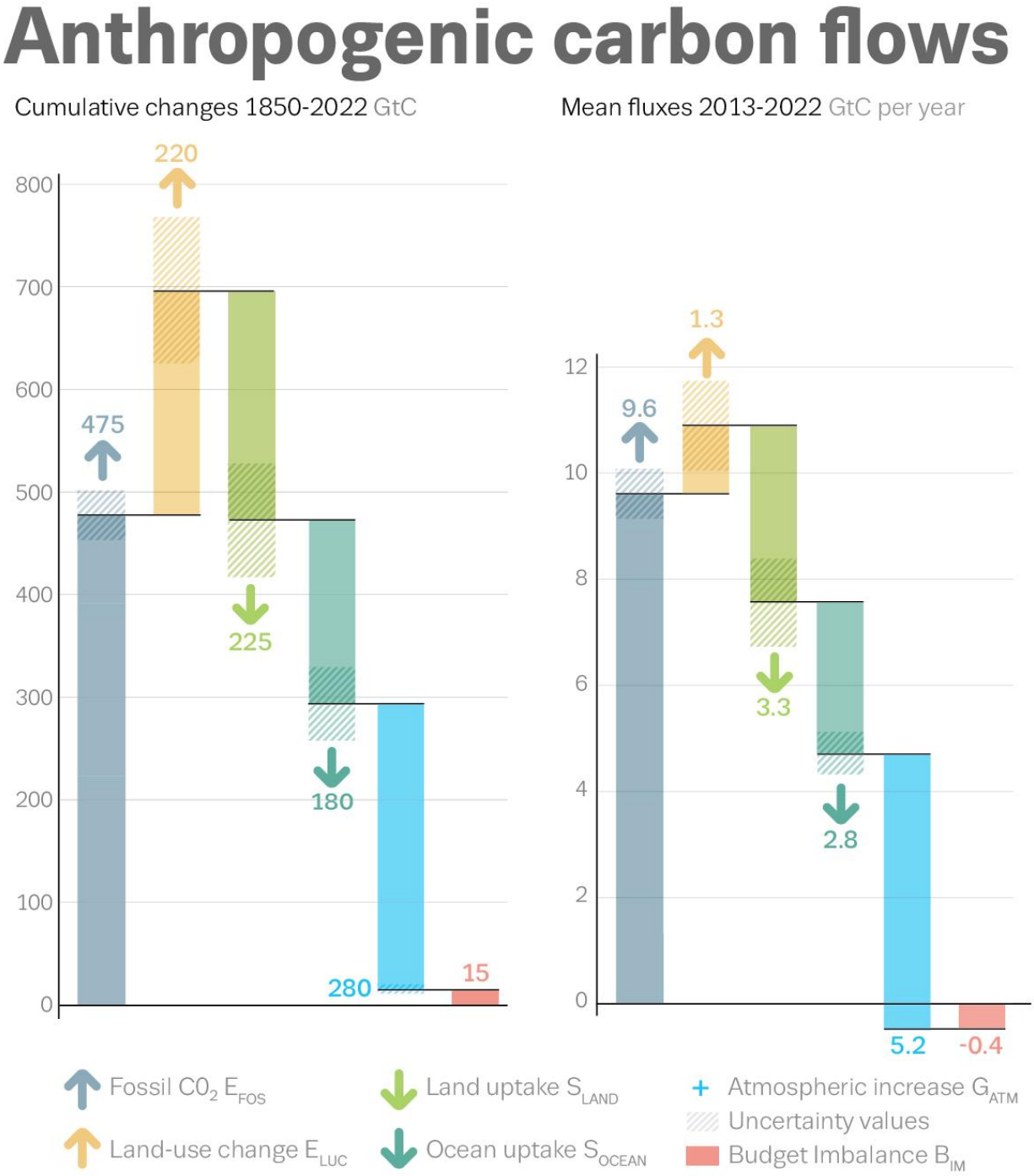

Figure 15. Cumulative changes over the 1850-2022 period (left) and average fluxes over the 2013-2022 period (right) for the anthropogenic perturbation of the global carbon cycle. See the caption of Figure 3 for key information and the methods in text for full details.

Figure 16. Kaya decomposition of the main drivers of fossil CO_2 emissions, considering population, GDP per person, Energy per GDP, and CO_2 emissions per energy, for China (top left), USA (top right), EU27 (middle left), India (middle right), Rest of the World (bottom left), and World (bottom right). Black dots are the annual fossil CO_2 emissions growth rate, coloured bars are the contributions from the different drivers to this growth rate. A general trend is that population and GDP growth put upward pressure on emissions (positive values), while energy per GDP and, more recently, CO_2 emissions per energy put downward pressure on emissions (negative values). Both the COVID-19 induced drop during 2020 and the recovery in 2021 led to a stark contrast to previous years, with different drivers in each region. The EU27 had strong Energy/GDP improvements in 2022.